UCRL-18066
cy. 2

SEMIANNUAL REPORT BIOLOGY AND MEDICINE

Donner Laboratory
and
Donner Pavilion

Fall 1967

TWO-WEEK LOAN COPY

This is a Library Circulating Copy which may be borrowed for two weeks. For a personal retention copy, call Tech. Info. Division, Ext. 5545

UCRL-18066
cy. 2

LAWRENCE RADIATION LABORATORY · UNIVERSITY OF CALIFORNIA · BERKELEY

DISCLAIMER

This document was prepared as an account of work sponsored by the United States Government. While this document is believed to contain correct information, neither the United States Government nor any agency thereof, nor the Regents of the University of California, nor any of their employees, makes any warranty, express or implied, or assumes any legal responsibility for the accuracy, completeness, or usefulness of any information, apparatus, product, or process disclosed, or represents that its use would not infringe privately owned rights. Reference herein to any specific commercial product, process, or service by its trade name, trademark, manufacturer, or otherwise, does not necessarily constitute or imply its endorsement, recommendation, or favoring by the United States Government or any agency thereof, or the Regents of the University of California. The views and opinions of authors expressed herein do not necessarily state or reflect those of the United States Government or any agency thereof or the Regents of the University of California.

UCRL-18066
UC-48 Biology and Medicine
TID-4500 (51st Ed.)

FALL 1967

SEMIANNUAL REPORT BIOLOGY AND MEDICINE

John H. Lawrence, M.D., Editor

DONNER LABORATORY AND DONNER PAVILION

LAWRENCE RADIATION LABORATORY UNIVERSITY OF CALIFORNIA
BERKELEY, CALIFORNIA

AEC Contract No. W-7405-eng-48

Foreword

The twenty-one papers comprising this issue tell of progress in several areas of biomedical research, but all areas of research activity cannot, of course, be covered. The first three papers concern erythropoietin. Using a technique based upon endogenous production of ^{14}CO in the breath following the injection of glycine-2-^{14}C to study red-blood-cell survival in LAF_1 mice and buffalo rats following hypoxia, erythropoietin injection, repeated phlebotomy, or phenylhydrazine-induced anemia, one study revealed minimal alterations in red-blood-cell survival despite marked erythropoietic stimulation and indicated that the red blood cells were remarkably normal (page 1). An investigation of the behavior of erythropoietin-sensitive cells during recovery from 200 R whole-body irradiation demonstrated results consistent with a model of hemopoiesis which assumes that a population of cells derived from the "stem cell" rather than of "stem cells" themselves is sensitive to the differentiative action of erythropoietin (page 15). The last report describes the presence of an erythropoietin-enhancing factor in the serum of a calf with primary familial polycythemia (page 23).

Three papers in radiation genetics describe radiation-induced mitotic segregation (page 26), reciprocal translocation (page 38), and radiation-sensitive mutants in yeast (page 43). A karyotype analysis of the M3-1 tissue culture line of Chinese hamster fibroblasts showed that the M3-1 cell "line" was no longer diploid and that there was no cell subline with a "normal" Chinese karyotype, thus justifying the doubts raised concerning the continued "normal" character of this line (page 48).

Pioneering work in the biomedical applications of the scanning electron microscope continues. Scanning electron micrographs of familiar biological specimens (tobacco mosaic virus, polystyrene latex spheres, lipoprotein macromolecules, and collagen) are presented as reference material for testing the performance of the instrument and demonstrating the kinds of information already available; such standard biological test specimens may pave the way for increased use of the scanning electron microscope in obtaining valuable information in biological and medical investigations (page 50). Two studies describe further uses of the electron microscope in research: one reports preliminary studies of microdomain structure-analysis of biological specimens which hopefully will lead to a method for obtaining diffraction patterns from a single cell membrane (page 64); the other reports macromolecular studies of structure of human serum lipoproteins (page 74). The next four reports are lipoprotein studies: the first describes the programming method for graphic presentation of data obtained in the computer analysis of Schlieren photographs of serum lipoprotein distributions, and shows how these computer-produced graphs allow rapid visual evaluation, comparison of samples, and error detection (page 85); the next describes a method for analysis of the principle lipid constituents of blood serum by a single measurement of the carbonyl band area (page 89); another presents an evaluation of changes in human serum lipoprotein distribution following heparin and ethyl-p-chlorophenoxyisobutyrate administration *in vivo*, using a computerized technique for analysis of ultracentrifugal films (page 95); and the last describes a procedure for the separation of serum $S_f > 400$ lipoproteins into three subfractions and the subsequent measurement of the

protein content of each protein subfraction and calculation of surface protein coverage, suggesting that the increase in surface-volume ratio with decreasing particle size is just compensated for by an increase in protein content, and therefore protein coverage remains the same for all serum $S_f > 400$ lipoproteins (page 102).

One report presents data obtained with a radioactive catheter and the scintillation camera in cardiac catheterization, instead of with fluoroscopy, which contributes a relatively large dose of radiation exposure to the child (page 58). This method could be a very important alternate.

There is a report on the physical characteristics of negative pion beams, including the energy-loss distribution and Bragg curves (page 108). Further investigations of growth hormone are then reported, using the very sensitive radioimmunoassay in selected mammalian species (page 123). This is an effort to understand the control of growth hormone release by the pituitary gland. Continued investigations of the biological effects of heavy particles are reported in a paper concerning comparative effects on the proliferative capacity of lymphoma ascites tumor cells in vivo of X rays and helium ions of several LET's (page 151). The oxygen enhancement ratio was greatest for 230 kV X rays and least for the higher LET (80 and 210 MeV-cm^2/g) helium ions. The RBE's were close to 1, except for the high-LET (Bragg peak) helium ions (1.8 and 1.9). The next paper describes the use of a modified insulin tolerance test to measure pituitary reserve in pituitary syndromes—such information being of great value in diagnosing pituitary disorders as well as in discerning the effect of heavy particles in therapy (page 166). Another paper presents a literature survey and a report on delayed radionecrosis of the central nervous system, indicating the great individual variation in susceptibility (page 173). The final paper describes the use of heavy particle radiosurgery in the treatment of Cushing's disease (page 193).

Table of Contents

The Effects of Graded Erythropoietic Stimulation on Red Blood Cell Survival in the Mouse and Rat
STEPHEN A. LANDAW 1

Studies on the Behavior of Erythropoietin-Sensitive Cells in the Mouse During Recovery from 200 R Whole-Body Irradiation
JOHN C. SCHOOLEY, JUDITH M. HAYES, LINDA N. CANTOR AND VIRGINIA W. HAVENS 15

Erythropoietin-Enhancing Factor in Serum of a Calf with Primary Familial Polycythemia
DONALD C. VAN DYKE, MARY L. NOHR AND B. TENNANT 23

Radiation-Induced Mitotic Segregation in Yeast
SAYAKA NAKAI AND ROBERT K. MORTIMER 26

A Reciprocal Translocation in *Saccharomyces cerevisiae*
TOMMY JAMES McKEY 38

Radiation-Sensitive Mutants in Yeast
MICHAEL A. RESNICK AND ROBERT K. MORTIMER 43

A Karyotype Analysis of the M3-1 Tissue Culture Line of Chinese Hamster Fibroblasts
WILLIAM D. LOUGHMAN 48

Standard Biological Test Specimens for Use in the Scanning Electron Microscope
THOMAS L. HAYES, JaRUE S. MANNING AND ROBERT M. GLAESER 50

Cardiac Catheterization Using a Radioactive Catheter and the Scintillation Camera
DONALD C. VAN DYKE, HAL O. ANGER, FREDERICK DUFFY, STANLEY HIGASHINO AND JOYCE WILSON 58

Microdomain Structure-Analysis of Biological Specimens by Electron Diffraction
ROBERT M. GLAESER 64

Structure of Human Serum Lipoproteins as Observed with the Electron Microscope after Negative Staining
GERTRUDE M. FORTE, ALEX V. NICHOLS AND ROBERT M. GLAESER 74

Graphic Presentation of Computer-Derived Schlieren Lipoprotein Data
LIN C. JENSEN, THOMAS H. RICH AND FRANK T. LINDGREN 85

Integrated Absorption Intensities of the Ester Carbonyl Bands of Lipids and Their Analytical Applications
NORMAN K. FREEMAN, LIN C. JENSEN AND VIRGINIA C. LEW 89

Analysis of Change in Ultracentrifugal Lipoprotein Profiles Following Heparin and Ethyl-p-Chlorophenoxyisobutyrate Administration
ALEX V. NICHOLS, EDWARD H. STRISOWER, FRANK T. LINDGREN, GERALD L. ADAMSON AND ELAINE L. COGGIOLA 95

Subfractionation of $S_f > 400$ Serum Lipoproteins by Successive, Cumulative, Density Gradient Centrifugation
WALTER J. LOSSOW, FRANK T. LINDGREN, JACK C. MURCHIO AND LIN C. JENSEN 102

A Calculation of the Physical Characteristics of Negative Pion Beams—Energy-Loss Distribution and Bragg Curves
STANLEY B. CURTIS AND MUDUNDI R. RAJU 108

Investigation of Growth Hormone Secretion in Selected Mammalian Species
JOSEPH F. GARCIA AND IRVING I. GESCHWIND 123

The Measurement of the Effects of X Rays and Helium Ions on the Proliferative Capacity of Lymphoma Ascites Tumor Cells in vivo
JOSE M. FEOLA, JOHN H. LAWRENCE, AND GRAEME P. WELCH 151

Use of a Modified Insulin Tolerance Test to Measure Growth Hormone Reserve in Pituitary Diseases
JOHN A. LINFOOT, JOSEPH F. GARCIA, NORTON J. SNYDER, EDWARD MANOUGIAN, RICHARD A. CARLSON, ROBERT A. FINK, JAMES L. BORN AND JOHN H. LAWRENCE 166

Delayed Radionecrosis of the Central Nervous System
LARRY W. McDONALD, JAMES L. BORN, JOHN H. LAWRENCE AND JOHN T. LYMAN 173

Heavy Particle Radiosurgery in Cushing's Disease
JOHN A. LINFOOT, EDWARD MANOUGIAN, CORNELIUS A. TOBIAS, JAMES L. BORN, NORTON J. SNYDER, RICHARD A. CARLSON AND JOHN H. LAWRENCE 193

Staff Publications 199

Author Index 205

Personnel 207

The Effects of Graded Erythropoietic Stimulation on Red Blood Cell Survival in the Mouse and Rat

Stephen A. Landaw

Controversy exists with regard to the effect of increased erythropoietic rate on the survival of red blood cells (RBC). While certain previously published results indicate that increasing the rate of RBC production results in diminution in the survival of such cells in the circulation (1-6), other results indicate that increasing erythropoiesis has no effect on RBC survival (7-9). This question is by no means trivial since it has implications in such problems as the biochemical basis of RBC survival and in understanding the kinetic mechanisms involved when erythropoietic rate is increased.

Recently, a method was developed for the determination of the distribution of circulating RBC survival times by measurement of ^{14}CO in the breath of animals following the injection of glycine-2-^{14}C (10). This continuous, quantitative, in vivo method obviates the necessity of obtaining any blood samples, and is independent of changes in total body RBC volume. It is the purpose of this article to present results using this method in the mouse and rat following graded erythropoietic stimulation by hypoxia, bleeding, erythropoietin (ESF) injection, or phenylhydrazine (PHH)-induced anemia.

MATERIALS AND METHODS

Animals used for this study were female LAF_1 mice (Jackson Memorial Laboratory, Bar Harbor, Maine) and male buffalo rats (Simonsen Laboratory, Gilroy, California). The mice, weighing approximately 20 g each, were studied in groups of five animals, each mouse receiving 10 μCi of labeled glycine (specific activity: 20-28 millicuries per millimole; New England Nuclear Corp., Boston, Mass.) intravenously without anesthesia. The rats, weighing 300-350 g each, were studied individually, each rat receiving 50 μCi of labeled glycine intravenously under light ether anesthesia.

Labeled carbon monoxide was detected in the expired air of these animals by a method previously presented (11). Essentially, this method entails the removal of contaminating $^{14}CO_2$ from the expired air by means of soda lime, oxidation of the ^{14}CO to $^{14}CO_2$ by means of a Hopcalite catalyst (Mine Safety Applicances Co., Pittsburgh, Pa.), and absorption of the $^{14}CO_2$ thus generated in ethanolamine, followed by liquid scintillation counting. Previous studies have shown that this method is an accurate means of measuring degradation of labeled heme in the intact animal, and that contamination by endogenously produced $^{14}CO_2$ and other volatile compounds in the breath, urine, and feces is negligible (11). A similar method has

been introduced by White, Coburn, Williams, and co-workers for performing the same type of studies in man (12).

Production of ^{14}CO was divided into "early" and "late" phases by methods previously described (10, 11). The "early peak" was determined in one of two manners, as follows:

1) All of the ^{14}CO exhaled by the animal during the first 3-5 days following injection of the labeled glycine was measured. On subsequent days the quantity of exhaled ^{14}CO was measured for 5-hr periods. In this manner the exact magnitude and shape of the early peak could be accurately determined.

2) Labeled CO was collected at frequent 5-hr intervals during the period 3-18 days following injection of the labeled glycine.

In either method, the data points obtained after the third post-injection day could be approximated by a single exponential regression line, using a visual best-fit to the data points on semilogarithmic paper. The quantity of ^{14}CO excreted secondary to early peak processes was estimated in method 1 by adding the total activity obtained during the period of continuous collection of ^{14}CO to the calculated excretion from the end of the period of continuous collection to infinity, assuming a single exponential form to the ^{14}CO excretion data during this period. In method 2 the quantity of ^{14}CO excreted related to the early peak processes was estimated from the single exponential regression line alone, in the period from the time of injection to infinity. This was done by dividing the zero time extrapolate by the slope of the curve relating ^{14}CO excretion rate to time after injection of glycine-2-^{14}C.

After correction for the single exponential component due to continuation of the early peak, the late peak of ^{14}CO excretion was analyzed by fitting the corrected data obtained after the 20th day to appropriate mathematical functions (10, 13) utilizing a CDC 6600 digital computer. When thus applied to the data, this computer program provides the following parameters describing the distribution of RBC survival:

k = rate of random hemolysis (percent per day)

T = mean potential RBC lifespan (days)

σ = standard deviation of lifespans about the mean potential lifespan (days)

C = fractional incorporation of labeled glycine into circulating RBC heme (percent).

Hematocrit determinations were performed using a semi-micro method. Hemoglobin concentrations and reticulocyte counts were performed using standard methods. The length of time for sampling the expired air ranged from 1-5 hr. Samples for liquid scintillation counting of the trapped ^{14}CO (as $^{14}CO_2$) were prepared in duplicate, and counted for a sufficient length of time so that the counting error would be less than 2%. Sample count rate (CPM) was converted to absolute disintegration rate (DPM) by the use of an internal standard of toluene-^{14}C (New England Nuclear Corp., Boston, Mass. and Nuclear-Chicago Corp., Des Plaines, Illinois). The maximum excretion rates for ^{14}CO obtained in this study were approximately 2000 DPM per hour during the early peak, and 500 DPM per hour during the late peak.

For the cross-transfusion experiments, donor cells labeled by glycine-2-^{14}C during the preceding 24 hr were removed via aortic puncture, and washed three times in isotonic saline.

The hematocrits were then adjusted to 45-55% by the addition of normal saline after the final wash, and the cells were transfused intravenously via a lateral tail vein into normal compatible hosts.

Phenylhydrazine solutions were made fresh daily, and injected in a dose of 4 mg per 100 g of body weight intraperitoneally on days 0, 1, and 2. Labeled glycine was then injected into rats 2, 3, 4, 5, 7, or 11 days following the last injection of the phenylhydrazine. A complete early peak determination was made in the rats given labeled glycine 3 or 5 days following the last injection of phenylhydrazine (method 1). In all the rats given this drug, the early peak magnitude was also estimated by method 2.

Rats were bled one-third of their calculated blood volume, or 1.5% of their body weight (14) each day for three consecutive days, either by cardiac puncture or tail vein puncture, under light ether anesthesia. In an effort to avoid the production of lowered levels of serum iron as a direct result of the repeated bleeding, injections of iron dextran (Imferon, Lakeside Laboratories, Inc., Milwaukee, Wisconsin) were given subcutaneously on the day preceding each phlebotomy, for a total dose of 15-20 mg of elemental iron per rat. This is approximately twice the iron present in the entire circulating blood volume of rats of this size. Labeled glycine was then injected intravenously 1, 2, 3, 4, 7, or 11 days following the last bleeding, and the early and late peaks studied as outlined above.

Erythropoietin (sheep erythropoietin, Step I, 0.5 units/mg, Connaught Medical Research Laboratory, Toronto, Canada) was injected as a single dose of either 1 or 12 units dissolved in normal saline, via the intravenous route, to normal female LAF_1 mice. Labeled glycine was injected 50 hr after the injection of the crude erythropoietin solution.

Hypoxia was achieved in LAF_1 mice in an altitude chamber at an atmospheric pressure corresponding to an altitude of 18,000-19,000 ft above sea level. The air in the chamber was monitored for O_2 and CO_2 concentrations, which were found to be essentially the same as ordinary room air. The mice were pre-treated with injections of iron dextran to prevent emergence of iron-deficient RBC as a result of the increased erythropoietic rate, each mouse receiving 2 mg of elemental iron by subcutaneous injection 24 hr before being placed in the chamber. This is approximately 4 times the iron content of the circulating RBC of mice of this size. The mice were placed in the altitude chamber for 72 hr, following which time they were returned to normal atmospheric pressures and injected with 10 μCi of labeled glycine each, and then returned to the altitude chamber for an additional 72 hr. They were then returned to normal atmospheric pressures for the remainder of the experiment. Breath collection was begun 4 days after the injection of the labeled glycine, so that the early peak could be studied only by method 2 in these animals.

Animals used in this study were bred from specific pathogen-free breeder stock, and splenectomy of mice and rats in the animal colony of this laboratory has failed to induce anemia, reticulocytosis, or RBC inclusion bodies characteristic of bartonella-infected animals. Although it is difficult or impossible to rule out the presence of these organisms in our

animals, it appears that the animals used in these experiments do not have significant hemolysis resulting from infection with this organism.

RESULTS

I. HYPOXIA IN THE LAF_1 MOUSE Hematologic parameters for the hypoxic mice are shown in Table 1, and results of the determination of parameters of RBC survival are shown in Table 2. Although there was an unequivocal increase in hematocrit, hemoglobin concentration, reticulocyte count, and fractional incorporation of labeled glycine into RBC heme, it is apparent that there was no significant alteration of RBC survival in these hypoxic mice. Although the period of hypoxia following the injection of glycine did not allow for a complete early peak determination, the downslope of the early peak could be determined, and early peak fractionation performed by method 2 (Table 3). This component averaged 19% of total ^{14}CO production in the hypoxic mice, while the comparable figure for normal mice is 17%. Inspection of the ^{14}CO production curves in the 2 groups of hypoxic animals failed to disclose any evidence of a significant component of extremely short-lived RBC, thus ruling out the possibility of a double population of RBC or of a significant degree of ineffective erythropoiesis in these animals.

II. ERYTHROPOIETIN STIMULATION IN THE LAF_1 MOUSE Results for these experiments are shown in Tables 1-3. They indicate that although a single injection of 1 or 12 units of crude sheep ESF did not significantly alter hemoglobin concentration or hematocrit 5 days after injection, a significant increase in reticulocyte percentage and increased fractional glycine incorporation was achieved. Parameters of RBC survival (Table 2) were somewhat irregularly changed in these animals, but the only statistically significant change was a diminution of the mean potential lifespan in all three experimental groups ($p < 0.01$), although the greatest shortening noted was only 6% less than normal. Examination of total ^{14}CO production by method 1 showed a normal early peak fractionation in all experimental groups, without evidence for increased ineffective erythropoiesis or the production of a component of extremely short-lived RBC.

III. PHENYLHYDRAZINE-INDUCED ANEMIA IN THE RAT Results for these experiments are shown in Tables 1-3, and document a maximal anemia on day 4, maximal glycine incorporation on day 5, and a maximal reticulocytosis on day 6, following injection of this drug on days 0, 1, and 2. Red blood cell survival patterns show that the only statistically significant changes have occurred in the mean potential lifespan, with a maximum shortening to 65% of normal in the cohort of cells labeled 2 days after the last injection of phenylhydrazine. Thereafter, the mean potential lifespan returned towards normal values at approximately the same rate as the venous hematocrit returned towards normal. Eleven days after the last injection of phenylhydrazine, when the hematocrit had returned to normal, the reticulocyte percentage was still markedly elevated, fractional glycine incorporation was more than 3 times normal, while the mean potential lifespan was only 4% shorter than normal.

Total ^{14}CO fractionation, as measured by either method 1 or 2 showed that the ratio of the early peak to total ^{14}CO production was increased in the cohorts labeled 2 days after

Table 1. Hemoglobin concentration, hematocrit, and reticulocyte percentage in the study animals. For the hypoxic mice, HCT and HGB were obtained 10 days after the start of hypoxia, while reticulocyte concentration was studied 3 days after start of hypoxia. For the mice treated with erythropoietin, HGB, HCT, and reticulocyte percentages were determined 5 days after injection of ESF. Values for the bled and phenylhydrazine-treated rats were obtained on the day of injection of labeled glycine. Normal values are ± 1 S. D.

Group / Time of injection of labeled glycine	Reticulocytes (%)	Hematocrit (%)	Hemoglobin (g %)
Normal LAF_1 mouse	1.6	51.6 ± 2.0	16.8 ± 0.8
Hypoxic LAF_1 mouse	6.5	60	19.6
1 unit ESF, LAF_1 mouse	5.9	53	16.9
12 units ESF, LAF_1 mouse	10.1	53	17.2
Normal buffalo rat	1.7	46.7 ± 2.0	
2 (Days after last PHH injection)	45	25	
3	80	32	
4	83	37	
5*	41	41	
7	64	43	
11	20	48	
Normal buffalo rat	1.7	46.7 ± 2.0	
1 (Day(s) after last phlebotomy)	22	23	
2	46	28	
3	49	31	
4	46	37	
7	16	47	
11	9	47	

*This animal was studied and injected at a different time from all the other phenylhydrazine-treated rats.

the last injection of PHH, normal in the cohort formed 3 days after the last dose, and subnormal in subsequent cohorts, although none of the changes are statistically significant because of the great variability of this ratio in the normal rats. Detailed examination of the shape of the early peak disclosed an indistinct but constant alteration during the first 24 hr following injection of labeled glycine only in the animal injected with glycine 3 days after the last injection of PHH. The changes, which were not present in the study conducted 5 days after the last dose of PHH, consisted of a displacement of the time of maximum excretion of ^{14}CO from the normal 2-3 hr to about 6 hr (Fig. 1), with an indistinct secondary rise 9-14 hr after glycine injection (unpublished results). Other than these early peak alterations, there was no evidence for a significant population of RBC with an extremely short lifespan.

Table 2. Parameters of RBC survival in the study animals. Normal values are ± 1 S. D.

Group / Time of injection of labeled glycine	Mean potential lifespan (MPLS) (days)	Standard deviation of lifespans about MPLS (days)	Random hemolysis (%/day)	Incorporation of glycine into circulating RBC heme (%)
Normal LAF_1 mouse	53.1 ± 0.4	8.7 ± 1.2	0.84 ± 0.37	0.41 ± 0.17
Hypoxic LAF_1 mouse, group I	53.0	8.6	0.60	1.14
Hypoxic LAF_1 mouse, group II	52.1	8.9	0.62	1.16
1 unit ESF, LAF_1 mouse	51.4	12.3	0.67	0.87
12 units ESF, LAF_1 mouse, group I	49.8	8.4	0.77	1.03
12 units ESF, LAF_1 mouse, group II	50.7	7.5	1.04	1.16
Normal buffalo rat	65.7 ± 1.5	8.4 ± 1.3	0.60 ± 0.20	0.27 ± 0.02
2 (Days after last PHH injection)	42.4	10.6	0.14	1.87
3	50.5	8.5	0.31	2.35
4	54.7	6.8	0.25	2.33
5*	59.0	7.8	0.60	1.65
7	56.9	7.4	0.35	1.67
11	63.0	9.8	0.53	1.04
Normal buffalo rat	65.7 ± 1.5	8.4 ± 1.3	0.60 ± 0.20	0.27 ± 0.02
1 (Day(s) after last phlebotomy)	52.9	6.6	0.68	1.34
2	50.0	8.0	0.63	2.10
3	55.9	8.9	0.40	1.80
4	57.1	8.4	0.55	1.73
7	60.1	8.0	0.42	1.47
11	67.0	8.0	0.54	0.65

*This rat was studied and injected with phenylhydrazine at a different time from all the other rats in the group.

Results of the cross-transfusion experiments are shown in Table 4. Normal, labeled RBC survive normally in a normal rat host, with the exception of a shortening of the mean potential lifespan of about 5%. However, cells produced in a phenylhydrazine-treated rat had a markedly altered survival pattern when transfused into a normal host. The slight mean potential lifespan shortening is again seen, but there is also the presence of a marked increase in random hemolysis, the maximum observed rate being 60 times normal. In addition, hemolysis of the washed, labeled cells was noted *in vitro*, whereas this was not seen with the normal cells. In all, there were up to three components of random hemolysis in the cross-transfused phenylhydrazine-treated donor cells, instead of the usual one. Most of these cells were destroyed in the first 2 weeks following the cross-transfusion, but the cells remaining in the circulation were still subjected to increased rates of random destruction up to twice normal.

Table 3. Early peak fractionation in study animals. Values given are for the ratio of the early peak to total ^{14}CO production, as calculated either by method 1 or method 2 (see Materials and Methods). Normal values are ± 1 S. D.

Group / Time of injection of labeled glycine	Ratio: early peak to total ^{14}CO production	
	Method 1	Method 2
Normal LAF_1 mouse	0.27	0.17
Hypoxic LAF_1 mouse	--	0.19
1 unit ESF, LAF_1 mouse	0.24	--
12 units ESF, LAF_1 mouse	0.25	--
Normal buffalo rat	0.35 ± 0.10	0.29 ± 0.09
2 (Days after last PHH injection)	--	0.38
3	0.35	0.31
4	--	0.17
5	0.20	0.13
7	--	0.17
11	--	0.16
Normal buffalo rat	0.35 ± 0.10	0.29 ± 0.09
1 (Day(s) after last phlebotomy)	--	0.11
2	--	0.07
3	0.16	0.05
4	--	0.06
7	--	0.09
11	--	0.11

IV. BLOOD LOSS ANEMIA IN THE RAT Previous studies (15) have shown that pretreatment of bled rats with iron dextran prevents the production of low serum iron levels in these animals. In one of the animals studied in this series, the serum iron concentration on the day following the last of three daily phlebotomies, in a rat pretreated with iron dextran, was 267 micrograms percent (normal control: 168 micrograms percent).

Results of this study show a maximal anemia on day 3, maximal fractional glycine incorporation on day 4, and maximal reticulocytosis on day 5, when phlebotomy was performed on days 0, 1, and 2. Again, parameters of RBC survival were unchanged with the exception of statistically significant shortening of the mean potential lifespan, which was maximally shortened to 75% of normal in the cohort produced 2 days following the last phlebotomy (day 4). Thereafter the mean potential lifespan returned towards normal at a rate approximating the rate of return of the venous hematocrit towards normal. Eleven days after the last phlebotomy, at a time when the venous hematocrit had been normal for at least the preceding 4 days,

Table 4. Parameters of RBC survival in cross-transfusion experiments. Normal values given are ± 1 S. D.

Group	Mean potential lifespan (MPLS) (days)	Standard deviation about MPLS (days)	Random hemolysis (%/day)
Normal control animals	65.7 ± 1.5	8.4 ± 1.3	0.60 ± 0.20
Normal donor A cross-transfused into normal host I	63.2	9.4	0.58
Normal donor B cross-transfused into normal host II	62.1	8.3	0.44
Glycine injected 3 days after last of three consecutive daily doses of phenylhydrazine:			
Survival in original host	50.5	8.5	0.31
Survival of donor C cells after cross-transfusion into normal host III	46.3	6.0	1.35, 6.5, 35.0
Survival of donor C cells after cross-transfusion into normal host IV	46.6	6.1	0.97, 12.0*

*This animal was not studied until the 8th day after cross-transfusion, so that an earlier, third component of random hemolysis, if present, could not be detected.

the reticulocyte percentage was still elevated and the fractional glycine incorporation was twice normal, although RBC survival was entirely normal.

Fractionation of total ^{14}CO production by methods 1 and 2 showed that the early peak-total CO ratio was below normal in all the bled animals. There was no evidence of an alteration in the shape of the early peak (Fig. 1), and no evidence for a population of extremely short-lived RBC in any of the rats so treated.

DISCUSSION

The method used in this study for evaluating RBC survival in animals with stimulated erythropoiesis offers distinct advantages over techniques previously used. Subsequent to most forms of erythropoietic stimulation there is a significant change in total body RBC volume. Thus, when RBC survival is studied by measurement of circulating heme specific activity, independent measures must be made of total circulating RBC mass in order to correct for changes due to an expanding or contracting RBC mass. The ^{14}CO method yields results which are independent of these changes, since it measures only the catabolism of heme in the cohort of cells labeled following the injection of glycine-2-^{14}C. The necessity of repeated anesthesia and venesections, which may in themselves alter erythropoiesis, is avoided with the method used in this study. The cross-transfusion studies have shown *in vitro* and *in vivo* hemolysis of the cells formed shortly after the cessation of phenylhydrazine treatment.

Therefore, it is possible that techniques requiring blood sampling, handling, and washing of cells prior to determining heme specific activity may actually be destroying some of the more fragile labeled cells before they can be counted.

While the ^{14}CO method provides a means for estimating the fraction of labeled heme degradation associated with ineffective hemoglobin synthesis and non-hemoglobin heme turnover (early peak), as well as determination of the parameters of survival of circulating RBC, there are a number of inherent approximations and assumptions. Quantitative fractionation of the early peak into its two main components is not yet possible. Since the turnover of hemoglobin heme in the marrow and non-hemoglobin hemes in the rest of the body may be totally independent processes, and since it is only the ratio of the former process to the "late peak" that is of interest in this regard, a better understanding of ineffective erythropoiesis awaits the improved definition of this fractionation.

It has been demonstrated that, subsequent to the administration of labeled glycine, there is a prolonged presence of label in the glycine pool (16), due in large part to the re-entry of labeled glycine from catabolized, labeled protein. This phenomenon is not specifically corrected for in the present method. One of the consequences of this continued availability of label in the glycine pool is an overestimation of the mean potential lifespan. Such an overestimation is probably quite small, and cannot exceed 6%, as indicated from the cross-transfusion studies herein presented (Table 4). Additionally, in cross-transfusion experiments the labeled RBC are subjected to the stresses attendant to cross-transfusion, which may alone cause the shortening noted.

When the size and gross turnover rates of the glycine pool are constant, the relative fraction of labeled glycine incorporated into circulating RBC heme is a good measure of the relative increase in effective hemoglobin synthesis. In the present experiments, some of the erythropoietic stimuli might be associated with an overall increase in the net turnover rate of the glycine pool. Under these circumstances, the relative fractional glycine incorporation underestimates the increase in hemoglobin synthesis. One can thus conclude that the relative increase in effective hemoglobin synthesis is either equal to or greater than the relative fractional glycine incorporation into circulating RBC heme.

Exposure of female LAF_1 mice to 6 days at a simulated altitude of 18,000 ft, or injection of a single dose of 1 or 12 units of crude sheep erythropoietin increased RBC production, as evidenced by increases in reticulocyte count and fractional glycine incorporation, with the maximum glycine incorporation being slightly less than 3 times normal. In the hypoxic mice, parameters of RBC survival were entirely normal. There was a minimal, but statistically significant, decrease in the mean potential lifespan in the mice treated with the crude sheep erythropoietin, with greater shortening found at the higher dosage level. There was no consistent evidence of increased ineffective erythropoiesis, or early RBC death in the mouse experiments.

Three daily injections of phenylhydrazine (PHH) or three daily phlebotomies in the buffalo

rat produced almost identical changes in the venous hematocrit, but marked differences in reticulocyte percentage and fractional glycine incorporation. Examination of the results shown in Tables 1 and 2 reveals that rats treated with either PHH or phlebotomy, with either comparable hematocrits or reticulocyte percentage, do not show comparable alterations in the mean potential lifespan, the only parameter showing statistically significant alterations. It is only when the fractional incorporation of glycine is comparable that the mean potential lifespan shortening is also comparable. Figure 2 shows that there is nearly a linear increase in the degree of shortening of the mean potential lifespan with increased fractional glycine incorporation in the range from 2-8 times normal. The same figure shows that increases in glycine incorporation of less than 3 times normal are associated with minimal or no changes in mean potential lifespan, results that are in agreement with some of the previously published studies (7, 8, 9). The points on the graph which show the linear relation least well are from animals in which the fractional glycine incorporation was still submaximal (1 and 2 days after the last of 3 phlebotomies, and 2 days after last injection of PHH), suggesting that the earliest cells produced following these stresses are more abnormal than those cells produced subsequently. This finding is in general agreement with recent theories of response to such stimuli, which state that the initial response to intense erythroid stimuli may be achieved without an increase in marrow cellular components (17), by decreasing intramedullary maturation time and skipping terminal divisions (18, 19), while maximal responses are obtained by increasing total marrow cellularity, which allows for increased RBC production without producing the markedly abnormal cells seen initially.

Examination of the shape of the early peak in all the experimental animals revealed no significant alterations from normal with the exception of the animals studied less than 4 days after the last of 3 daily injections of phenylhydrazine. The qualitative and quantitative changes in the latter instance indicate a moderate increase in ineffective erythropoiesis, which occurred along with fractional glycine incorporation approximately 6 times normal. Since these changes were not seen in a bled animal with a similar fractional glycine incorporation, this is most probably due to a direct toxic effect of the drug on developing erythroid cells. In all other instances, early peak:total CO fractionation was either normal or subnormal, suggesting that erythropoiesis becomes <u>more</u> effective as erythropoietic rate increases above normal. However, as noted earlier, until the early peak can be accurately described in terms of its two general components, this fractionation will have only grossly qualitative significance in the study of ineffective erythropoiesis.

The cross-transfusion experiments document that the changes herein described are due to an intrinsic defect in the RBC (Table 4), but also point out the fact that the cells produced in a PHH-treated rat do not survive normally following the cross-transfusion procedure, more than one-third of the transfused cells being destroyed by random processes before the third week after labeling. Similar results have recently been presented by Robinson (20), who found that of normal cross-transfused labeled RBC, 1.6% of the labeled heme was converted into bile pigment in three days, while in cross-transfused labeled cells produced following phlebotomy, 7.6% was converted to bile pigment in the same time period. These results are fully compatible with the observation that newly formed RBC are markedly fragile <u>in vitro</u>, although the

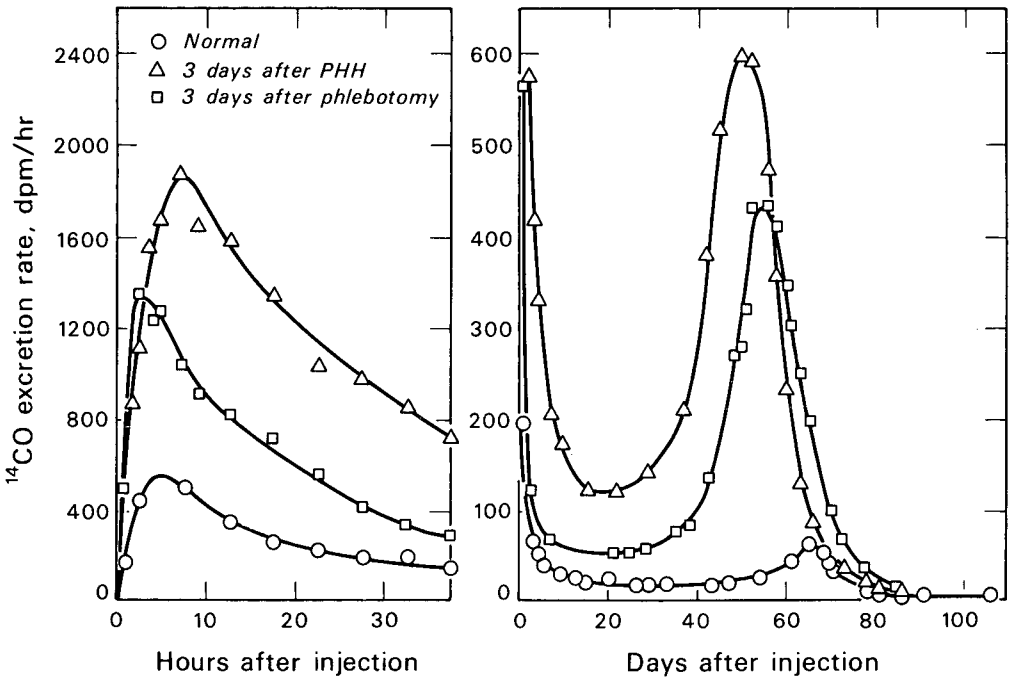

Fig. 1. ^{14}CO production in a normal rat, a phlebotomized rat, and a phenylhydrazine-treated rat. Note the difference in the ordinate and abscissa scales for the time periods 0-35 hr and 1-100 days following injection of labeled glycine. Labeled CO excretion rates are expressed in DPM of ^{14}CO per hour. DBL 682-4568

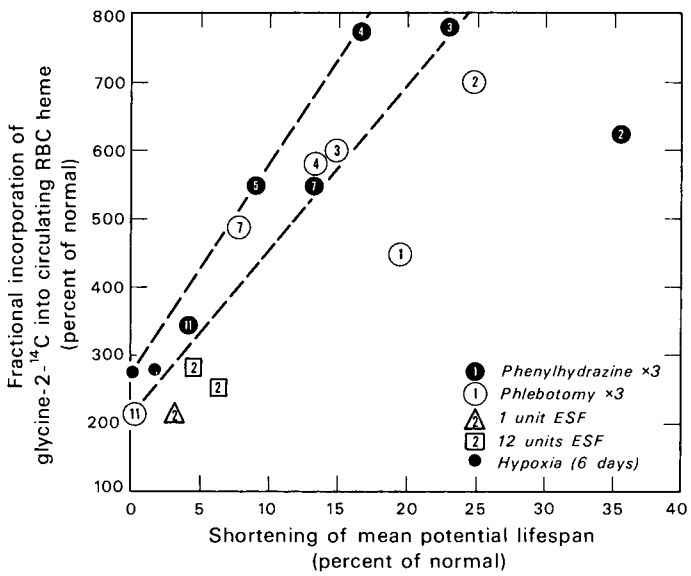

Fig. 2. Graph showing the relationship between shortening of the mean potential lifespan (in percent) and the increase in fractional incorporation of glycine into circulating RBC heme (as percent of normal) for all the experimental animals. Numbers inside the symbols indicate the length of time in days between the last injection of phenylhydrazine or the last phlebotomy and the injection of the labeled glycine. Note that those experimental points falling outside of the area enclosed by the dashed lines all involve intervals between the time of last treatment and injection of labeled glycine of 2 days or less.

DBL 682-4569

in vivo studies did not show increased rate of random destruction, suggesting an artifactual nature of the observations in the cross-transfused animals.

The maintenance of a finite, but minimally shortened (less than 35%) mean potential lifespan, without concomitant evidence of ineffective erythropoiesis (except as noted in one animal), production of a double population of cells, or increased random hemolysis speaks for functional normalcy of these cells. That they maintain their normally distributed survival about a shorter mean lifespan suggests that they have simply aged faster than normal. Whether this increased aging is due to a decreased amount of a critical material initially given to the cell, or to an increased rate of degradation of a critical component is not known.

Recent work by Marks (21) has shown that non-hemoglobin protein formation in the fetal mouse erythron is directly under the control of messenger RNA, since it can be almost completely suppressed with actinomysin. However, actinomysin does not depress hemoglobin formation in the same cells. Thus, when the nucleus is extruded from the cell, it is possible that non-hemoglobin protein synthesis stops abruptly, while hemoglobin synthesis continues. Since the enzymes of the pentose-phosphate shunt and Embden-Myerhof pathways are included in this former group, and are of critical importance in maintaining normal survival (22), any shortening of intramedullary time will most likely decrease the time over which these enzymes can be manufactured, leading to decreased levels in the emerging RBC. Under these circumstances, one might expect the emerging cell to reach a critically low content of these materials sooner than normal, resulting in a decreased mean potential lifespan.

SUMMARY

Red blood cell survival was studied in LAF_1 mice and Buffalo rats following hypoxia, erythropoietin injection, repeated phlebotomy, or phenylhydrazine-induced anemia, using a technique based upon the endogenous production of ^{14}CO in the breath following the injection of glycine-2-^{14}C. Despite estimated hemoglobin synthesis rates 8 or more times normal, in no instances were there any increases in the rate of random destruction of the produced RBC, nor was there the production of a component of extremely short-lived cells. Ineffective hemoglobin synthesis appeared to be either normal or decreased, with the exception of rats studied shortly after injection of phenylhydrazine, suggesting a toxic effect of the drug in this time period. A modest but significant shortening of the mean potential lifespan (senescent destruction) was seen, which increased linearly with increasing hemoglobin synthesis rate. This shortening never exceeded 35% and no shortening of any significant degree was seen unless estimated hemoglobin synthesis rates were more than 2-3 times normal. The minimal alterations in RBC survival noted in these experiments despite marked erythropoietic stimulation lead one to conclude that these cells are remarkably normal.

ACKNOWLEDGMENTS

The author is indebted to Miss Sandra Stoddard for her invaluable technical assistance, and to Drs. H. Saul Winchell and Donald C. Van Dyke for their helpful suggestions during all phases of this study. This work was supported in part by a Special Fellowship from the

National Heart Institute, and also by the U. S. Atomic Energy Commission, and the National Aeronautics and Space Administration under contract W-7405-eng-48.

REFERENCES

1. Neuberger, A., and Niven, J. S. F.; Haemoglobin formation in rabbits. J. Physiol. 112: 292, 1951.
2. Berlin, N. I., and Lotz, C.; Lifespan of the red blood cell of the rat following acute hemorrhage. Proc. Soc. Exptl. Biol. Med. 78: 788, 1951.
3. Harriss, E. B., and Belcher, E. H.; Radioisotope techniques in the study of red cell lifespan in experimental animals; in IXth International Congress of Radiology, Vol. II, edited by B. Rajewsky, Stuttgart, Georg Thieme Verlag, 1959, p. 905.
4. Stohlman, F.; Humoral regulation of erythropoiesis VII. Shortened survival of erythrocytes produced by erythropoietine or severe anemia. Proc. Soc. Exptl. Biol. Med. 107: 884, 1961.
5. Cline, M. J., and Berlin, N. I.; Red blood cell lifespan using DFP^{32} as a cohort label. Blood 19: 715, 1962.
6. Stohlman, F.; Brecher, G., and Moores, R. R.; Humoral regulation of erythropoiesis VIII. The kinetics of red cell production and the effect of erythropoietin; in Erythropoiesis, edited by L. O. Jacobson and M. Doyle, New York, Grune and Stratton, 1962, p. 162.
7. Van Dyke, D. C., and Berlin, N. I.; Production of normal-lived erythrocytes with erythropoietin. Proc. Soc. Exptl. Biol. Med. 104: 573, 1960.
8. Pollycove, M.; Winchell, H. S., and Lawrence, J. H.; Classification and evolution of patterns of erythropoiesis in polycythemia vera as studied by iron kinetics. Blood 28: 807-829, 1966.
9. Robinson, S. H.; Tsong, M.; Brown, B. W., and Schmid, R.; The sources of bile pigment in the rat: studies of the "early labeled" fraction. J. Clin. Invest. 45: 1578, 1966 (Fig. 7).
10. Landaw, S. A.; Studies of RBC lifespan distribution using endogenous ^{14}CO production; in Semiannual Report, Donner Laboratory, Lawrence Radiation Laboratory Report UCRL-17481, Spring 1967, p. 43.
11. Landaw, S. A., and Winchell, H. S.; Endogenous production of carbon-14 labeled carbon monoxide: an in vivo technique for the study of heme catabolism. J. Nucl. Med. 7: 696, 1966.
12. White, P.; Coburn, R. F.; Williams, W. J.; Goldwein, M. I.; Rother, M. L., and Shafer, B. C.; Carbon monoxide production associated with ineffective erythropoiesis. J. Clin. Invest. 46: 1986, 1967.
13. Eadie, G. S., and Brown, I. W.; Red blood cell survival studies. Blood 8: 1110, 1953.
14. Berlin, N. I.; Huff, R. L.; Van Dyke, D. C., and Hennessy, T. G.; The blood volume of the adult rat, as determined by Fe^{59} and P^{32} labeled red cells. Proc. Soc. Expt. Biol. Med. 71: 176, 1949.
15. Parker, H., and Van Dyke, D. C.; unpublished results.
16. Berlin, N. I.; Hewitt, C., and Lotz, C.; Hippuric acid synthesis in man after the administration of (α-^{14}C) glycine. Biochem. J. 58: 498, 1954.

17. Van Dyke, D. C.; Anger, H. O., and Pollycove, M.; The effect of erythropoietic stimulation on marrow distribution in man, rabbit, and rat as shown by Fe^{59} and Fe^{52}. Blood 24: 356, 1964.
18. Stohlman, F.; Some aspects of erythropoiesis. Seminars in Hematology 4: 304, 1967.
19. Hillman, R. S., and Finch, C. A.; Erythropoiesis: normal and abnormal. Seminars in Hematology 4: 327, 1967.
20. Robinson, S. H.; Reticulocyte death: a source of early labeled bile pigment. J. Clin. Invest. 46: 1109, 1967.
21. Marks, P. A.; J. Mol. Biol., in press.
22. Carson, P. E., and Frischer, H.; Glucose-6-phosphate dehydrogenase deficiency and related disorders of the pentose phosphate pathway. Am. J. Med. 41: 744, 1966.

Studies on the Behavior of Erythropoietin-Sensitive Cells in the Mouse During Recovery from 200 R Whole-Body Irradiation

John C. Schooley, Judith M. Hayes, Linda N. Cantor and Virginia W. Havens

INTRODUCTION

Studies on the temporal restoration of the functional integrity of the hematopoietic system after mild irradiation have provided some insight into the kinetics of proliferation of the most primitive precursor cells of the hematopoietic tissue. One valuable means of quantitating changes in the functional state of erythroid precursors after sublethal irradiation is the measurement of the responsiveness of the polycythemic mouse to a standard amount of erythropoietin. The essential pattern of the recovery by irradiated polycythemic mice of the ability to respond to erythropoietin has been established by several investigators (1, 2, 3). It is characterized by a marked depression in responsiveness immediately after irradiation, followed by a return to normal or above-normal responsiveness by about 10 days after irradiation. The magnitude of the depression and the extent of recovery apparently depend not only on the dose of irradiation but on the challenging dose of erythropoietin used. These findings have been discussed recently by Lajtha (4).

Gurney (5) has discussed some of the limitations of the method of measuring responsiveness of the polycythemic mouse to erythropoietin, and has emphasized the importance of the fact that erythropoietin has a biological half-life, and that an effective concentration of erythropoietin must exist. Thus, it is likely that the test dose of erythropoietin does not act instantaneously, but rather during an appreciable portion of the entire test period of 5 days, while conditions within the hematopoietic tissue are changing both as a result of recovery from irradiation and as a result of the initial action of erythropoietin upon sensitive cells. Some aspects of these problems have been previously studied in the unirradiated polycythemic mouse (6), using antibody against erythropoietin as a means of limiting the duration of action of erythropoietin in the test system.

In the present experiments the response of the mildly irradiated polycythemic mouse to a 6-hr exposure to erythropoietin was measured 10 days after irradiation. In addition, the responsiveness of these mice to fractionated doses of erythropoietin was determined.

MATERIALS AND METHODS

Female C_3H Cum mice weighing about 20 g and 6-8 weeks of age were made polycythemic by the intraperitoneal injection of isologous red blood cells. The red cells were washed three

times with saline before injection and the buffy coat removed after each washing. Each mouse was injected with 1 ml of packed red blood cells on 2 successive days, and was retransfused at weekly intervals by intravenous injections of 1 ml of packed red blood cells in order to maintain the polycythemic state during the course of the experiment. Mice having hematocrits less than 55% at the time of sacrifice were not included in the experiments.

Polycythemic mice were irradiated with 200 R ^{60}CO γ rays, 5 days after the 2nd intraperitoneal injection of red blood cells. The mice were irradiated 1.22 meters from a ^{60}CO source with a dose rate in air of 15.5 R/min, measured with a Victoreen condenser R-meter. Under these conditions the average tissue dose in the mouse was approximately 0.94 rad/R in air.

Step I sheep plasma erythropoietin (obtained from Connaught Medical Research Laboratories, Toronto, Canada) had a potency of 0.5 I. R. P. (International Reference Preparation) units/mg dry weight (1.0 I. R. P. is approximately 1.0 cobalt unit). The appropriate dose of erythropoietin (ESF) was dissolved in 0.5 ml saline. All injections were made intravenously. Fifty-six hours after the first erythropoietin injection, 0.5 μCi of ^{59}Fe as iron citrate (specific activity approximately 10 μCi/μg) was injected intravenously, and 72 hr later a blood sample was taken by cardiac puncture. In all experiments the intervals between the first injection of erythropoietin, the injection of ^{59}Fe, and the time of sacrifice remained constant. In some experiments anti-erythropoietin immune serum was injected intravenously 6 hr after the injection of erythropoietin. Simultaneous injection of erythropoietin and immune serum did not stimulate erythropoiesis. In other experiments a second dose of erythropoietin was injected into groups of irradiated or unirradiated mice at various intervals after the first injection. The radioactivity present in a 0.5 ml sample of blood was measured at the time of sacrifice, and the percent of the injected ^{59}Fe incorporated into total blood volume was calculated. It was assumed that the blood volume of the polycythemic mice was 7% of the total body weight. There were 6 to 10 mice per group in each experiment. The standard error of the mean was calculated for each value.

Immune serum capable of neutralizing the biological activity of sheep plasma erythropoietin was obtained from rabbits immunized with human urinary erythropoietin. The schedule of immunizations, and the characteristics of the immune serum have been described previously (7).

RESULTS

The effect of limiting the duration of action of 0.5 unit of erythropoietin to 6 hr in the unirradiated and the irradiated polycythemic mouse is shown in Fig. 1. It was assumed that injection of the antibody neutralized the biological activity of all the erythropoietin that had not acted during the 6-hr period. The polycythemic mice were tested 9, 10, 11, and 12 days after 200 R irradiation. For comparison, the responsiveness of similar groups of mice receiving the same dose of erythropoietin but no antibody is also indicated. It is evident that 3 or 4 times as many cells are available during a 6-hr period to be stimulated by erythropoietin in the irradiated mice at these times after irradiation as in unirradiated mice, and that one-third

to one-half of the total response to erythropoietin takes place during this 6-hr period in the irradiated mice. The responsiveness of the irradiated mice to the unlimited action of erythropoietin is slightly higher at these times after irradiation than that of unirradiated polycythemic mice.

Figure 2 shows the effect of varying the interval between the successive injections of two identical doses of 0.5 unit of erythropoietin on the erythropoietic response of unirradiated and irradiated polycythemic mice 10 days after irradiation. The 72-hr ^{59}Fe uptakes are plotted as a function of the interval between the first and second erythropoietin injections. In unirradiated polycythemic mice an ^{59}Fe uptake of $8.7 \pm 0.51\%$ was observed after the injection of one unit of erythropoietin, and the values obtained after fractionating the same total dose of erythropoietin in unirradiated polycythemic mice were calculated relative to this value. Similarly in irradiated polycythemic mice an ^{59}Fe uptake of $14.4 \pm 1.4\%$ was observed after the injection of one unit of erythropoietin and the values obtained after fractionating the dose of erythropoietin in these mice were calculated relative to this value. The erythropoietic response of unirradiated and irradiated mice to one unit of erythropoietin is significantly different ($P < 0.001$).

In both irradiated and unirradiated mice, fractionating the dose of erythropoietin stimulated erythropoiesis, as measured by ^{59}Fe uptakes, to a greater extent than the response observed when the same total dose of erythropoietin was given at one time. However, in the irradiated groups of mice the relative erythropoietic stimulation was much less than in the unirradiated groups of mice, particularly when the interval between the first and second dose of erythropoietin was greater than 20 hr. For example, when the interval between the two doses was 24 hr, the relative response in the unirradiated polycythemic mice was more than 3 times that observed when the dose was not fractionated in unirradiated mice, but the relative response in the irradiated polycythemic mice at 24 hr was only about 1.5 times that observed in irradiated mice when the dose was not fractionated. The data in Fig. 2 have been plotted in relative terms to emphasize the fact that the irradiated polycythemic mouse does not respond to a second dose of erythropoietin 24 hr after the first, to the same degree as the unirradiated polycythemic mouse. It should be emphasized that after 24 hr it is the erythropoietic response relative to the unfractionated dose of erythropoietin that varies, not the actual response.

The erythropoietic response of unirradiated polycythemic mice to the intravenous injection of 12 units of erythropoietin was $41.1 \pm 2.6\%$, whereas 10 days after irradiation polycythemic mice had an ^{59}Fe uptake of $30.4 \pm 1.8\%$ after receiving the same dose of erythropoietin. This difference is significant ($P < 0.005$). Thus, as summarized in Table 1, when a large dose of erythropoietin was injected, the erythropoietic response of the irradiated mouse was significantly less than the unirradiated mouse. But, in contrast, when a small dose of erythropoietin was injected the opposite occurred, and the erythropoietic response of the irradiated mouse was greater than in the unirradiated mouse.

DISCUSSION

It has generally been assumed that erythropoietin acts directly on a self-maintaining

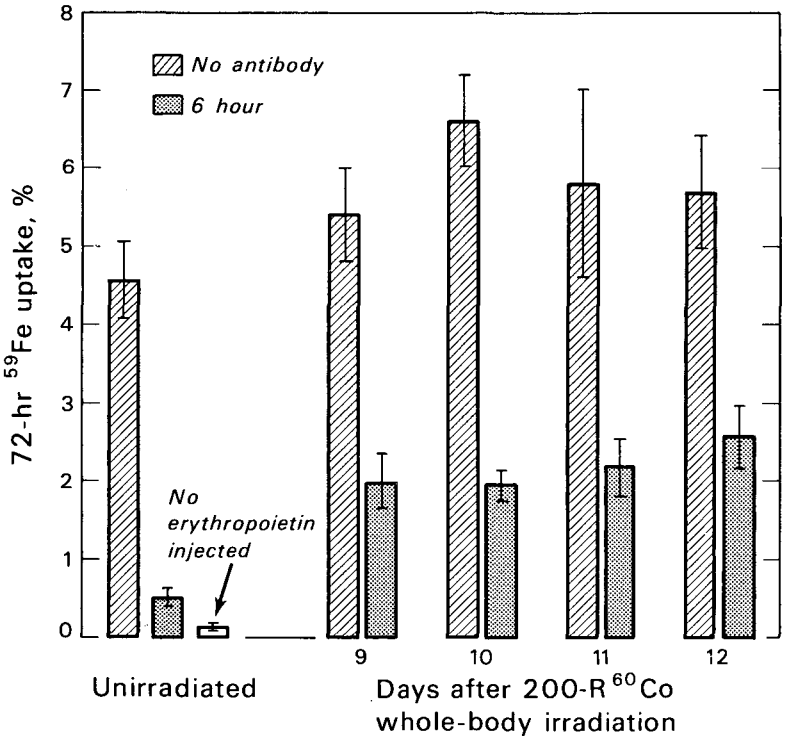

Fig. 1. Effect of limiting the duration of action of 0.5 unit of erythropoietin to 6 hr by the injection of anti-erythropoietin immune serum in the unirradiated and irradiated polycythemic mice on the 72-hr ^{59}Fe uptake. The 72-hr ^{59}Fe uptakes in similar groups of mice receiving no immune serum are given for comparison.
DBL 682-4570

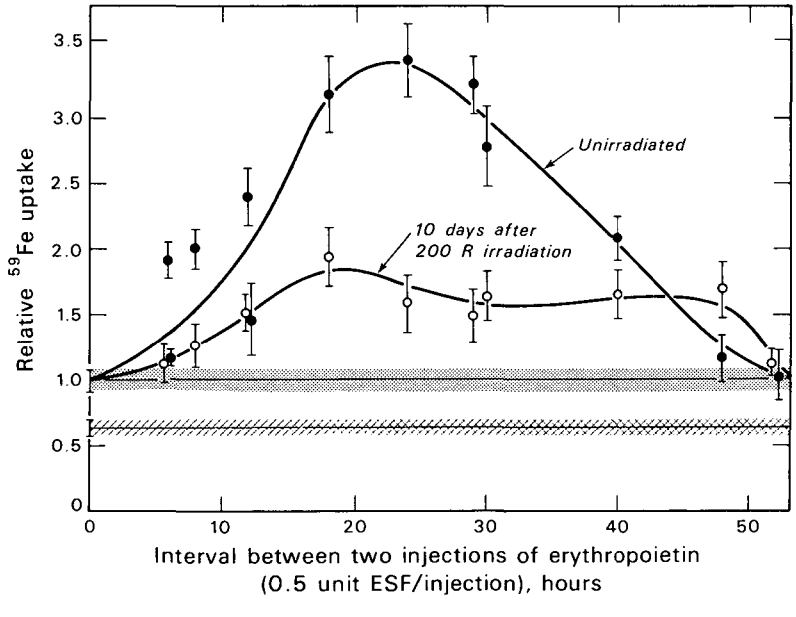

Fig. 2. Effect of fractionating the dose of erythropoietin on the relative ^{59}Fe uptake of unirradiated and irradiated polycythemic mice. Unit response is defined as that observed following a single intravenous injection of 1.0 unit of erythropoietin. Each curve is plotted relative to its own unit response. The values are plotted as a function of the interval between the first and second erythropoietin injections. The lower hatched line shows the response to 0.5 unit of erythropoietin.
DBL 682-4571

Table 1. 72-hr ^{59}Fe uptake.

	1.0 I. R. P. unit of erythropoietin	12 I. R. P. units of erythropoietin
Unirradiated	8.7 ± 0.5%	41.1 ± 2.6%
10 days after 200 R irradiation	14.4 ± 1.4%	30.4 ± 1.8%

population of primitive hematopoietic stem cells, but this assumption has been challenged by some recent observations. Till and McCulloch (8) have demonstrated the presence of cells in hematopoietic tissue which, upon injection into lethally irradiated hosts, settle down in the spleen, proliferate, and give rise to discrete nodules on its surface. These nodules often contain mature cells characteristic of the erythroid, granulocytic, and megakaryocytic series. Becker et al. (9) have presented evidence indicating that these nodules are derived from a single cell. Bruce and McCulloch (10) and Schooley (11) concluded that some descendant of the spleen colony-forming cell, rather than the colony-forming cell itself, was sensitive to erythropoietin stimulation. Some evidence was also presented (11) suggesting that the progeny of the colony-forming cell, which responds to erythropoietin, is unipotential, i.e., it can only be stimulated to become erythroid cells. Morse and Stohlman (12) studied the effect of vincristine on megakaryocytopoiesis and erythropoiesis, and also concluded that a compartment of cells existed between the most primitive precursor of the hematopoietic system and the populations of differentiated hemopoietic cells. The present results then will be discussed in terms of a model of hematopoiesis that postulates a population of cells derived from a primitive precursor (probably the spleen colony-forming cell), and sensitive to erythropoietin, which upon stimulation gives rise to differentiated erythroid cells. Erythropoietin is thus not assumed to act directly upon the "stem cell."

The present results indicate that 10 days after whole-body irradiation the hematopoietic system of the polycythemic mouse contains 3 or 4 times as many erythropoietin-sensitive cells available during a 6-hr period for differentiation into erythroid cells by erythropoietin as found in unirradiated polycythemic mice. Alexanian et al. (3) found that erythropoietic responsiveness was much less depressed after the second of two irradiations 12-14 days apart than after a single irradiation. They concluded that not only were the available erythropoietin-sensitive cells increased at this time, but that a twofold increase in actual "stem cell" numbers had occurred. In terms of the present model, a twofold increase in erythropoietin-sensitive cells rather than "stem cells" would be assumed. The pattern of recovery of the response of irradiated mice to fractionated doses of erythropoietin suggests to us that although the pool of available and potentially available erythropoietin-sensitive cells is significantly increased, the total numbers of primitive precursors or "stem cells" are not increased. It has been suggested previously (6) that following the initial exposure of a polycythemic mouse to erythropoietin the actually available erythropoietin-sensitive cells are immediately triggered to differentiate into erythroid cells, while a recruitment of cells into a state receptive to erythropoietin occurs. In terms of the present model this recruitment would be envisaged

as a result of 1) the division of "stem cells" and their subsequent movement into the erythropoietin-sensitive cell pool, and 2) the movement of the potentially available portion of the erythropoietin-sensitive cell pool into a state actually receptive to the action of erythropoietin. We suggest that 10 days after irradiation the first injection of erythropoietin uses the available erythropoietin-sensitive cells, and that more available erythropoietin-sensitive cells are recruited from the total erythropoietin-sensitive cell pool, so that a second dose of erythropoietin acts on these recruited cells. The total erythropoietin-sensitive cell pool (actually and potentially available) must be derived eventually from a more primitive precursor population, and we suggest that this precursor population is still depressed in the irradiated mouse at the 10th day after irradiation. The depression of this pool then limits the ability of the irradiated mouse to respond to fractionated doses of erythropoietin.

The finding that injections of large doses of erythropoietin (12 units) stimulate erythropoiesis significantly more in unirradiated mice, whereas small doses (1 unit) actually do the reverse and stimulate erythropoiesis more in the irradiated mouse is consistent with the above interpretation of the effect of fractionated doses of erythropoietin. The large dose of erythropoietin is undoubtedly present in effective levels in the mouse for most of the test period. In the irradiated and unirradiated polycythemic mouse the available erythropoietin-sensitive cells are immediately triggered to differentiate, and more erythropoietin-sensitive cells are recruited from both the potentially available erythropoietin-sensitive cell pool and its precursor population, the stem cell. The unirradiated mouse can continually derive erythropoietin-sensitive cells from the precursor pool, but the irradiated mouse has a diminished precursor pool and can only slowly repopulate the erythropoietin-sensitive cell pool once the cells have actually been triggered to differentiate. Small doses of erythropoietin stimulate erythropoiesis more in the irradiated mouse because the pool of available erythropoietin-sensitive cells is larger, and recruitment from the precursor pool is not required before the erythropoietin has disappeared.

The spleen colony-forming cell is probably the immediate precursor of the erythropoietin-sensitive cell. The total number of colony-forming cells that can be demonstrated in the spleen and bone marrow of the 200R irradiated mouse is markedly depressed immediately after irradiation and remains depressed for 13 to 15 days (13, 14). Increased responsiveness to erythropoietin precedes by almost a week any measurable increase in transplantable colony-forming cells in the spleen and bone marrow of polycythemic mice. This suggests again two populations of cells, and suggests that at this dose of irradiation the repopulation of erythropoietin-sensitive cells has priority over the restoration of colony-forming cells. Porteous and Lajtha (15) have also found that recovery of colony-forming cells did not occur before the 10th day when measured by grafting techniques; however, using a bone marrow shielding technique, they concluded it was not necessary to postulate two kinds of stem cells. It should be emphasized that other experiments previously cited favor the concept of several precursor populations from which the differentiated hematopoietic cells are derived.

The conclusions arrived at in this paper are necessarily speculative. If a separate population of erythropoietin-sensitive cells exists and it is assumed to be unipotential, other

similar populations of cells which are the more immediate precursors of granulocytic and megakaryocytic cells must also exist in the bone marrow. The various feedback mechanisms which regulate the movement of the primitive precursor into these intermediate populations, as well as the extent of division within the various intermediate populations, remain unsolved problems. Some preliminary observations suggest that hypoxia or something, other than erythropoietin, produced as a result of hypoxia may regulate the movement of the precursor cell into the erythropoietin-sensitive cell population (14).

SUMMARY

Ten days after 200 R ^{60}CO whole-body irradiation the hematopoietic system of the polycythemic mouse contains 3 to 4 times as many cells available during a 6-hr period for stimulation by erythropoietin into erythroid cells as does the unirradiated mouse. The irradiated polycythemic mouse does not, however, respond to fractionated doses of erythropoietin as does the unirradiated polycythemic mouse. Paradoxically, the irradiated mouse exhibits a greater response to a small dose of erythropoietin than an unirradiated mouse, although it shows a lower response to a large dose of erythropoietin. These results are discussed relative to a model of hemopoiesis which assumes that a population of cells derived from the "stem cell" rather than the "stem cell" itself is sensitive to the differentiative action of erythropoietin.

ACKNOWLEDGMENTS

This work was supported in part by the U. S. Atomic Energy Commission and in part by Cancer Research Funds of the University of California.

REFERENCES AND NOTE

1. Gurney, C. W., and Wackman, N.; Impairment of erythropoiesis by irradiation. Nature 190: 1017-1018, 1961.
2. Gurney, C. W.; Lajtha, L. G., and Oliver, R.; A method for investigation of stem-cell kinetics. Brit. J. Haemat. 8: 461-466, 1962.
3. Alexanian, R.; Porteous, D. D., and Lajtha, L. G.; Stem-cell kinetics after irradiation. Int. J. Rad. Biol. 7: 87-94, 1963.
4. Lajtha, L. G.; Response of bone marrow stem cells to ionizing radiations; in Current Topics in Radiation Research, Vol. I., edited by M. Ebert and A. Howard, Amsterdam, North-Holland Publishing Co., 1965, pp. 141-163.
5. Gurney, C. W.; Effect of radiation on the mouse stem cell compartment in vivo. Perspectives Biol. Med. 6: 233-245, 1963.
6. Schooley, J. C.; Responsiveness of hematopoietic tissue to erythropoietin in relation to the time of administration and duration of action of the hormone. Blood 25: 795-808, 1965.
7. Schooley, J. C., and Garcia, J. F.; Some properties of serum obtained from rabbits immunized with human urinary erythropoietin. Blood 25: 204-217, 1965.
8. Till, J. E., and McCulloch, E. A.; A direct measurement of the radiation sensitivity of normal mouse bone marrow cells. Radiation Res. 14: 213-222, 1961.
9. Becker, A. J.; McCulloch, E. A., and Till, J. E.; Cytological demonstration of the clonal nature of spleen colonies derived from transplanted mouse marrow cells. Nature 197: 452-454, 1963.

10. Bruce, W. R., and McCulloch, E. A.; The effect of erythropoietic stimulation on the hemopoietic colony-forming cells of mice. Blood 23: 216-232, 1964.

11. Schooley, J. C., The effect of erythropoietin on the growth and development of spleen colony-forming cells. J. Cell Physiol. 68: 249-262, 1966.

12. Morse, B. S., and Stohlman, F., Jr.; Regulation of erythropoiesis. XVIII. The effect of vincristine and erythropoietin on bone marrow. J. Clin. Invest. 45: 1241-1250, 1966.

13. Schooley, J. C.; Cantor, L. N., and Havens, V. W.; Relationship between growth of colony-forming cells and erythropoietin-sensitive cells in mice irradiated with 200 R of ^{60}Co gamma rays. Exp. Hemat. 9: 55-56, 1966.

14. Schooley, J. C.; Garcia, J. F.; Cantor, L. N., and Havens, V. W.; A summary of some studies on erythropoiesis using anti-erythropoietin immune serum. Ann. N. Y. Acad. Sci., in press.

15. Porteous, D. D., and Lajtha, L. G.; On stem-cell recovery after irradiation. Brit. J. Haemat. 12: 177-188, 1966.

This paper has been published in Radiation Research (32: 875-883, 1967).

Erythropoietin-Enhancing Factor in Serum of a Calf with Primary Familial Polycythemia

Donald C. Van Dyke, Mary L. Nohr and Bud C. Tennant

Primary familial polycythemia occurs occasionally in calves of an inbred Jersey herd maintained at the University of California, Davis. The genetic pattern of this disease suggests a simple autosomal recessive mode of inheritance (1). In the course of investigation of the etiology of this disease, it was discovered that serum from the one currently surviving calf with polycythemia, although itself devoid of measurable erythropoietic activity, when incubated with erythropoietin resulted in a 4-fold enhancement of activity. Incubation with normal calf serum did not enhance the activity of erythropoietin in the assay system employed in these studies.

Gardner et al. (2) have reported enhancement of purified erythropoietin by serum from normal human beings, normal rabbits, and normal mice. Although in these studies serum from normal calves consistently failed to enhance erythropoietin activity, incubation of erythropoietin with sera from other species, dog, monkey, and man, was found to increase erythropoietin activity 1.5- to 2.3-fold.

Serum was obtained from the 6-month-old female calf with familial primary polycythemia and from 4 normal Jersey female calves of the same age in the herd. All sera were frozen immediately after separation and stored thus until use. Hematocrit of the polycythemic calf was 65%; hemoglobin was 21 g/100 ml. Hematocrit of the normal calves was 31, 34, 39.5, and 39%; hemoglobin was 11.7 and 10.8 g/100 ml (calves C and D not measured).

Assays for erythropoietic activity were done in hypertransfused female mice of the Balb/c strain, according to the method of DeGowin et al. (3). Erythropoietin was obtained from the urine of a patient with aplastic anemia (4) and concentrated by collodion adsorption (5). This erythropoietin was standardized by comparison with the International Reference Preparation (6), using either saline or serum as diluent.

All sera were incubated with erythropoietin for 2 days in the cold (8°C). Erythropoietin alone and serum alone were incubated under the same conditions.

Table 1 shows the enhancement of erythropoietin after incubation with various amounts of polycythemic calf serum. Serum obtained before 8-1/2 months of age produced a consistent and significant enhancement of activity of erythropoietin even with as little as 0.1 ml of polycythemic calf serum. No enhancement of activity occurred from incubation with serum from

Table 1. Erythropoietin-enhancing factor in serum of a polycythemic calf.

Group (no. of mice)	Activity (× ESF control)	Significance of difference*
Polycythemic calf		
1 ml serum + ESF (6)	4.0	0.001
0.5 ml serum + ESF (10)	3.0	0.001
0.1 ml serum + ESF (10)	2.4	0.001
1 ml serum & ESF at 2 sites (7)	1.8	0.1
Normal calves: 1 ml serum + ESF		
Calf A (6)	0.7	0.02
Calf B (9)	0.7	0.001
Calf C (8)	1.0	--
Calf D (9)	1.4	0.3

*Fisher's "t" test.

normal calves. Repetition of this experiment using serum collected a fortnight later gave identical results, 1 ml of serum giving a 4-fold enhancement of erythropoietin activity. Also presented in the table are the results of simultaneous subcutaneous injections of erythropoietin and polycythemic calf serum at different sites; significant enhancement was not observed.

These findings indicate that the serum of this polycythemic calf contained something not present in normal calf serum which in itself had no erythropoietic effect but which on incubation with erythropoietin resulted in 4-fold enhancement of the activity. Spontaneous recovery has been observed in affected calves which survive for more than 1 year, and in an attempt to ensure survival of this calf until remission occurred, phlebotomies were done at approximately monthly intervals. Assay for the erythropoietin-enhancing activity in serum from successive bleedings revealed a decrease in activity at 8-1/2 months with complete disappearance of enhancing activity by 10 months (Table 2). Although it seemed reasonable to assume that this factor was causally related to the polycythemia in this calf and to the severe and often fatal polycythemia occurring in other calves of this herd, it was found that there was no remission in polycythemia corresponding to or within 5 months following the disappearance of the detectable level in the serum.

Enhancement of erythropoietin by incubation with renal erythropoietic factor (REF) (7) suggested the possibility that the enhancing factor present in this calf might be REF. However, further investigation of the physiological and chemical characteristics of the enhancing factor in the intact mouse assay system being employed, which requires relatively large amounts of material, was not possible. The small remaining supply of active serum (from bleedings at 6 and 7 months) was reserved for study in the *in vitro* system described in the

Table 2. Decrease in erythropoietin enhancing factor with age of polycythemic calf.

Age (months)	Hct (%)	Activity (× ESF control)		
		1 ml	0.5 ml	0.1 ml
5.3	66	2.9	2.4	2.4
6.4	64.5	4.0	3.0	2.4
7.2	66	4.2	3.7	3.9
8.5	69	1.6	1.9*	--
9.5	67	1.0	1.0	--
10.0	70	0.6	--	--

*Average of 10 assays, one of which was negative.

accompanying report by Borsook et al. (8). Further investigation of this subject must await birth of another calf afflicted with primary familial polycythemia.

ACKNOWLEDGMENTS

This work was supported in part by the U. S. Atomic Energy Commission and in part by Grant 5ROICA08370-02 from the National Cancer Institute of the National Institutes of Health.

REFERENCES AND NOTE

1. Tennant, B.; Asbury, A. C.; Laben, R. C.; Richards, W. P. C.; Kaneko, J. J., and Cupps, P. T.; J. Am. Vet. Med. Assoc. 150: 1493, 1967.
2. Gardner, E., Jr.; Wright, C.-S.; Lewis, J. P., and Moores, R. R.; Brit. J. Haematol. 13: 317, 1967.
3. DeGowin, R. L.; Hofstra, D., and Gurney, C. W.; Proc. Soc. Exptl. Biol. Med. 110: 48, 1962.
4. Van Dyke, D. C.; Layrisse, M.; Lawrence, J. H.; Garcia, J. F., and Pollycove, M.; Blood 18: 187, 1961.
5. Van Dyke, D. C.: Haemopoiesis, London, J. & A. Churchill, 1960, p. 397.
6. Cotes, P. M., and Bangham, D. R.; Bull. World Health Organ. 35: 751, 1966.
7. Zanjani, E., personal communication, 1967. Cf. also Contrera, J. F.; Gordon, A. S., and Weintraub, A. H.; Blood 28: 330, 1966.
8. Borsook, H.; Ratner, K.; Tattrie, B.; Teigler, D., and Lajtha, L. G.; Nature, submitted for publication.

Dr. B. Tennant is with the Department of Veterinary Medicine, University of California, Davis.

Radiation-Induced Mitotic Segregation in Yeast

Sayaka Nakai[*] *and Robert K. Mortimer*

The genotype of mitotically dividing diploid cells is generally assumed to be maintained with relatively high precision. However, phenotypic expression of recessive genes, formerly in heterozygous state, does occur at a low frequency in some organisms. Stern (1936) observed concomitant expression of recessive linked traits in Drosophila in the form of "twin spots" and concluded that mitotic crossing over was causally associated with this event. Subsequently, mitotic segregation has been observed in various fungi: in Aspergillus nidulans by Pontecorvo, Roper, Hemmons, MacDonald, and Bufton (1953), in Aspergillus niger by Pontecorvo, Roper, and Forbes (1953), in Penicillium chrysogenum by Pontecorvo and Sermonti (1954), in Saccharomyces cerevisiae by James (1955), and Roman (1956), and in Ustilago maydis by Holliday (1961). Mitotic segregation of genetic traits has been observed both in organisms with and without a normal sexual cycle. In the latter, it has provided an approach to genetic analysis.

From their studies of ultraviolet-induced sectoring of galactose genes in yeast, James and Lee-Whiting (1955) concluded that mitotic crossing over was the responsible event. Hurst and Fogel (1964) also concluded that there was crossing over followed by mitotic centromere disjunction, but added that there is "generalized chromosome synapsis and crossing-over in a four strand stage at normal meiotic rates." A positive correlation between the frequency of homozygosis and meiotic centromere distance of different genes is expected if mitotic crossing over is involved. Wilkie and Lewis (1963) observed a negative or no correlation for various groups of linked genes in ultraviolet-irradiated yeast and accordingly favored crossing over followed by meiotic centromere disjunction and restitution of diploidy. In contrast, Mortimer (1959), and Haefner (1966) observed a positive correlation between mitotic segregation frequency and centromere distance for an assortment of genes located on different chromosomes.

James and Lee-Whiting (1955) and Johnston (1961) performed genetic analyses on both sectors of a number of sectored colonies. In most of these colonies one sector was homozygous recessive and the opposite sector homozygous dominant for the sectored traits. Linked markers sectored together. These dates are consistent with mitotic crossing over as the responsible event. In contrast, Yamasaki, Ito, and Matsudaira (1964) analyzed both sectors of 13 colonies in which sectoring of an adenine gene had been induced by X rays. In none

[*]Present address: Division of Genetics, National Institute of Radiological Sciences, Chiba-shi, Japan.

were reciprocal genotypes found in opposite sectors as would have been expected for mitotic crossing over.

This lack of agreement concerning the mechanism of radiation-induced mitotic segregation in diploid yeast perhaps suggests that there are a variety of possible mechanisms. For example, in addition to mitotic crossing over, mitotic nondisjunction, haploidization, deletion of a chromosome segment carrying the dominant gene, mutation of the dominant gene to a recessive allele, or a process akin to gene conversion (Roman, 1963) all could lead to mitotic descendants of heterozygous diploid cells that express the recessive phenotype. The relative importance of these different events might depend on the inducing agent or on the genes involved. The availability of a linkage group marked by seven genes and a centromere for which all intergenic distances could be measured by tetrad analysis prompted our reinvestigation of induced sectoring in yeast with the hope that a coherent explanation for the phenomenon could be obtained.

MATERIALS AND METHODS

YEAST STRAINS Most of the yeast strains used in this study were derived from the Berkeley yeast culture collection. In the initial experiments, which are described in a following section, a number of haploid strains bearing one or more unmapped genes were crossed to a strain carrying the recessive actidione resistance gene, $\underline{ac}_2^r$. This gene was shown by Hawthorne to be located on the left arm of chromosome VII (Hawthorne and Mortimer, 1960) and the experiments were designed to screen for markers linked to this resistance gene.

For the principal part of this experiment, the following hybrid was constructed:

$$\text{XS144: } o\frac{a}{\alpha}o\frac{\underline{le}_1\ \underline{tr}_5\ \underline{ac}_2^r\ \underline{met}_{13}\ \underline{ty}_3\ \underline{ly}_5\ \underline{ad}_{5,7}}{\underline{LE}_1\ \underline{TR}_5\ \underline{AC}_2^s\ \underline{MET}_{13}\ \underline{TY}_3\ \underline{LY}_5\ \underline{AD}_{5,7}}.$$

This hybrid is heterozygous for mating type and for seven genes located on the left arm of chromosome VII. The symbols used in this paper to designate different genes conform to those agreed upon at the Carbondale Yeast Genetics Conference (1963). ad, ar, hi, is, le, ly, met, tr, ty, ur correspond to genes controlling the synthesis of adenine, arginine, histidine isoleucine and valine, leucine, lysine, methionine, tryptophan, aromatic amino acids, and uracil, respectively. Lower case (ad) corresponds to the recessive allele which is phenotypically expressed as a requirement for the corresponding metabolite. Upper case (AD) corresponds to the dominant allele and the nonrequiring phenotype. $\underline{ac}_2^r$ is a recessive mutation conferring resistance to cycloheximide (actidione). $\underline{AC}_2^s$ is the sensitive, dominant allele of this gene. a and α are the complementary mating type alleles. The subscripts refer to particular genetic loci.

MEDIA:

1) Growth medium (YEPD): 1% Difco yeast extract, 2% Difco peptone, 2% (or 1/4%) dextrose, (for solid medium, 2% agar).

2) Synthetic complete (SC): per liter, Difco Yeast Nitrogen Base without amino acids, 6.4 g; adenine, arginine, histidine, leucine, lysine, methionine, phenylalanine, tryptophan,

tyrosine, and uracil, 20 mg each; dextrose, 10 g; agar, 20 g.

3) Omission media: a series of media in which one of the amino acids or bases has been omitted from synthetic complete; e. g., (-AR) is SC minus arginine, etc. The $\underline{ty}_3$ mutation confers a requirement for tyrosine, phenylalanine, and tryptophan. To score $\underline{tr}_5$ in the presence of this gene the (-TR) medium was supplemented with indole, which can be used by $\underline{ty}_3$ but not $\underline{tr}_5$ strains (Manney, 1964).

4) Minimal medium (MV): per liter, Difco Yeast Nitrogen Base without amino acids, 6.4 g; dextrose, 10 g; agar, 20 g.

5) Actidione medium: SC plus 1.8 μg/ml actidione.

6) Sporulation medium: per liter, potassium acetate, 9.8 g; glucose, 1.0 g; yeast extract, 2.5 g (McClary, Nulty, and Miller, 1959).

TETRAD ANALYSIS Sporulated cultures were treated with snail digestive juice and individual tetrads isolated by micromanipulation (Johnston and Mortimer, 1959). Spore colonies were transferred to a YEPD master plate which, after incubation at 30°C, was replica-plated onto appropriate media. From the patterns of growth/nongrowth of the spore colonies on the various media, the genotype of the diploid culture could be determined. These procedures and the method of establishing linkages are described in more detail in an earlier publication (Hawthorne and Mortimer, 1960).

INDUCTION AND ISOLATION OF SECTORED COLONIES Diploid cells from stock slants (YEPD) maintained at 2°C were inoculated into double-strength liquid YEPD medium contained in an Erlenmeyer flask. The cultures were grown for 3 days at 30°C with aeration obtained by rotary shaking. The stationary phase cells were washed and diluted in sterile distilled water. Approximately 200 cells were plated on each of a number of YEPD (1/4% dextrose) plates. The cells were then irradiated. After irradiation, the plates were incubated for 7 to 9 days at 30°C. The colonies were then replica-plated onto minimal medium (MV) for studies with XS144, or onto SC plus actidione for screening of markers for linkage to $\underline{ac}_2^r$. After 24 hr incubation, colonies that were sectored on the diagnostic media were scored. If the plates were stamped onto minimal medium, a sectored colony was evidenced by growth/nongrowth instead of growth of the entire colony. On actidione medium, the majority of colonies fail to grow, since $\underline{ac}_2^r$ is recessive; colonies sectored for growth/nongrowth then signal sectoring of this gene. From the original YEPD plate, both sides of the sectored colonies were isolated and transferred to a master YEPD plate. After 1 to 2 days incubation, these plates were replica-plated onto omission media (-LE, -TR, etc.) to determine phenotypic sectoring of other characters in the diploid.

IRRADIATION SOURCES A beryllium-window X-ray tube (MACHLETT OEG-60) operated at 50 kV and 20 mA was used as a source of X rays. The dose rate was 200 R/sec. Low pressure mercury vapor lamps were the source of ultraviolet radiation. The cells were irradiated at an intensity of 35.8 ergs/mm^2/sec.

RESULTS

SURVEY OF GENES FOR LOCATION ON CHROMOSOME VII The left arm of chromo-

some VII in Saccharomyces cerevisiae was known to carry the genes le_1, tr_5, and ac_2^r (Hawthorne and Mortimer, 1960, Mortimer and Hawthorne, 1966). Because of detailed studies on two of these genes (Manney, 1964, Nakai and Mortimer, 1967) a search was undertaken for additional genes that might be located on this chromosome arm. A number of previously unmapped genes were surveyed for linkage using radiation-induced mitotic segregation. Hybrids heterozygous for ac_2^r and for one or more unmapped genes were constructed. Sectoring of ac_2^r was induced with X rays (see Material and Methods) and the resultant sectors were analyzed for coincident sectoring of the unmapped genes. Of 27 genes analyzed, 4 showed mitotic linkage to ac_2^r, i.e., $ad_{5,7}$, ly_5, met_{13}, and ty_3 (Table 1). These four genes and the three genes already located on this chromosome arm were then tested for meiotic linkage using tetrad analysis. The linkages indicated by mitotic segregation were confirmed by meiotic analysis. The results for hybrid XS144, which is heterozygous for these seven genes, are presented in Table 2. The gene order determined from these data and from an analysis of crossover patterns in individual asci is: centromere VII - le_1 - tr_5 - ac_2^r - met_{13} - ty_3 - ly_5 - $ad_{5,7}$. All intergenic distances are determinable from the tetrad data and their sum is 165 centimorgans.

MITOTIC RECOMBINATION Strain XS144 was exposed to three doses of X rays: 15, 40, and 80 krad, and to ultraviolet light (45 sec). The corresponding survivals for these four treatments were 0.95, 0.75, 0.50, and 0.28. The survivors, which were on YEPD (1/4% dextrose) medium, were replica-plated to minimal medium (MV) to detect sectoring of the nutritional genes. The percentages of sectored colonies were 2.9, 4.0, 2.0, and 2.4 for the respective treatments. In addition, approximately equal percentages of completely negative colonies were observed. These latter colonies most likely arise from coincidence sectoring of nutritional genes and lethality in the divisions immediately following treatment (Haefner, 1965, James and Werner, 1966). In this experiment they were not studied further.

Both sectors of colonies that were sectored for growth/nongrowth on MV were isolated from the corresponding YEPD plates and transferred to a series of YEPD master plates. The phenotypes of these sectors were then determined by replica-plating the masters to a series of omission plates. The results of these tests are summarized in Table 3. Only the phenotypes of the auxotrophic sectors are recorded because the initial screening determined the phenotype (except at the ac_2^r locus) of the opposite sectors; i.e., prototrophic on minimal medium.

For classes 1 to 7, sectoring involves characters determined by all genes located distal to one of the seven genes on this chromosome arm. For example, class 4 is not sectored for le_1, tr_5, or ac_2^r but is sectored for the four genes beyond ac_2^r; i.e., met_{13}, ty_3, ly_5, and $ad_{5,7}$. These seven classes can most easily be explained by a single mitotic crossover in one of the seven regions on this chromosome arm; i.e., class 1 would be due to a crossover in the region between the centromere and le_1, class 2 between le_1 and tr_5, etc. The two daughter cells formed subsequent to the recombination event would presumably form the two sectors of the colony. The majority of sectored colonies fall into one of classes 1 to 7. For the 15 krad exposure, 79% of the sectored colonies are in these classes and can be explained by a single

Table 1. Survey of unmapped genes for mitotic linkage to ac_2^r.

Gene	No. of colonies sectored for ac_2^r	No. of colonies with coincident sectoring	Gene	No. of colonies sectored for ac_2^r	No. of colonies with coincident sectoring
ad_4	26	1	ly_8	20	0
$ad_{5,7}$	23	17	ly_9	29	0
ar_1	23	0	ly_{10}	21	0
ar_2	29	0	met_4	29	0
ar_7	42	0	met_5	21	0
hi_5	33	0	met_6	13	0
hi_7	30	0	met_7	40	0
hi_8	10	0	met_{13}	23	15
is_2	12	0	ty_2	30	0
le_3	21	0	ty_3	16	8
ly_3	10	0	ur_1	23	0
ly_4	31	0	ur_2	15	0
ly_5	21	19	ur_4	26	0
ly_6	32	0			

Table 2. Tetrad data for genes located on the left arm of chromosome VII in hybrid XS144.

Gene pair	Ascus type: Parental ditype	Nonparental ditype	Tetratype	Intergenic distance (cm)
le_1-tr_5	77	0	46	18.7
tr_5-ac_2^r	34	3	86	42.3
ac_2^r-met_{13}	78	2	43	22.4
met_{13}-ty_3	83	1	39	18.3
ty_3-ly_5	107	1	15	8.5
ly_5-$ad_{5,7}$	34	9	80	54.5

mitotic crossover. Genetic analyses, to be described in a later section, show that this explanation is valid except for class VII for which other events also are involved.

The remaining 23 classes cannot be explained by a single mitotic crossover. Classes 8 to 22 involve sectoring of only a single gene or of two or more adjacent genes. The classes for which only one gene character is sectored, i.e., 8, 12, 15, 18, 20, and 22 are the most frequent in this group of sectored colonies. It is possible to explain the colonies in classes 8 to 22 by assuming that two mitotic crossovers have been induced. To explain the excess of colonies for which only one gene is sectored, it is necessary to add the additional condition

Table 3. Phenotypes of auxotrophic sectors of colonies formed by irradiated cells of strain XS144.

	Phenotype of negative sector*							Treatment			
								X ray (15 kR)	X ray (40 kR)	X ray (80 kR)	X ray (45 sec)
	-AD	-LY	-TY	-MET	+AC	-TR	-LE	No. of sectored colonies	No. of sectored colonies	No. of sectored colonies	No. of sectored colonies
1	(-	-	-	-	+	-	-)	9	2	0	8
2	(-	-	-	-	+	-)	+	7	3	2	4
3	(-	-	-	-	+)	+	+	118	8	3	24
4	(-	-	-	-)	-	+	+	14	3	2	12
5	(-	-	-)	+	-	+	+	38	1	1	5
6	(-	-)	+	+	-	+	+	3	1	5	1
7	(-)	+	+	+	-	+	+	125	16	28	35
8	+	+	+	+	-	+	(-)	4	5	5	1
9	+	+	+	+	-	(-	-)	0	2	0	2
10	+	+	+	+	(+	-	-)	0	0	0	2
11	+	(-	-	-	+	-	-)	1	0	0	1
12	+	+	+	+	-	(-)	+	13	1	1	3
13	+	+	+	+	(+	-)	+	2	1	0	1
14	+	+	(-	-	+	-)	+	0	1	0	0
15	+	+	+	+	(+)	+	+	6	1	1	2
16	+	+	+	(-	+)	+	+	5	2	0	3
17	+	(-	-	-	+)	+	+	4	1	0	2
18	+	+	+	(-)	-	+	+	19	3	2	3
19	+	(-	-	-)	-	+	+	0	0	0	2
20	+	+	(-)	+	-	+	+	9	1	1	4
21	+	(-	-)	+	-	+	+	2	1	2	0
22	+	(-)	+	+	-	+	+	7	6	0	6
23	(-	-	-	-	+)	+	(-)	3	0	0	0
24	+	+	+	+	(+)	+	(-)	1	0	0	0
25	+	+	+	(-	+)	+	(-)	1	0	0	0
26	+	+	+	(-)	-	+	(-)	1	0	0	0
27	(-)	+	+	+	(+)	+	+	1	0	0	2
28	(-)	+	+	(-	+)	+	+	1	0	0	0
29	(-)	+	+	(-)	-	+	+	1	0	0	0
30	(-)	+	(-)	+	-	+	+	0	0	1	0
				Total sectors				397	59	54	123
				Total colonies examined				13345	1471	2673	5220
				Percent sectored colonies				2.9%	4.0%	2.0%	2.4%

*Sectored phenotypes are enclosed in parentheses.

that crossovers in adjacent intervals are more probable. However, the colonies sectored for only one gene could have been caused by mitotic gene conversion, mutation, or deletion at the locus. Only through genetic analyses of the sectors is it possible to decide among these possibilities.

Classes 23 to 30 are minor classes. They can be explained by three or more mitotic crossovers or by a combination of events at different loci or in different regions.

No pronounced differences in the distributions of phenotypic classes were observed for the different X-ray doses or for the ultraviolet exposure.

In Fig. 1 are plotted the relative frequencies of homozygosity of the different genes as a function of their distance from the centromere using the 15 krad data of Table 3. It is clear that there is a positive correlation between sectoring frequency of a gene and its centromere distance, as expected if mitotic crossing over is the predominant event.

GENETIC ANALYSES Genetic analyses were performed on both sectors of 65 sectored colonies representing 14 phenotypic classes. Six to eight tetrads from each sector were analyzed for segregation of the seven genes located on the left arm of chromosome VII. The sample of colonies selected for analysis is not representative with regard to the distribution of phenotypic classes. It was found that homozygosity for some of the recessive genes, particularly $\underline{ty}_3$, greatly reduced the ability of the diploids to form spores. This precluded extensive genetic analysis of many classes of sectored colonies. The results of the genetic analyses are summarized in Table 4. The sectored colonies could be grouped into three main categories: A--those for which the genotypes in opposite sectors were reciprocal for the sectored genes; B--those colonies whose genotypes in opposite sectors were nonreciprocal for the sectored genes; i.e., heterozygous in one sector and homozygous recessive in the opposite sector; and C--those colonies whose genotypes indicated a more complex event or sequence of events.

Colonies that were sectored reciprocally (category A) were mainly those that sectored for two or more adjacent genes; i.e., classes 1 to 6 and 13, 16 and 17. Nonreciprocal events (category B) were mainly observed for colonies that sectored only for the phenotype of a single gene, i.e., classes 7, 8, 12, 18, and 22. Colonies that were sectored for just the distal marker, $\underline{ad}_{5,7}$ (Class 7), were found to be about equally divided between the reciprocal and nonreciprocal categories.

Of the 65 colonies analyzed genetically, all but 6 can be explained either by one or two reciprocal mitotic crossovers (category A), or by mitotic gene conversion of a single gene (category B). The genotypes of both sectors of the 6 exceptional colonies are summarized in Table 5.

The two exceptional colonies in phenotypic class 6 (colonies 31 and 57) were sectored for the two distal genes $\underline{ly}_5$ and $\underline{ad}_{5,7}$. For both colonies, the genotypes in opposite sectors for

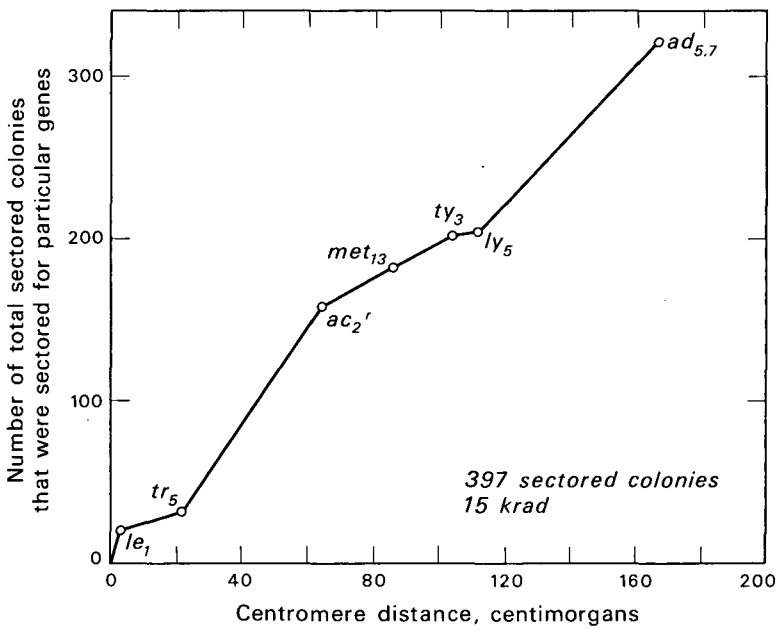

Fig. 1. DBL 681-4515

these two genes were reciprocal, consistent with a mitotic crossover event between $\underline{ty}_3$ and $\underline{ly}_5$. However, for both colonies, nonreciprocal segregation of $\underline{ty}_3$ also was observed. The sector that was homozygous dominant for $\underline{LY}_5$ and $\underline{AD}_{5,7}$ also was homozygous for the dominant allele $\underline{TY}_3$. The negative sector was heterozygous in both colonies. In addition, in colony 31, $\underline{ty}_3$ was in repulsion to $\underline{met}_{13}$ instead of in coupling as in XS144 or colony 57, an effect that can be accounted for by mitotic crossing over. Colony 57 can be explained by a crossover event that is nonreciprocal for the region including $\underline{ty}_3$. For colonies 36, 50, 54, and 46, the region of nonreciprocity extends over two or more genes. These colonies can be explained only by a combination of unusual events. Without the knowledge that the sectors analyzed represent the entire progeny of the irradiated cell, it is difficult to propose plausible explanations. X-ray-induced sectoring of lethality in diploid yeast is a common event at the doses used in this experiment (Haefner, 1965, James and Werner, 1966).

A number of the sectors were found to segregate for recessive lethals. Of the 65 colonies analyzed, 28 were free of lethals in both sectors, 13 were heterozygous for a lethal in both sectors, and 7 contained a lethal in only one sector. The remaining 17 colonies could not be classified in this fashion because analysis of the negative sector was hindered by homozygosity for certain nutritional genes, particularly $\underline{ty}_3$. In these colonies, very few asci were recovered from the negative sector and in these spore viability was consistently very low. It appeared unlikely that recessive lethals were the only source of reduced spore viability in these cases. None of the lethals observed were linked to the genes that were sectored. This rules out deletion or nondisjunction of one of a homologous pair of chromosomes as a causal factor in radiation-induced sectoring.

Table 4. Genetic analysis of sectored colonies formed by X-irradiated XS144 cells.

Phenotypic class*	No. of colonies analyzed	Genotypes of sectors† A Reciprocal	B Nonreciprocal	C Exceptional
1	2	2		
2	1	1		
3	8	8		
4	2	2		
5	1	1		
6	2			2
7	23	11	12	
8	8		8	
12	3		2	1
18	3		3	
22	8	2	4	2
13	1	1		
16	2	1		1
17	1	1		
	65	30	29	6

*See Table 3.

†On the basis of genetic analyses the sectored colonies can be divided into the following classes:

A - Reciprocal genotypes in opposite sectors. All sectored genes were homozygous dominant in one sector, homozygous recessive in the opposite sector. Nonsectored genes were heterozygous in both sectors.

B - Nonreciprocal genotypes in opposite sectors. Sectored gene(s) were homozygous recessive in the negative sector, heterozygous in the positive sector. Nonsectored genes were heterozygous in both sectors.

C - Exceptional, see Table 5.

DISCUSSION

These experiments demonstrate that the principal mechanism of radiation-induced sectoring in diploid yeast is mitotic crossing over. Approximately 80% of the colonies were sectored for all genes distal to one of the seven intergenic regions. Genetic analysis showed that these colonies were reciprocal with respect to the genotypes of opposite sectors. A positive correlation between sectoring frequency and centromere distance was observed, as is expected for

Table 5. Genotypes of exceptional sectored colonies.

Phenotypic class	Colony number	Sector	Recessive phenotype expressed	Genotype*						
				$ad_{5,7}$	ly_5	ty_3	met_{13}	ac^r_2	tr_5	le_1
6	31	Pos.		(+/+	+/+	+/+)	+/-	-/+	+/-	+/-
		Neg.	ly ad	(-/-	-/-	-/+)	+/-	-/+	+/-	+/-
6	57	Pos.		(+/+	+/+	+/+)	+/-	-/+	+/-	+/-
		Neg.	ly ad	(-/-	-/-)	+/-	+/-	-/+	+/-	+/-
12	36	Pos.		(+/+	+/+	+/+	+/+	-/-)	+/-	+/-
		Neg.	tr	+/-	+/-	+/-	+/-	-/+	(-/-)	+/-
16	46	Pos.	ac^r	+/-	+/-	+/-	+/-	(+/+)	+/-	+/-
		Neg.	met	+/-	+/-	+/-	(-/-)	-/+	+/-	+/-
22	50	Pos.		(+/+	+/+	+/+	+/+)	-/+	+/-	+/-
		Neg.	ly	(+/+	-/-)	+/-	+/-	-/+	+/-	+/-
22	54	Pos.		+/-	+/-	+/-	+/-	-/+	+/-	+/-
		Neg.	ly	+/-	(-/-	+/+	+/+)	-/+	+/-	+/-

*Genotypes different than that of XS144 are enclosed in parentheses.

mitotic crossing over. The failure of Wilkie and Lewis (1963) to find a correlation between centromere distance and sectoring frequency might be explained by the fact that high ultraviolet doses were employed in their experiments. It is possible that mitotic gene conversion, which should show no centromere dependence, predominates at these high exposures. If only a fraction of the population of cells was competent for mitotic crossing over, this event could saturate at relatively low doses, allowing other events such as gene conversion to predominate.

Mitotic gene conversion, i.e., nonreciprocal sectoring, was observed in the present experiments, but in nearly all cases its effect was restricted to single genes. If two or more adjacent genes sectored, the event involved in nearly every case was mitotic crossing over. It is not known if the conversion-type events observed in this study correspond to the intragenic events involved in reversion of heteroallelic diploids (Roman and Jacob, 1958). They are analogous to the aberrant 1:3 segregations observed in meiosis of yeast and other fungi.

Radiation induces a relatively high frequency of recombination (3% for one chromosome arm) at doses that cause relatively little killing. This role of radiation in altering the genotype of cells that survive radiation might be of importance in assessing the long-term effects of exposure to radiation.

ACKNOWLEDGMENTS

Mrs. Ruth Lerner and Mr. T. McKey contributed greatly to the success of these experiments. Their excellent assistance in all phases of the study is greatly appreciated.

This work was partially supported by the U. S. Atomic Energy Commission and the National Aeronautics and Space Administration (S. N.).

REFERENCES

Carbondale Yeast Genetics Conference, 1963, Microbial Genet. Bull. 19 (Suppl).

HAEFNER, K., 1965: Zum Inaktivierungs-kriterium fuer Einzelzellen unter besonderer Beruecksichtigung der Teilungsfaehigkeit Roentgen- und UV-bestrahlter Saccharomyces Zellen verschiedenen Ploidiegrades. Intern. J. Radiation Biol. 9: 545-558.

HAEFNER, K., 1966: Zum Mechanismus der Entstehung auxotropher Zellen in heterozygoten Saccharomyces-Stämmen nach UV- und Röntgen-Bestrahlung. Z. Vererbungsl. 98: 82-90.

HAWTHORNE, D. C., and R. K. MORTIMER, 1960: Chromosome mapping in Saccharomyces: Centromere linked genes. Genetics 45: 1085-1110.

HOLLIDAY, R., 1961: Induced mitotic recombination in Ustilago maydis. Genet. Res. 2: 231-248.

HURST, D. D., and S. FOGEL, 1964: Mitotic recombination and heteroallelic repair in Saccharomyces cerevisiae. Genetics 50: 435-458.

JAMES, A. P., 1955: A genetic analysis of 'sectoring' of ultraviolet-induced variant colonies of yeast. Genetics 40: 204-213.

JAMES, A. P., and B. LEE-WHITING, 1955: Radiation-induced genetic segregations in vegetative cells of yeast. Genetics 40: 826-831.

JAMES, A. P., and M. M. WERNER, 1966: Radiation-induced lethal sectoring in yeast. Radiation Res. 29: 523-536.

JOHNSTON, J. R., 1961: Ph. D. dissertation, University of California, Berkeley. Studies in meiotic and mitotic recombination in Saccharomyces cerevisiae.

JOHNSTON, J. R., and R. K. MORTIMER, 1959: Use of snail digestive juice in isolation of yeast spore tetrads. J. Bacteriol. 78: 292.

MANNEY, T. R., 1964: Action of a super-suppressor in yeast in relation to allelic mapping and complementation. Genetics 50: 109-121.

McCLARY, D. O., W. L. NULTY, and G. R. MILLER, 1959: Effect of potassium versus sodium in the sporulation of Saccharomyces. J. Bacteriol. 78: 362-368.

MORTIMER, R. K., 1959: Invited discussion. Radiation Res. Suppl. 1: 394-402.

MORTIMER, R. K., and D. C. HAWTHORNE, 1966: Genetic mapping in Saccharomyces. Genetics 53: 165-173.

NAKAI, S., and R. MORTIMER, 1967: Induction of different classes of genetic effects in yeast using heavy ions. Radiation Res. Suppl. 7: 172-181.

PONTECORVO, G., J. A. ROPER, L. M. HEMMONS, K. D. MacDONALD, and A. W. J. BUFTON, 1953: The genetics of Aspergillus nidulans. Advan. Genet. 5: 141-238.

PONTECORVO, G., J. A. ROPER, and E. FORBES, 1953: Genetic recombination without sexual reproduction in Aspergillus niger. J. Gen. Microbiol. 8: 198-210.

PONTECORVO, G., and G. SERMONTI, 1954: Parasexual recombination in Penicillium chrysogenum. J. Gen. Microbiol. 11: 94-104.

ROMAN, H., 1956: A system selective for mutations affecting the synthesis of adenine in yeast. Compt. Rend. Trav. Lab. Carlsberg, Sér. Physiol. 26: 299-314.

ROMAN, H., 1963: Genic conversion in fungi. pp. 209-227. Methodology in Basic Genetics. Edited by W. J. Burdette. Holden-Day, San Francisco.

ROMAN, H., and F. Jacob, 1958: A comparison of spontaneous and ultraviolet-induced allelic recombination with reference to the recombination of outside markers. Cold Spring Harbor Symp. Quant. Biol. 23: 155-160.

STERN, C., 1939: Somatic crossing over and segregation in Drosophila melanogaster. Genetics 21: 625-730.

WILKIE, D., and D. LEWIS, 1963: The effect of ultraviolet light on recombination in yeast. Genetics 48: 1701-1716.

YAMASAKI, T., T. ITO, and Y. MATSUDAIRA, 1964: The whole- and fractional-colony mutation induced by soft x-rays in yeast. Jap. J. Genet. 39: 147-150.

A Reciprocal Translocation in *Saccharomyces cerevisiae*

Tommy James McKey

INTRODUCTION

Yeast is a versatile organism for genetical research since both mitotic products and meiotic tetrads are analyzable. This versatility permits genetic investigations of chromosome aberrations without recourse to cytological techniques. Hopefully, in the future, genetic studies will be augmented by cytological correlations. This paper reports the detection and analysis of reciprocal translocation in yeast.

MATERIALS AND METHODS

A haploid strain (1375) with a single nutritional requirement for arginine (ar_{4-28}) arose as a mutant spore from a diploid sporulated in the presence of acridine. This strain was provided by Dr. G. E. Magni, Università di Parma. It was crossed to the haploid tester strain X1491-5A bearing the markers ad_{2-1}, p_1 and the suppressor S_d. The resulting hybrid (X1834) was sporulated and tetrad analysis was undertaken initially to determine suppressibility of the ar_{4-28} mutation. The analysis was extended when it was observed that the tetrads produced viability classes which were suggestive of a chromosomal rearrangement (Esser and Kuenen, 1965; Perkins, 1966); i.e., most tetrads yielded either 4:0, 2:2, or 0:4 ratios for viable : inviable spores.

Asci were dissected by the method of Johnston and Mortimer (1959).

Tetrad analysis was performed by the method described by Gilmore (1967).

Yeast strains:

1375	$a\ ar_{4-28}$
X1491-5A	$\alpha\ ad_{2-1}\ p_1\ S_d$
X901-26A	$\alpha\ thr_2\ tr_5\ le_1\ hi_6\ tr_1\ ar_{4-2}\ thr_1\ cu_1$
JB 112	$\alpha\ tr_{5-4}$
DT 29	$\alpha\ tr_{5-1}$
X160-2C	$\alpha\ ur_3\ thr_3\ hi_1\ ar_6\ is_1\ tr_2\ ad_1$
X1834	X1491-5A × 1375
XY7	1375 × JB112
XY10	1375 × XY7-2B

Media: The media used in this experiment include YEPD, GNA, RA, synthetic complete, synthetic omission, and petite, as described by Gilmore (1967).

RESULTS

INITIAL DETECTION OF CHROMOSOMAL REARRANGEMENT IN X1834 A total of 119 4-spored asci were analyzed from X1834 (1375 × X1491-5A). All markers segregated normally but viability was sharply reduced. The following classes of viable : inviable spores per ascus were observed:

Table 1.

	Viable:inviable spores per ascus				
	4:0	3:1	2:2	1:3	0:4
No. of asci	30	3	62	6	18

Among the five viability classes are three major classes: 4:0, 2:2, and 0:4. The remaining two classes can be explained by the superimposition of random spore death on these classes, since only 95% of the spores dissected from normal hybrids are viable. Thus, the 4:0 and the 3:1 asci probably represent one class (4:0), while the 2:2 and 1:3 asci represent another class (2:2).

Sixty-two of the 119 asci analyzed from X1834 hybrid fell in the 2:2 viability class and each of the 62 asci segregated 1:1 for the $\underline{ar}_{4-28}$ marker. Since $\underline{ar}_4$ is close (8 cM) to a centromere (Mortimer and Hawthorne, 1966), most of the 2:2 asci are presumed to contain two viable spores that are non-sister, i.e., spores derived from products segregated at the first meiotic division. This observation and the pattern of spore viability suggested that X1834 was heterozygous for a translocation.

OUT CROSSES AND BACK CROSSES In an attempt to demonstrate that parent 1375 contributed the translocation, this strain was outcrossed to several normal strains. The resultant hybrids in each instance showed the same viability classes as were observed in the spore tetrads from X1834.

In this study a total of 211 4-spored asci were analyzed from hybrids heterozygous for the presumed chromosomal rearrangement.

The results were as follows:

Table 2.

	Viable:inviable spores per ascus				
	4:0	3:1	2:2	1:3	0:4
No. of asci	47	10	112	14	28

The haploid 1375 was crossed to JB112, a known normal strain, and asci from the resulting hybrid XY7 were of the same viability classes as observed with X1834. A spore isolate, XY7-2B, from the XY7 hybrid, which was deduced to carry the chromosomal rearrangement, was backcrossed to the original 1375 haploid and 42 dissected asci from the resulting hybrid XY10 were analyzed for spore viability. It was expected that XY10 would be homozygous for the translocation and 96% of the spores were viable (Table 3), a result consistent with normal spore viability.

Table 3.

	Viable : inviable spores per ascus				
	4:0	3:1	2:2	1:3	0:4
No. of asci	37	3	2	0	0

INTRA-ASCAL CROSSES A 4-spored ascus from a hybrid heterozygous for the chromosomal rearrangement in which all four spores formed colonies was selected. All possible crosses were made among the four spores. The four resulting hybrids were sporulated and analyzed for spore viability. At least 30 asci were dissected from each hybrid and each hybrid gave the viability classes observed with X1834 (Table 4).

Table 4.

	Viable : inviable spores per ascus				
Hybrids	4:0	3:1	2:2	1:3	0:4
Ax B	8	0	17	0	7
Ax D	14	1	27	4	11
Cx B	6	0	21	0	5
Cx D	4	2	22	0	4
Total no. of asci	32	3	87	4	27

Presumably the translocation (T) and mating type segregated in a ditype configuration in this ascus such that all four crosses were heterozygous for both mating type and translocation. When the two viable spores from a single 2:2 ascus were crossed and tetrad analysis performed, the same viability classes as observed with X1834 were observed.

In other intra-ascal crosses, normal viability has been obtained, presumably reflecting normal/normal or translocation/translocation genotype.

STAGES OF SPORE DEATH Though it is clear that meiosis and sporogenesis proceed

to completion in translocation heterozygotes, some asci contain either 2 or 4 potentially lethal spores. Thirty asci were dissected from X1834 and each spore was examined after 24 hr incubation. Some of the spores divided 2 to 4 times, forming large branched cells, some merely enlarged without dividing, while about 5% of the spores showed no obvious change. Some 50% of the spores formed normal colonies. Since most of the spores analyzed from X1834 went through several divisions or partial division before dying, an attempt was made to mate those potentially lethal spores.

A total of 16 asci were dissected from a hybrid heterozygous for the chromosomal rearrangement and one spore of each ascus was paired with a normal strain D160-2C, which carried markers on three chromosomes. Of the 16 pairs, five formed unmistakable zygotes. These were isolated and allowed to develop into colonies. In each case the phenotype of the D160-2C haploid parent was expressed in the zygotic colonies. This implies that nuclear fusion and cell fusion are uncoupled.

The 1375 strain was crossed to several haploid strains with mapped chromosomal markers for linkage studies in an attempt to locate the translocation break points. No linkage has been found to date. However, these studies are still in progress.

DISCUSSION

The viability classes observed are those expected from a reciprocal translocation or an inversion (Perkins, 1966). For an inversion, the 0:4 class can only occur when there is a 4-strand double crossover in the inverted segment. This class should represent one-fourth of the double crossovers, a comparatively rare event. The 3-strand double crossovers should yield 2:2 asci as is the case for single crossovers, while the 2-strand double crossovers and the non-crossovers should yield 4:0 asci. If the 1375 haploid carried an inversion the data are explicable only if the frequency of double exchanges exceeded the single exchanges within the inverted segment.

The data best fit the expectation for a reciprocal translocation in which one break is distantly removed from the centromere while the other break is sufficiently close to the centromere that an exchange between the centromere and the break point is highly improbable. Since $\underline{ar}_4$ segregated 1:1 in all sixty-two 2:2 asci from X1834, this marker might be linked to the rearrangement. The $\underline{ar}_4$ marker is 8 cM from the centromere and should have yielded some 2:0 or 0:2 asci for arginine even if all 62 asci contained non-sister spores.

The 4:0 and 0:4 viability classes are expected in a 1:1 ratio for a translocation. However, the data reported here approximate a 2:1 ratio (see Table 2). The deficit of 0:4 asci could be due to early breakdown during sporogenesis of potential 0:4 asci. A deficit for this ascus category has been observed in Neurospora crosses known to be heterozygous for a reciprocal translocation (Perkins, 1966). However, among the intra-ascal crosses in the present study the 4:0 and 0:4 asci appeared in equal frequency. A longer sporulation period was involved in this series of crosses and it is conceivable that the 0:4 asci mature more slowly than the other ascus classes. Thus, they could have been selected against in the analysis of X1834.

The 2:2 asci are readily explained by the occurrence of crossing over between the centromeres and the breakpoints. The frequency of 2:2 asci depends upon the map distance between the centromeres and the breakpoints in each chromosome and this may assume any value from zero to greater than two-thirds. Approximately 60% of the asci are 2:2, which indicates that the sum of the centromere-breakpoint intervals is on the order of 30 cM.

Theoretically, one does not expect the 3:1 and 1:3 viability classes from translocation heterozygotes. However, these classes can be explained by random spore death as pointed out earlier.

The consequences of non-disjunction of homologous centromeres which would yield 0:4 asci were ignored in this study.

Another translocation in yeast has been found by Esposito (personal communication). In addition, viability patterns expressed in spore tetrads from a number of other diploids used in recent studies in this laboratory (Stromnaes, in preparation; Mortimer, personal communication; Fogel, personal communication) are suggestive of other chromosomal structural alternations in this organism.

ACKNOWLEDGMENTS

I wish to thank Professor Robert K. Mortimer for his helpful discussion and advice. I also want to thank Dr. S. Fogel for his assistance and Dr. Michael Esposito for providing data on his work with a translocation in yeast.

REFERENCES

1. Gilmore, R. A., 1967; Super-suppressors in Saccharomyces cerevisiae. Genetics 56: 641-658.
2. Mortimer, R. K., and Hawthorne, D. C., 1966; Genetic Mapping in Saccharomyces cerevisiae. Genetics 53: 165-173.
3. Johnston, J. R., and Mortimer, R. K., 1959; J. Bacteriol. 78: 292.
4. Esser, K., and Kuenen, R., 1965; Genetik der Pilze, Springer-Verlag, Berlin.
5. Perkins, D. D., Neurospora Newsletter #9, pp. 10-12, June, 1966.

Radiation-Sensitive Mutants in Yeast

Michael A. Resnick and Robert K. Mortimer

The modification of radiation damage has been shown in many organisms to be under genetic direction. Extensive work with bacteria suggests a genetically controlled system for recognizing and excising ultraviolet-induced pyrimidine dimers (1). Lesions resulting from ionizing radiation are thought to be repaired by the same or a similar system. An alternative to the stepwise repair of ultraviolet (UV) lethal damage is photoreactivation (2). Photoreactivation (PR) involves splitting the dimer by an enzyme that requires activation by light of longer wavelength (3). In bacteria this process has also been demonstrated to be under genetic control (4).

To examine the role of repair and the nature of the lesion or lesions in such radiation-induced processes as mutagenesis, recombination, and killing in Saccharomyces cerevisiae, mutations which markedly increase the sensitivity to radiation were induced. These mutants are sensitive to UV, X rays, or both. Although mutants in the first two classes have been described previously (5, 6), there has been no report of a mutant in yeast that is sensitive to both UV and X rays.

The radiation-sensitive mutations were induced in strain X1687-101B (α ar_{4-17} hi_{5-2} ly_{1-1} ad_{2-1} le_{1-12}) using 0.1 M $NaNO_2$ for 60 min (approximately 30% survival). Employing the technique of Nakai and Matsumoto (6), sensitive mutants were detected by 1) replica-plating the surviving clones, 2) lightly irradiating the replica imprints, and 3) examining for the presence or absence of growth. The types of mutants and their frequency in a sample of 3282 survivors of $NaNO_2$ treatment are as follows: UV-sensitive, 3; X-ray sensitive, 4; UV and X-ray sensitive, 1. Tetrad analysis performed on the mutant strains after crossing with other nonsensitive strains has revealed that these characteristics segregate as single gene traits. The mutants were tested for allelism by determining the sensitivity of diploids formed by all pairwise combinations of the mutants (Table 1). Allelism was indicated if the diploid was sensitive since other tests had shown that all the mutants were expressed recessively. The centromere-linked mutants (KC 370, KC 371, and KC 373) were found to be allelic to centromere-linked mutants described by Snow (5) and by Nakai and Matsumoto (6). None of the other strains described by these investigators were tested against the remaining mutants in this study.

The responses to UV of the UV-sensitive mutants are presented in Fig. 1. Survival of these mutants is comparable to that of the corresponding mutants of Snow (5) and Nakai and Matsumoto (6) with which they are allelic (see Table 1). The uxs mutant is less sensitive to

Table 1.

Mutant strain	Sensitivity	Centromere-linked?	Allelism	Mutant gene designation
KC 370	UV	Yes	KC 371	uvs 9-2
KC 371	UV	Yes	KC 370 and uvr-9*	uvs 9-3
KC 373	UV	Yes	UV_1^s †	uvs 1-2
KC 372	UV and X ray	No		uxs 1
KC 376	X ray	No		xs 1
KC 377	X ray	No	KC 383	xs 2-1
KC 381	X ray	No		xs 3
KC 383	X ray	No	KC 377	xs 2-2

*Snow (reference 5).

†Nakai and Matsumoto (reference 6).

UV than the other mutants; however, it is still much more sensitive than the wild type strain. X-ray survival of some of the mutants is shown in Fig. 2. There is either a lowered "tail" or no tail at all on the survival curves of the uxs and xs mutants when compared with the wild type strain. This tail has been shown to be due to the budding cells in the population which are resistant to X-ray killing (7). The fraction of budding cells in the experiments presented in Fig. 2 was comparable for all strains.

Possibly, the X-ray repair system in haploid yeast is only active during the budding stage which corresponds to DNA synthesis (8). The repair enzymes must be short-lived because after budding the sensitivity returns. The xs and uxs mutants may have defective or permanently repressed repair systems.

It should be noted that the genetic control of repair of X-ray damage in yeast differs from that in bacteria. In bacteria all the X-ray sensitive mutants are also UV sensitive; however, not all UV-sensitive mutants are X-ray sensitive (9). This would suggest that in bacteria a component of the UV repair mechanism is able to repair damage due to ionizing radiation. The existence in yeast of three classes of mutants, uvs, xs, and uxs, may indicate that there are two separate pathways for the repair of X-ray damage, one of which is part of the UV repair system. An alternative to this model would be a common pathway for repair with branches that act only on UV or X-ray damage.

Besides the above mutants a mutant which is "photoreactivationless" (phr) was also isolated. Photoreactivation of UV damage is not observed with this mutant. There have been no previous reports of such a mutant in a eukaryotic organism. This mutant was isolated in a strain which was UV sensitive (uvs 9-3). As shown in Fig. 3, survival after PR is relatively

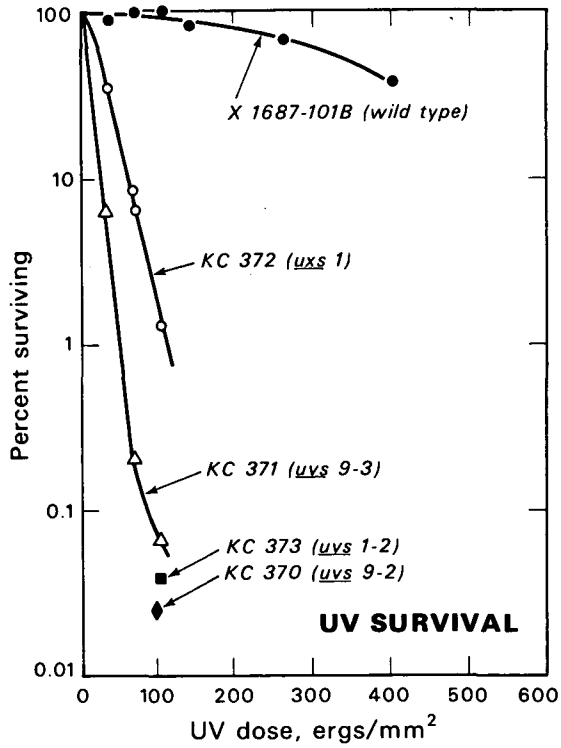

Fig. 1. DBL 682-4580

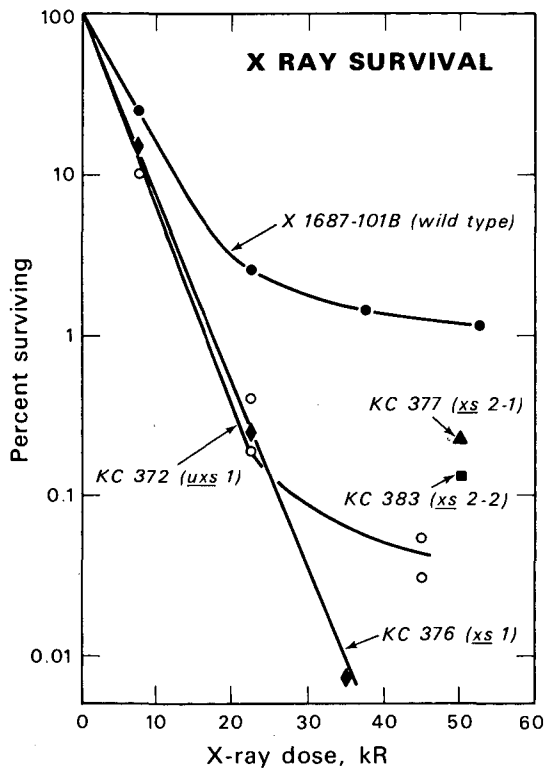

Fig. 2. DBL 682-4581

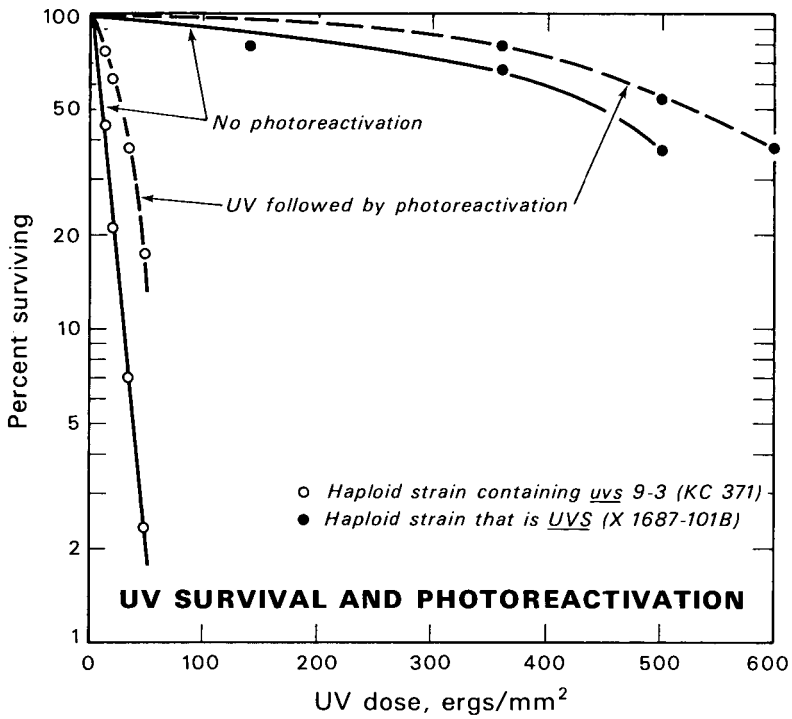

Fig. 3. DBL 682-4582

much higher in the uvs than in the UVS strain. Therefore, a phr mutant can be more easily identified in the uvs strain. The mutant was obtained by a method similar to that used for obtaining UV-sensitive mutants. Instead of using nitrous acid, UV was employed as the mutagen. After the UV treatment (about 20% survival), the cells were plated to nutrient agar. Each plate of colonies which emerged was replica-plated to two plates both of which were exposed to UV. Immediately following this, one plate was placed in the dark and the other was illuminated by visible light. One day later the replica imprints were examined. The uvs phr mutant had a low level of growth on both plates while the other colonies (uvs) had much more growth on the plates exposed to light. The phr characteristic segregates as a single gene trait (phr 1). It is neither linked to uvs 9 nor is it centromere-linked.

The survival of the phr mutant after UV exposure is the same with or without photoreactivation. In the uvs PHR strain the kinetics of survival with PR is much different than without (Fig. 3). However, in the UVS PHR strain the kinetics before and after PR are similar with a dose-modifying factor of about 1.25. The effects of the phr mutant in a diploid and in UVS strains are presently being examined.

SUMMARY

Three classes of mutants which increase sensitivity to radiation have been isolated in yeast: UV-sensitive, X-ray sensitive, and UV and X-ray sensitive. Another mutant prevents photoreactivation of lethal damage following UV. These mutants are being used to study radiation-induced recombination, lethality, mutagenesis, and lethal sectoring.

REFERENCES

1. Haynes, R. H.; Radiation Res. Suppl. 6: 1, 1966.
2. Setlow, J. K.; in Current Topics in Radiation Research, Vol. II, edited by Ebert and Howard, Amsterdam, North-Holland Publishing Co., 1966, p. 195.
3. Rupert, C. S., and Harm, W.; in Advances in Radiation Biology, Vol. II, edited by Augenstein and Mason, New York, Academic Press, Inc., 1966, p. 1.
4. Harm, W., and B. Hillebrandt; Photochem. Photobiol. 1: 271, 1962.
5. Snow, R.; J. Bacteriol. 94: 571, 1967.
6. Nakai, S., and S. Matsumoto; Mutation Res. 4: 129, 1967.
7. Beam, C. A.; Mortimer, R. K.; Wolfe, R. G., and Tobias, C. A.; Arch Biochem. Biophys. 49: 110, 1954.
8. Williamson, D. H.; J. Cell. Biol. 25: 517, 1965.
9. Howard-Flanders, P., and Boyce, P.; Radiation Res. Suppl. 6: 156, 1966.

A Karyotype Analysis of the M3-1 Tissue Culture Line of Chinese Hamster Fibroblasts

William D. Loughman

In 1964 Todd (1) reported results of biophysical investigations which utilized, in part, cells derived from bone marrow cultures of a male adult Chinese Hamster. The particular subline utilized, called M3-1, was determined to have a proportion of normal diploid cells near 90%, with an apparently normal diploid male karyotype. The remaining 10% of cells were essentially tetraploid. This "normal" chromosome constitution had been maintained for about one and one-half years.

This same cell line is still used occasionally at Donner Laboratory for a variety of radiobiological investigations. Recently, doubts have been expressed as to its continued "normal" character. Specific questions were: 1) Is the cell line still diploid with a normal karyotype, and 2) Is the cell line still a single cell line, or are several "clonal derivatives" coexisting?

In May and June of 1967, samples of the M3-1 line were obtained and the cells were subjected to detailed karyotype analysis following established procedures. The normal male Chinese Hamster karyotype given by Yerganian (2) was used as a standard. In the normal diploid karyotype containing 22 chromosomes, the first two large submetacentric pairs have been labeled Group A, the next two medium submetacentric pairs Group B, the next three small metacentric pairs Group C, the last three acrocentric pairs Group D. The large submetacentric X and Y chromosomes were separately identified. Five hundred cells were counted and categorized as essentially diploid, essentially tetraploid, or as essentially higher-ploid. An additional 600 cells in the diploid range were subjected to exact chromosome counts. Twenty-five high magnification photographic karyotypes were prepared. Information from the karyotypes as to gain or loss of chromosomes, and structural abnormalities of chromosomes, was coded on punched cards. These were sorted to detect underlying chromosome patterns, if any.

From this analysis, it was found that 92% of the cells were in the diploid range; the remaining 8% were in the tetraploid range, only a single octaploid or higher ploidy cell being seen. This agrees with the estimate of Todd (1). The exact chromosome counts gave the following distribution, for cells in the diploid range:

Chromosomes per cell:	21	22	23	24
Percent of cells:	6.18	38.6	48.6	6.18

(In 600 cells, 1 cell each had 9, 10, 33, and 67 chromosomes)

From the karyotype analysis, three major cell types could be distinguished:

1) Usually no loss in groups A-D; loss if found is restricted to Group D;
   No minute chromosomes;
   Sporadic loss of the Y chromosome;
   Gain of chromosomes of miscellaneous morphology but medium to small size;
   Stemline number inconstant, but usually 22 or 23 in roughly equal numbers.
2) Usually no loss in groups A-D; loss if found is restricted to Group D;
   Minute ("dot") chromosome always present, sometimes in duplicate;
   Sporadic loss of the Y chromosome;
   Gain of medium acrocentrics often seen; no gain of metacentrics or submetacentrics;
   Inconstant stemline, usually 22 or 23 in equal numbers, with a few 24.
3) Always loss in Group C, often two or more; sometimes loss in Group D;
   Almost always a "dot" chromosome, usually associated with a large acrocentric;
   Y chromosome usually present;
   Gain of small to medium metacentrics, never large metacentrics, occasional gain of small to medium submetacentrics;
   Stemline 22 to 23, with more 23 and never 24 or higher.

Each cell type was remarkably constant according to the above five general criteria. Within a given "subline," over 50% of the cells met all five criteria, over 70% met the same four criteria, and over 90% met the same three criteria. A few tetraploid cells were karyotyped, and proved to be simple duplications of one or another of the three basic chromosome patterns.

While the foregoing does not constitute rigorous proof for the existence of exactly three sublines, with the properties specified, in the frequencies assigned, it does constitute proof that 1) the M3-1 cell "line" is no longer diploid, nor even mostly diploid, 2) it is not a single cell line, and 3) there is no clear evidence for the existence of any cell subline with a "normal" Chinese Hamster karyotype.

REFERENCES

1. Todd, Paul W.; Reversible and irreversible effects of ionizing radiations on the reproductive integrity of mammalian cells cultured in vitro. Lawrence Radiation Laboratory Report UCRL-11614, August 18, 1964.
2. Yerganian, G.; Chromosomes of the Chinese Hamster (Cricetulus griseus) I. The normal compliment and identification of the sex chromosomes. Cytologia 24: 66, 1959.

Standard Biological Test Specimens for Use in the Scanning Electron Microscope

Thomas L. Hayes, JaRue S. Manning and Robert M. Glaeser

INTRODUCTION

The scanning electron microscope (SEM) is rapidly being accepted as a research tool in the fields of biology and medicine (1, 2). It would be useful for investigators in these areas to have test specimens for this instrument. These test specimens should meet certain requirements dictated by the properties of the scanning electron microscope itself and by the type of work carried on with the instrument. Some of these requirements are:

1) The specimen should have structural detail in the size range of the resolution limit of presently available scanning electron microscopes (200-400 Å).

2) The specimen should be a biological structure rather than some inorganic system.

3) The dimensions of the biological structure should be well known from other techniques such as transmission electron microscopy (EM).

4) The test material should be familiar to biologists and it should be relatively easy to obtain in a biological laboratory.

This paper suggests four materials that satisfy these conditions and demonstrates the appearance of these materials in the scanning electron microscope.

METHODS

Samples were checked by viewing the specimen in the light microscope and standard transmission microscope following observation in the scanning electron microscope. In order to allow direct comparison of transmission and scanning images of the same specimen, a special holder (Fig. 1) was designed for the scanning electron microscope that allows one to view standard transmission EM grids in the SEM. After being studied in the scanning electron microscope, the grid is removed and placed in the transmission EM for correlative study. A holder was also constructed which allowed standard glass microscope slides to be viewed in the SEM, thus permitting direct correlation between the light microscope and the SEM.

Details of preparation are discussed under the separate materials. All scanning electron micrographs were taken using the instrument at Donner Laboratory, a Japan Electron Optics Co. Model JSM scanning electron microscope.

The sample preparation techniques were as follows:

1) Tobacco mosaic virus. Paracrystalline (birefringent) needles were precipitated from an isolated preparation of a common strain of tobacco mosaic virus (TMV) in distilled

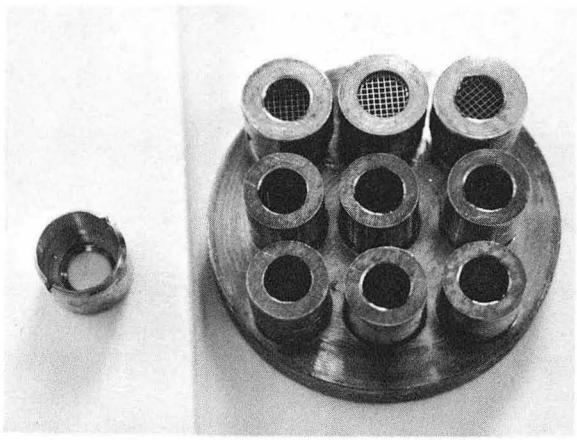

Fig. 1. Holder used for viewing standard transmission electron microscope grids in the scanning electron microscope.
XBB 681-376

water.* Concentrated NH_4Ac-HAc was added in a dropwise fashion to 2 ml of a virus suspension containing approximately 2 mg/ml of virus. The concentrated NH_4Ac-HAc solution was made by adding glacial acetic acid to saturated ammonium acetate until the pH was reduced to 4.7. Specimens for scanning and transmission electron microscopes were placed on Formvar-coated grids, frozen in liquid nitrogen, lyophilized, and coated on the top surface with carbon. A negatively stained preparation was obtained by forming paracrystalline needles in a solution containing 1% phosphotungstic acid (final concentration) and then air drying the sample. The sample for phase contrast light microscopy was prepared by EtOH drying of glutaraldehyde-fixed paracrystals.

2) Polystyrene latex 880 Å diameter spheres. This material is very familiar to electron microscopists and can be obtained from the manufacturer (Dow Chemical Co., Bioproducts Dept., Midland, Michigan). The diameter of 880 Å has a standard deviation of 80 Å. A suspension of 10% solids in deionized water was diluted and a drop placed on a Formvar-coated grid. Following air drying, the specimen was coated with a layer of Pt-Pd alloy evaporated at normal incidence to the surface in a manner otherwise similar to that used for shadowing specimens for transmission electron microscopy.

3) Serum lipoprotein macromolecules. Human serum lipoproteins were isolated by centrifugal techniques (3), fixed and stained with 1% buffered (pH 7.4) osmium tetroxide. The diameter of these particles prepared in this way has been measured using the transmission electron microscope and averaged 350 Å (4).

4) Collagen fibrils. The collagen material was prepared for scanning electron microscopy by the sectioned tissue technique (5), from rat skin. The same section was observed in both the SEM and the light microscope by using standard-size glass microscope slides in a specially adapted holder in the SEM. The sections were coated with an evaporated layer of Pt-Pd alloy for conduction, but this did not seem to interfere with subsequent viewing with the light microscope.

*The authors wish to thank Prof. C. A. Knight of the Department of Molecular Biology for supplying the virus strain used.

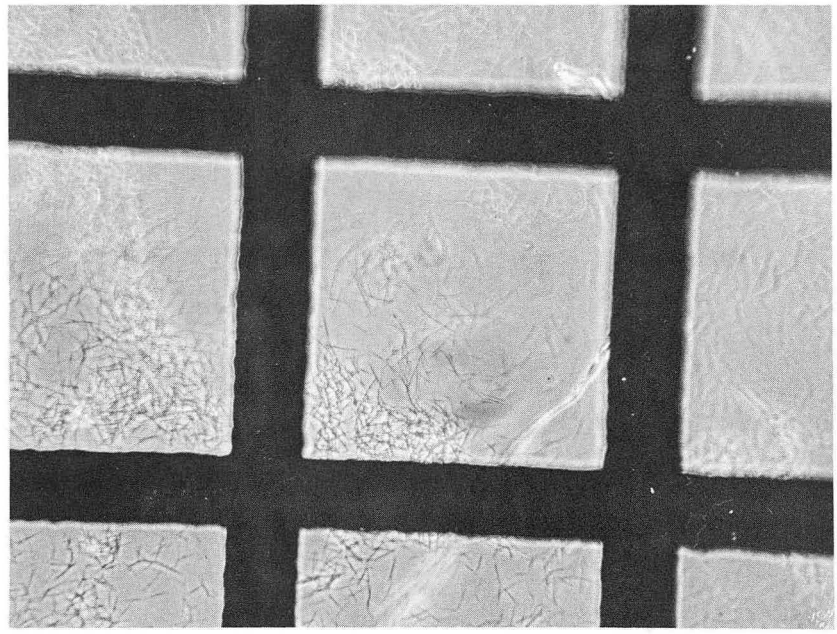

Fig. 2. Tobacco mosaic virus (TMV) paracrystals. Phase contrast light microscopy. × 175.
XBB 681-304

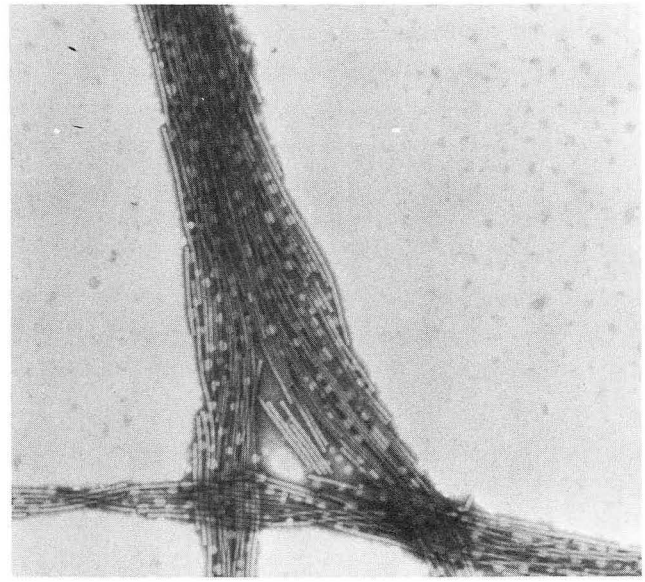

Fig. 3. TMV paracrystals. Negative stain transmission electron microscopy. × 30,000. Center-to-center distance between virus particles is 240 Å. Globular electron-transparent regions are probably due to the deposit of NH_4Ac during staining. Those deposits subsequently volatilized.
XBB 681-305

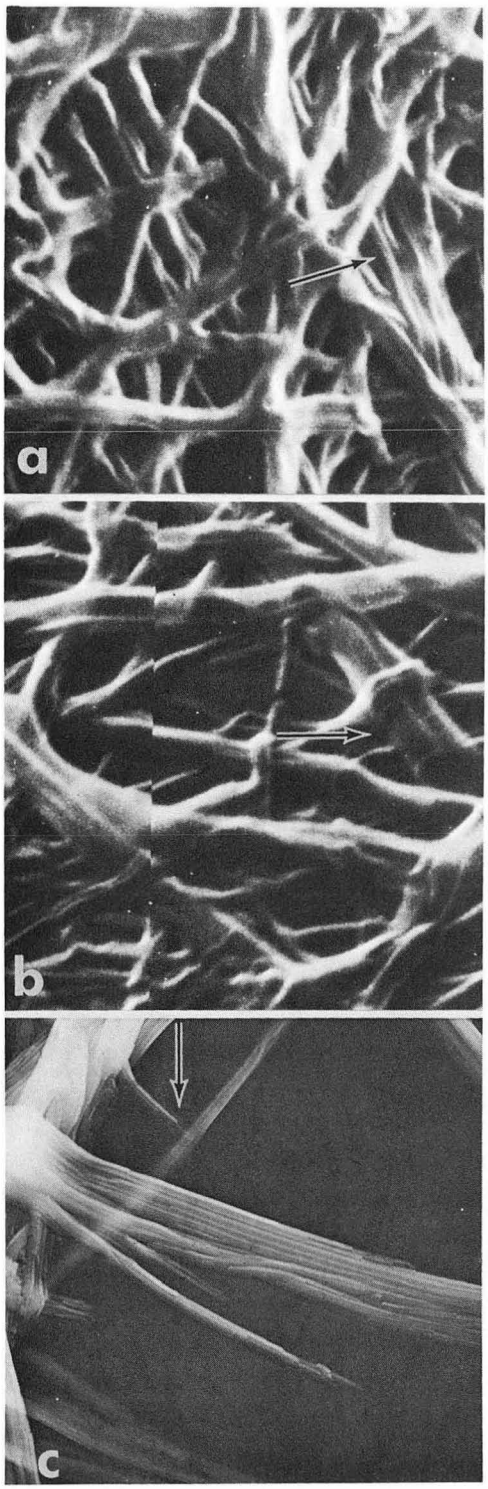

Fig. 4. TMV paracrystals. Arrows point to areas where individual particles can be seen. (a) and (b) Scanning electron micrographs. × 22,000. (c) Transmission electron micrograph. × 22,000

XBB 679-5295, XBB 679-5292, and XBB 681-306

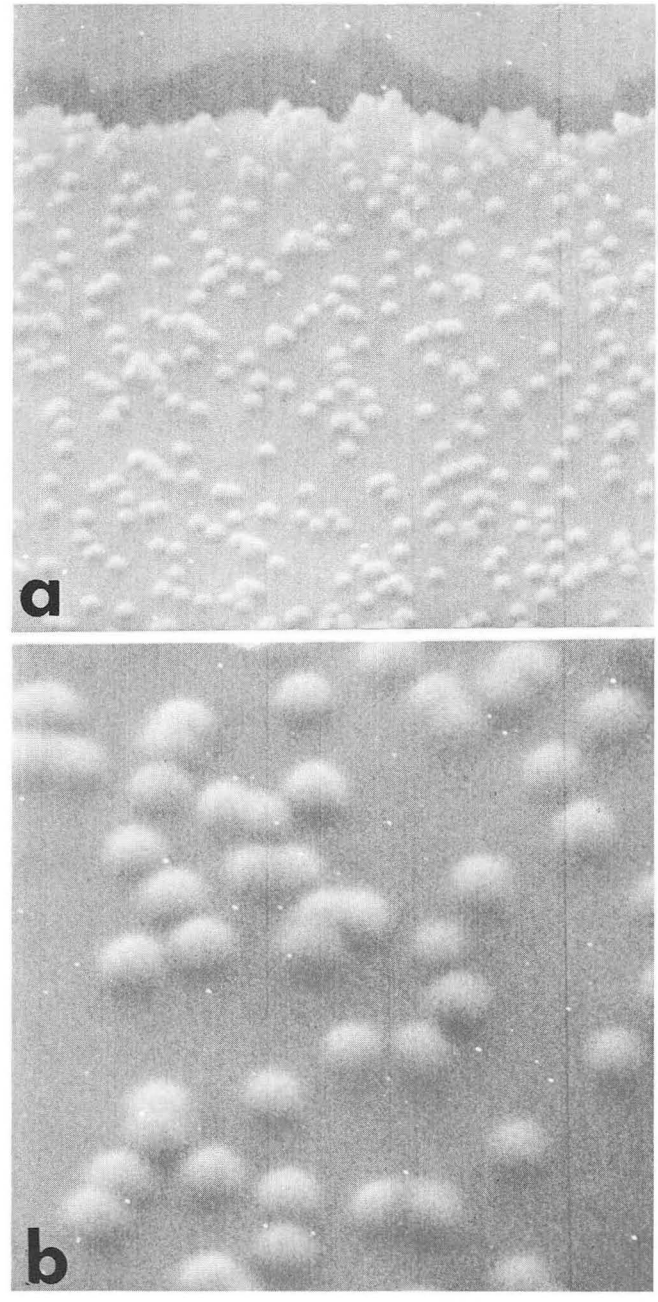

Fig. 5. Polystyrene latex particles. 880 Å diameter, scanning electron microscope. (a) × 26,000, (b) × 75,000. XBB 679-5095 and XBB 679-5093

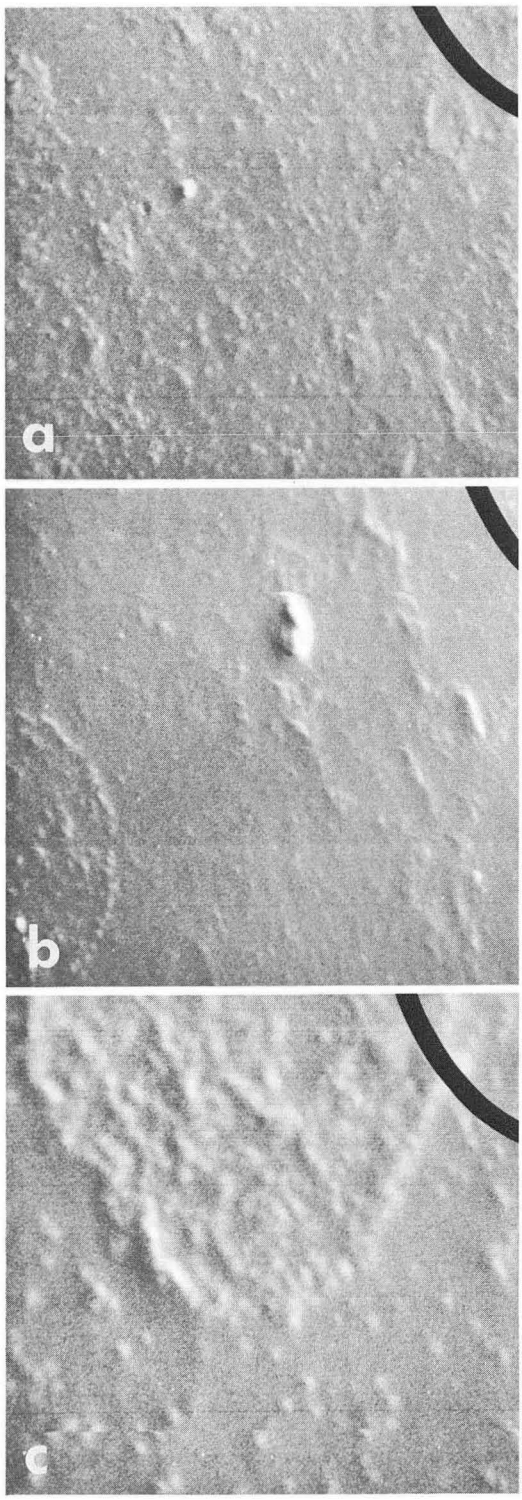

Fig. 6. Serum lipoprotein macromolecules. 350 Å diameter, (a) × 20,000, (b) × 20,000, (c) × 60,000.

XBB 679-5226, XBB 679-5213, and XBB 679-5228

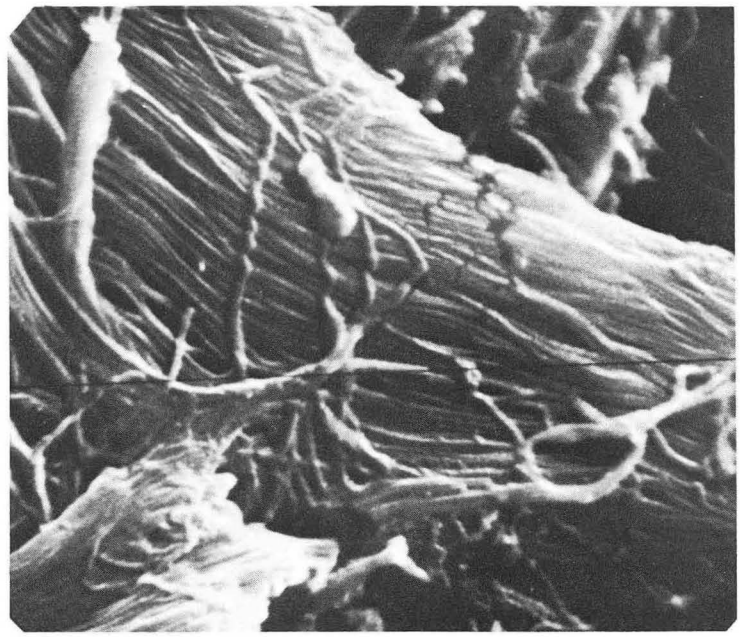

Fig. 7. Collagen fiber and filaments. Scanning electron microscope. × 10,000. The dimensions of the filaments have been reported as about 200 Å diameter with 100 Å spacing between filaments (6). The beading seen on the filament represents the characteristic striation width of about 500 Å. Correlations can be made directly to standard transmission electron micrographs (7). XBB 681-307

RESULTS AND DISCUSSION

The scanning electron micrographs of these materials along with correlative light and transmission electron micrographs are shown in Figs. 2 through 7. Comments concerning the dimensions and other information found in each image are contained in the figure legends. The point-to-point resolution shown is about 300 Å.

It is hoped that photographs of familiar biological subjects will help to serve as reference material for biologists testing the performance of a scanning electron microscope and may also demonstrate the kinds of information available at this time through the use of this instrument.

SUMMARY

Scanning electron micrographs of familiar biological specimens (tobacco mosaic virus, polystyrene latex spheres, lipoprotein macromolecules, and collagen) are presented as reference material for testing the performance of a scanning electron microscope and to demonstrate the kinds of information available at the present time with this instrument.

ACKNOWLEDGMENT

This work was supported by the U. S. Atomic Energy Commission.

REFERENCES

1. Hayes, T. L.; Pease, R. F. W., and McDonald, L. W.; Applications of the scanning electron microscope to biologic investigations. Lab. Invest. 15: 1320-1326, 1966.
2. Hayes, T. L., and Pease, R. F. W.; Applications of the scanning electron microscope in biology and medicine, in Advances in Biological and Medical Physics, Vol. 12, edited by John H. Lawrence and John W. Gofman, New York, Academic Press, Inc., 1968.
3. Lossow, W. J.; Lindgren, F. T.; Murchio, J. C., and Jensen, L. C.; Subfractionation of $S_f > 400$ serum lipoproteins by successive, cumulative, density gradient centrifugation, in this Report.
4. Hayes, T. L., and Hewitt, J. E.; Visualization of individual lipoprotein macromolecules in the electron microscope. J. Appl. Physiol. 11: 425, 1957.
5. McDonald, L. W.; Pease, R. F. W., and Hayes, T. L.; Scanning electron microscopy of sectioned tissue. Lab. Invest. 16: 532, 1967.
6. Bryant, W. M.; Greenwell, J. E., and Weeks, P. M.; Alterations in collagen organization during dilation of the cervix uteri. Surg. Gynecol. Obstet. 126: 27, 1968.
7. Porter, K. R., and Bonneville, M. A.; Plate 13 in An Introduction to the Fine Structure of Cells and Tissues, Philadelphia, Lea & Febiger, 1963.

Cardiac Catheterization Using a Radioactive Catheter and the Scintillation Camera

Donald C. Van Dyke, Hal O. Anger, Frederick Duffy, Stanley Higashino and Joyce Wilson

The speed and resolution of the scintillation camera (1, 2) are such that the course and movements of a catheter labeled with a gamma emitter can readily be seen on the camera's oscilloscope screen. By projecting this image on a roentgenogram of the patient's chest, one can visualize passage of the catheter through the vascular channels of the heart in the same way that a radio-opaque catheter is seen under fluoroscopy. Anatomic information is provided by a single roentgenogram of the chest, resulting in a significant reduction in radiation dose to the patient.

In the hands of experts and in spite of all efforts to keep fluoroscopy time to a minimum, the usual diagnostic cardiac catheterization procedure requires a minimum of 7 minutes of fluoroscopy time. With up-to-date image intensifier and field of view as restricted as practicable, the patient receives an entrance dose of approximately 0.3-0.5 R/min to a large part of the chest, 90-95% of which is absorbed (3). In children such a dose of irradiation is justifiable when it provides the only approach to successful treatment of the disease, but it would be desirable to further reduce the irradiation dose by an order of magnitude.

This report will attempt to evaluate the usefulness of the labeled catheter technique for cardiac catheterization on the basis of a limited trial in children conducted by the staff of the Donner Laboratory and the cardiology unit of the Children's Hospital Medical Center, Oakland, California.

MATERIALS AND METHODS

The Donner Laboratory scintillation camera, which has a 9- to 10-in. field of view, has been described in detail elsewhere (1, 2). The camera was placed beside the fluoroscope so that the patient could be viewed with either instrument simply by moving the fluoroscope table, Fig. 1. This arrangement allowed the physician to check the position of the catheter by the standard fluoroscopic technique and to utilize fluoroscopic cineradiography. The 4-in. scintillation camera oscilloscope screen was enlarged to life size by means of closed circuit television, Fig. 2. Radio-opaque gamma-emitting markers were placed in the suprasternal notch and over the xiphoid, and a 6-ft X ray of the chest was taken. The magnification and orientation of the television image was adjusted by placing the X ray over the television monitor so that the radio-opaque markers were superimposed on the gamma-emitting scintillations, Figs. 2-4.

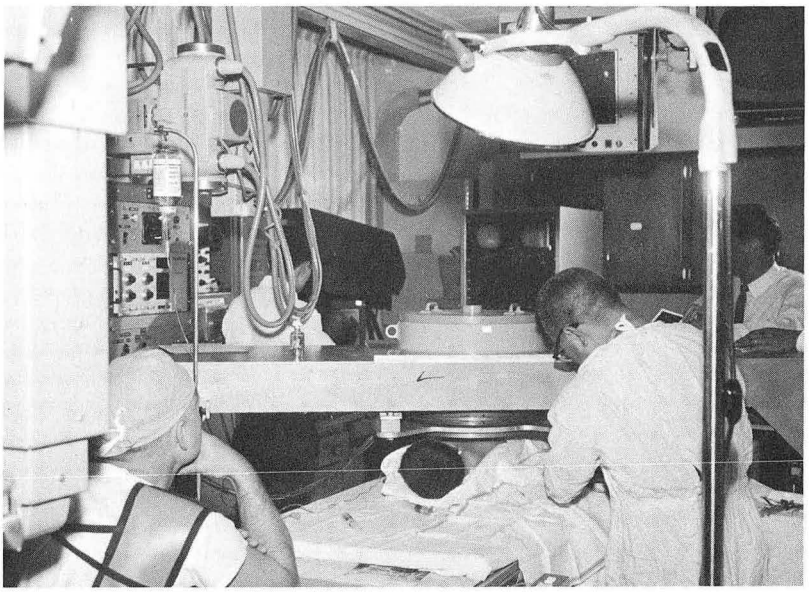

Fig. 1. The patient is positioned under the scintillation camera detector head during the catheterization procedure. XBB 670-5749

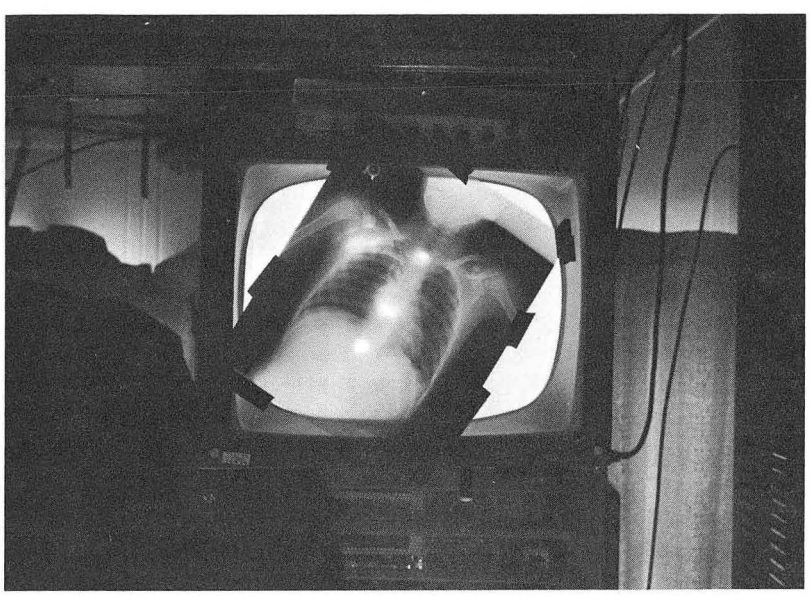

Fig. 2. A closed circuit television displays the camera image of the catheter life-size. By placing a roentgenogram of the patient's chest over the screen the catheter is seen superimposed on the film. The dots in the sternal notch and over the xiphoid are the radioactive markers used to ensure proper orientation. XBB 670-5736

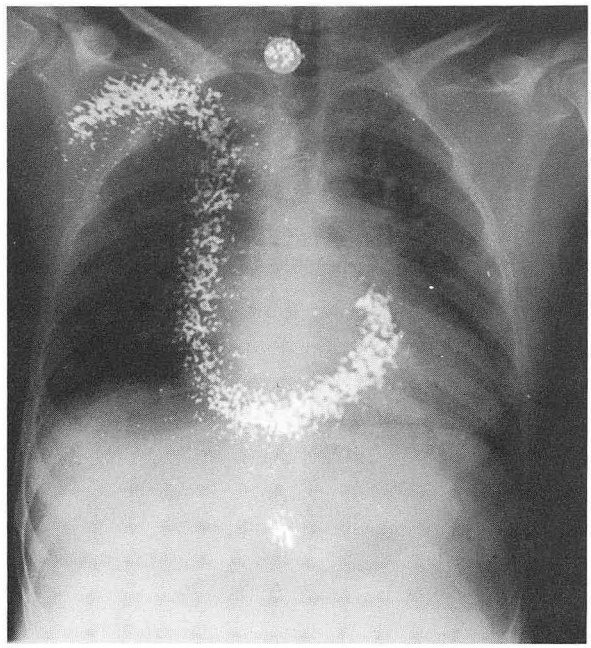

Fig. 3. Labeled catheter seen through the roentgenogram fixed over the television screen. Exact magnification and orientation obtained by superimposing images of the radio-opaque, radioactive markers placed above the sternal notch and over the xiphoid.

XBB 683-1013

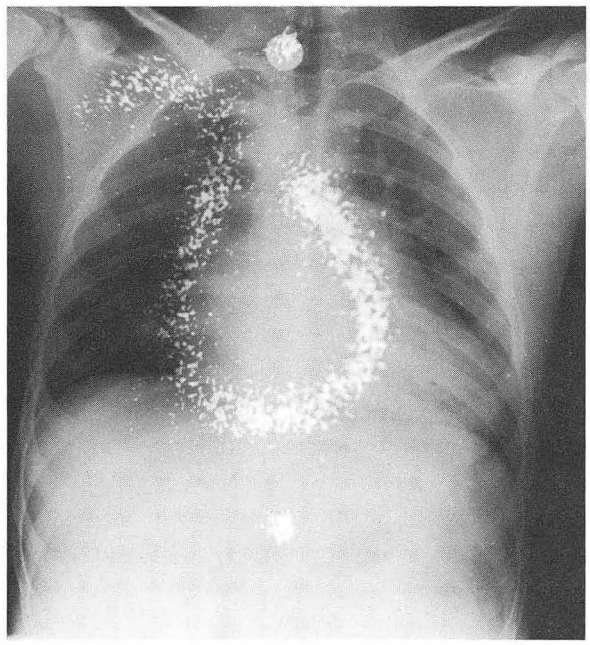

Fig. 4. Same as Fig. 3 with catheter advanced into the pulmonary artery.

XBB 683-1014

Standard commercially available cardiac catheters were labeled by drying a solution of cerium-141 on the surface and sealing it with two coats of varnish. From 1-3 mCi of cerium-141 were applied, the amount depending on the length of the labeled region. The most satisfactory distribution of label was 20-30 cm long with more at the tip.

RESULTS

Following initial studies in dogs and monkeys, the scintillation camera was moved to the cardiology unit of Children's Hospital for evaluation of the technique in children undergoing routine cardiac catheterization for diagnostic purposes. The technique was used by two physicians in five routine cases. Three were not successful because of technical difficulties with the labeled catheter itself: either proper size was not available or there was insufficient label for clear visualization. In the two cases where a well-labeled catheter of the proper size was available, each of the participating physicians, who were skilled in catheterization but unfamiliar with the scintillation camera, had no difficulty in placing the catheter with complete assurance. The two successful cases done by this technique were an 8-year-old boy with a pre-catheterization diagnosis of valvular pulmonic stenosis and a 17-1/2-year-old boy with ventriculo-septal defect and pulmonic stenosis (Figs. 3 and 4).

DOSE MEASUREMENTS

Radiation dose from the G. E. Fluoricon fluoroscope with image intensifier was measured* with Victoreen ionization chambers and dental X-ray film, using lucite phantoms. The entrance dose was 560 mR/min. The exit dose was 10% for a small and 5% for a large child. The dose measured is 70% higher than that reported by Evans (3).

The radiation dose from the cerium-141 labeled catheter used in this study is calculated to be 0.09 rad/min to the vessel wall where the catheter touches the wall, if 3 mCi of cerium-141 is contained within the catheter and there is 0.3 mm of absorber to absorb internally converted electrons from the cerium. At a point 2 in. from the catheter the tissue dose is calculated to be 1.5 mR/min.

A summation of the total dose to the patient from a complete cardiac catheterization study using conventional fluoroscopy, image-amplification fluoroscopy, or a labeled catheter and the scintillation camera is given in Table 1, modified from Evans (3). Included in the table are the dose measurements from image-amplification fluoroscopy given by Evans, as well as the higher dose from image-amplification fluoroscopy measured in this study.

DISCUSSION

On the basis of this limited trial, both physicians who compared the new technique with their routine fluoroscopic procedure were satisfied that placement of the catheter by the new method presented no difficulty. Successful application of this technique requires properly labeled catheters in a variety of sizes and lengths.

---

*The authors are indebted to William Nolan of the Lawrence Radiation Laboratory for the dose measurements.

Table 1. Pediatric cardiac evaluation (15-cm infant).

Procedure	Number of roentgens			
	Conventional fluoroscopy	Image-amplification fluoroscopy		Scintillation camera + image-amplification fluoroscopy
		Evans	CHMC	
Chest films (4 views)	0.12	0.12	0.12	0.15*
Fluoroscopic screening (3 min)	9.00	0.90	1.50	0.90
Cardiac catheterization (7 min)	21.0	2.10	3.50	0.03†
Cineradiography (10 sec)	0.20	0.20	0.30	0.30
Total	30.3	3.3	5.4	1.4

*One extra chest film with two radio-opaque and gamma-emitting sources for superimposition of images.

†1.5 mR/min 2 in. from catheter (20 min for the total procedure since the catheter cannot be turned on and off).

From Table 1 it can be seen that the radiation dose received by the patient when conventional fluoroscopy is used (entry dose: 30 R) is clearly excessive. The use of image-amplification fluoroscopy has reduced the dose by almost an order of magnitude to approximately 4 R/min. The use of the scintillation camera for the catheterization procedure combined with image-amplification fluoroscopy for screening and cineradiography resulted in a total dose of 1.4 R, of which 60% comes from the period of fluoroscopic screening.

Complete evaluation of the labeled catheter-scintillation camera technique will require much more extensive experience than was possible in this pilot study, but the conclusion was that with properly manufactured labeled catheters, no difficulty would be encountered in catheter placement.

Caffey (4) has stated "The most pressing current problem in pediatric radiology is the reduction of hazards to the patient from exposure to ionizing radiation." Of all radiologic procedures, cardiac catheterization under fluoroscopy contributes the largest single source of exposure to a child. In the future the scintillation camera or similar devices may provide an alternate to fluoroscopy for much of the procedure of cardiac catheterization.

ACKNOWLEDGMENTS

This work was supported in part by the U. S. Atomic Energy Commission and in part by Grant 5ROICA08370 from the National Cancer Institute of the National Institutes of Health.

REFERENCES AND NOTE

1. Anger, H. O.; Van Dyke, D. C.; Gottschalk, A.; Yano, Y., and Schaer, L. R.; The scintillation camera in diagnosis and research. Nucleonics 23 (1): 57, 1965.
2. Anger, H. O.; Gamma-ray and positron scintillation camera. Nucleonics 21 (10): 56, 1963.
3. Evans, John A.; Hazards of diagnostic radiology in pediatrics. Am. J. Surg. 107: 400-405, 1964.
4. Caffey, J.: Pediatric X-Ray Diagnosis, 4th ed., Chicago, Yearbook Publishers, Inc., 1961.

Frederick Duffy, Stanley Higashino, and Joyce Wilson are with the Children's Hospital Medical Center, Oakland.

Microdomain Structure-Analysis of Biological Specimens by Electron Diffraction

Robert M. Glaeser

INTRODUCTION

The electron microscope is an instrument that is well suited for electron diffraction studies on the structure of thin specimens. By varying the focal lengths of the electromagnetic lenses it is possible to vary the effective camera length of a single instrument by a factor of 10^4. This flexibility allows one to examine ordered or crystalline structures with repeat distances varying from less than 1.0 Å to more than 1000 Å.

Electron diffraction has numerous practical advantages in the study of complex biological structures. One principle advantage results from the fact that electrons are scattered by the specimen with much greater efficiency than are X rays. This makes it possible to obtain diffraction data from 1) sub-microscopic crystals of materials that are difficult to crystallize as samples large enough to be practical for X-ray work, 2) small domains of large specimens with good local crystallinity but poor long-range order (e.g., oriented fibers), 3) internally-ordered structures that cannot themselves be crystallized or stacked together. Perhaps one of the most significant problems open to investigation by electron diffraction is that of the structure of cell membranes. A specimen that is but one membrane thick should be well suited for analysis by electron diffraction.

Other advantages include 1) the speed of data recording (seconds or minutes as compared with hours or days for X-ray diffraction), due in part to the fact that electrons are recorded with much greater efficiency than X-rays are, 2) the fact that the diffracted beams can be focused by the electromagnetic lenses to give high-resolution, directly visual information about the structure of the specimen.

This report describes the current results of preliminary studies which are being carried out in order to determine the feasibility of obtaining 1) diffraction patterns from single cell membranes and 2) high-resolution diffraction data from crystalline macromolecules. Results obtained with "model" specimens have revealed a number of instrumental limitations of the conventional electron microscope for such studies. The data reported here indicate that one of the most urgently needed improvements would be a data-monitoring device that is significantly more sensitive or more efficient than the conventional fluorescent screen.

THEORETICAL

The electron microscope is similar to the light microscope in that a periodic specimen

will produce a sharp diffraction pattern in the back focal plane of the objective lens (see Fig. 1), and an enlarged image of the diffraction pattern can be formed by a second lens which is set so that its object plane corresponds to the back focal plane of the objective lens.

In order to understand the formation of the diffraction pattern one must first recall that the back focal plane is defined as the two-dimensional surface upon which parallel rays are focused to a point. All rays parallel to the optical axis are brought to focus on the optical axis, and parallel rays at some given angle are all brought to focus at a given point off the optical axis.

A periodic specimen will either transmit radiation in the forward direction without scattering or it will scatter the radiation in discrete angles according to the Bragg equation

$$2 \sin \theta = \frac{\lambda}{d},$$

where

θ = scattering angle,

λ = wavelength of radiation,

d = a given repeat distance.

Thus, each spot in the diffraction pattern corresponds to a bundle of parallel rays scattered by one of the "repeat distances" or crystalline planes in the specimen.

Further along the optical axis the rays are again recombined according to their point of origin (and not according to their scattering angle). This plane of recombination is the image plane of the objective lens. As indicated in Fig. 1, it is common practice to insert a small aperture in the back focal plane in order to prevent the scattered radiation from reaching the image plane. The purpose for doing this is to increase the contrast in the image.

It is perhaps poorly appreciated in biological electron microscopy that electrons scattered from structures with repeat distances of 10 Å or more will pass through apertures 20 μ or more in diameter. This coherently scattered radiation will have a certain phase shift relative to the central, unscattered beam. When the two are recombined on the image plane of the objective lens, certain interference patterns will result. This interference contrast or "Fourier contrast" can be important in determining the contrast, and hence the apparent structure, of most ordered biological specimens. As a consequence, the precise interpretation of electron microscope images obtained with ordered biological structures requires the recording of the diffraction pattern as well as the direct image from the same area of the specimen.

RESULTS

In preparing for diffraction experiments with cell membranes one may expect to observe ordered structures with repeat distances of approximately 50 to 100 Å. The diffraction maxima thus occur at very small angles. The three-lens method of Ferrier and Murray (1) provides very good resolution of such large repeat distances. A number of specimens with large repeat distances were tested, and good diffraction patterns were obtained from an hexagonal array of 880 Å polystyrene spheres, Fig. 2, and from striated frog muscle in thin section,

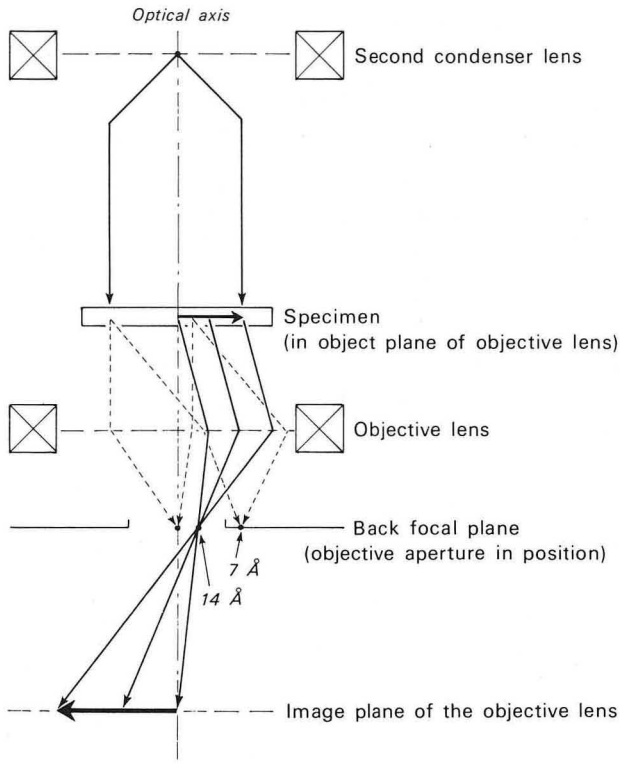

Fig. 1. Schematic diagram of the second condenser lens and the objective lens of an electron microscope, showing the formation of a diffraction pattern in the back focal plane and the subsequent formation of an image partially depleted of scattered radiation.
DBL 682-4562

Fig. 3. Attempts have been made to obtain diffraction patterns from the layered-membrane system of frog retinal rods, but these have not been successful so far, in spite of the fact that this is a highly ordered system, Fig. 4.

All low-angle diffraction experiments were performed with a 15 μ diameter condenser aperture. This limits the area of the specimen that is illuminated to approximately 10 μ in diameter, and greatly improves the sharpness of the diffraction patterns with samples that have good local crystallinity but poor "macroscopic" order.

At the same time a low-angle diffraction pattern from such a small area is so weak that it is not visible on the fluorescent screen. This makes it impossible to scan the specimen in the diffraction mode, looking for highly ordered structures. This is not a serious problem if the specimen has a uniform degree of order over relatively large areas, as with the polystyrene spheres and the striated muscle. It is a serious problem, however, if the highly ordered domain is embedded in a large area of non-crystalline or amorphous structure, as with the retinal rod preparation. It is also a serious problem if one wishes to obtain diffraction patterns from single membranes supported on some kind of thin film. These current results seem to indicate that some type of image intensification will be required in order to monitor the diffraction pattern while the specimen is being scanned for areas of interest.

A metal-shadowed carbon-replica technique has been used by the author to examine cell surface structure (2, 3), and these data suggest that the erythrocyte membrane has a modular

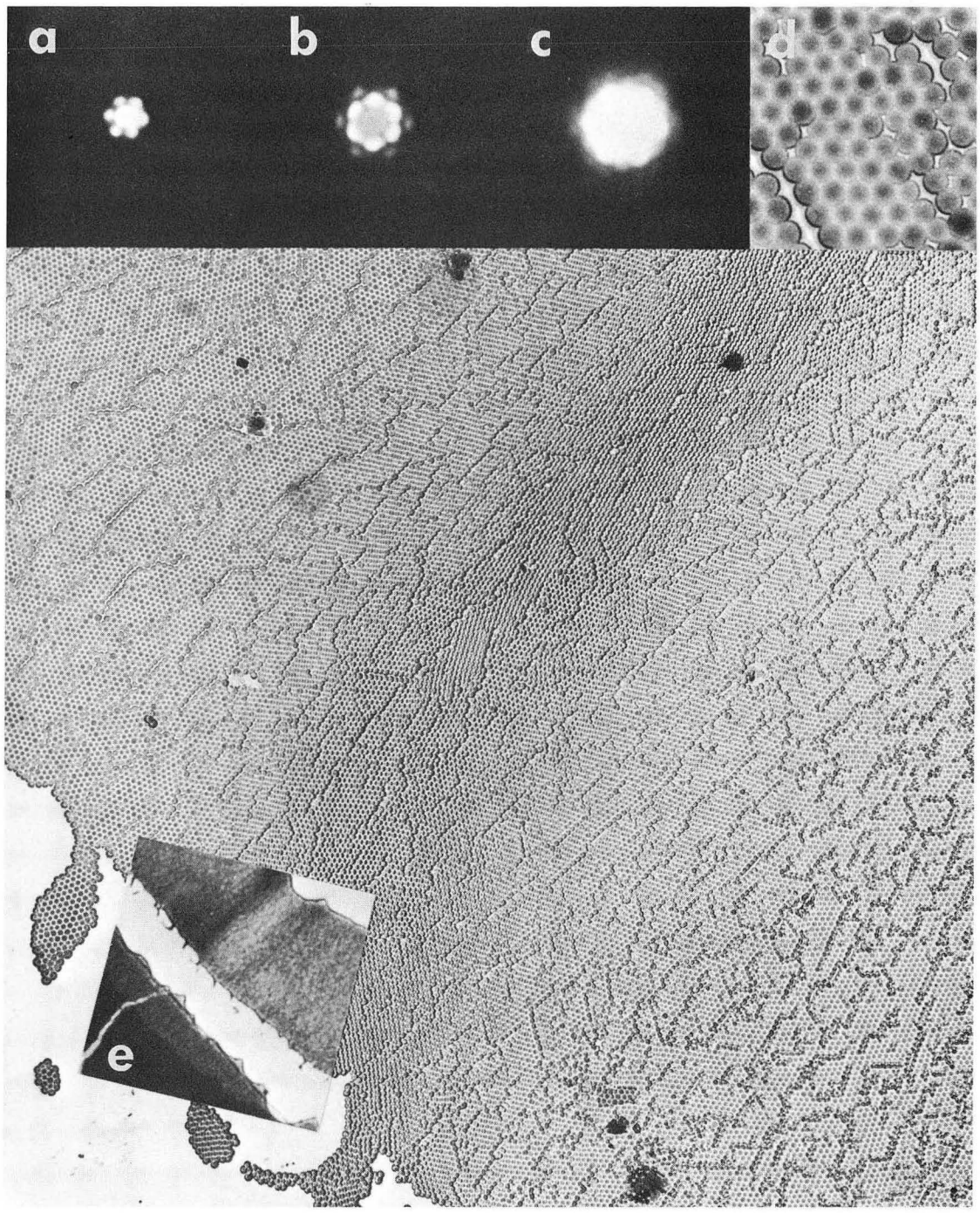

Fig. 2. 880 Å polystyrene latex spheres in a two-dimensional, hexagonal array. The average center-to-center spacing is actually 670 Å, presumably due to compressional effects in packing. Numerous packing faults are evident.

Insets (a), (b), and (c) are low-angle diffraction patterns recorded with different exposure times, inset (d) is a high-magnification photograph of a hexagonal domain of the sample, and inset (e) is a very low power micrograph of the two-dimensional sheet.

XBB 681-510

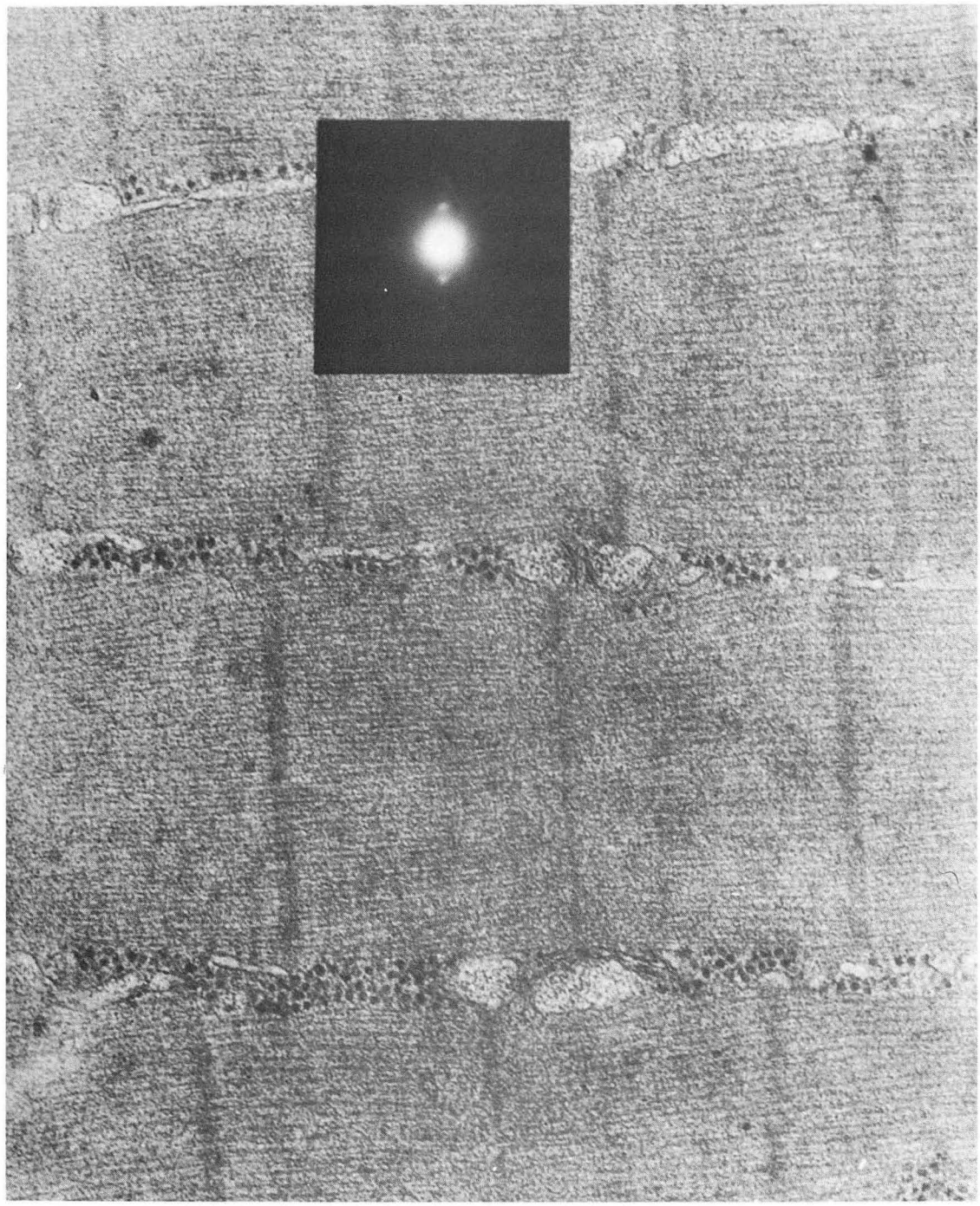

Fig. 3. Frog striated muscle in longitudinal thin section. The inset shows low-angle diffraction maxima from a two-dimensional hexagonal lattice of filaments with a unit cell dimension of 450 Å.

XBB 681-511

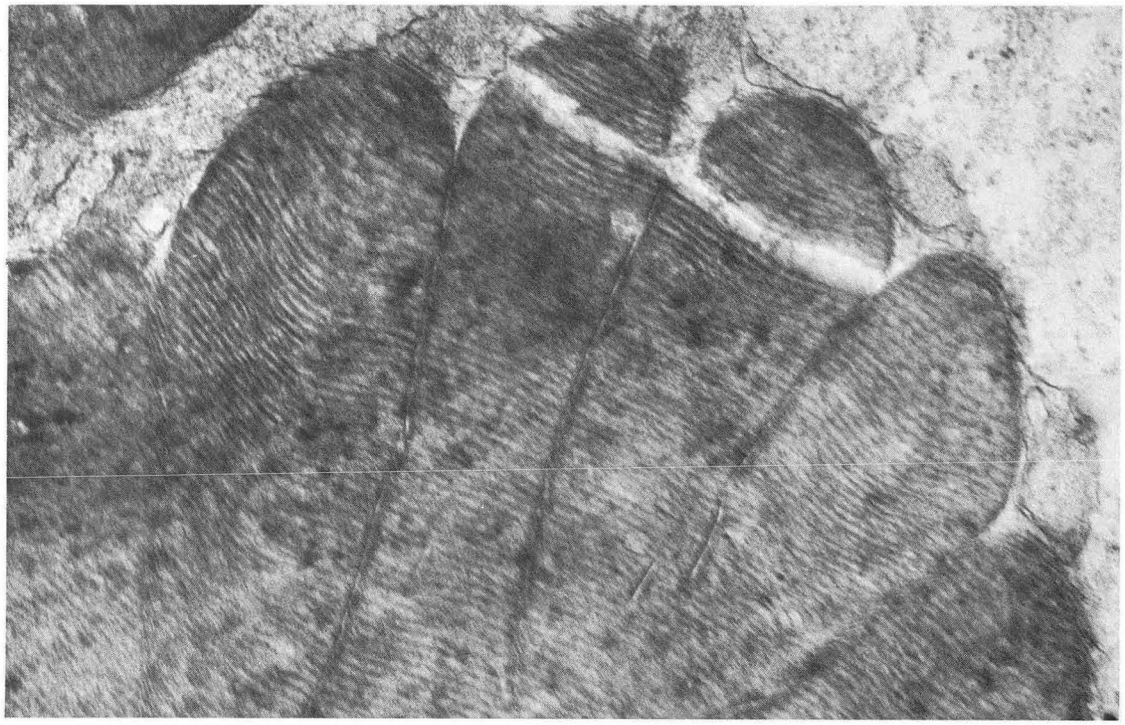

Fig. 4. Transmission electron micrograph of the layered system of membranes in the outer segment of frog retinal rods.
XBB 681-517

or subunit structure. Figure 5 is an electron micrograph of such a chromium-shadowed replica, Fig. 6 is the wide-angle diffraction pattern formed by the randomly ordered crystalline grains of chromium, and Fig. 7 is a dark-field image of the shadowed replica, produced by a small portion of the electrons scattered into the (1, 1, 1) Bragg reflection. The grain size over the cell surface is the same as that over the smooth background. This shows that the modular appearance of the RBC membrane is not an artifact due to the formation of unusually large metal grains on the biological surface.

High-resolution structure analysis of crystalline macromolecules ought to be possible by operation of the microscope in the conventional "selected-area diffraction" mode (4). The author is not aware of any successful attempt to obtain high-resolution diffraction patterns from crystalline proteins, nucleic acids, etc., although high-resolution data have been obtained from paraffins (5), cellulose (5), fibers of polyadenylic acid (6), and synthetic polypeptides (6, 5). Low-angle diffraction patterns have been obtained from crystalline ferritin and catalase (1).

In view of the apparent failure to obtain high-resolution electron diffraction data from crystalline proteins, a series of experiments were begun with a variety of crystalline amino acids. All have given strong diffraction patterns, but the greatest success to date has been with ℓ-glutamic acid, air-dried at room temperature from distilled water on a Formvar-

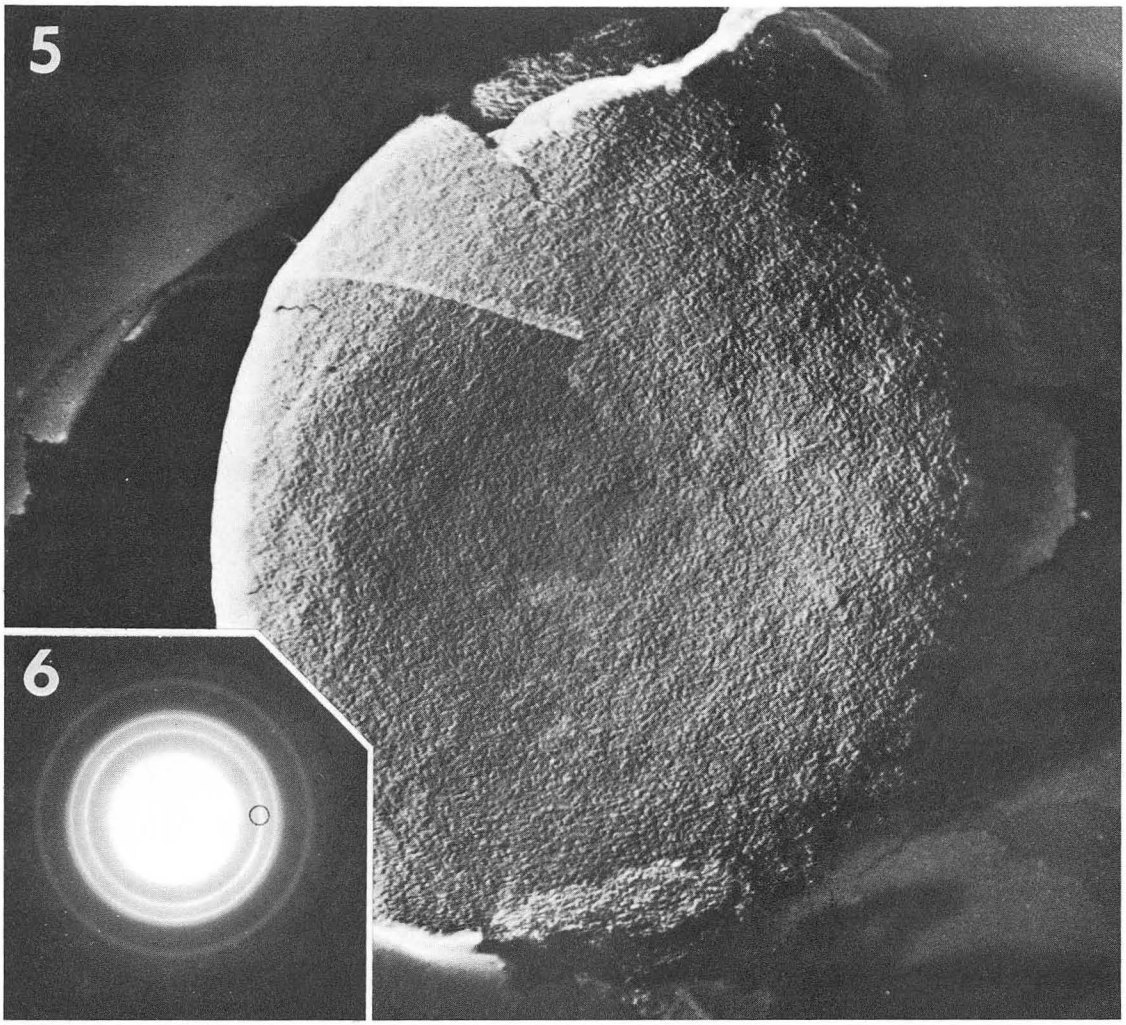

Fig. 5. Transmission electron micrograph of an OsO_4-fixed, freeze-dried human RBC surface: chromium-shadowed carbon replica.

Fig. 6. Wide-angle diffraction pattern produced by metal grains, approximately 25 Å in diameter, covering the carbon replica in Fig. 5. The circle indicates the approximate source of scattered electrons which were used to form the dark-field image in Fig. 7.

XBB 681-516

coated E. M. specimen grid, and Fig. 8 is an example of the kind of diffraction pattern obtained with the glutamic acid samples in the Hitachi HU11 microscope, and Fig. 9 is an example of a valine diffraction pattern obtained with the JEOL 1-MeV electron microscope.

In order to obtain such diffraction data it has been found necessary to be unusually careful not to damage the specimen by too intense an electron beam. In the Hitachi HU11 it was found necessary to use a small condenser aperture (15 μ is satisfactory; 150 μ is too large), a

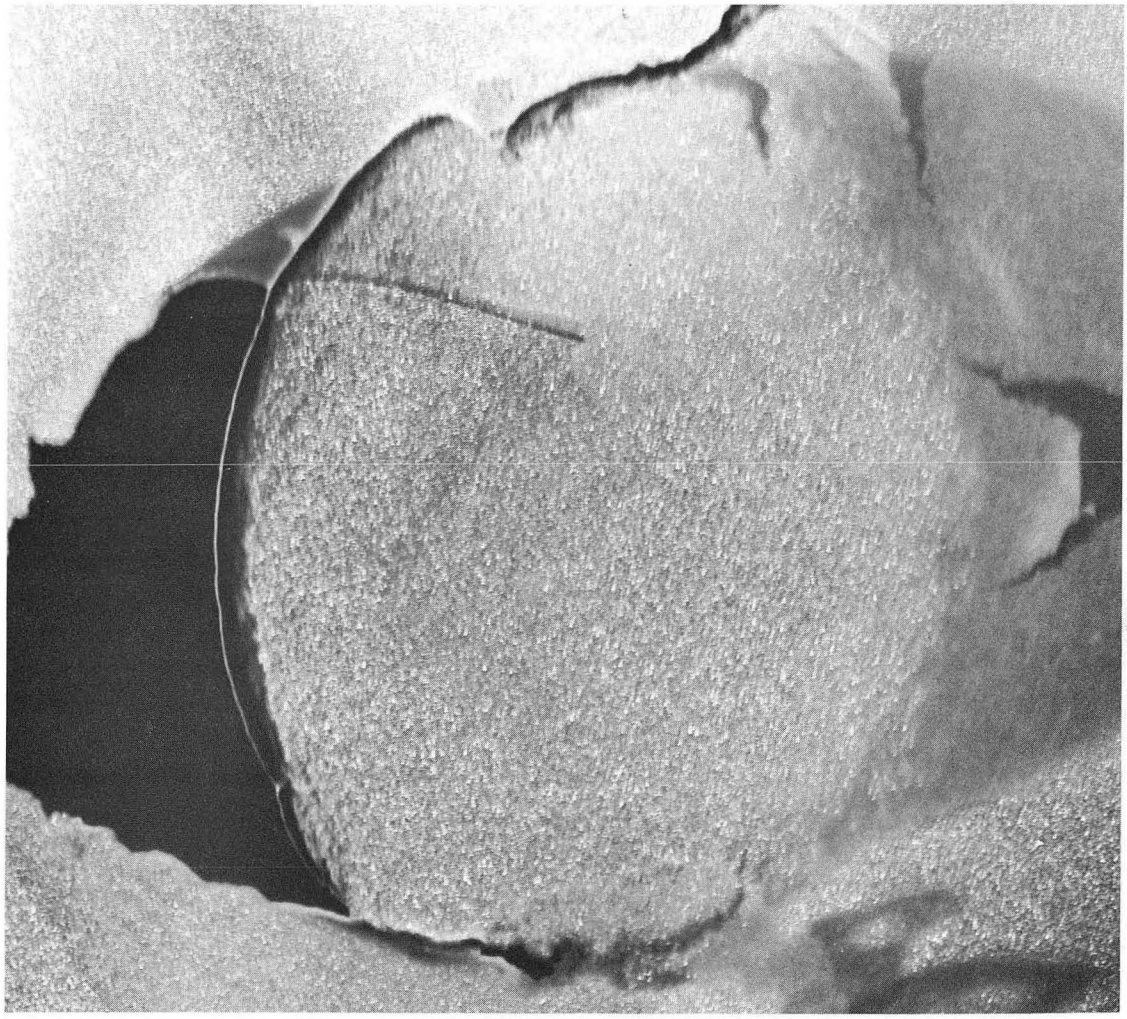

Fig. 7. Dark-field electron micrograph of RBC surface replica. The objective aperture was positioned so as to block the central, transmitted beam and to admit a portion of the (1, 1, 1) Bragg-reflected ring onto the image plane of the objective lens.

XBB 681-519

minimum obtainable beam current, the first condenser lens set at maximum defocus, and the second condenser lens at near maximum defocus. Deviation from these conditions results in fading of the diffraction pattern over the period of minutes or even seconds; operation of the microscope in the way customary for normal transmission microscopy produces instantaneous fading of the diffraction patterns of crystalline amino acids.

On the basis of the present results with the crystalline amino acids it seems almost

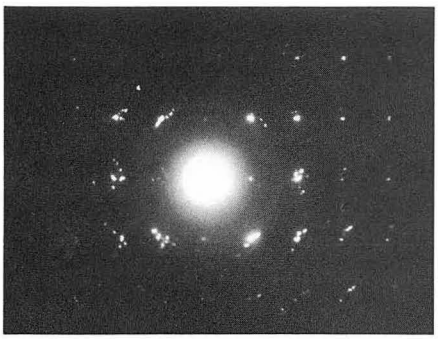

Fig. 8. Wide-angle diffraction pattern of ℓ-glutamic acid. Hitachi HU11 electron microscope, 75 kV, 15 μ condenser aperture. XBB 681-514

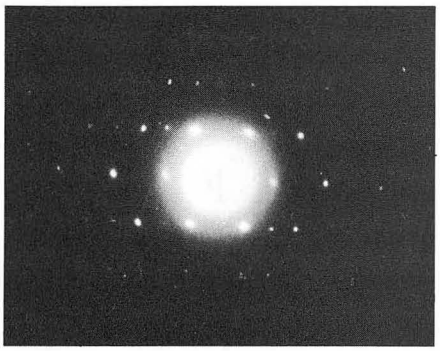

Fig. 9. Wide-angle diffraction pattern of ℓ-valine. JEOL JEM-1000 electron microscope (sample sent to Tokyo through the courtesy of Mr. Steven Pinson). XBB 681-518

certain that if the electron microscope is operated at a level of illumination sufficient to allow careful focus at high magnification (say greater than 20,000 ×), then most, if not all, biological structure will be randomized at the level of 10 Å and less. It is self-evident that when a high-resolution diffraction pattern cannot be obtained from a crystalline or ordered array of macromolecules, then it is hopeless as well to expect to obtain a high-resolution image. Furthermore, experimental conditions which do not allow high-resolution images of a crystal will not be any more suitable for producing high-resolution images of single (free) macromolecules.

Our present data would suggest that biological specimens appear to have random contrast below 10 to 20 Å because the structure is in fact randomized by too intense a level of illumination. The use of some form of image intensification during focus and/or the use of higher accelerating voltages may provide the way for examining crystalline macromolecules without destroying them at the same time.

ACKNOWLEDGMENTS

This work was supported in part by the U. S. Atomic Energy Commission and in part by U. S. Public Health Service grant GM 15129-01.

The author acknowledges active participation in this work by Prof. Gareth Thomas, Department of Mineral Technology and Inorganic Materials Research Division, Lawrence Radiation Laboratory.

REFERENCES

1. Ferrier, R. P., and Murray, R. T.; Roy. Microscop. Soc. 85 (3): 323, 1966.
2. Glaeser, R. M.; Hayes, T. L.; Mel, H. C., and Tobias, C. A.; Exp. Cell Res. 42: 467, 1966.
3. Glaeser, R. M., and Scott, T. B.; in Proc. E. M. Soc. Amer., 25th Annual Meeting, 1967, p. 120.
4. Alderson, R. H., and Halliday, J. S.; in Techniques for Electron Microscopy, edited by D. H. Kay, Philadelphia, F. A. Davis Co., 1965.
5. Vainstein, B. K.: Diffraction of X-Rays by Chain Molecules, New York, Elsevier Publishing Co., 1966.
6. Parsons, D.; in 6th International Congress for Electron Microscopy, Kyoto, 1966, p. 121.

Structure of Human Serum Lipoproteins as Observed with the Electron Microscope after Negative Staining

Gertrude M. Forte, Alex V. Nichols and Robert M. Glaeser

INTRODUCTION

Human serum lipoproteins exhibit a wide range in their physical and chemical properties such as density, particle size, molecular weight, and lipid and protein composition (14, 3). Ultracentrifugal analysis shows that they fall naturally into several groups which may be specified by either density or rate of flotation range. The four major groups of human serum lipoproteins are: 1) high-density lipoproteins (HDL) with densities of 1.063-1.20 g/ml, 2) low-density lipoproteins (LDL) with densities of 1.006-1.063 g/ml and flotation rates of S_f 0-20, 3) very low density lipoproteins (VLDL) with densities of 0.96-1.006 g/ml and flotation rates of S_f 20-400, and 4) lipoproteins frequently called chylomicrons, with densities less than 0.96 g/ml and flotation rates greater than S_f 400. Within each class of lipoproteins there is an apparently continuous spectrum of macromolecules varying in chemical composition and molecular size (15).

Although the chemical composition and physical properties of the various lipoprotein classes have been fairly well defined, comparatively little is known about their shape and structural organization. Of the four major classes, the VLDL and the chylomicron groups have been the ones most extensively investigated by electron microscopy. Kay and Robinson (12) and Hayes et al. (11) have examined lipoproteins within these fractions after osmium fixation and found them to be spherical structures ranging in diameter between 275-5000 Å. Visualization of the LDL and HDL lipoproteins, on the other hand, has been more difficult. Beischer (2) and Hayes, Murchio, Lindgren and Nichols (10) have examined LDL particles after osmium tetroxide fixation, but the data are less definitive than with the VLDL. Comparison of molecular weights calculated from the data of Hayes et al. with those obtained by other physical methods showed the microscope values to be approximately double the other. To explain this discrepancy, the authors proposed that the viewed structures were dimers of LDL macromolecules. Hayes and Hewitt (9) reported that fixed and shadowed preparations of high-density lipoproteins revealed spherical structures 150 Å in diameter; however, this configuration has not been confirmed by other data.

In this investigation the major classes of human serum lipoproteins were examined with the electron microscope, using the negative staining technique. This technique was chosen since Brenner and Horne (5) and Lucy and Glauert (18) have shown that the structure of proteins and phospholipid micelles, respectively, can be visualized with high resolution by its application. Since serum lipoproteins contain both proteins and phospholipids, as well as

other lipids, we expected negative staining methods to be applicable to the determination of 1) lipoprotein sizes and shapes, and 2) existence of possible substructure in the various lipoproteins.

MATERIALS AND METHODS

ULTRACENTRIFUGAL ISOLATION OF LIPOPROTEIN FRACTIONS Samples of venous blood were drawn from nonfasting normal adults. Serum was separated from clotted blood by ultracentrifugal procedures previously described by de Lalla and Gofman (8). Isolation of lipoprotein fractions was performed by preparative ultracentrifugal techniques reported by Lindgren, Nichols and Wills (17). Three ultracentrifugal fractions were obtained: a fraction containing lipoproteins of density < 1.006 g/ml designated S_f 20-10^5 or VLDL-plus-chylomicron fraction; a fraction of density 1.006-1.063 g/ml designated S_f 0-20 or LDL; and a fraction of density 1.063-1.20 g/ml designated HDL. All salt solutions used in adjusting the solution densities for the successive stages of preparative ultracentrifugation were made up with deionized water and contained 100 mg/liter disodium salt of EDTA. Following isolation, each of the lipoprotein fractions was dialyzed for 18 hours with 3 changes against 0.95% ammonium acetate-ammonium carbonate buffer, pH 7.4, containing 5 mg/liter EDTA. Negative staining and electron microscopy immediately followed dialysis.

NEGATIVE STAINING OF PREPARATIONS FOR ELECTRON MICROSCOPY Samples were prepared for microscopy by mixing equal volumes of lipoprotein and 2% sodium phosphotungstate, pH 7.2 (PTA) in a small test tube. Mixing was achieved by gently swirling the tube by hand. The final concentration of the lipoproteins in the suspension was approximately 2 mg/ml. One drop of the suspension was placed on a Formvar-carbon coated grid and allowed to remain there for 60 sec; after this interval excess fluid was removed by touching the edge of the grid with filter paper.

A total of 3 experiments were carried out for each lipoprotein fraction and in each case similar structures were found, indicating that the methods of isolation and staining were reproducible. Electron microscopy of purified ovolecithin (Applied Science Labs., Inc.) suspended by sonication in the ammonium acetate-carbonate buffer and stained by the procedures described above showed lamellar structures similar to those described by Bangham and Horne (1).

ELECTRON MICROSCOPY Electron micrographs were obtained with the Hitachi HU11 electron microscope operating at an accelerating voltage of 75 kV with a 50 μ objective aperture. Instrumental magnifications of 15,000 to 60,000 were used and plates were photographically enlarged 2 to 6 times.

Particle diameters were obtained from the electron micrographs by edge-to-edge measurement of the electron-transparent images. These measurements may be subject to error from at least two sources. In the case of HDL, and probably LDL as well, where the protein content is substantial (approximately 50% and 20% of the lipoproteins, respectively), PTA may be positively staining and thereby reducing our estimates of particle size. Another

source of error might be a flattening or spreading of the lipoproteins during drying. By virtue of its high triglyceride and low protein content, the VLDL-plus-chylomicron fraction might be more subject to this error. Indeed, as shown in the Results section, some particles in this fraction often appear somewhat flattened and amorphous.

RESULTS AND DISCUSSION

STRUCTURE OF THE HIGH-DENSITY LIPOPROTEINS Figure 1 is a representative electron micrograph of the HDL fraction as seen after negative staining with PTA. The lipoprotein structures appear as electron-transparent images set in a dense matrix of PTA. The freestanding particles average 86 Å in diameter (range 74-98 Å) and many have an electron-dense central region (arrows on Fig. 1 indicate these particles). Large aggregations of particles are usually seen as well and probably result from poor dispersion of the particles. The outline of the particle image is not smooth but shows indentations similar to those frequently seen in electron micrographs of negatively stained protein preparations, such as micrographs of carboxydismutase recently published by Branton and Park (4). The net visual impression of the separate-particle image is one of a structure made up of an aggregation of subunits. The numbers on Fig. 1 indicate the number of such subunits observed in the overall image. A ring-like structure composed of about 4-5 subunits is the configuration most frequently seen. Occasionally two ring-like structures are seen in close apposition where one of the subunits appears to be shared by both rings. Isolated single units usually do not appear in our micrographs. The inset on Fig. 1 is a line drawing depicting the various subunit configurations for the particles seen in the micrograph. The inset also indicates apparent dimers composed of two ellipsoidal units observed in this figure. From our micrographs it is difficult to resolve the actual shape of the subunit structure. The spherical or globular subunits which make up the ring-like structures have an apparent average diameter of 36 Å (range 31-40 Å) while ellipsoidal or cylindrical subunits have an apparent short axis of 36 Å and a long axis of 78 Å. An ellipsoidal shape might result from poor penetration of PTA around a four-subunit particle; on the other hand, the subunit may truly be elliptical and the images observed would be aggregates of ellipsoidal subunits standing with the long axis perpendicular to the plane of the grid surface.

A structure composed of subunits is highly reasonable in light of recent investigations of Levy and Fredrickson (13) and Scanu and Granda (21) on HDL degradation. These investigators were able to produce a "lipid-poor" HDL fraction by freeze-thawing or successive ultracentrifugation of serum. Delipidation of this fraction produced peptide subunits of approximately 20,000 molecular weight which were similar to the intact protein of HDL (21). Both groups of investigators have suggested that multiples of a similar subunit may produce the various HDL subclasses, namely, HDL_2 and HDL_3. Recently Shore and Shore (22) found 3 peptide chains of 30,000 molecular weight for the HDL_3 subfraction and they concluded that this lipoprotein may be made up of 3 protein subunits. Despite the discrepancies between the data of the above authors, the fact that similar peptide subunits are found on the HDL prompts us to suggest that the apparent electron microscopical subunits may correspond to the actual peptides associated with the HDL.

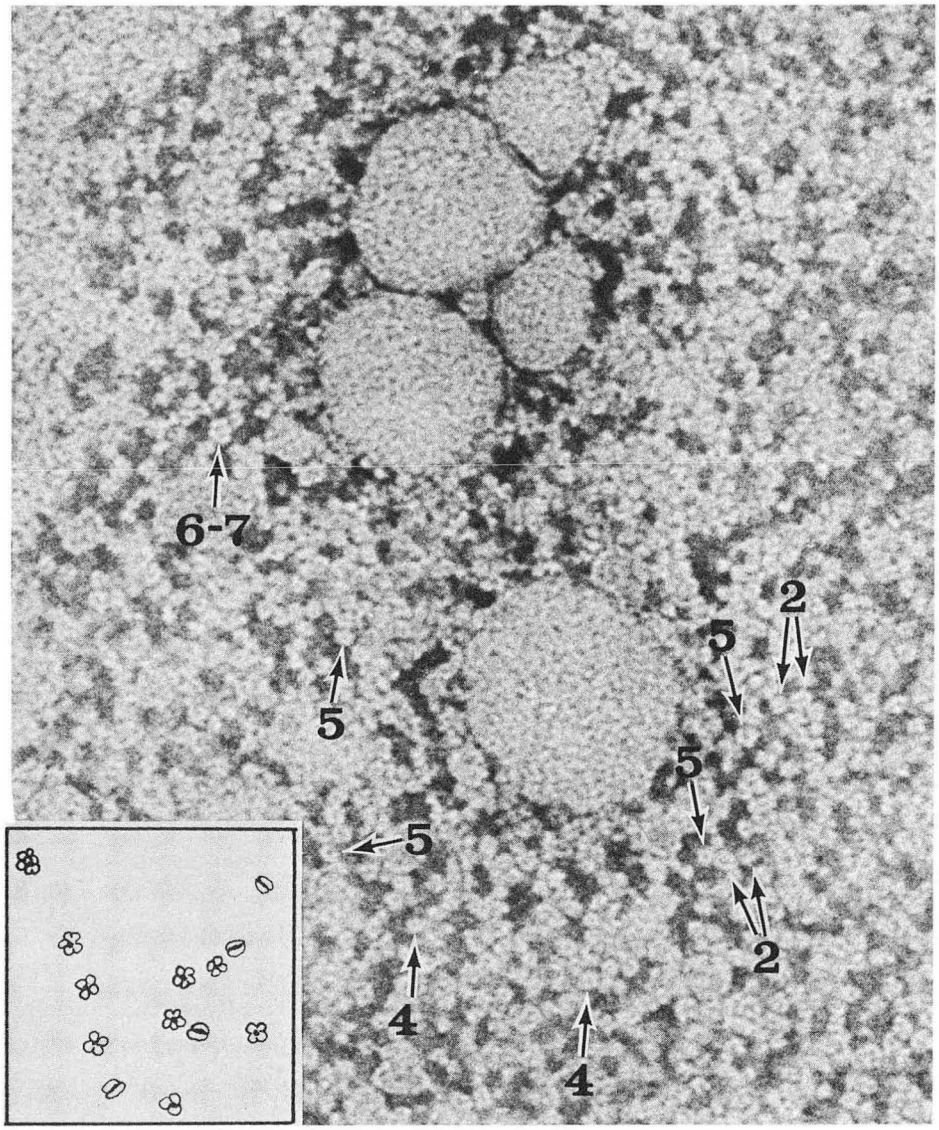

Fig. 1. A representative electron micrograph of the high-density lipoproteins negatively stained with sodium phosphotungstate. Arrows indicate some of the particles and the digit refers to the number of subunits which appear to make up the molecule. The line-drawing inset describes some of the particle configurations seen in the micrograph. × 256,000.

XBB 683-1007

If one considers the images of the HDL preparation as spherical particles and disregards their substructural aspects, then it is possible to calculate approximate molecular weights from the following expression:

$$\text{Molecular weight} = \frac{4}{3}\pi r^3 \rho N,$$

where r is the particle radius,

ρ is the density of the lipoprotein,

N is the Avogadro's number.

By using the radii obtained from the micrographs and the available densities of the two HDL subfractions, HDL_3 and HDL_2, two ranges of molecular weights can be calculated (see Table 1). Our calculated molecular weight for particles of an average diameter of 86 Å actually lies between the HDL_3 and HDL_2 values determined by Scanu and Granda (21) from ultracentrifugal and other data. Our molecular weight value is probably a function of the known heterogeneity of the HDL particles. If the calculations are carried out with our observed maximum and minimum diameters, the values are in good agreement with those of Scanu and Granda.

STRUCTURE OF THE LOW-DENSITY LIPOPROTEINS Where favorable quantities of negative stain have been entrained between particles, the freestanding low-density lipoproteins appear as roughly spherical macromolecules with a mean diameter of 216 Å (range 170-260 Å). The arrows on Fig. 2 indicate LDL particles which appear spherical; since single particles never appear elongated and are never seen on-edge there is no direct evidence that they are ellipsoids or disks. It is quite apparent, however, in the same micrograph that the particles upon contact with one another exhibit a polygonal shape. The macromolecules, therefore, display a degree of deformability which would be consistent with the view of Vandenheuvel (23) that the LDL protein forms a thin shell around a lipid core and is not necessarily a structural protein. Figure 3, which is a high-resolution micrograph of the LDL macromolecules, shows very clearly the distribution of particle sizes and the non-uniformity of shape of the packed particles. Another feature which is also noticeable is the constancy of distance between adjacent particles; the electron-dense interparticle space is estimated to be 15-20 Å.

The LDL particles seen on Fig. 3 have a granular appearance which is again suggestive of substructure. This granularity is reminiscent of that shown by Brenner and Horne (5) for turnip yellow mosaic virus and thought by these authors to be indicative of structural detail in the virus. This micrograph also reveals that PTA penetration between particles is not always complete so that regions of low electron density bridge adjacent molecules; such bridge-like connections are indicated by arrows. These bridges may arise through contact of apposed protruding regions at the surface of 2 particles as depicted in the highly schematic diagram in Fig. 4. At this point, however, one can only conjecture upon the structure and composition of these bridges.

The data presented above strongly suggest that the intact LDL lipoprotein is spherical or globular in shape. Preliminary electron microscopic studies which we have carried out on freeze-dried and shadowed particles also substantiate this conclusion. Our micrographs do

Table 1. Molecular weights of the high-density lipoproteins calculated from observed particle diameters.*

Particle diameter (Å) (from electron micrograph)	Mol. wt. using HDL_3 density 1.149 g/ml	Mol. wt. using HDL_2 density 1.094 g/ml
98	341,000	331,000
86	231,000	219,000
74	147,000	140,000
Molecular weight from ultracentrifugation data of Scanu and Granda (21)	158,000-180,000	340,000-380,000

*The particle diameters include the average diameter (86 Å) as well as the maximum and minimum values which were measured from micrographs. Density values used in the calculation were the hydrated densities for HDL_3 and HDL_2 given by Scanu and Granda (21).

not suggest that the low-density lipoproteins are prolate ellipsoids which form dimers as proposed by Hayes et al. (10). There is also a discrepancy between these data and the work of Bjorklund and Katz (6) whose light-scattering data indicate that the LDL may consist of prolate ellipsoids with dimensions of 350 Å by 160 Å.

The present data are in good agreement with an LDL diameter of 200 Å calculated from ultracentrifugal data by Lindgren and Nichols (16) and based on the assumption that the particles are spherical. When the molecular weight of the LDL macromolecule is calculated on the basis of a particle diameter of 216 Å and a density of 1.035 g/ml, a value of 3.29×10^6 is obtained. Compared with the value of $2.8\text{-}3.0 \times 10^6$ obtained by Bjorklund and Katz (6), our figure is somewhat high but may be a reflection of the distribution of particle sizes in our samples.

Oncley, Gurd, and Melin (20) and Cook and Martin (7) have postulated that the low-density lipoprotein may consist of a lipid core surrounded by an outer protein layer. Margolis and Langdon (19), on the other hand, have proposed from data on partial proteolysis of these lipoproteins, that the LDL molecules may be composed of several subunits which in themselves resemble miniature lipoproteins similar to the Oncley et al. model. In our present investigation we were unable to find any definitive indication of a small number of subunits such as those considered by Margolis and Langdon (19). The configuration of the LDL lipoproteins rather suggests a structure similar to that proposed by Oncley et al. (20) and Cook and Martin (7).

The electron-transparent regions connecting adjacent low-density lipoprotein particles are extremely interesting. These bridge-like entities could be functionally very significant

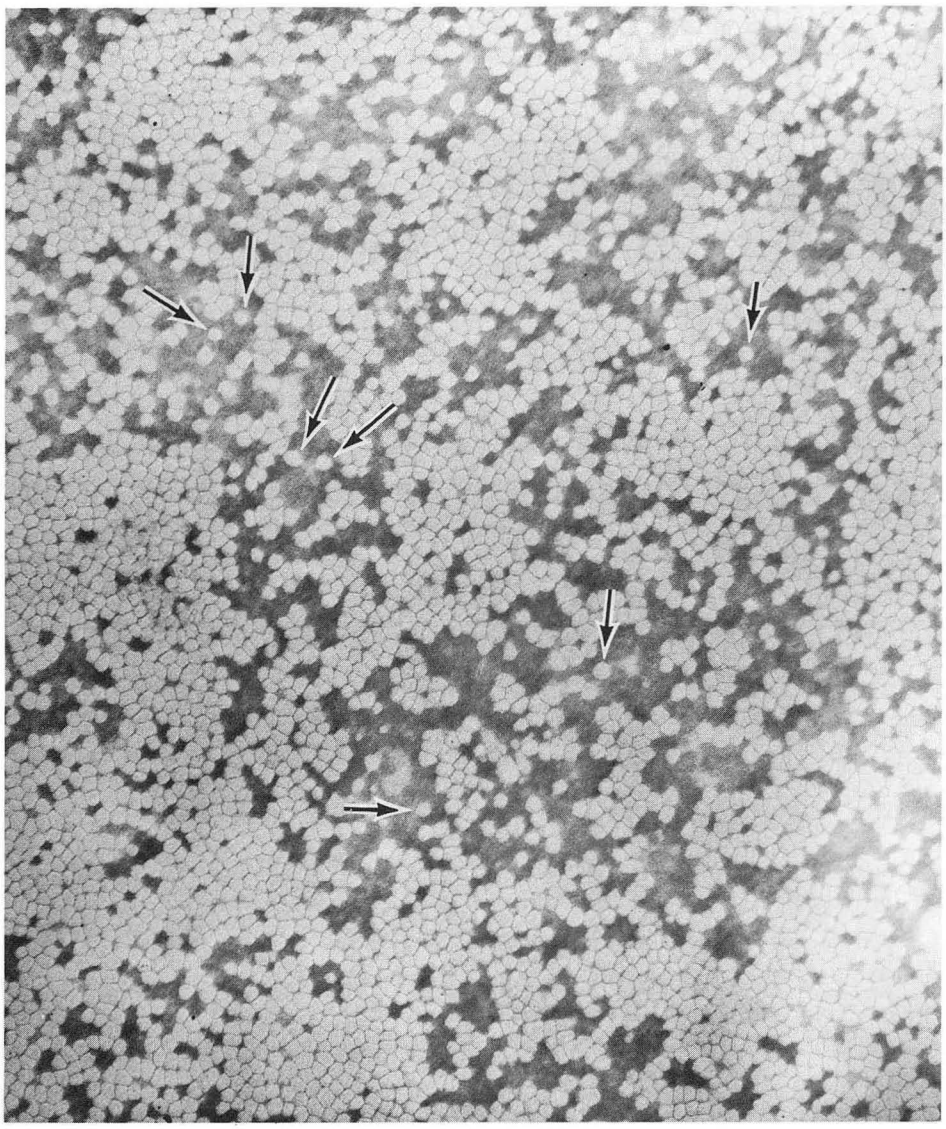

Fig. 2. An electron micrograph of the low-density lipoproteins negatively stained with sodium phosphotungstate. Arrows indicate single particles which appear to be spherical. × 90,000.

XBB 683-1008

in the exchange and net transfer of molecules from the LDL structure and also may play a role in aggregation and fusion of the particles. Figure 5 shows LDL lipoproteins in various stages of aggregation or fusion. Small aggregates are only the size of two low-density lipoprotein structures while others approach the size of chylomicrons (1500 Å).

STRUCTURE OF THE VERY LOW DENSITY LIPOPROTEINS PLUS CHYLOMICRONS

The very low density lipoprotein plus chylomicron fraction as visualized in Fig. 6 by the nega-

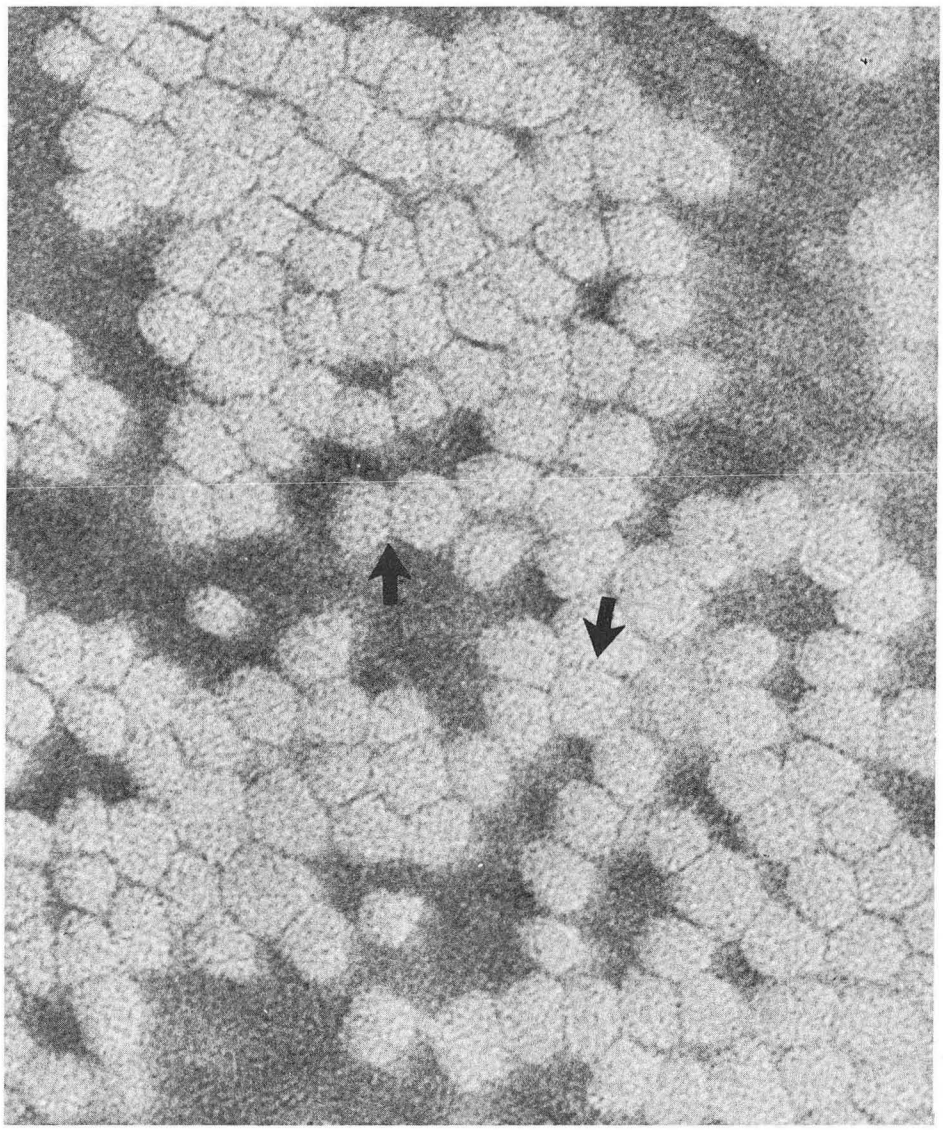

Fig. 3. A high resolution micrograph of the low-density lipoproteins negatively stained with sodium phosphotungstate. The arrows indicate regions in which there are bridge-like connections between adjacent particles. × 420,000.

XBB 683-1009

tive staining procedure exhibits a diversity of size and shape. Smaller molecules are more or less spherical and, like the LDL, are easily deformed. Larger particles, however, are often amorphous in appearance. These latter shapes may result from a flattening of the structures during drying. The range of size of this lipoprotein class varies from 230-5000 Å in diameter. This range reflects the heterogeneity of the fraction which also includes the very large chylomicrons. It is of interest to note that these lipid-rich particles are very electron transparent. In Fig. 6 (arrow) one can see areas where one particle overlays another yet both particles are still visible.

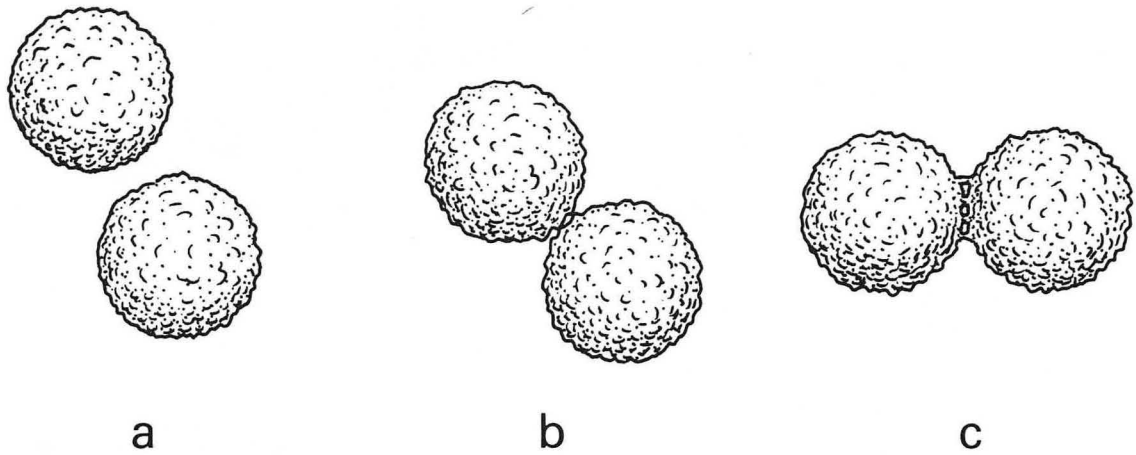

Fig. 4. A highly schematic representation of the bridge-like structures sometimes seen between adjacent low-density lipoprotein particles. Individual particles are represented in (a); (b) shows 2 particles beginning to form bridge-like connections, and (c) shows the completed bridge-like regions between the particles.

DBL 682-4586

The structure of the VLDL plus chylomicron fraction revealed by negative staining corroborates the findings of Hayes et al. (11) that the very low density serum lipoproteins are spherical structures with a wide range in size. Our results reveal no fine structure either within or at the periphery of these large particles.

SUMMARY

Human serum lipoproteins were separated by ultracentrifugation into 3 fractions: high-density lipoproteins, low-density lipoproteins, and very low density lipoproteins plus chylomicrons. The structures of the various fractions were studied with the electron microscope after negative staining with sodium phosphotungstate.

The high-density lipoproteins appear to be structures 86 Å in diameter and possessing an electron-dense central region. The particles are composed of subunits approximately 36 Å in diameter.

The low-density lipoproteins appear spherical with a mean diameter of 216 Å and they display a high degree of deformability. Bridge-like connections between adjacent particles also appear to be present.

The very low density lipoproteins plus chylomicrons are extremely heterogeneous in size and shape and range from 230-5000 Å in diameter. The smaller molecules seem to be spherical while the extremely large ones are flattened and irregular in shape.

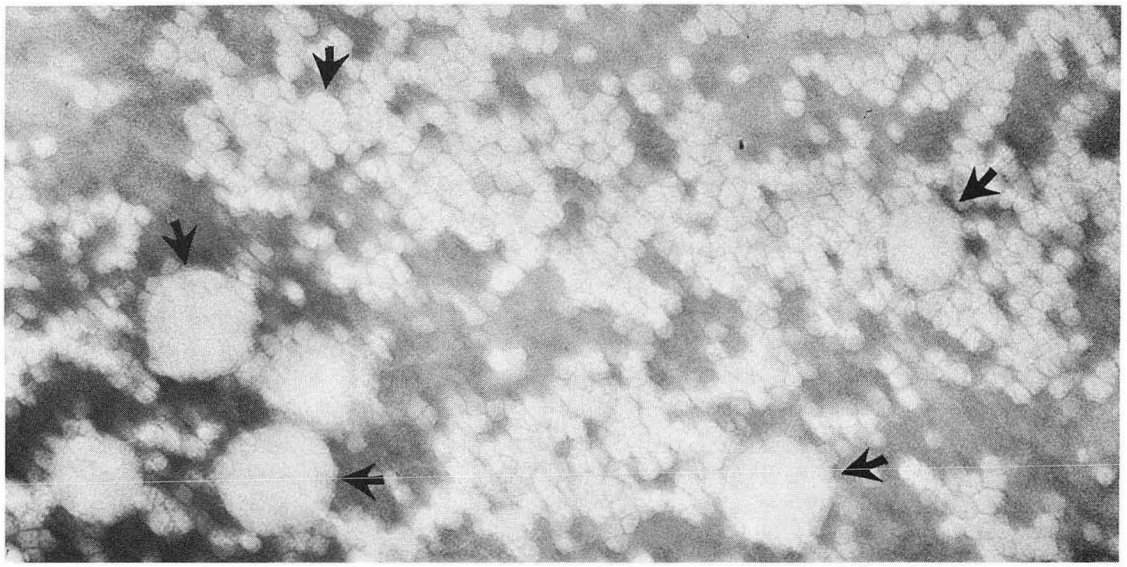

Fig. 5. A negatively stained preparation of the low-density lipoproteins in which various sized aggregations of the particles are visible as indicated by the arrows. × 135,000.

XBB 683-1010

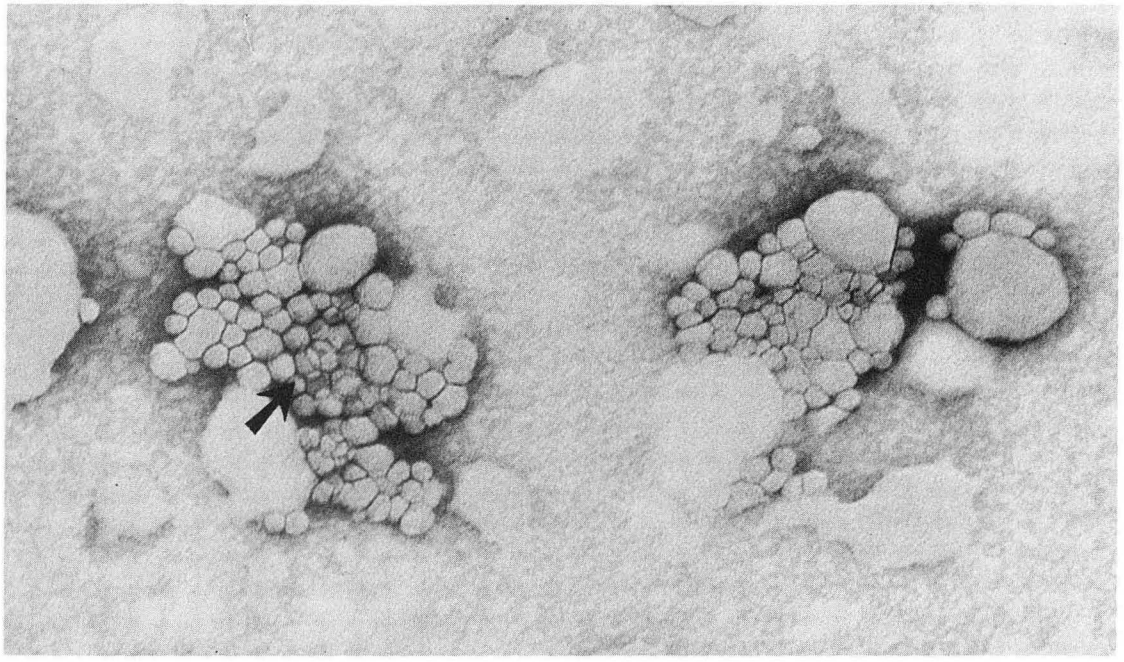

Fig. 6. An electron micrograph of the very low density lipoproteins plus chylomicrons negatively stained with sodium phosphotungstate. A great heterogeneity in size of particles is readily seen. The arrow points to a region in which one sees particles superimposed on each other. × 120,000.

XBB 683-1011

ACKNOWLEDGMENTS

The authors gratefully acknowledge the valuable technical assistance of Elaine Coggiola, Elaine Yokoyama, and Walter Ho. We also would like to thank Drs. T. L. Hayes, F. T. Lindgren, and W. J. Lossow for their helpful discussions during the preparation of this manuscript.

This work was supported in part by USPHS Research Grant HE 10878-02 (PC) from the National Heart Institute, U. S. Public Health Service, and by the U. S. Atomic Energy Commission. G. M. Forte is also the recipient of a Bay Area Heart Research Fellowship.

REFERENCES

1. Bangham, A. D., and Horne, R. W.; J. Mol. Biol. 8: 660, 1964.
2. Beischer, D. E.; Circulation Res. 2: 164, 1954.
3. Bragdon, J. H.; Havel, R. J., and Boyle, E.; J. Lab. Clin. Med. 48: 36, 1956.
4. Branton, D., and Park, R. B.; J. Ultrastruct. Res. 19: 283, 1967.
5. Brenner, S., and Horne, R. W.; Biochim. Biophys. Acta 34: 103, 1959.
6. Bjorklund, R., and Katz, S.; J. Am. Chem. Soc. 78: 2122, 1956.
7. Cook, W. H., and Martin, W. G.; Canad. J. Biochem. Physiol. 40: 1273, 1962.
8. de Lalla, O. F., and Gofman, J. W.; in Methods of Biochemical Analysis, Vol. 1, edited by D. Glick, New York, Interscience Publishers, Inc., 1954, p. 459.
9. Hayes, T. L., and Hewitt, J. E.; J. Appl. Physiol. 11: 425, 1957.
10. Hayes, F. T.; Murchio, J. C.; Lindgren, F. T., and Nichols, A. V.; J. Mol. Biol. 1: 297, 1959.
11. Hayes, T. L.; Freeman, N. K.; Lindgren, F. T.; Nichols, A. V., and Bierman, E. L.; in Protides of the Biological Fluids, edited by H. Peeters, Amsterdam, Elsevier Publishing Company, 1966, p. 273.
12. Kay, D., and Robinson, D. S.; Quart. J. Exptl. Physiol. 47: 258, 1962.
13. Levy, R. I., and Fredrickson, D. S.; J. Clin. Invest. 44: 426, 1965.
14. Lindgren, F. T.; Elliott, H. A., and Gofman, J. W.; J. Phys. Colloid. Chem. 55: 80, 1951.
15. Lindgren, F. T.; Nichols, A. V., and Freeman, N. K.; J. Phys. Chem. 59: 930, 1955.
16. Lindgren, F. T., and Nichols, A. V.; in The Plasma Proteins, Vol. 2, edited by F. Putnam, New York, Academic Press, Inc., p. 1.
17. Lindgren, F. T.; Nichols, A. V., and Wills, R. D.; Am. J. Clin. Nutr. 9: 37, 1961.
18. Lucy, J. A., and Glauert, A. M.; J. Mol. Biol. 8: 727, 1964.
19. Margolis, S., and Langdon, R. G.; J. Biol. Chem. 241: 485, 1966.
20. Oncley, J. L.; Gurd, F. R. N., and Melin, M.; J. Am. Chem. Soc. 72: 458, 1950.
21. Scanu, A., and Granda, J. L.; Biochemistry 5: 446, 1966.
22. Shore, V., and Shore, B.; Biochemistry 6: 1962, 1967.
23. Vandenheuvel, F. A.; Canad. J. Biochem. Physiol. 40: 1299, 1962.

Graphic Presentation of Computer-Derived Schlieren Lipoprotein Data

Lin C. Jensen, Thomas H. Rich and Frank T. Lindgren

The computer analysis of schlieren photographs of serum lipoprotein distributions has been described in detail by Ewing et al. (1). This computer program yields numeric output fully corrected to standard conditions in terms of lipoprotein concentration of the original sample, allowing valid comparisons from sample to sample to be made. In order to extend and improve the computer analysis of lipoprotein distributions, a program has been written to present this data in graphic form, allowing rapid visual evaluation, comparison of samples, and error detection.

PROGRAMMING METHOD

The computer input data consist of lipoprotein concentrations for a series of standard flotation rate (S_f or F rate) intervals in the card format produced by the schlieren analysis program (1). Although the low-density analysis is presented here in terms of S_f values, the program is similarly used for high-density graphical analysis. The plotting program converts these S_f rates into appropriate linear dimensions and lipoprotein concentrations into areas equivalent to those of the corrected schlieren patterns, routinely presented at 3 times the concentration of serum. It then calculates frequent points along a best fit curve through the resulting histogram, from which the graph is subsequently plotted on a physical device. At the same time the program sums lipoprotein concentrations of the total pattern and those of specified component regions (S_f 0-12, S_f 12-20, S_f 20-100, and S_f 100-400 in the standard low-density run), as well as determining the S_f rate where the maximum concentration occurs. The final steps are to draw a rectangle around each frame, with tick marks and frame boundaries which normally correspond to the template upon which the schlieren pattern was initially traced, label the plot, and print standard interval lipoprotein concentration values. It is possible to plot several patterns on one frame, or to plot the mean and/or standard deviation of a group of cases.

At the present time we normally use an S_f rate scale identical to that of the 3 time frame template used for tracing the enlarged schlieren pattern (see Fig. 1). However, the montage of three frames (taken at different times required to include all the low-density lipoproteins) results in a discontinuous curve representing what is essentially a continuous spectrum. In Fig. 2c, a logarithmic scale has been chosen arbitrarily to achieve continuity while roughly preserving the relative widths represented by the individual schlieren frames. Another potentially useful scale using the square root of S_f rate would yield a scale nearly linear in particle diameter.

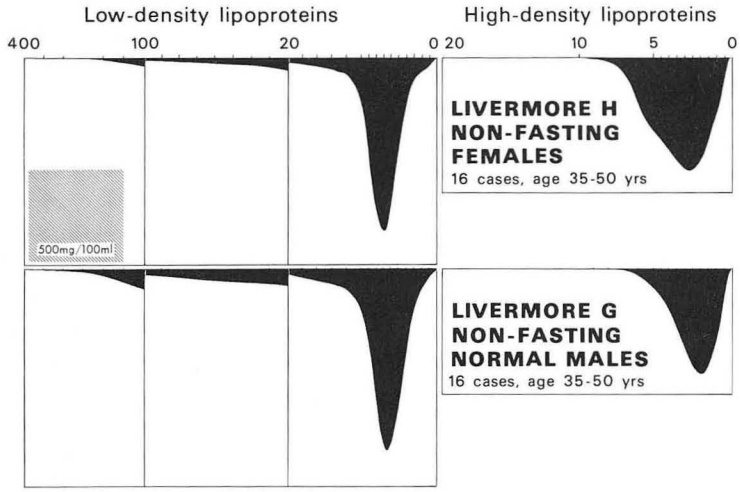

Fig. 1. Typical low- and high-density lipoprotein spectra drawn by a Cal-Comp plotter and shaded and labeled for publication. DBL 682-4583

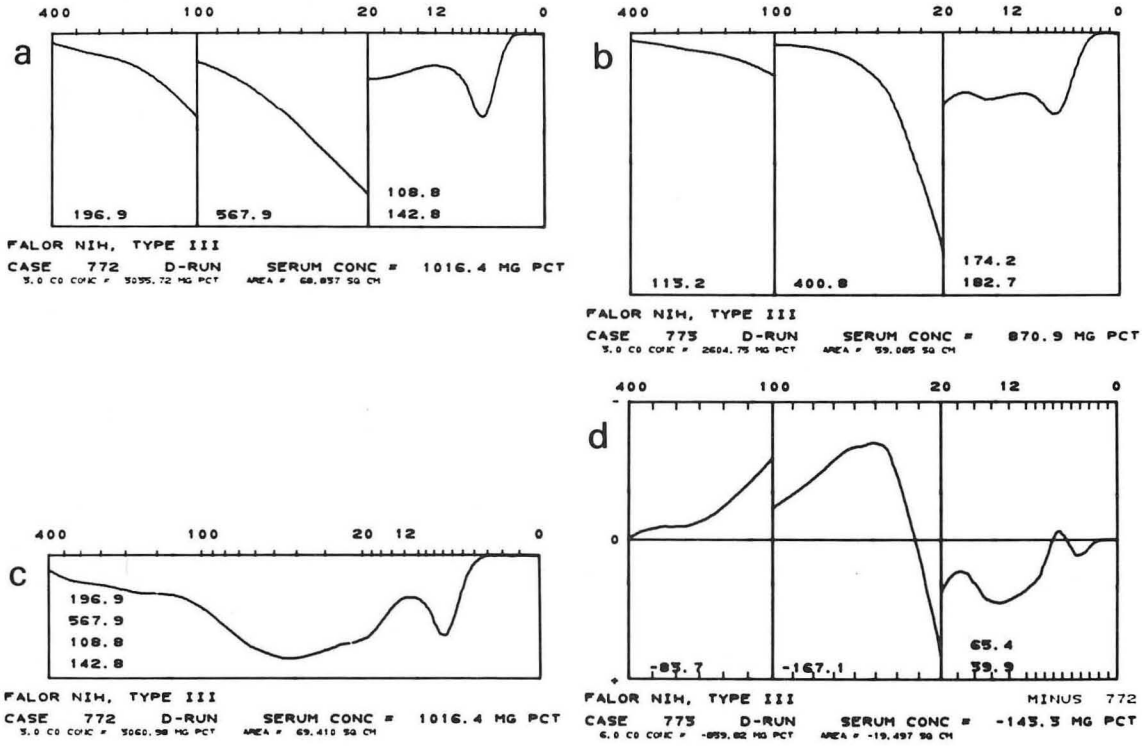

Fig. 2. Cathode ray tube (CRT) plots of low-density lipoprotein spectra. 2a and 2b show a patient before and after drug therapy. 2c duplicates 2a using a continuous logarithmic scale. 2d shows 2a subtracted from 2b magnified twofold. DBL 682-4584

Although patterns may be compared by holding them side by side, or plotting them on a single graph, small but significant differences still may be hard to see. A modified version of the program has been developed which subtracts the first pattern of a series from each subsequent one and plots the difference at a specified magnification. For example, Fig. 2d shows 2a subtracted from 2b magnified twofold.

GRAPHIC MEDIA

Figure 1 was drawn on a CalComp plotter, which moves a pen about a segment of chart paper under computer control. To present a visually effective profile, the pattern has been shaded and mounted, producing a high quality figure. Since the CalComp plotter is accurate to 1/100 of an inch, it is therefore also useful in drawing master templates for tracing schlieren patterns from the film. However, the main disadvantage of the CalComp plotter is that it is a relatively slow process requiring extensive operator intervention; thus, plotting on it, especially in any quantity, is expensive and subject to delays.

In contrast, the plots in Fig. 2 were traced electronically on a cathode ray tube (CRT) and photographed on 35 mm film. This CRT system lacks the resolution and absolute dimensions given by the CalComp, but it is rapid and requires only the occasional removal of film. Rough 8-1/2- × 11-in. prints in any quantity usually are available on an overnight basis.

PROGRAM USAGE

Logically there is one plotting program with an extra input routine to handle population means. It is written for the CDC-6600 computer, using plotting routines of the Lawrence Radiation Laboratory, Berkeley, computer center. For reasons of technical efficiency, separate but similar versions for CalComp and CRT plotting are used. The program itself is quite flexible. After selecting the proper version, one specifies by optional control cards such requirements as input intervals, number of curves to plot on one frame, template dimensions, magnification factors, positions of S_f rate labels, frame boundaries, and concentration subregions. Standard values or procedures are assumed unless overridden by special options.

DISCUSSION

This program was conceived as a means for preparing data, such as Fig. 1, for publication in place of the tediously hand-drawn graphs previously required (1). As soon as the initial version of the program was running, it was obvious that one had such a clear and immediate visual presentation that it would be valuable to have for all schlieren data. Emphasis was then given to ease of use and conversion to the CRT medium when it became operational. Routinely, now, the program is run following computer analysis of the schlieren tracing as part of the same job (i. e., without human intervention) so that prints are available almost as soon as the total numerical output.

Many errors are now caught which before graphic presentation undoubtedly went undetected. Our reduction of schlieren film to punch-card numbers involves two technicians and two keypunch operators. Occasional human errors are inevitable. To illustrate a typical error, suppose some interval on the tracing is 1.36 cm but is read by the computer as 1.86 cm.

This error does not stand out at all in a column of figures; however, on the plot it immediately is detected as a large bump on an otherwise smooth curve.

SUMMARY

Computer-produced graphs of lipoprotein spectra present a large amount of information rapidly to the eye and greatly facilitate error detection. Data derived from schlieren patterns in the analytical ultracentrifuge are fully corrected to standard conditions, allowing valid comparison of serum lipoprotein concentrations and profiles. The computer program is flexible enough to provide appropriate representations for many types of spectra and several possibilities for comparison of data.

ACKNOWLEDGMENTS

This work was supported by Research Grant 5-RO1-HE-01882-14 from the National Heart Institute, Public Health Service, Bethesda, Maryland, and by the U. S. Atomic Energy Commission.

REFERENCE

1. Ewing, A. M.; Freeman, N. K., and Lindgren, F. T.; in Advances in Lipid Research, Vol. 3, edited by R. Paoletti and D. Kritchevsky, New York, Academic Press, Inc., 1965, Chap. 2, p. 25.

Integrated Absorption Intensities of the Ester Carbonyl Bands of Lipids and their Analytical Applications

Norman K. Freeman, Lin C. Jensen and Virginia C. Lew

A total lipid extract from blood serum has as its major constituents three types of fatty acid esters, viz., cholesteryl esters, triglycerides, and glycerophosphatides. The infrared absorption bands of the carbonyl stretching vibrations for these ester classes are shown in Fig. 1, together with the absorption of unesterified fatty acid (UFA) in the same spectral interval. For all four curves the concentrations of fatty acid is the same. It may be noted that for the three ester curves shown there is a point of approximately equivalent absorptivity at 1746 cm^{-1}. In a method described earlier (1) this equivalence was used as the basis for measurement of the total esterified fatty acids (TEFA) in serum lipid extracts.

Another approach to the analysis for TEFA is to use the integrated absorption intensity (band area) instead of absorbance at a single frequency. In part, the rationale for this approach is the general observation that integrated intensities for a particular type of band are likely to remain constant under the influence of intramolecular structural changes or solvent interactions, whereas such effects can displace peak positions or alter peak heights. Integrated intensities are also less affected by instrumental factors such as slit width and wavelength reproducibility. This investigation was undertaken to determine the integrated carbonyl absorption intensities of the major blood lipids, and to assess their usefulness for esterified fatty acid analysis.

EXPERIMENTAL

MATERIALS Triolein (>99%), oleic acid (>99%), and cholesterol (99%) were obtained from The Hormel Institute, Austin, Minn. Cholesteryl oleate (>99%) and egg lecithin (highly purified) were obtained from Applied Science Laboratories, State College, Pa.

MEASUREMENTS Infrared absorption measurements were made with a Perkin-Elmer Model 421 grating spectrophotometer. Samples were dissolved in carbon tetrachloride, and the absorption cell had a path length of 1.0 mm. Transmittance curves were recorded in the usual manner over the frequency interval 1700-1800 cm^{-1}, using twice-normal slit width (ca 0.25 mm), expanded frequency scale (2 $\times$ abscissa), and the minimum scanning speed. A digital data recorder, Perkin-Elmer Model DDR-2C, was coupled to the spectrophotometer output and used to record measurements in binary coded decimal form on punched paper tape. The operating mode selected was to record a transmittance value at each 0.5 cm^{-1} interval as indicated on the frequency counter (uncorrected).

COMPUTATIONS All computations were performed on a CDC-6600 computer, which is equipped to read the punched paper tape and transfer the information to magnetic tape for further handling by the computer. All transmittance measurements are first converted to absorbances, $A_\nu = \log T_0 - \log T_s$, where T_0 = transmittance of solvent and T_s = transmittance of sample solution at frequency ν. The set of absorbance values representing the spectral curve may then be fed into the remainder of the calculation program and stored on magnetic tape for future reference.

For the analytical purpose under consideration, the integrated intensity is taken as the band area, which is simply calculated as a summation over 200 half-wavenumber intervals.

$$B = \text{band area} = \sum_{\nu_1}^{\nu_2} A_\nu \Delta\nu = 0.5 \sum_{1700}^{1800\ \text{cm}^{-1}} A_\nu .$$

The quantity B is functionally related to sample concentration C in the same manner as absorbance. A calibration of B vs. C may be established in either graphical or numerical form and used to determine C from a measurement of B.

RESULTS AND DISCUSSION

Calculated band areas (B) are listed in Table 1 for the pertinent lipids, over appropriate ranges of concentration. In addition to the three principal ester types found in serum, methyl oleate is included for comparison. Unesterified fatty acid and cholesterol are serum constituents which also need to be considered in the analytical problem. The third column in Table 1 shows numerical values of B/C; and constancy of this ratio for each substance indicates linearity of B vs. C plots. The fourth column shows B/C_{FA}, the area per unit fatty acid concentration. Here the value remains constant (within about 2%) over all four ester classes, showing independence of ester type.

Results for some simple binary mixtures are given in Table 2. Agreement with the prepared composition is within 2%. A mixture of this type is sometimes obtained in the analysis of low-density lipoproteins (LDL), which contains very little unesterified fatty acid. A total lipid extract from LDL is treated with an adsorbent to remove phospholipids, leaving a solution of mainly triglycerides and cholesteryl esters. A series of such preparations was analyzed, with results as shown in Table 3. Two sets of results are given for band area measurement. One set is for band areas measured from 1700-1800 cm^{-1}, using an average of the ester factors (B/C_{FA}) from Table 1. The other set (last column) is based on a narrower band which was chosen to eliminate as much as possible of the major free fatty acid peak (Fig. 1) and very little of the ester band area. The discrepancies from peak height analyses were thereby reduced from 2-3% to about 1% or less in most cases.

Some duplicate serum lipid analyses were carried out, with the results given in Table 4. In these extracts all three ester types are present, as well as unesterified fatty acid and cholesterol. From Table 1 and the estimated cholesterol concentration it may be inferred that the error due to cholesterol is less than 0.5%. Unesterified fatty acids, on the other hand, may account for 5-15% of the total band area in the 1700-1800 cm^{-1} interval. In Table 4 the

Table 1. Carbonyl band areas for representative lipids (1700-1800 cm^{-1}).

Compound	C (mg/ml)	B, band area	B/C	B/C_{FA}*
Triolein	0.89	3.72	4.16	4.35
	1.81	7.51	4.16	4.35
	2.70	11.12	4.12	4.31
	3.54	14.51	4.09	4.28
Cholesteryl oleate	1.94	3.70	1.91	4.40
	3.88	7.43	1.92	4.42
	5.53	10.12	1.83	4.22
	7.75	14.61	1.89	4.34
Lecithin (egg)	2.38	7.71	3.24	4.44
	2.98	9.53	3.20	4.41
	3.97	12.64	3.18	4.38
	5.96	19.16	3.21	4.42
Methyl oleate	0.78	3.20	4.11	4.32
	1.52	6.32	4.16	4.37
	3.23	13.28	4.11	4.31
	5.29	21.50	4.06	4.26
Oleic acid	0.75	4.23	5.63	5.63
	1.56	8.87	5.69	5.69
	2.10	12.00	5.71	5.71
	3.04	17.28	5.69	5.69
Cholesterol (no carbonyl)	2.02	0.1276	0.063	--
	4.55	0.2556	0.056	--
	6.06	0.3209	0.053	--
	9.09	0.4806	0.053	--

*C_{FA} = conc. of fatty acid.

TEFA values calculated from this interval are about that much higher than the corresponding values from peak height measurement. When the narrower band (1720-1780 cm^{-1}) is used, these discrepancies are reduced to 3-9%, as shown in the last column of Table 4.

In an experiment to assess further the effect of free fatty acids on these measurements, some mixtures of triolein and cholesteryl esters were prepared with various amounts of added oleic acid. Figure 2 shows a plot of the percent error in TEFA measurement vs. the percent fatty acid present. Using the 1720-1780 cm^{-1} frequency interval, it appears that the error in TEFA determination is less than 5% if the UFA content does not exceed 10% of the total fatty acids. This is in agreement with the data from total serum lipid extracts. As a rough

Table 2. Determination of total esterified fatty acids in mixtures of triolein (TO) and cholesteryl oleate (CO) (conc. in mg/ml).

Mixture	TO	CO	FA_{TO}	FA_{CO}	Σ FA	TEFA*
1	0.90	2.76	0.86	1.20	2.06	2.10
2	0.45	4.15	0.43	1.80	2.23	2.27
3	1.36	1.38	1.30	0.60	1.90	1.93
4	2.06	0.55	1.97	0.24	2.21	2.24
5	1.37	2.51	1.31	1.09	2.40	2.39

*Calculated from band areas (1700-1800 cm^{-1}).

Table 3. Determination of total esterified fatty acids in nonphospholipid fractions of S_f 0-20 lipoprotein lipids (conc. in mg/ml).

Sample	TG*	CE*	FA_{TG}†	FA_{CE}†	Σ FA†	TEFA‡ (1700-1800 cm^{-1})	TEFA‡ (1720-1780 cm^{-1})
1	0.82	4.19	0.79	1.82	2.61	2.66	2.62
2	0.81	3.64	0.78	1.58	2.36	2.41	2.38
3	0.91	5.11	0.87	2.22	3.09	3.20	3.14
4	0.90	3.30	0.86	1.43	2.29	2.33	2.30
5	1.07	4.97	1.03	2.16	3.19	3.29	3.25
6	0.68	3.82	0.65	1.66	2.31	2.37	2.33
7	1.19	5.51	1.14	2.39	3.53	3.64	3.59

*Analysis by peak heights (triglycerides and cholesteryl esters).

†Calculated from analyzed composition.

‡Calculated from band areas.

Table 4. Total esterified fatty acids in lipid extracts from serum (conc. in mg/ml).

Sample	TEFA (peak height)	TEFA (1700-1800 cm^{-1})	TEFA (1720-1780 cm^{-1})
1	3.44, 3.43	3.77, 3.78	3.54, 3.54
2	3.11, 3.10	3.63, 3.57	3.38, 3.35
3	3.15, 3.25	3.50, 3.56	3.35, 3.40

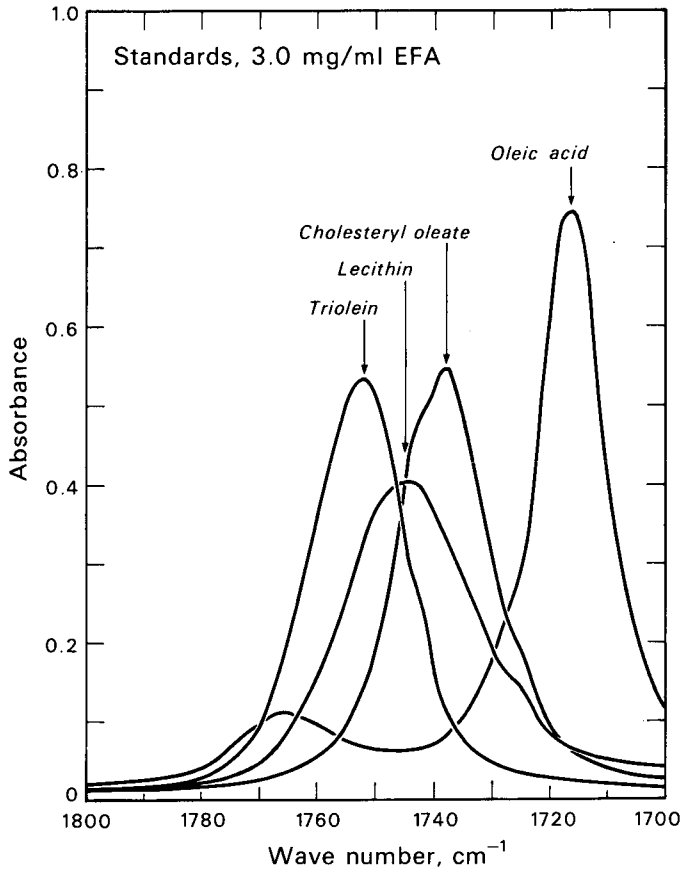

Fig. 1. Carbonyl absorption bands of representative serum lipids. Concentration in each case is adjusted to a fatty acid content of 3.0 mg/ml. Absorbing path length is 1.0 mm.

DBL 682-4589

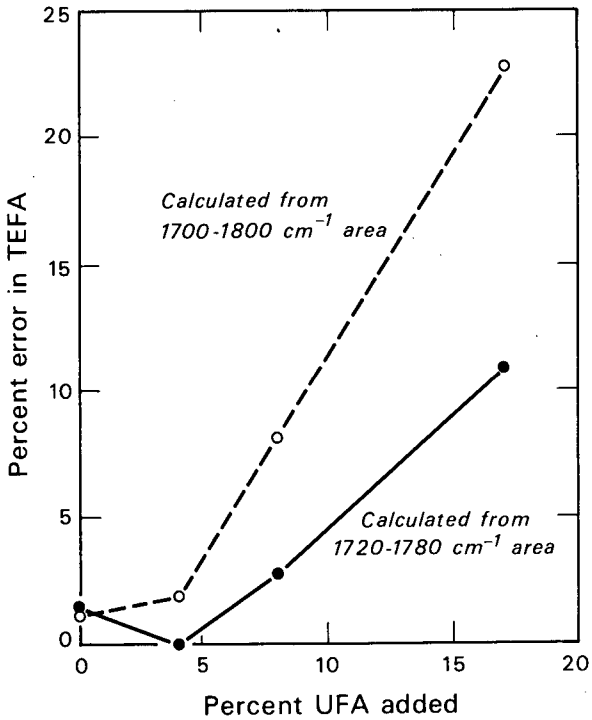

Fig. 2. Relative error in TEFA determination as a function of UFA content.

DBL 682-4588

criterion, the ratio of the area in the 1700-1720 cm^{-1} interval to the total area may be used to judge whether or not UFA exceeds 10%.

Methods of estimating the free fatty acids more accurately from band area measurements are being investigated. Such an analysis will probably be based on empirical relationships between areas of subintervals, where the system is regarded as two components—esters and fatty acids.

SUMMARY

Integrated absorption intensities over the frequency interval 1700-1800 cm^{-1} have been measured for the principal lipid constituents of blood serum. A very nearly identical value has been obtained for the integrated absorbance per mole of fatty acid in triglycerides, cholesteryl esters, and lecithin, as well as for methyl oleate. Mixtures of these substances can therefore be analyzed for total esterified fatty acids by a single measurement of the carbonyl band area. The corresponding band areas for cholesterol and unesterified fatty acids have also been measured, since they normally occur in small amounts in serum lipid extracts. The contribution by cholesterol at its normal level is less than 0.5% of the total band area. Interference by unesterified fatty acids is more significant, and some evaluation of its extent has been made.

Computation of integrated band areas by computer has been facilitated by direct recording of spectrophotometric data on punched paper tape.

REFERENCE

1. Freeman, N. K.; Ann. N. Y. Acad. Sci. 69: 131-144, 1957.

Analysis of Change in Ultracentrifugal Lipoprotein Profiles Following Heparin and Ethyl-p-Chlorophenoxyisobutyrate Administration

Alex V. Nichols, Edward H. Strisower, Frank T. Lindgren, Gerald L. Adamson and Elaine L. Coggiola

Administration of heparin (1) or ethyl-p-chlorophenoxyisobutyrate (CPIB) (2) to humans results in significant reduction of elevated serum levels of very low density lipoproteins (VLDL, d < 1.006 g/ml) which include the S_f 20-400 ultracentrifugal class of lipoproteins. Concomitant with the reduction of VLDL concentrations following heparin, increases in more dense lipoprotein species occur. These changes after heparin suggest a possible degradation of VLDL into more dense lipoprotein moieties which float under centrifugation with the S_f 0-20 or low density lipoproteins (LDL, d 1.006-1.063 g/ml) and the high density lipoproteins (HDL, d 1.063-1.21 g/ml). Since available data indicate that two protein components of VLDL are identical to protein moieties normally associated with the LDL and HDL (3, 4), degradation of VLDL could be expected to yield lipoproteins with ultracentrifugal properties similar if not identical to LDL and HDL. Concentration changes in ultracentrifugal lipoprotein classes other than the VLDL have also been noted in sera of subjects receiving CPIB (2). While the changes in the ultracentrifugal properties of VLDL have been extensively reported, a quantitative description of changes in ultracentrifugal profiles of the LDL and HDL following heparin or CPIB is lacking. Recent developments in the computerized analysis of ultracentrifugal lipoprotein patterns have greatly facilitated quantitative resolution and evaluation of changes in lipoprotein distributions (5). In this preliminary report, the feasibility of applying these developments to the quantitation of changes in ultracentrifugal lipoprotein profiles of hypertriglyceridemic subjects receiving separately heparin and CPIB is evaluated.

METHODOLOGY

SUBJECTS Serum lipoprotein changes were studied in two hypertriglyceridemic subjects. Subject A. S. is a 74-year-old, moderately obese, clinically well woman, with mild maturity-onset diabetes controlled by diet. Fasting blood sugars ranged between 118-120 mg% during the heparin study and from 97 to 105 mg% during the CPIB study.

Subject S. B. is a 55-year-old, clinically well man with small elbow lesions typical of xanthoma tuberosum. A complete medical evaluation showed no detectable abnormalities on physical examination except for the xanthomas on the elbow and standard laboratory studies showed normal thyroid function, absence of renal and hepatic disease, and normal glucose

tolerance. In consequence his hyperlipidemia is of a primary type, not related to or caused by other diseases.

Each subject received an intravenous injection of 100 mg of heparin in the fasting state on the morning of the experiment and subsequent (18 and 75 minute postheparin) 25 ml blood samples were drawn from the opposite arm into evacuated tubes containing 1.5 mg thimerosal and 1.0 mg of protamine sulfate with 1.0 mg of sodium chloride in a volume of 0.1 cc water. Both patients maintained their fasting state during the heparin study.

Blood samples were drawn in the fasting state before and during CPIB administration (dose CPIB: 2 g/day). In this report, the changes in serum lipoprotein profiles encountered after 35 days (subject A. S.) and 38 days (subject S. B.) of CPIB administration will be presented. Both patients maintained their weight within ±2 lb during the CPIB study.

ULTRACENTRIFUGAL AND COMPUTER ANALYSIS OF SERUM LIPOPROTEIN DISTRIBUTION Serum was separated from subjects' blood by procedures previously described (6). Ultracentrifugal isolation and flotation analyses of low and high density lipoproteins were performed as described earlier (5).

Data obtained from the ultracentrifuge schlieren films of low and high density lipoproteins were analyzed by computer techniques described by Lindgren et al. (5). In this analysis, the low density lipoprotein distribution (from S_f° 0 to S_f° 400) is subdivided into 29 intervals; and the high density distribution (from $F_{1.20}^\circ$ 0 to $F_{1.20}^\circ$ 9.0) is subdivided into 15 intervals. Flotation rates described by $S_f^{\circ *}$ values are rates in Svedberg units for lipoproteins in a medium of density 1.063 g/ml (NaCl, 26°C, 52,640 rpm). Flotation rates designated by $F_{1.20}^{\circ *}$ values are rates in Svedbergs for lipoproteins in a medium of density 1.20 g/ml (NaCl-NaBr, 26°C, 52,640 rpm). The lipoprotein concentration within each one of these flotation intervals is calculated via a computer program after manual analysis of the schlieren patterns. The concentration data for the subdivided low or high density lipoprotein distributions may subsequently be processed via computer to obtain a condensed schematic representation of the lipoprotein distribution.

In this study we evaluated the changes in lipoprotein distributions, following administration of heparin and CPIB, by comparing the concentration changes within each of the intervals of the subdivided distribution. This quantitative comparison was made by subtracting the initial subdivided distribution, interval by interval, from the subdivided distributions obtained postheparin and during CPIB administration. In this way, the concentration change, positive or negative, is sharply defined in terms of its magnitude and flotation rate interval.

The replicability of concentration measurements within each of the flotation intervals of the subdivided lipoprotein distribution was evaluated. The percentage error encountered in

*Flotation rates designated by S_f° and $F_{1.20}^\circ$ are rates corrected for concentration and Johnston-Ogston effects. Rates designated S_f and $F_{1.20}$ are uncorrected rates.

determinations of serum concentration within flotation subintervals averaged 7% for concentrations equal to or greater than 10 mg/100 ml.

RESULTS

In Fig. 1, schematic lipoprotein profiles for subject A. S., before and following heparin administration, show shifts in the S_f° 0-400 lipoprotein distribution qualitatively similar to those previously described (1). The characteristic features of this shift are marked decreases in S_f° 20-400 lipoprotein species and increases in the S_f° 0-20. Figure 1 also shows the changes in HDL ultracentrifugal profiles following heparin.

The bar graphs in Fig. 2 show the quantitative changes of lipoprotein concentrations which occur within each of the 29 S_f° intervals of the subdivided S_f° 0-400 lipoprotein profiles of subject A. S. These graphs readily show the S_f° intervals within which positive or negative concentration changes occur. In the 18 minute postheparin sample decreases in concentration occur in the subintervals within the S_f° 20-400 (-76%) and S_f° 1-5 (-21%) ranges, and increases are observed in the subintervals within the S_f° 5-20 (+77%) range. The preheparin concentrations were 671 (S_f° 20-400), 355 (S_f° 5-20), and 269 (S_f° 1-5) mg/100 ml. The bar graph for the 75 minutes postheparin sample shows the S_f° ranges of major concentration change to be approximately S_f° 20-400 (-76%) and S_f° 6-16 (-69%). An increase in the S_f° 2-4 range is also observed (+23%). Preheparin concentrations were 671 mg/100 ml (S_f° 20-400), 212 mg/100 ml (S_f° 6-16), and 142 mg/100 ml (S_f° 2-4). Comparison of the HDL lipoprotein profile for the 18 minutes postheparin with the preheparin sample shows a slight shift of the HDL distribution to higher $F^\circ_{1.20}$ values with a low order increase of concentration in the $F^\circ_{1.20}$ 1.0-7.0 range. Similar comparisons for the 75 minute postheparin sample show a marked increase in HDL concentration in the $F^\circ_{1.20}$ 1.0-6.0 range.

Bar graphs of lipoprotein concentration changes per S_f° and $F^\circ_{1.20}$ intervals for subject S. B. following heparin are presented in Fig. 3. In the 18 minute postheparin sample the S_f° ranges of major concentration change are approximately S_f° 30-400 (-39%) and S_f° 8-30 (+17%). Changes in the ranges S_f° 5-8 and S_f° 3-5 are also observed but are of relatively lower magnitude than in the broader S_f° ranges noted above. Preheparin concentrations were 444 mg/100 ml (S_f° 30-400) and 262 mg/100 ml (S_f° 8-30). At 75 minutes postheparin, the major changes in concentration are observed in approximately the S_f° 20-400 (-43%) and S_f° 7-20 (+40%) ranges. Again, low magnitude changes are observed in the S_f° 5-7 and S_f° 3-5 ranges. Preheparin concentrations were 543 mg/100 ml (S_f° 20-400) and 184 mg/100 ml (S_f° 7-20). The bar graphs of concentration changes in HDL profiles for both the 18 and 75 minute postheparin samples show an increase in approximately the $F^\circ_{1.20}$ 0.5-3.5 and a decrease in approximately the $F^\circ_{1.20}$ 3.5-8 ranges.

Figure 4 presents examples of bar graphs of lipoprotein concentration changes observed in both subjects during prolonged administration of CPIB. These particular data are presented because they represent samples showing maximal reduction in S_f° 20-400 lipoproteins during the course of CPIB treatment. Such samples might also be expected to show maximal changes of concentration in other regions of the overall lipoprotein spectrum. Interpretation of small

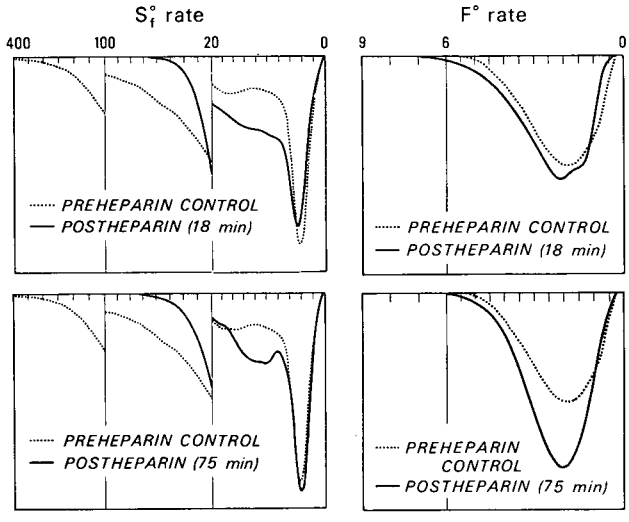

Fig. 1. Schematic representation of S_f° 0-400 (left) and $F^\circ_{1.20}$ 0-9, HDL (right) lipoprotein profiles 18 min (upper) and 75 min (lower) after heparin for subject A. S. DBL 6712-1906

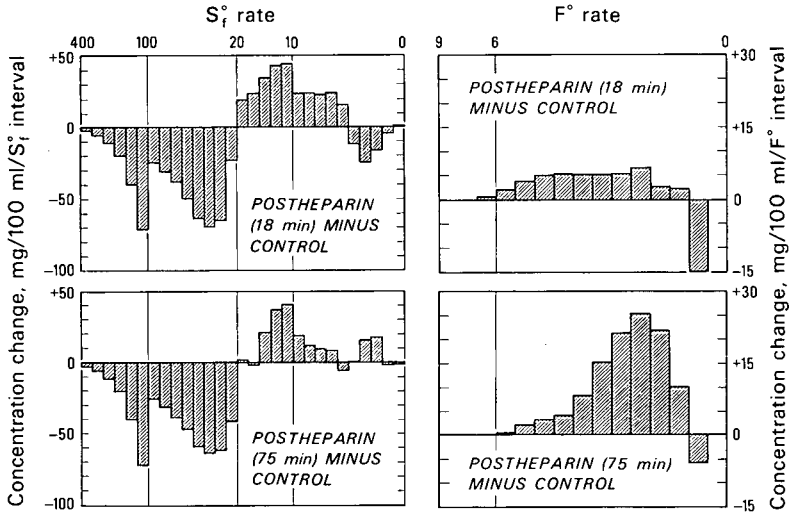

Fig. 2. Bar graphs of concentration changes in S_f° 0-400 (left) and HDL (right) profiles 18 min (upper) and 75 min (lower) after heparin for subject A. S. DBL 6712-1907

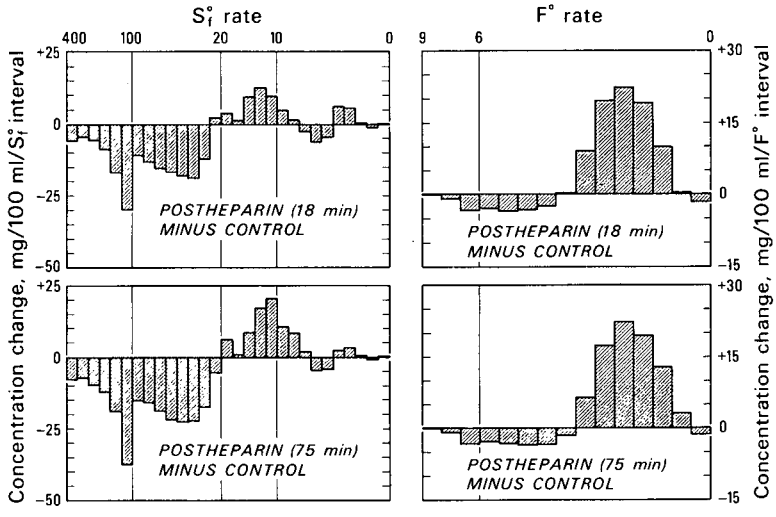

Fig. 3. Bar graphs of concentration changes in S_f° 0-400 (left) and HDL (right) profiles 18 min (upper) and 75 min (lower) after heparin for subject S. B. DBL 679-1813

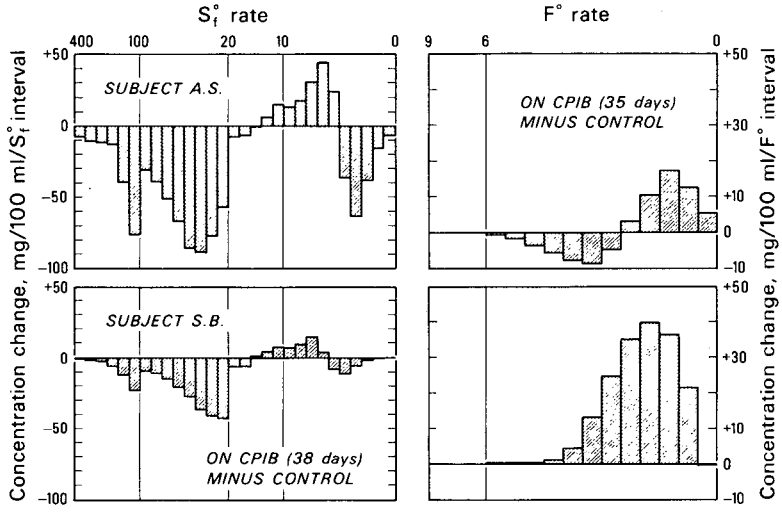

Fig. 4. Bar graphs of concentration changes in S_f° 0-400 (left) and HDL (right) profiles for subjects A. S. (upper) and S. B. (lower) 35 and 38 days, respectively, on CPIB. DBL 679-1817

changes in lipoprotein concentrations in the CPIB data are made with due regard to the limitation imposed by lack of rigid diet control; however, both patients were well motivated to keep their diets constant and maximal weight changes were within ± 2 lb.

In subject A. S. the concentration changes in the S_f° 0-400 profile appear in the following ranges: S_f° 14-400 (-60%), S_f° 5-14 (+67%), and S_f° 0-5 (-65%). Pre-CPIB concentrations were 1116 mg/100 ml (S_f° 14-400), 230 mg/100 ml (S_f° 5-14), and 245 mg/100 ml (S_f° 0-5). In the HDL profile of subject A. S. there appears to be a decrease (36%) in the $F_{1.20}^\circ$ 2.5-6.0 range with an increase (28%) in the $F_{1.20}^\circ$ 0-2.5. The data for subject S. B. show concentration changes in the S_f° 16-400 (-50%), S_f° 6-16 (+23%), and S_f° 0-6 (-35%) ranges. Pre-CPIB concentrations were 510 mg/100 ml (S_f° 16-400), 211 mg/100 ml (S_f° 6-16), and 77 mg/100 ml (S_f° 0-6). The concentration change observed in the HDL profile of subject S. B. is substantial (+74% relative to pre-CPIB concentration of 242 mg/100 ml) and occurs primarily within the $F_{1.20}^\circ$ 0.5-6.0 range.

DISCUSSION

In most analytic ultracentrifugal studies on changes in lipoprotein distributions rather broad flotation intervals have usually been used. In the low density region, the S_f° intervals primarily studied were the S_f° 0-12, S_f° 12-20, S_f° 20-100, and S_f° 100-400. By means of the currently available computerized analysis it is possible to analyze quantitatively the specific flotation intervals wherein positive or negative concentration changes occur. Detailed ultracentrifugal information on heparin-induced changes in lipoprotein distributions is now of special interest in light of the participation of the LDL and HDL protein moieties, as proteins or as lipoproteins, in VLDL structure (4, 7). Detailed delineation of the properties of the degradation products following heparin-induced lipolysis may provide insight into the roles of LDL and HDL in the removal of VLDL-triglyceride from the bloodstream.

The quantitative data of this report, in agreement with earlier qualitative observations, show the major degradation products in the low density lipoprotein distribution to appear within the S_f° 5-30 flotation interval. Paper electrophoretic analyses of postheparin plasma have also shown increases in β lipoprotein (7). Since either β lipoprotein or its protein moiety is part of the structure of VLDL, it is interesting that lipolytic degradation of this lipoprotein class leads to accumulations of products only within the S_f° 5-30 and not the entire S_f° 0-30 or total β lipoprotein range. The chemical composition data of Shore and Shore (8) showed that the postheparin products in the S_f 11-20 interval are very similar to physiologic S_f 12-20. If comparable lipolytic processes occur in the physiologic removal of VLDL-triglyceride and these degrade the VLDL only down to the S_f° 5-30, then the step leading to final physiologic removal of the S_f° 5-30 or its triglyceride is apparently an open question of considerable importance to our understanding of lipoprotein metabolism.

The lipolytic degradation of VLDL also leads to products in the HDL flotation interval. This observation would be expected because of the reported presence of HDL or HDL protein on VLDL. Our data confirm the results of Levy et al. (9) who, using paper electrophoresis, found increases in α or HDL lipoproteins following heparin. Our data are insufficient to

establish any specificities in flotation properties of these HDL products.

The data representative of the maximal changes in lipoprotein profiles following long-term administration of CPIB show a marked depression in serum concentrations of S_f° 16-400 lipoproteins in both subjects. At the same time there is also a decrease in concentration in the S_f° 0-6 interval which is associated with an increase in the S_f° 6-16 interval. These concentration changes in the S_f° 0-16 range result in an apparent increase in the flotation rate of the major peak in the S_f° 0-20 profile. The data are insufficient to draw any conclusions regarding similarities or differences in changes of lipoprotein profiles in response to heparin and CPIB. It should be noted, however, that with both agents the fall in VLDL levels is associated with increased concentrations in the approximate range of S_f° 5-30.

The present observations on the effects of heparin and CPIB on VLDL and HDL levels are in agreement with available data demonstrating inversely related responses of HDL and VLDL concentrations during periods when VLDL levels are altered (9).

SUMMARY

Changes in human serum lipoprotein distribution following heparin and ethyl-p-chlorophenoxyisobutyrate administration in vivo are evaluated by application of a computerized technique for analysis of ultracentrifugal films. Flotation rate ranges within which concentration changes occur are delineated for the two agents.

ACKNOWLEDGMENTS

This work was supported in part by USPHS Research Grants HE 10878-02 and HE 07220-03 from the National Heart Institute, U. S. Public Health Service, and by the U. S. Atomic Energy Commission.

The authors gratefully acknowledge the valuable technical assistance of Julia Tsai, Lin C. Jensen, and Robert E. Doyle.

REFERENCES

1. Graham, D. M.; Lyon, T. P.; Gofman, J. W.; Jones, H. B.; Yankley, A.; Simonton, J., and White, S.; Circulation 4: 666, 1951.
2. Strisower, E. H.; J. Atherosclerosis Res. 3: 445, 1963.
3. Gustafson, A.; Alaupovic, P., and Furman, R. H.; Biochemistry 5: 632, 1966.
4. Fredrickson, D. S.; Levy, R. I., and Lees, R. S.; New Engl. J. Med. 276: 215, 1967.
5. Lindgren, F. T.; Ewing, A. M.; Freeman, N. K., and Wills, R. D.; in Progress in Biochemical Pharmacology, Vol. 2, edited by D. Kritchevsky, R. Paoletti, and D. Steinberg, Basel/New York, Karger, 1966, p. 475.
6. de Lalla, O., and Gofman, J. W.; in Methods of Biochemical Analysis, Vol. 1, edited by D. Glick, New York, Interscience Press, 1954, p. 459.
7. Fredrickson, D. S.; Levy, R. I., and Lees, R. S.; New Engl. J. Med. 276: 94, 1967.
8. Shore, B., and Shore, V.; J. Atherosclerosis Res. 2: 104, 1962.
9. Levy, R. I.; Lees, R. S., and Fredrickson, D. S.; J. Clin Invest. 45: 63, 1966.

Subfractionation of $S_f > 400$ Serum Lipoproteins by Successive, Cumulative, Density Gradient Centrifugation

Walter J. Lossow, Frank T. Lindgren, Jack C. Murchio and Lin C. Jensen

"Chylomicrons" is the term introduced by Gage in 1920 (1) to describe particles readily discernible with the dark-field microscope that appear in plasma after a fatty meal. When present in plasma, they constitute the largest entities of the plasma lipoprotein spectra. They are usually isolated in the preparative ultracentrifuge in the S_f range of 400-10^5 (which includes particles approximately 750-11,000 Å in diameter) because $S_f > 400$ marks the upper limit for quantitation of lipoproteins by schlieren analysis in the analytical ultracentrifuge. The $S_f > 400$ serum lipoproteins consist of approximately 90% triglyceride and small amounts of cholesterol, phospholipid, and protein. By using a swinging bucket rotor and density gradient procedure, which effectively eliminate convective disturbances, and a computer program for calculating S_f recoveries, this class of very low density lipoproteins, precisely defined in terms of included S_f range, can be isolated following a single centrifugation free from significant contamination with serum protein or lipoproteins of lower flotation rates (2). Using this procedure, we have isolated $S_f > 400$ lipoproteins from thoracic duct chyle and from serum of rats, and determined their protein content by elemental NCH analysis coupled with a phospholipid assay (3). The weight percent protein of $S_f > 400$ lipoproteins isolated from chyle and from serum after fat loading was on the average 0.76 and 2.2%, respectively. On the basis of experiments in which rat chyle was incubated with serum or serum fractions, we have concluded that a net uptake of protein by $S_f > 400$ chyle lipoproteins occurs in serum and that the protein taken up is derived principally from higher density lipoproteins rather than other serum proteins (3).

All of the chylomicron protein appears to be associated with a surface "membrane" of which phospholipid is the principal lipid constituent (4). The proportion of the surface of chylomicrons covered by a given amount of protein will, of course, depend upon its molecular arrangement. We have calculated that, even if the surface protein existed in the form of an expanded monomolecular film 10 Å thick, no more than 27% of the surface of a chylomicron in the thoracic duct lymph of rats 3000 Å in diameter (containing 0.76% protein) could be covered with protein. After acquiring additional protein in serum (and raising the protein percentage to 2.2), 81% of its surface could be covered with protein. If the surface layer is 20 or 40 Å thick, the protein coverage will, of course, be about one-half or one-quarter of the above values.

While it is known that throughout the lipoprotein spectra the weight percent protein of serum lipoprotein increases with decreasing size, it is not known whether a precisely defin-

able relationship exists between lipoprotein size and protein content. For example, with respect to the largest group of lipoproteins, the $S_f > 400$ class, one might ask whether the relationship is such that, if surface coverage is calculated for a given surface layer thickness (and protein configuration), will a decrease in particle size (and an increase in surface-volume ratio) be just compensated for by an increase in protein percentage so that the same proportion of the surface will be covered with protein in all size groups isolated? Discontinuities in the relationship would indicate either changes in protein coverage (assuming no alteration in protein configuration) or changes in protein configuration. Pronounced discontinuities might suggest the occurrence of the latter. Investigation of this question requires a procedure for the isolation of discrete subfractions of the $S_f > 400$ lipoproteins. Development of such a procedure seems particularly desirable at this time because it would make possible the study not only of the question raised above but also other closely related problems, such as the investigation of changes in particle size distribution in lymph and serum during fat absorption and the more discrete distinction between exogenous and endogenous particles.

In this report we describe a density gradient procedure for the subfractionation of serum $S_f > 400$ lipoproteins and its evaluation by a comparison of the particle sizes at the boundaries of the subfractions calculated from the predicted S_f recoveries with a particle size vs. mass histogram derived by a computer program from direct measurements made on electron micrograph prints of each fraction. In addition, preliminary data is presented for the protein content and calculated surface protein coverage of three subfractions of $S_f > 400$ lipoproteins isolated from human serum.

METHOD

In the previously described procedures for isolating $S_f > 400$ lipoproteins from serum, in the first step 1 ml of serum was overlayered with 5 ml of a NaCl solution gradient in a preparative ultracentrifuge tube (2). For subfractionating the $S_f > 400$ lipoproteins we have scaled up this density gradient system to 3 ml of sample and a 14 ml NaCl solution gradient. The same salt solutions are used to prepare the gradients, but in the following volumes (from highest to lowest density): 1 ml each of the first two solutions and 3 ml each of the remaining four. This gradient is nonlinear. It is steepest just above the sample, to restrict the formation of negative gradients arising from the migration of particles from the layered boundary, and declines gradually in steepness thereafter. Two modifications have been introduced in the initial steps of the procedure. Solid, epoxy, hemispherical inserts which fit snugly into the bottom of the centrifuge tubes are placed in the tubes (over a few drops of NaCl solution of the same density as the sample) before the addition of the sample. This is done to eliminate the curvature in the lower boundary of the sample. To facilitate the transfer of the sample to the centrifuge tube without touching the inside walls of the tube with the transfer pipette (which would contaminate the overlayering salt solutions with sample), a lucite sleeve, measuring approximately one-third of the length of the tube, is inserted into the tube to act as a guide for the pipette.

The computer program developed for calculating the recovery of $S_f > 400$ lipoproteins in the top 1 ml of the centrifuge tube after centrifuging 1 ml of serum overlayered with a density

gradient (2) enables us to calculate the centrifugal conditions for the recovery of lipoproteins of a given flotation rate range in the top layer as well as their positions in the tube at any time during the centrifugation. One of two procedures could be adopted for the subfractionation. We could, after a single centrifugation under a given set of conditions, remove a number of layers, starting from the top of the tube. Alternatively, we could centrifuge repeatedly under prescribed conditions and successively remove layers from the top after each centrifugation. The principal advantage of the latter procedure is that, by bringing all fractions to the top in such a manner, it increases the distance traveled by each and concentrates them into thin top layers. As a result, the difference between 100% and threshold recovery calculated for any given subfraction is reduced. This also means that the theoretical overlap among fractions is reduced. In addition, a thin, top, packed layer can be more readily removed without contamination by its underlying layer than broad layers spread throughout the tube. The chief disadvantage of a procedure involving successive centrifugations is the disturbance of the layers each time a fraction is removed and the rotor moved from and to the centrifuge. It was our judgment, on the basis of our experience with these methods, that the advantages of a cumulative, successive fractionation procedure would outweight any disadvantage.

In our initial trials, therefore, we adopted the following procedures for a 3-stage subfractionation of samples of serum obtained from a diabetic at Highland Hospital 8 hours after the patient consumed a mixture containing 100 g of safflower oil: As described above and in reference 2, 3 ml of the serum samples, raised to a background density of 1.063 with solid NaCl, were placed in heavy-walled centrifuge tubes ($5/8 \times 4$ in.) and overlayered with the 14 ml NaCl solution gradient. They were centrifuged in a 25.3 swinging bucket rotor in a Spinco model L2-65 ultracentrifuge (modified to achieve temperature stability to $\pm 0.2°C$ during a run and rotor speed stability to ± 30 rpm) at room temperature at 12,000 rpm for a period of time calculated to bring 100% of the $S_f > 3200$ lipoproteins into the top 0.5 ml. At 23°C this centrifugation, including acceleration and deceleration, is equivalent to 0.734×10^6 g min. The initial rotor temperature determined the exact shut-off time (generally on the order of 38 min). The top 0.5 ml was quantitatively transferred (2) to 8 ml vials, which were then sealed with plastic-lined caps. Second and third 0.5 ml top layers were collected in the same manner following centrifugations first at 12,000 rpm and finally at 20,000 rpm for periods of time calculated to bring into the top 0.5 ml, successively, $S_f > 1100$ and $S_f > 400$ lipoproteins. The approximate times for the second and third centrifugations were 70 min (1.310×10^6 g min at 23°C) and 63 min (3.36×10^6 g min at 23°C). After collecting the third 0.5 ml fraction, an additional 0.5 ml layer was removed for measurement of the background salt density and possible serum protein contamination. The precise 100% and threshold recoveries of each of the three fractions were calculated (2) from the centrifugal conditions, including the mean rpm, the initial and final rotor temperatures, and the up-to-speed, shut-off, and deceleration times. The total mass of each fraction was determined by elemental NCH analysis (2).

Electron micrographs of each fraction were obtained as follows: Aliquots were diluted 1:100 with glass-distilled H_2O. Drops, containing approximately 0.005 ml, were placed on collodion-covered stainless steel grids and fixed with OsO_4 vapor in a humidity chamber.

After air drying they were shadowed with uranium in a vacuum evaporator. Electron micrographs were taken at known magnifications with an RCA-2D microscope. The diameters of the lipoprotein particles were measured on 8-1/2 × 10 in. prints (representing a total magnification of 24,280 ×) of each photomicrograph, using a pair of dividers and a vernier caliper calibrated to 0.02 mm. A computer program converted these measurements into angstroms, sorted all particles of a given fraction into an ascending sequence of diameter, and calculated the molecular weight of each particle, assuming a uniform hydrated density of 0.93 g/ml. From these data a mass vs. particle size histogram showing each fraction was constructed by a CalComp plotter, in which each fraction was normalized to its proportion of the total mass by including in the program values for lipoprotein mass obtained by NCH analysis. The histogram intervals for each fraction studied were chosen to represent 10% or more of the total molecular weight, resulting in rectangles of approximately equal area. In addition, the sum of all fractions was manually plotted above the histogram in order to show the mass vs. particle size distribution for the total $S_f > 400$ lipoproteins.

RESULTS

Shown in the upper part of Fig. 1 are the anticipated S_f values for the recovery of 100% and 0% (threshold recovery) of the lipoproteins in each fraction and the particle diameters at the fraction boundaries calculated from these recoveries. Plotted for each fraction in the lower part of Fig. 1 is lipoprotein mass vs. particle diameter, derived from the particle size measurements made on electron micrograph prints.

The predicted mean particle diameter at the boundary between fractions I and II was 2012 Å. According to the histograms, 97.7% of the mass of fraction I was isolated as particles larger than that dimension, and 84.4% of the mass of fraction II was isolated as particles smaller than that size. The anticipated mean particle diameter at the boundary between fractions II and III was 1175 Å. On the basis of the histograms, 97.3% of the mass of fraction II was recovered as particles larger than that size while 55.3% of the mass of fraction III was recovered as smaller particles. Essentially 100% of the mass of fraction III was recovered as particles larger than the particle size predicted for the lower boundary of that fraction. The one major discrepancy then between the predicted particle sizes and the particle size distribution derived from electron microscopy measurements was the recovery, calculated from the histograms, of 45% of the mass of fraction III as particles larger than predicted from the S_f recoveries. Apart from that discrepancy, for which there does not appear to be an obvious explanation, the data may be considered to show a quite satisfactory agreement between the predicted and measured particle sizes.

Shown in Table 1 are the values for the weight percent protein of each lipoprotein fraction calculated from the N/N+C+H ratios and phospholipid content (2), the latter determined by a phosphorous assay (5). The protein percentages decreased with decreasing particle size. Listed also are the values calculated for the protein coverage of particles representing the average size (derived from the histograms) in each fraction. In these calculations the density of the protein was assumed to be 1.33 g/cc and that of the lipid moiety 0.93 g/cc. Protein coverage was calculated as 100 times the ratio of the experimentally determined weight percent

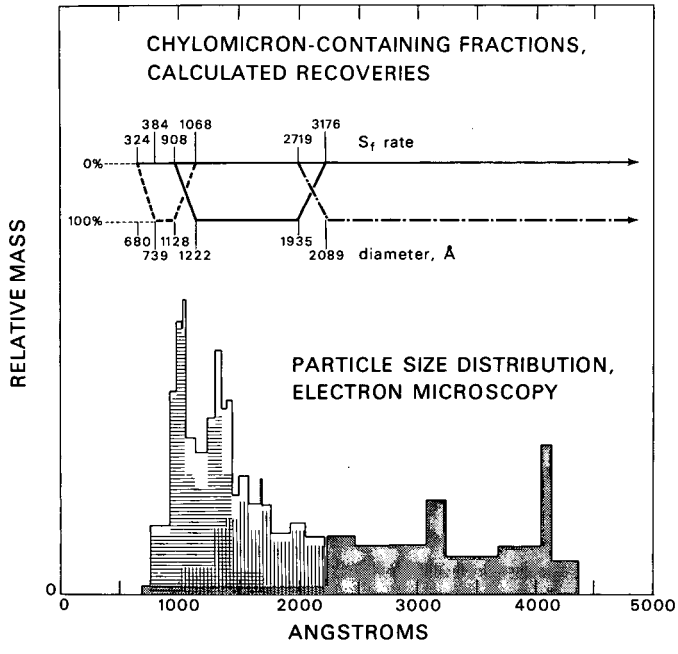

Fig. 1. Subfractionation of $S_f > 400$ serum lipoproteins.

Upper part: Diagrammatic representation of predicted 100% and threshold (0%) recoveries for each subfraction, and the particle diameters at the boundaries calculated from these recoveries.

Lower part: Plot of lipoprotein mass vs. particle diameter, derived from measurements of particle diameter on electron micrograph prints. Each subfraction is normalized according to its total mass determined by elemental NCH analysis.

DBL 681-4535

protein to the weight percent protein calculated for 100% coverage of a particle with a surface layer 20 Å thick. The percent coverage calculated for the three fractions was quite similar. This suggests that as the particle size decreases the increase in weight percent protein just compensates for the increased surface-volume ratio so that the protein constitutes the same proportion of the outer "membrane" for all $S_f > 400$ lipoproteins.

SUMMARY

A procedure is described for the separation of serum $S_f > 400$ lipoproteins into three subfractions by successive, cumulative centrifugation in a density gradient, with the removal of thin top layers after each centrifugation. Particle sizes of each subfraction calculated from the predicted S_f recoveries were compared with the particle size distribution derived from measurements of particle diameters on electron micrograph prints. The single discrepancy between the particle sizes predicted and measured by these techniques was the observation in the third subfraction of a sizeable proportion of particles by measurement larger in diameter than predicted from the S_f recoveries. Measurement of the protein content of each lipoprotein subfraction and calculation of surface protein coverage suggest that the increase in surface-volume ratio with decreasing particle size is just compensated for by an increase in protein content, so that protein coverage remains the same for all serum $S_f > 400$ lipoproteins.

ACKNOWLEDGMENTS

This study was supported by Research Grant 5 R01-HE-1882-CA from the National Heart Institute, and by the U. S. Atomic Energy Commission. We are indebted to Dr. Laurance W. Kinsell, Director of the Institute for Metabolic Research, Highland General Hospital, Oakland,

Table 1. Elemental analysis and protein content of three subfractions of $S_f > 400$ serum lipoproteins.

Fraction	Σ μg NCH/0.1 ml	N/N+C+H (× 10^3)	Weight % phospholipid*	Weight % protein	% of surface covered with protein†	Mean mass % lipoprotein
I	385, 395	2.67, 2.40	2.6	1.28, 1.12	24.0, 21.0	43.4
II	206, 214	4.76, 3.65	5.1	2.21, 1.56	22.3, 15.7	23.5
III	296, 295	7.10, 6.44	8.7	3.16, 2.77	21.1, 18.5	33.1

*Mean of duplicate phosphorus analysis. Total phospholipid = 25 × P.
†Calculated for an outer "membrane" 20 Å thick.

California, for kindly supplying blood specimens obtained from a patient in the metabolic ward of the hospital.

REFERENCES AND NOTE

1. Gage, S. H.; The free granules (chylomicrons) of the blood as shown by the dark-field microscope. Cornell Veterinarian 10: 154-155, 1920.
2. Hatch, F. T.; Freeman, N. K.; Jensen, L. C.; Stevens, G. R., and Lindgren, F. T.; Ultracentrifugal isolation of serum chylomicron-containing fractions with quantitation by infrared spectrometry and NCH elemental analysis. Lipids 2: 183-191, 1967.
3. Lossow, W. J.; Lindgren, F. T., and Jensen, L. C.; Net uptake of rat serum protein by $S_f > 400$ lymph chylomicrons in vitro. Biochim. Biophys. Acta 144: 670-677, 1967.
4. Zilversmit, D. B.; The composition and structure of lymph chylomicrons in dog, rat, and man. J. Clin. Invest. 44: 1610-1622, 1965.
5. Bartlett, G. R.; Phosphorous assay in column chromatography. J. Biol. Chem. 234: 466-468, 1959.

Jack C. Murchio is associated with the Department of Public Health, Division of Air and Industrial Hygiene, Berkeley, California.

A Calculation of the Physical Characteristics of Negative Pion Beams
Energy-Loss Distribution and Bragg Curves

Stanley B. Curtis and Mudundi R. Raju

INTRODUCTION

Considerable interest has been shown in the past several years in the possibility of using a negative pion (π^--meson) beam in radiotherapy (1-4). Negative pions have unique properties not shared by any of the radiations now used in radiotherapy. The pions travel through matter at low ionization levels and, when they come to rest, are captured by nuclei and undergo violent nuclear interactions, causing low-energy highly ionizing particles to be emitted as the nuclei break up. The depth of pion penetration depends on the initial energy of the particle. Most of the particles in an incoming beam survive and come to rest at the end of their range; the rest either decay or undergo nuclear interaction in flight. When the negative pion comes to rest in water, it is captured by either a proton or oxygen nucleus, forming a π^--mesic atom. If it is captured by a proton, the resulting neutral atom diffuses through the medium until an oxygen nucleus is encountered. The pion is then captured by the oxygen nucleus, since the resulting energy of the system is lower; that is, the pion can be more tightly bound. The pion cascades down through the energy levels in the π^--mesic atom until it reaches the ground state. The overlap of the nucleus and pion is then such that the probability of a nuclear interaction is unity and the interaction occurs. All this happens in times short compared with the mean lifetime of the pion of 2.6×10^{-8} sec. Some work (2, 5, 6) has been done on the identification of the particles emerging from these nuclear interactions, or "stars" as they are called in nuclear emulsion.

An attempt is made here to calculate a few of the physical characteristics of pion beams (both pure and contaminated with other particles) which are of interest in evaluating the potentialities of such a beam for radiotherapy. It should be emphasized at the outset that the following calculation is only as good as the input experimental data and the subsequent assumptions and approximations allow it to be. The final test of the suitability of pion beams for radiotherapy will come from the laboratory, where controlled experiments can be conducted on biological systems and the resulting effects can be carefully measured.

Throughout the calculation, many of the geometrical and physical input data reflect experimental conditions in the meson cave of the 184-inch cyclotron at the Lawrence Radiation Laboratory, where much of the experimental work is being carried out (3, 4). One artificial assumption is made: The incident pion beam is initially parallel and uniformly distributed. This

is difficult to achieve experimentally, but it is certainly possible to achieve a beam parallel enough and with great enough uniformity to allow the following analysis to be valid. As comparison with experimental results shows, the analysis predicts well the gross features of the variation of ionization with depth in water, and there is no reason to believe that the resulting distribution of dE/dx is not roughly correct also.

The input data of the differential energy spectra of particles emerging from a pion interaction at rest come from the fine experiments performed in water-impregnated emulsion by P. H. Fowler and his group at the University of Bristol (2). By a subtraction process, they obtained the spectra of the various particles: protons, α particles, ^{7}Li ions, and the heavy recoils (boron, carbon, and nitrogen) which result from the capture of a negative pion by an oxygen nucleus in water. To simplify the calculation, all the heavy recoils are assumed here to be carbon nuclei. The pion rest-mass energy of 140 MeV is available for overcoming the binding energy in the nucleus and giving kinetic energy to the emitted particles.

THE dE/dx DISTRIBUTION

We first define a function, $F(\epsilon)$, which we call the dE/dx or energy-loss distribution (sometimes called the LET spectrum). $F(\epsilon)$ is defined so that

$$\int F(\epsilon)d(\log\epsilon) = \text{total energy deposited per unit mass at the point in question per incident pion/cm}^2. \tag{1}$$

Here ϵ is the collision or ionization energy loss per unit length, dE/dx. We use the differential of the logarithm of ϵ because of the wide range in dE/dx involved in this problem. It will be convenient to plot the distribution logarithmically in dE/dx, and so equal distances along the abscissa will have equal weights if $F(\epsilon)$ is defined as above. The integral we note is proportional to the dose deposited at the point. We assume that all the energy is deposited locally, i.e., δ-ray corrections are small.

From the standard manner in which doses are calculated from particle fluxes, we can form the equality

$$\frac{dJ}{dE}\,\epsilon dE = F(\epsilon)d(\log\epsilon), \tag{2}$$

where dJ/dE is the differential energy spectrum at the point, i.e., the number of particles per unit energy interval, area, and incident fluence. From equation 2 we solve for $F(\epsilon)$, obtaining

$$F(\epsilon) = 2.303\,\frac{dJ}{dE}\,\epsilon^2/\frac{d\epsilon}{dE}\,. \tag{3}$$

For a given ϵ, we can easily calculate $d\epsilon/dE$, which is the slope of the dE/dx-vs.-E curve (7). In the low-energy region, the work of Northcliffe has been used (8). A more difficult task is the determination of dJ/dE at the point in question for the various particles emerging from the pion stars. This quantity is calculated for one particle type in Appendix I, and the result is given here:

$$\frac{dJ}{dE} = \frac{\rho(Z)}{\epsilon}\int_E^{E_{max}} \frac{dJ}{dE_0}\,dE_0, \tag{4}$$

where $\rho(Z)$ = density of stopping pions at a depth Z in the water per incident pion fluence,

ϵ = dE/dx of particle of energy E,

E_{max} = maximum energy of particles emitted from a star–the exact value of E_{max} is not important, since the spectrum drops off steeply as a function of energy,

$\frac{dJ}{dE_0}$ = differential energy spectrum per pion star for the particle type in question,

E_0 = initial energy of particles emerging from the star.

Substituting equation 4 into 3, we have, for the energy-loss distribution,

$$F(\epsilon) = \frac{2.303\ \rho(Z)\ \epsilon}{d\epsilon/dE} \int_E^{E_{max}} \frac{dJ}{dE_0}\, dE_0. \tag{5}$$

Note that

$$\int_E^{E_{max}} \frac{dJ}{dE_0}\, dE_0$$

is just the total number of particles emerging from the star with initial energy greater than E. The total $F(\epsilon)$ for the stars is the sum of the contributions from each particle type:

$$F(\epsilon)_{\text{total star}} = F(\epsilon)_{\text{proton}} + F_{\alpha}(\epsilon) + F_{^7\text{Li}}(\epsilon) + F_{^{12}\text{C}}(\epsilon). \tag{6}$$

CONTRIBUTIONS FROM OTHER PARTICLES IN THE BEAM

The presently available pion beams unfortunately contribute low dE/dx components to the ionization deposited in the star region. Those pions which have not yet stopped have dE/dx higher than minimum but lower than the high dE/dx of the charged particles emitted in the star. This contribution is calculated as follows. It is necessary to know the momentum or energy spread of the beam in order to calculate how many pions at any point have not yet stopped. We have assumed an initial beam of mean momentum 190 MeV/c, with the particle momenta in a Gaussian distribution with standard deviation 5 MeV/c. These are values taken from our experimental beam at the 184-inch cyclotron. The energy-loss distribution is calculated from equation 3, with

$$\frac{dJ}{dE}\,\epsilon = \frac{dJ}{dp_0}\,\frac{dp_0}{dE_0}\,\epsilon_0 \exp(-Z/\lambda), \tag{7}$$

where λ = the pion interaction mean free path (= 68 cm, the "geometric" mean free path, in this calculation)

$$\frac{dJ}{dp_0} = \frac{1}{\sigma(2\pi)^{1/2}} \exp\left[-\frac{1}{2}\left(\frac{p_0 - \bar{p}}{\sigma}\right)^2\right],$$

where $\bar{p}$ = the mean initial pion momentum,

p_0 = the initial pion momentum,

σ = the standard deviation,

E_0 = the initial pion energy,

Z = depth into the water,

ϵ_0 = dE/dx of the pions of initial energy E_0.

The exponential factor in equation 7 takes care of those pions lost from the beam through nuclear interaction before reaching the stopping region. We assume no dose contribution

from these interactions. We also neglect pion decay occurring in the water.

Accompanying the pions in the beam are muons and electrons of the same momentum. The approximate percentages of the various components of our initial beam are 65% pions, 25% electrons, and 10% muons (3). The muons are products of those pions which decay before reaching the final momentum-selection device. Their contribution to the energy-loss distribution is calculated in the same way as the pion contribution, with the omission of the exponential factor, because muons do not undergo absorption via the nuclear interaction. The electrons arise mainly from high-energy neutral pions decaying into two γ rays with subsequent electron-positron pair formation in the target. The electrons were assumed to have minimum ionization everywhere and to undergo a slight buildup because of electromagnetic shower production through the water. The electron dose was considered to increase linearly with depth and to reach 1.5 times the initial dose at 40 cm depth. For comparison, the peak region of the ionization curve for the stopping pions occurred at about 25 cm in our beam.

CONSTRUCTION OF THE BRAGG CURVE

The portion of this study dealing with the pion and muon contaminations lends itself to computer analysis, and a program was written for the CDC 6600 to calculate the energy-loss distributions for the pion and muon components as a function of water depth and then to integrate these to obtain the energy deposited per unit volume so that relative ionization depth-dose curves (Bragg curves) could be obtained. The contribution from the stars in the stopping region was included by multiplying the density of stars at the various points in the star region by a constant and adding it to the other contributions. This constant value, which is calculated to be 29 MeV, can be considered the intrinsic contribution of one star to the ionization deposited on the average in the medium. It is just

$$\frac{1}{\rho(Z)} \int_{-\infty}^{\infty} F(\epsilon)_{\text{total star}} \, d(\log\epsilon),$$

where $F(\epsilon)_{\text{total star}}$ is as given in equation 6.

RESULTS

The dE/dx distribution at 25.5 cm of water arising from all the components—stars, pions, muons, and electrons—are added together and shown in Fig. 1. The contribution from each component is also indicated. The spikes from the various components at high dE/dx arise at the point where $d\epsilon/dE$ goes through zero (see equation 3). It is seen from the figure that there is considerable contamination from low-dE/dx components. The area under the curve is proportional to the dose, and by integrating this function at several depths and normalizing the results to the dose at the entrance, a normalized central-axis depth-dose curve can be constructed. This is shown in Fig. 2 for a beam consisting only of pions, and in Fig. 3 for the contaminated beam described above, consisting of 65% pions, 10% muons, and 25% electrons. Also indicated in Fig. 3 is the contribution from neutrons, which is seen to be small. The calculation of the neutron contribution is outlined in Appendix II.

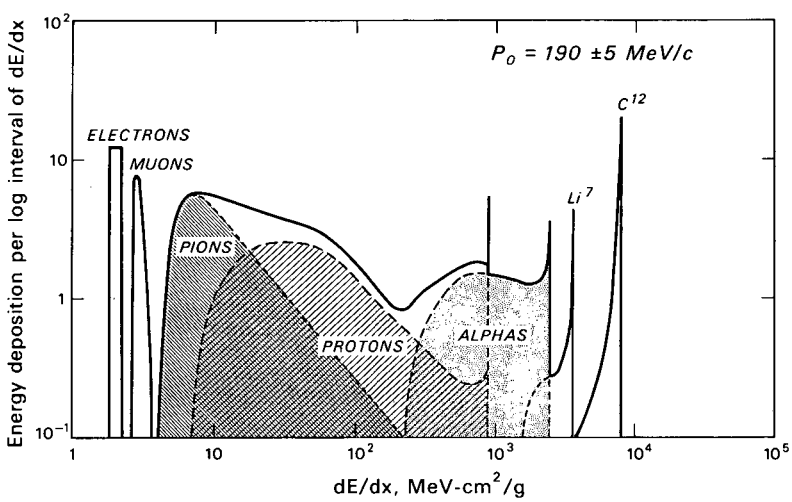

Fig. 1. The dE/dx distribution of a contaminated negative pion beam at 25.5 cm of water in the Bragg peak region calculated for an incident Gaussianly distributed momentum distribution 190 ± 5 MeV/c. The contribution of each component is shown. The beam was assumed to be composed initially of 65% pions, 25% electrons, and 10% muons. The ordinate is in MeV per gram per logarithmic interval of dE/dx per incident pion/cm^2.

DBL 673-1581

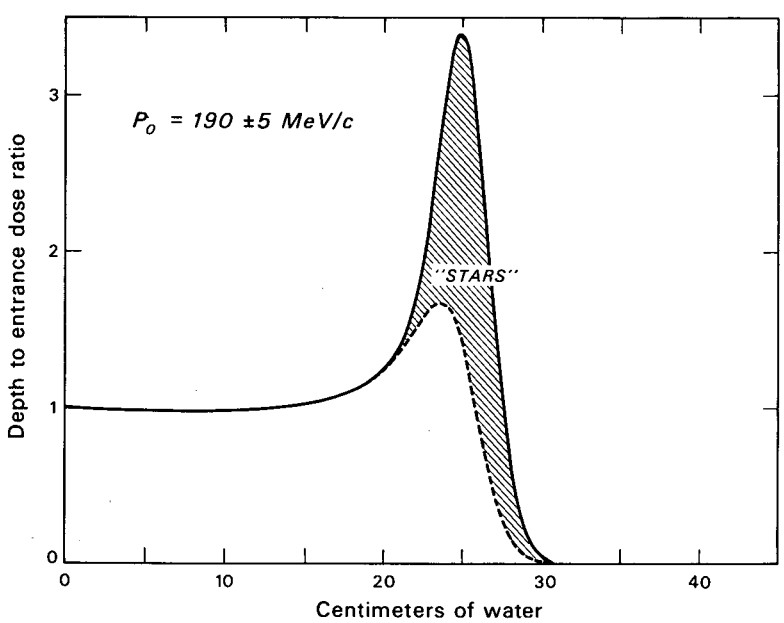

Fig. 2. A normalized central-axis depth-dose curve in water for a pure negative pion beam of incident momentum 190 ± 5 MeV/c. The additional contribution of dose in the peak region due to the pion interactions or stars is indicated.

XBL 674-1369

MULTIPLE SCATTERING AND STRAGGLING CONSIDERATIONS

We have neglected both multiple scattering of the beam and range-straggling effects. The multiple scattering is negligible because the calculated Bragg curve is a central-axis curve; the width of the multiple scattering distribution is small compared with the radius of the beam cross section used in our experiments. The standard deviation of the projected multiple scattering distribution of a pencil beam of stopping pions can be approximated well (see multiple scattering treatment in Appendix II) by

$$\sigma_{ms} = 7.63 \times 10^{-2} R_0^{0.95}$$
$$= 1.65 \text{ cm in the stopping pion region } (R_0 = 25.5 \text{ cm}).$$

Since this is small compared with the half-width of our beam of 3.8 cm, the spreading of the beam is appreciable only near the edges, and our central-axis value is relatively unaffected by multiple scattering. The correction on the beam axis would be 4%, assuming a uniform incident beam.

The amount of straggling can be approximated by using the graph and table given in the American Institute of Physics Handbook (9). The percentage change in the range due to straggling is Gaussianly distributed and the fractional standard deviation is given by

$$\sigma_s/R_0 = \left(\frac{102.2}{mc^2}\right)^{1/2} f(E/mc^2),$$

where m is the pion mass. The function $f(E/mc^2)$ is given as a function of energy in the graph for iron in the Handbook, and interpolation to other elements can be made by using the accompanying table. For pions of energy 96 MeV, the result in water is

$$\sigma_s/R_0 = 0.024 \text{ or } \sigma_s = 0.6 \text{ cm}.$$

Figure 4 shows the density (as a function of depth) of stopping pions, as calculated by the computer program. The shape of the curve is due to the initial momentum spread. A Gaussian approximation with standard deviation 1.6 cm is shown as the solid curve. It is seen that the pions stop in an approximately Gaussian distribution. The folding of two Gaussians produces another Gaussian of standard deviation,

$$\sigma = (\sigma_1^2 + \sigma_2^2)^{1/2},$$

where σ_1 and σ_2 are the standard deviation of each Gaussian. Thus, folding the straggling distribution into the distribution due to the initial momentum spread yields the total standard deviation,

$$\sigma = 1.7 \text{ cm}.$$

We see that the straggling correction adds only 1 mm to the spread due to momentum spread of the initial beam, therefore it has been neglected in the calculation.

Finally, there is a small correction to the straggling due to multiple scattering. This effect has been estimated and is a small fraction of the straggling correction and so is also neglected.

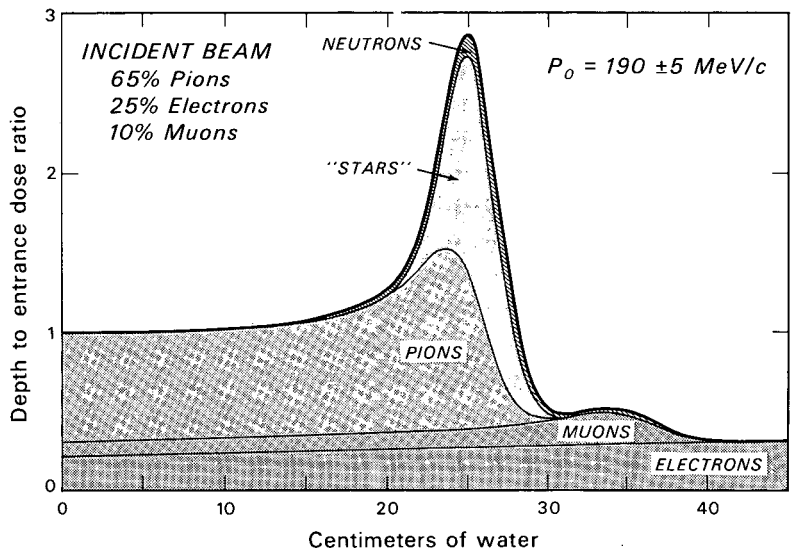

Fig. 3. A normalized central-axis depth-dose curve in water for a contaminated beam of negative pions of incident momentum 190 ± 5 MeV/c. The contributions from the contaminant particles are indicated.

DBL 673-1580

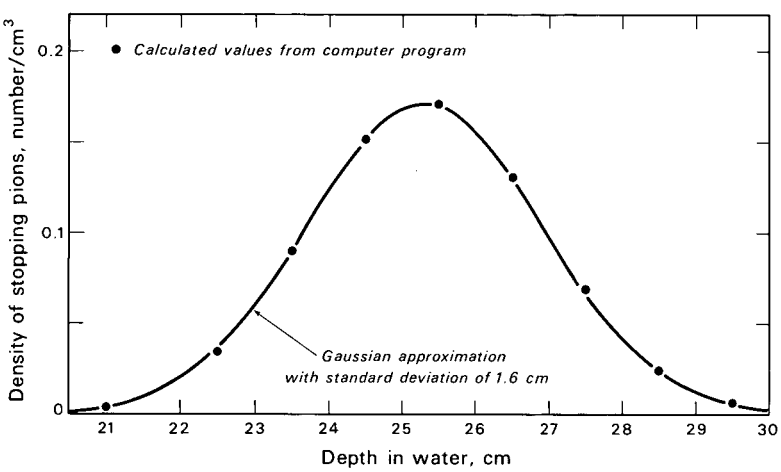

Fig. 4. The relative density of stopping pions of 190 ± 5 MeV/c in water as a function of depth through the stopping region. The points denote results from the computer program. The solid curve is a Gaussian fit with a standard deviation of 1.6 cm.

DBL 673-1583

DISCUSSION

It is seen from Figs. 2 and 3 that the dose in the stopping pion region is increased markedly by the presence of the particles produced in the nuclear interactions. For the pure pion beam, the maximum depth-to-entrance dose ratio is 3.4 and the full width at half maximum (i.e., the width of the curve when it has a value halfway between 1.0 and its maximum value) is 3.5 cm. For the contaminated beam, the maximum dose ratio is 2.9 and the full width at half maximum is 4 cm. The maxima of both these curves occur at 25 cm of water for a beam of 190 MeV/c initial momentum.

It is possible to calculate the relative contributions to the dose from the various types of particles at, for instance, the maximum of the dose curve. The percentage of dose caused by the pions which have not yet stopped varies greatly through the peak region. Table 1 gives percentage contributions from the various particles at 25.5 cm of water, near the maximum of the dose curve, for both the pure and contaminated beams. Here, the pions which have not yet stopped contribute 35% and 30% of the dose, respectively. It is seen that the most heavily ionizing components (^{4}He, ^{7}Li, ^{12}C ions, and neutrons) account for 32% and 28% of the dose for the pure and contaminated beams, respectively. The other 30% of the dose comes from the protons, which are seen from Fig. 1 to be mostly in the low dE/dx range. These percentages vary as a function of incident particle momentum as well as momentum spread of the beam.

Although this calculation was carried out under the assumption that the medium in which the pions stopped was water, it is of some interest to compare these results with preliminary data of a dose curve measured with a lithium-drifted silicon detector in the pion beam at the Berkeley 184-inch cyclotron, as reported by Raju et al. (10). This comparison is shown in Fig. 5. Experimentally, the linearity of the electronic system required is difficult to achieve over the large range of pulse heights present in the stopping pion region, and the experimental data presented must be considered of a preliminary nature (10). The agreement is good, however, and could probably be made better by adjusting the momentum spread of the incident beam used in the calculation. Computer runs were made with spreads of 3, 5, and 7 MeV/c and the best fit (5 MeV/c) was chosen. This is a reasonable value and had been estimated prior to these experiments by the physics groups using this pion beam.

The higher dose, beyond the pion peak in the experimental data, has not been completely explained, but may well be due to the contribution from negative muon-capture processes in the silicon detector. The probability for such processes rises as Z^4, for low Z, where Z is the atomic number of the stopping material. The probability for nuclear capture of the muon equals the probability for muon decay at $Z \approx 10$. Since silicon has a Z of 14 and oxygen has a Z of 8, capture processes will dominate in the detector while decay will dominate in water. The capture process is $\mu^- + p \rightarrow n + \nu$. The neutrino carries off most of the energy. The most probable fate of the resulting excited nucleus is for one or more low-energy neutrons to be "boiled off" in an evaporation process. This would lead to a small increase in dose in the silicon detector around the muon stopping region. Another process, which occurs with less probability, is the direct emission of charged particles. A theoretical calculation of this

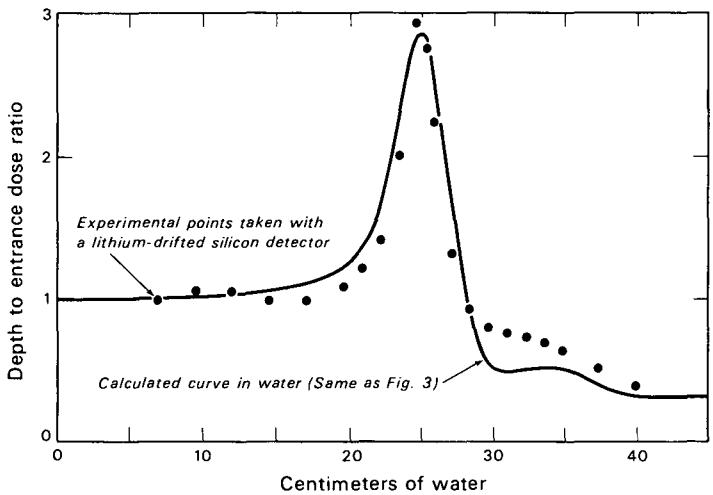

Fig. 5. Comparison of the calculated Bragg curve (Fig. 3) with experimental results obtained with a lithium-drifted silicon detector in a water phantom.
DBL 673-1582

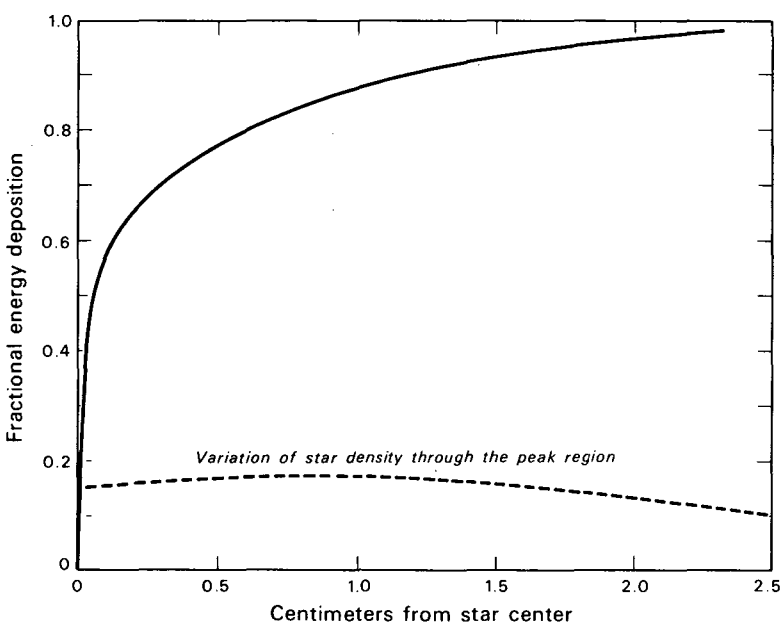

Fig. 6. The fraction of energy deposited by a single pion star inside a given distance plotted against distance from the star. The variation of an arbitrarily selected portion of the density of stopping pions (star density) is plotted through the peak of the star region for comparison.
XBL 674-1368

Table 1. Percentage contribution of various particles to the dose at the maximum of the dose curve.*

Particle type	Pure beam (no electrons or muons)	Contaminated beam (10% muons, 25% electrons in incident beam)
	(Percent contribution)	
Protons	33	28
He ions	14	12
^{7}Li ions	2	2
^{12}C ions	9	8
Neutrons	7	6
Pions (not yet stopped)	35	30
Electrons	--	10
Muons	--	4

*Beam Conditions: 190 ± 5 MeV/c-momentum beam in water.

correction for silicon has not been attempted. The dose in the muon stopping region in water arising from muon-decay electrons has been estimated to be not more than 10% of the muon contribution shown in Fig. 3, and so was not included in the figure.

In view of the fact that the calculation was made for water and the experimental data were obtained in a silicon detector with a somewhat nonuniform pion beam, the comparison between the theoretical and experimental results as shown in Fig. 5 is considered satisfactory. In fact, the similarity between the two results indicates that the nuclear interactions occurring when pions are captured in silicon do not produce significantly different particle types and spectra from those occurring in water. Thus, silicon detectors appear to be useful dosimeters for measuring the distribution of dose from pion beams in water.

SUMMARY

The physical properties of a stopping negative pion beam have been studied in connection with dosimetry experiments with such beams at the Berkeley 184-inch cyclotron. Calculations have been made of the dE/dx distribution in the stopping pion region, and central-axis depth-dose curves (Bragg curves) have been computed with the assumption of a uniform parallel incident beam with a large enough cross section so that multiple scattering can be neglected. A Gaussianly distributed incident momentum spread is assumed such that the width of the Bragg peak in the stopping region due to momentum straggling is large compared with range straggling effects. This approximates well our experimental situation. Although the calculations were carried out with water as the stopping medium, comparison of the resulting Bragg curve with an experimental curve obtained with a silicon detector shows good agreement. This result implies that the nuclear products emerging from a silicon nucleus after pion capture do not alter significantly the dose in silicon from the dose expected in water. Thus it appears

that silicon detectors can be used to obtain information on dose distributions of stopping pion beams in water phantoms.

ACKNOWLEDGMENTS

It is a pleasure to acknowledge the assistance of Mr. Michael Levitt, who was responsible for the numerical analysis of the neutron contribution presented in Appendix II, and Mr. John Sperinde, who helped with the considerations of multiple scattering effects. The suggestions and encouragement of Prof. C. Richman are gratefully acknowledged. We wish also to acknowledge the support of Profs. C. A. Tobias and J. H. Lawrence throughout the course of this work.

This work was performed under the auspices of the United States Atomic Energy Commission, the American Cancer Society, and the Office of Naval Research.

APPENDIX

I. CALCULATION OF dJ/dE AT DEPTH Z IN THE PION STOPPING REGION We assume a uniformly distributed parallel beam of incident pions to calculate dJ/dE at a depth of water, Z, in the pion stopping region on the central axis of the beam. The beam is assumed to have a large enough cross section so that edge effects are nonexistent on the central axis. We let dJ/dE_0 be the number of particles of a given type (e.g., protons) of energy between E_0 and $E_0 + dE_0$ emitted isotropically from a pion interaction. The quantity dJ/dE_0 is the differential energy spectrum per star. The spectra measured by Fowler (2) in oxygen have been used in this calculation. Now we let $f_D(E_0, r)$ equal the number of particles of initial energy between E_0 and $E_0 + dE_0$ crossing a unit area at a distance r from a star. If we integrate this function over a sphere, we must account for all the particles between E_0 and $E_0 + dE_0$ emitted from the star. Thus,

$$\int_{\text{sphere}} f_D(E_0, r)\, dA = \frac{dJ}{dE_0}, \tag{A1}$$

where $dA = r^2 \sin\theta\, d\theta\, d\phi$. Since r is constant on the sphere, the integration is trivial and yields

$$4\pi r^2 f_D(E_0, r) = \frac{dJ}{dE_0}. \tag{A2}$$

Now to calculate the number of particles per unit area at Z with energy greater than E from sources (stars) in the vicinity, we must integrate $f_D(E_0, r)$ over energy from E up to E_{max} and over volume to include all those stars that will contribute particles of energy E or greater at the point. We integrate the function $f_D(E_0, r)\, \rho(Z, r)$, where $f_D(E_0, r)$ is the number of particles crossing unit area <u>per star</u> at a distance r from the point and $\rho(Z, r)$ is the density of stars (i.e., number per unit volume) at a distance r from the point Z. We have

$$J(\geq E) = \int_E^{E_{max}} \int_0^{R(E_0) - R(E)} \int f_D(E_0, r)\, \rho(Z, r)\, dA\, dr\, dE_0. \tag{A3}$$

We now assume that the density of stars, ρ, varies linearly over the region where most of the energy from a star is deposited. That is, we make the approximation

$$\rho(Z, r) = \rho(Z) + K\, r \cos\theta, \tag{A4}$$

where $r \cos\theta$ is the distance along the z axis and $\rho(Z)$ is the density of stars at Z. Figure 6 shows to what extent this is a valid approximation for the pion beam we have used in our experiments to date. The density of stars is shown as a function of depth through the star region. The fraction of energy deposited by a star is shown as a function of distance from the star center, which is placed arbitrarily near the center of the star region. It is seen that within 6 mm, 80% of the star energy has been deposited. Over such a distance, the star density can be considered as varying linearly.

Substituting equations A2 and A4 into A3, and integrating over dA, we have

$$J(\geq E) = \rho(Z) \int_E^{E_{max}} \int_0^{R(E_0) - R(E)} \frac{dJ}{dE_0}\, dr\, dE_0. \tag{A5}$$

We note that the r^2 factors cancel. This is simply a result of the fact that although the flux through a unit area from a source falls as $1/r^2$, the number of sources on a spherical shell increases as r^2. Also, the term involving the linear variation of the density vanishes, since

$$\int_0^{\pi} \cos\theta \sin\theta\, d\theta = 0.$$

The upper limit for r in equation A5 is explained in Fig. 7. R(E) denotes the range of a particle with energy E. For stars further than $R(E_0) - R(E)$ from the point of interest, the particle with initial energy E_0 could not reach the point with energy E or greater and so should not be included in $J(\geq E)$. This upper limit, then, corresponds to those particles that arrive at the point of interest with energy E. Integration over dr yields

$$J(\geq E) = \rho(Z) \int_E^{E_{max}} [R(E_0) - R(E)] \frac{dJ}{dE_0}\, dE_0. \tag{A6}$$

The differential spectrum dJ/dE is obtained by differentiating equation A6 with respect to E, yielding, in absolute value,

$$\frac{dJ}{dE} = \frac{\rho(Z)}{\epsilon} \int_E^{E_{max}} \frac{dJ}{dE_0}\, dE_0. \tag{A7}$$

Here we have made use of the well-known relationship

$$\frac{d}{dx} \int_a^x f(y)\, dy = f(x),$$

and the fact that

$$\frac{dR(E)}{dE} = \frac{1}{\epsilon}.$$

II. SUMMARY OF THE TECHNIQUE FOR ESTIMATING THE NEUTRON CONTRIBUTION IN THE BRAGG PEAK The neutron differential energy spectrum from the pion-oxygen interactions was taken as the interpolated curve given in Fowler's paper (2). Depth-dose curves for wide parallel monoenergetic neutron beams with slab geometry were weighted according

to the neutron spectrum to yield a depth-dose curve corresponding to the neutron spectrum from a pion star. That is,

$$D(r) = \frac{\int D(E_0, r) \frac{dJ_n}{dE_0} dE_0}{\int \frac{dJ_n}{dE_0} dE_0}, \tag{B1}$$

where $D(r)$ = the dose per neutron/cm^2 at a distance r,

$D(E_0, r)$ = the neutron dose per incident neutron/cm^2 of initial energy E_0 at a distance r,

$\frac{dJ_n}{dE_0}$ = the differential energy spectrum of neutrons from a star.

$D(E_0, r)$ were obtained from the work of Snyder and Neufeld (11) and Zerby and Kinney (12). The above expression is for a parallel beam incident on a semi-infinite slab of tissue. Since the neutrons of interest here have rather high energies (average energy ≈ 23 MeV), we assume that a negligible number leave the slab in a direction opposite to the incident beam direction. We can then assume that from a point source (i.e., a pion star) the dose will fall off as $1/r^2$ times the above function $D(r)$, that is,

$$f(r) = \frac{3}{4\pi r^2} D(r) \text{ rads/star.} \tag{B2}$$

Here $f(r)$ is the rads per star deposited by neutrons at a distance r from the star. The factor of 3 arises because three neutrons on the average are emitted per star. The final expression for the central axis dose at point Z is given by

$$D(Z) = \frac{3}{4\pi} \iiint \rho(x, y, z) \frac{D(r)}{r^2} dxdydz, \tag{B3}$$

where $\rho(x, y, z)$ is the density of stars, number per unit volume at the point (x, y, z), and r is the distance from the volume element to the dose point at Z. The variation of the density along z was assumed to be that shown in Fig. 4. The variations along x and y were chosen to be identical and symmetrical. The initial beam was assumed uniform and square in shape with a width of 8 cm. It was then assumed that the beam spread out due to multiple scattering. The points of arrest of the pions, and so the density of pion stars, were described in the stopping region by a simplified theory of multiple scattering where $(1/p\beta)^2$ can be written to a good approximation as $K R^{-k}$, where K and k are constants and R is the residual range of the pion [see the Appendix of reference 1, for example]. We have used $K = 1.86 \times 10^{-3}$ and $k = 1.10$. The spread of one element of the beam is a Gaussian distribution in this case with a standard deviation 1.65 cm. Thus, an approximation of the 3-dimensional distribution of pion stars could be constructed. The resultant density as well as the $D(r)$ function were known only numerically; therefore, a numerical integration of equation B3 was performed. A computer program was developed for the CDC 6600 to perform the integration. The main feature of this program was a sliding interval size such that negligible error was introduced at small r, where $1/r^2$ is large.

Calculations were made every 2 cm through the star region except near the center, where values were computed every 1/3 cm. The results are shown in Fig. 8, and are also indicated on the Bragg curve in Fig. 3.

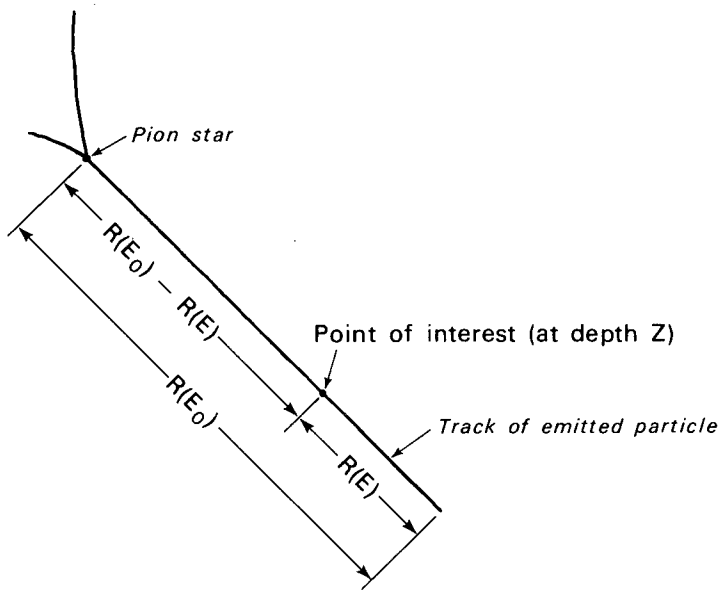

Fig. 7. Explanation of the upper limit of integration over r. R(E) denotes the range of a particle with energy E. The "point of interest" is the point where the dose is being calculated. Only those particles of initial energy E_0 that are emitted closer to the dose point than $R(E_0) - R(E)$ will reach it with energy greater than E.

DBL 673-1585

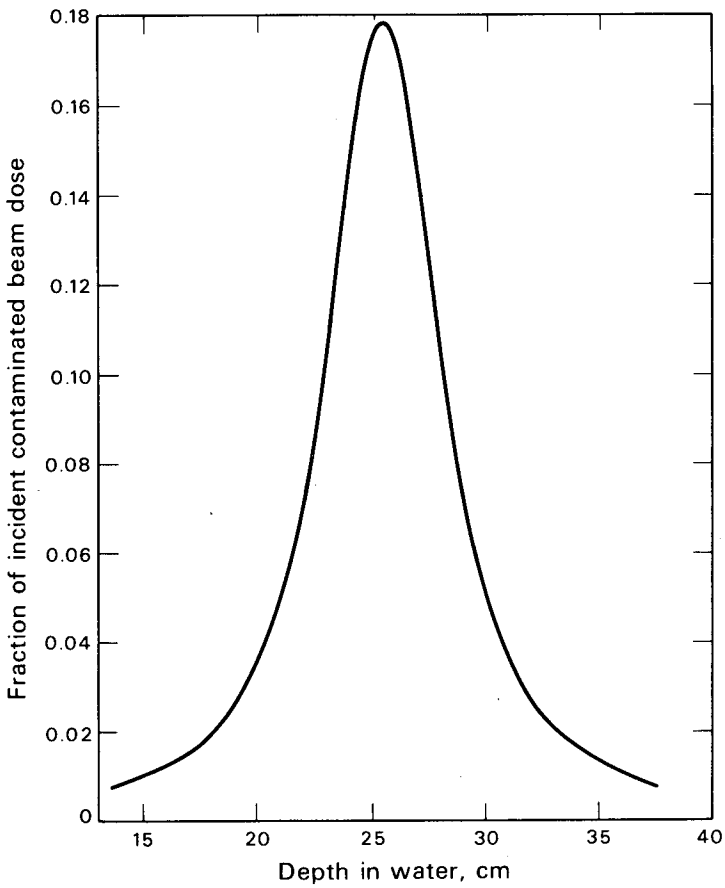

Fig. 8. Neutron contribution to the dose as a function of depth in water for the negative pion beam described in the text. The dose is normalized to the incident contaminated beam dose and is also plotted in Fig. 3.

DBL 673-1584

REFERENCES AND NOTES

1. Fowler, P. H., and Perkins, D. H.; The possibility of therapeutic applications of beams of negative π mesons. Nature 189: 524-528, 1961.
2. Fowler, P. H.; π Meson versus cancer? Proc. Phys. Soc. 85: 1051-1066, 1965.
3. Richman, C.; Aceto, H.; Raju, M. R., and Schwartz, B.; The radiotherapeutic possibilities of negative pions–preliminary physical experiments. Am. J. Roentgenol., Radium Therapy Nucl. Med. 96: 777-790, 1966.
4. Raju, M. R.; Aceto, H., and Richman, C.; Pion studies with silicon detectors. Nucl. Instr. Methods 37: 152-158, 1965.
5. Ammiraju, P., and Lederman, L. M.; A diffusion chamber study of very slow mesons. IV. Absorption of pions in light nuclei. Nuovo Cimento 4: 283-306, 1956.
6. Menon, M. G. K.; Muirhead, H., and Rochat, O.; Nuclear reactions produced by slow negative π-mesons. Phil. Mag. 41: 583-618, 1950.
7. As found in Barkas, W. H., and Berger, M. J.; Tables of energy losses and ranges of heavy charged particles; in Studies in Penetration of Charged Particles in Matter, Natl. Acad. Sci.-Natl. Res. Council Publication 1133: 103-172, 1964.
8. Northcliffe, L. C., Passage of heavy ions through matter. Ann. Rev. Nucl. Sci. 13: 67-102, 1963. Also found as Appendix B in publication referred to in Ref. 7 above, pp. 353-388.
9. Bichsel, H.; Passage of charged particles through matter; in American Institute of Physics Handbook, 2nd ed., New York, McGraw-Hill Book Co., Inc., 1963, Sec. 8c, pp. 8-37.
10. Raju, M. R.; Lampo, E. J.; Curtis, S. B.; Sperinde, J. M., and Richman, C.; Lithium-drifted silicon detector used as a pulse dosimeter; in Proceedings of the 13th Nuclear Science Symposium on Instrumentation in Space and Laboratory, Boston, Massachusetts, Oct. 19-21, 1966. IEEE Trans. Nucl. Sci. NS 10 [1]: 559, 1966.
11. Snyder, W. S., and Neufeld, J.; Calculated depth-dose curves in tissue for broad beams of fast neutrons. Brit. J. Radiol. 28: 342-350, 1955.
12. Zerby, C. D., and Kinney, W. E.; Calculated tissue current-to-dose conversion factors for nucleons below 400 MeV. USAEC Report ORNL-TM-1038, Oak Ridge National Laboratory, 1965.

Mudundi R. Raju is associated with the Southwest Center for Advanced Studies, Dallas, Texas.

This paper is Lawrence Radiation Laboratory Report UCRL-17606 and will be published in Radiation Research.

Investigation of Growth Hormone Secretion in Selected Mammalian Species

Joseph F. Garcia and Irving I. Geschwind

One major conceptual development and one major technical development have helped revolutionize and greatly broaden our concepts of the control of growth hormone release by the pituitary gland. The conceptual development is one that decrees that the pituitary gland secretion is controlled by the hypothalamus, and that this regulation is exerted through the medium of a humorally transported releasing factor. The evidence in support of this idea has recently been reviewed by Pecile and Müller [1966], who have considered experiments involving pituitary stalk-section, pituitary transplants and explants, hypothalamic lesions and stimulation, and the action of crude or purified growth hormone releasing factors (GRF) in vivo and in vitro. We shall return to a discussion of some of these lines of evidence below, after consideration of the major technical development referred to above—radioimmunoassay. This procedure, so brilliantly developed and exploited by Berson and Yalow and their associates, has allowed the determination of circulating levels of growth hormone in a number of mammalian species. The procedure has been utilized to determine the effects of normal and manipulated physiological and environmental states on circulating growth hormone levels, and the greatest portion of this work, that which has been done in the human, has recently been reviewed by Glick, Roth, Yalow, and Berson [1965]. Other such studies in which radioimmunoassay procedures were used have been carried out in the rhesus monkey by Meyer and Knobil [1967], and in the rat by Schalch [1966] and Schalch and Reichlin [1966].

The work to be outlined below was initiated with the hope of developing a satisfactory bioassay for GRF, utilizing the rhesus monkey [Garcia and Geschwind, 1966]. In order to achieve both greater economy in the use of materials and smaller variation in the responses of the test animals, we eventually turned to a study of the rat and rabbit, employing for these purposes highly purified homologous growth hormones and specific antisera. The evidence we are to present differs from much that has been demonstrated in man and in the rhesus monkey by radioimmunoassay, and in the rat by bioassay, so that it has raised more problems than it has solved.

By way of introduction, we should like to review the evidence in favor of a hypothalamic control of GH release, concentrating on the effect of crude or purified "GRF" in in vivo and in vitro experiments.

The first satisfactory evidence for a GRF came from the in vitro experiments of Deuben and Meites [1964], in which crude hypothalamic extracts promoted the release of GH from rat pituitary glands cultured for 6 days. These results were confirmed by Schally, Steelman, and Bowers [1954] who incubated rat pituitaries for 6 to 9 hr with porcine or bovine extracts and obtained a 2- to 7-fold increase in GH release. The demonstration of GRF activity in in vivo experiments was initially provided by Pecile, Müller, Falconi, and Martini [1965] in the rat, and the findings were subsequently confirmed by Ishida, Kuroshima, Bowers, and Schally [1965] and by Krulich, Dhariwal, and McCann [1965]. In the in vitro experiments, incubation medium growth hormone levels were measured, and in the in vivo experiments, decrease in pituitary GH within 15 to 30 min of the injection of extract; in both types of experiments results were obtained by bioassay.

These experiments seemed to show clearly that hypothalamic extract contained a factor that promoted depletion of pituitary GH (in vivo) and release of GH into the medium (in vitro). It appeared probable that the GH disappearing from the pituitary must be appearing in the circulation, and should be detected there by a sufficiently sensitive assay. At the time, radioimmunoassay of rat GH was not available and attention was turned to the macaque. Knobil [1966], Garcia and Geschwind [1966], and Smith, Katz, Root, Dhariwal, Bongiovanni, Eberlein, and McCann [1966], reported increases in circulating GH following the adminstration of crude hypothalamic extracts to the rhesus monkey. Subsequently, Machlin, Horino, Kipnis, Phillips, and Gordon [1967] reported similar effects in sheep infused with a hypothalamic extract.

Although these results are consistent with the earlier in vivo and in vitro findings, some disquieting reports and considerations have come to the fore. Thus, the significance of the bioassays of pituitary GH in the in vivo experiments has recently been questioned by Rodger, Beck, Burgos, and Guillemin [1967] who have concluded that "statistical analyses of the data... did not establish the certain presence" of an ovine GRF active in the rat. The specificity of the effect of hypothalamic extracts in the macaque has also been questioned by Knobil (personal communication) who, unable to obtain an effect with highly purified GRF (presumably effective in the rat) in the macaque, believes that the earlier results were due to vasopressin contamination. Finally, simple calculations indicate that the depletion in pituitary GH observed in the in vivo rat experiments should result in circulating GH levels in the microgram per milliliter range in short-term experiments. However, as is indicated below, such concentrations are not to be found by radioimmunoassay.

MATERIALS AND METHODS

The measurement of the plasma concentration of growth hormone in rhesus monkeys was carried out using a radioimmunoassay for human growth hormone (HGH) which has been described in detail elsewhere [Garcia, Linfoot, Manougian, Born, and Lawrence, 1967]. A double antibody technique was used, with antiserum to HGH produced in rabbits and antiserum to rabbit gamma globulin produced in goats; dilutions of rhesus monkey plasma give a parallel curve to that obtained for dilutions of standard HGH. Human growth hormone was kindly supplied by Prof. C. H. Li of the University of California, San Francisco.

The radioimmunoassay of rabbit and rat growth hormone has been set up along lines similar to those used for the assay of HGH. We obtained purified rabbit and rat growth hormones and their respective monkey antisera, and purified cat growth hormone through the kindness of Dr. Stanley Ellis of the Ames Research Center, Moffet Field, California. The rabbit GH had a potency of 1.3 units per mg and the rat GH, 2.9 units per mg, relative to the bovine GH standard. The second antibody used in the rabbit and rat GH assays was produced in goats immunized with monkey gamma globulin. More details of the rabbit and rat radioimmunoassays are presented in their respective sections below.

All of the growth hormone preparations used were labeled with iodine-125, using essentially the method of Greenwood, Hunter, and Glover [1963]. The iodine-125 was obtained from Abbott Laboratories and usually had a specific activity of approximately 40 mCi/ml. In all iodinations, 10 μg of hormone and 1 mCi of iodine-125 were used. This resulted in a preparation of labeled hormone with specific activities of approximately 70 μCi/μg.

The radioimmunoassays were carried out in 3 ml glass test tubes. Incubation periods at 4°C varied from 4 days for the rat GH assay to 6 days for the rabbit GH assay. After the incubation period, 0.1 mg monkey gamma globulin was added to each sample as a carrier. An amount of the precipitating antiserum was added which had previously been determined would maximally precipitate the monkey gamma globulin in the test tube and any labeled hormone that was antibody bound. After a 2 hr period the samples were centrifuged at 700×g in a refrigerated centrifuge for 30 min and the supernatant decanted. The iodine-125 radioactivity in the precipitates was then counted in a Nuclear-Chicago automatic scintillation counter.

Curves are plotted using semi-logarithmic paper with the growth hormone concentrations on the logarithmic scale and the percent of the labeled hormone that is bound to antibody on the linear scale. Tubes containing the same total amount of labeled hormone, but precipitated with 10% TCA, were counted to arrive at the 100% figure for labeled hormone presumably available to the antibody.

Barbital buffer, 0.07 M, pH 8.6, with 0.5 mg/ml bovine serum albumin added, was used as the diluent for all reactants in the radioimmunoassays. All plasma or serum samples were frozen as soon as possible after withdrawal and remained at -20°C until used in an assay.

Plasma glucose levels were determined by the method of Hoffman [1937], using a Technicon Autoanalyzer.

Extracts of sheep and rat hypothalami were prepared, using essentially the procedure described previously [Garcia and Geschwind, 1966]. The extracts were either freshly prepared and used immediately or were lyophilized and re-extracted with 0.01 M acetic acid in saline just prior to use.

Albino rabbits of the New Zealand strain, weighing between 3 and 5 kg, were obtained from Horton's Rabbitry, Los Gatos, California. All rats were of the Sprague-Dawley strain

and were supplied by Simonsen Laboratories, Gilroy, California. Genetic dwarf mice (dw) and LAF_1 hybrid mice were obtained from The Jackson Laboratory, Bar Harbor, Maine.

RESULTS

STUDIES ON MONKEYS We have previously reported on the ability to obtain a GH release in response to the stimulus of insulin hypoglycemia in the nembutalized monkey, indicating that the mechanisms responsible for the reflex release of GH are intact and that such a preparation can be used to study the release of GH [Garcia and Geschwind, 1966].

Responses to sheep hypothalamic extracts were studied in 10 experiments, in 9 of which a response with a release of GH was observed similar to those shown in Fig. 1. From basal levels the plasma GH concentration begins to rise 20 and 30 min after injection, attaining peak values from 45 to 60 min after the injection. These time relationships are consistent with the type of response seen following the injection of insulin. Similarly prepared extracts of cerebral tissue failed to produce any rise in PGH concentration within this time period.

Experiments were also carried out with the hypothalamic extract being injected while the blood glucose was raised and maintained at a high level by an infusion of glucose. One of these studies is depicted in Fig. 2. In the period immediately following the injection of the hypothalamic extract the blood glucose was in excess of 300 mg%. Even with such a high glucose level the response to the hypothalamic extract is not interfered with. In this instance the plasma concentration rises from a basal level of 2 mμg/ml to 90 mμg/ml at the peak of the response.

Although we observed no comparable responses following the injections of extracts of the cerebral cortex, it is highly probable that the latter is not a proper control for the hypothalamic extracts, which contain many pharmacologically active constituents in relatively high concentration. Knobil [1966] investigated the effect of one of these, vasopressin, in the conscious, restrained monkey and observed increases in plasma GH which were not dose dependent. We have employed nembutalized male animals whose GH levels have changed but little in response to either 5 units of Pitressin^R or 2.5 units of synthetic lysine vasopressin, the amount of vasopressin activity present in our hypothalamic extracts (Fig. 3). The highest PGH concentration following the injection was 5 mμg/ml, and when this was observed, it was in the first sample taken after the injection (approximately 15 min later). Greenwood and Landon [1966] have observed responses to Pitressin^R in human females but not in human males.

Although the time at which maximum elevation in plasma GH concentration in response to hypothalamic extract is rather constant, there is a great variation in the magnitude of the response. As pointed out above, this variation was one of the reasons which caused us to look into the possibility of using radioimmunoassay in some of the more common laboratory animal species, in the hope that with larger numbers this problem could be overcome.

STUDIES ON RABBITS Measurements of the plasma concentration of GH in the rabbit

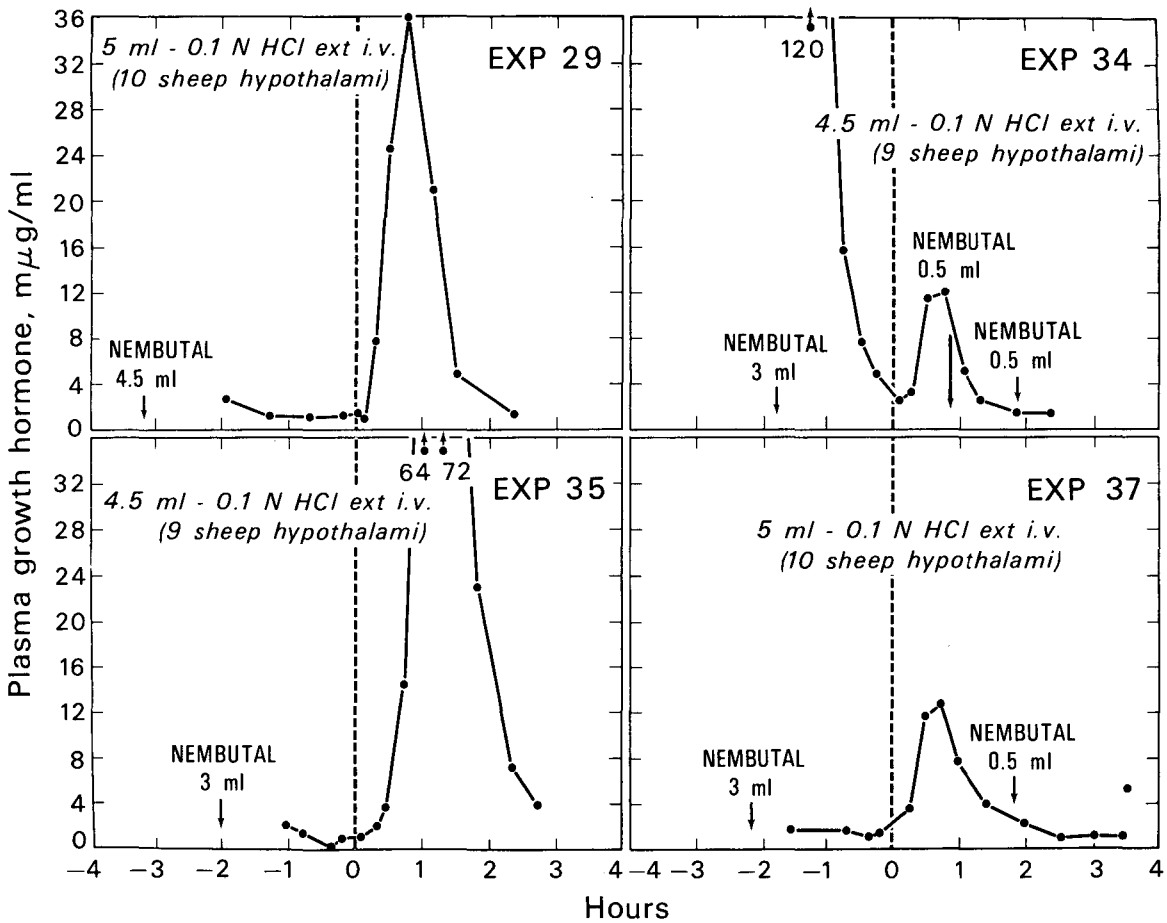

Fig. 1. The effect of ovine hypothalamic extract administered intravenously on circulating GH levels in nembutalized, male rhesus monkeys. (From Garcia and Geschwind, 1966).

MUB-9724

by radioimmunoassay or any other method have not as yet appeared in the literature. Figure 4 lists the amounts of the reactants used in the radioimmunoassay we have developed and depicts a typical curve obtained. A straight-line relationship is obtained between the logarithm of the concentration of unlabeled rabbit GH and the percent of the labeled rabbit GH, which is bound to the antibody from GH concentrations of approximately 1.5 to 25 mμg/ml. Initial studies with varying concentrations of anti-rabbit GH antiserum were tried before it was found that a dilution of 1:100,000 of the antiserum in the volume used (200 λ) would cover this range of rabbit GH concentration. The incubation period of 6 days was decided upon after observing that whereas shorter periods resulted in slopes which were not as steep, increasing the period beyond 6 days did not improve the slope. The amount of labeled hormone used was usually sufficient to give counting rates between 10,000 cpm for low GH concentrations down to 2000 cpm for high concentrations. The standard rabbit growth hormone concentrations used for such a curve were made up in the barbital diluent with 10 mg/ml rabbit albumin added in order to keep at least this minimal concentration of rabbit protein in the incubation. For measurement of plasma growth hormone concentration, 100 λ of the plasma to be assayed was substi-

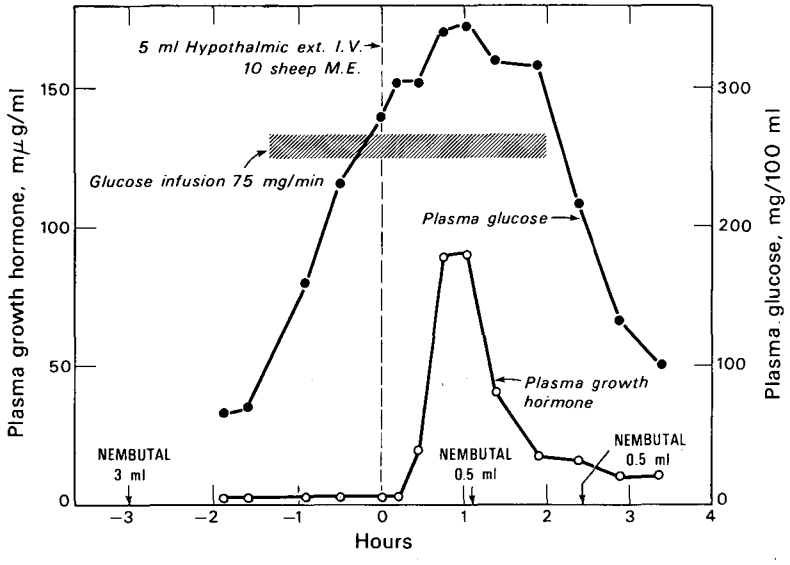

Fig. 2. The effect of ovine hypothalamic extract administered intravenously on the circulating GH level of a nembutalized, male rhesus monkey receiving a glucose infusion. DBL 678-1762

tuted for the standard rabbit growth hormone solution. Only the straight portion of such a curve was used for determining the plasma GH concentration.

Although not necessarily proof of identity, evidence supporting the identity of that material in plasma or tissue extracts with the specific hormone being studied, can, in radioimmunoassay terms, be obtained by showing that slopes of the assay curves of both materials are parallel. Some studies were done making such comparisons of pituitary extracts of various laboratory animals with the purified rabbit GH used in this radioimmunoassay. The tissue was homogenized in a tissue homogenizer with 10 ml of barbital buffer. After centrifugation, 10-fold dilutions of the supernate were made in order to determine the approximate dilution range which would give a curve within the range of the standard rabbit GH curve; when this was found, halving dilutions of the extract were made. Figure 5 presents the results of such a study on rabbit pituitary and placenta extracts. It would appear that dilutions of both fetal and adult rabbit pituitary extracts react with the antibody to purified rabbit GH with an affinity equal to that of the standard rabbit GH itself. The fetal rabbit pituitary extract was made from a pool of 4 glands taken 1 day before expected birth. Comparison of these rabbit pituitary dilution curves with the curve for standard rabbit GH reveals a pituitary GH concentration of approximately 4 μg/mg in fetal rabbit pituitary as compared with 13.3 μg/mg in the adult rabbit pituitary, or approximately 1/3 the adult rabbit pituitary concentration. However, plasma from 6 of the fetal rabbits taken at the same time revealed a range of plasma GH concentration from 60 to 144 mμg/ml, with an average value of 91 mμg/ml, compared with 18 mμg/ml for the plasma concentration in the pregnant rabbit. This several-fold higher plasma GH concentration with a much lower pituitary concentration than in the adult rabbit would indicate that in the fetal rabbit the kinetics of pituitary GH turnover are much different from those in the adult. One of the rabbit placentas was homogenized and treated in the same way as the

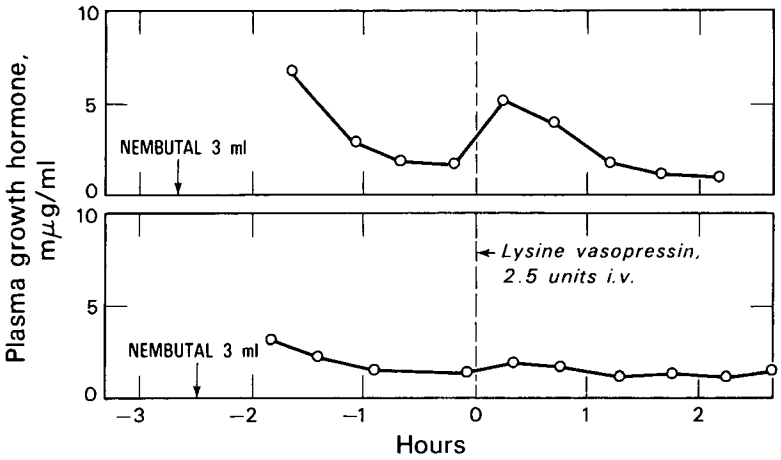

Fig. 3. The effect of 2.5 units synthetic lysine vasopressin administered intravenously on circulating GH levels in nembutalized, male rhesus monkeys.
DBL 678-1758

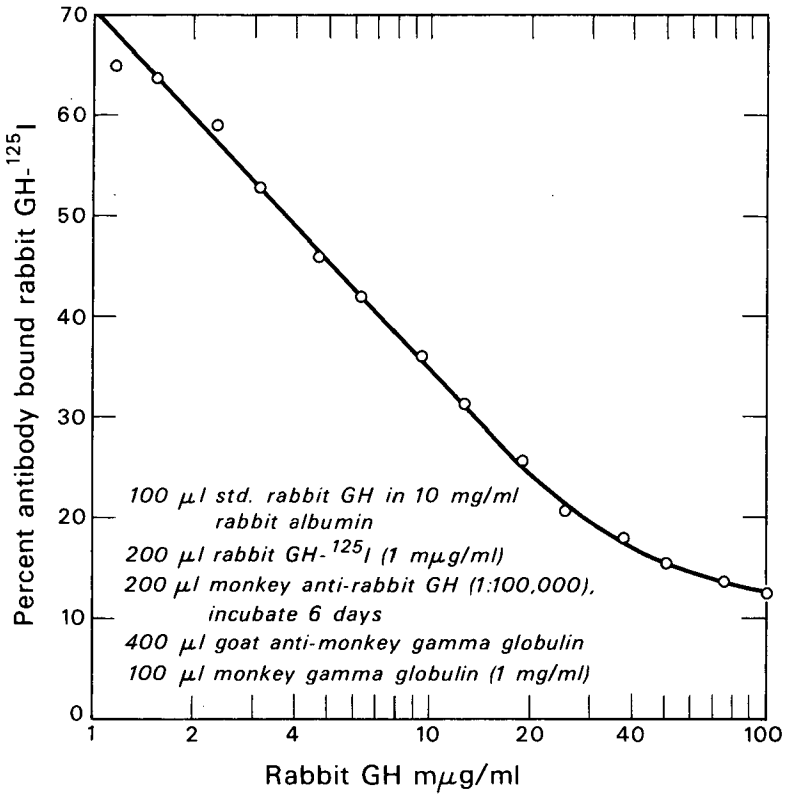

Fig. 4. The radioimmunoassay of rabbit GH: conditions, and a typical standard curve. The response is linear with the logarithm of GH concentration in the range of 1.5 to 25 mμg/ml.
DBL 678-1747

pituitary, and although the data are insufficient to permit the drawing of the same parallel relationship as for the pituitary extract, if the highest concentration is read off the curve, a GH concentration of 30 mμg/g of placenta is obtained. This amount of growth hormone is not inconsistent with the assumption that all of this GH may be in the blood remaining in the tissue. However, more data on this point will have to be accumulated before ruling out the possibility of a placental GH-like factor in the rabbit similar to that shown to exist in human placenta (cf. results in the rat, below).

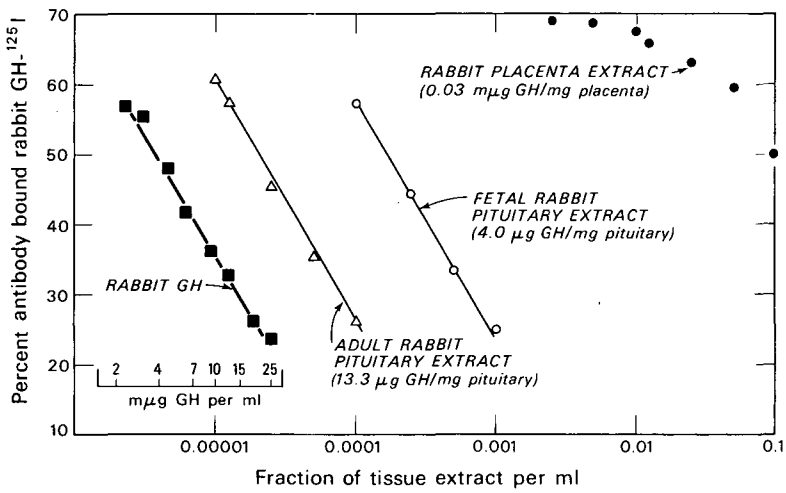

Fig. 5. The radioimmunoassay of rabbit GH, adult and fetal rabbit pituitary extract, and rabbit placenta extract: dilution-response curves.
DBL 678-1753

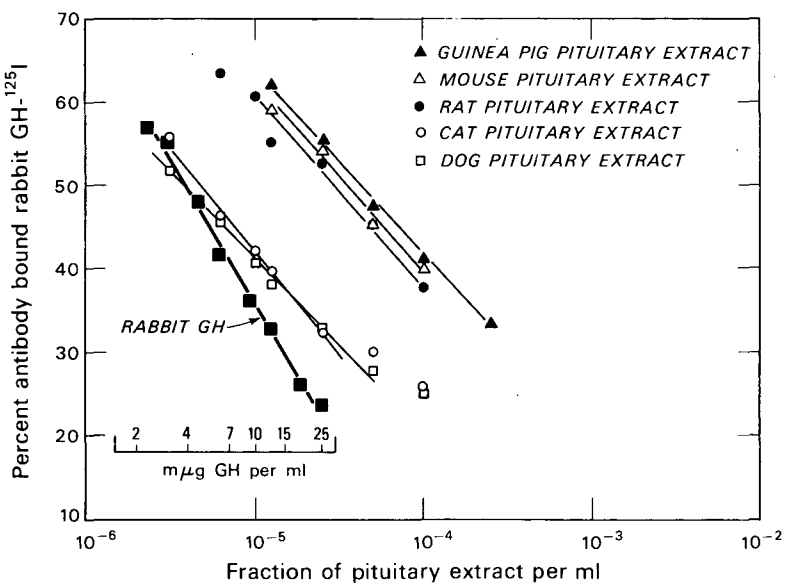

Fig. 6. Dilution-response curves for pituitary extracts of the guinea pig, mouse, rat, cat, and dog in the radioimmunoassay for rabbit GH.
DBL 678-1759

Pituitaries from several other laboratory animals were homogenized, diluted in the same way, and compared for their ability to compete with labeled rabbit GH for antiserum to rabbit GH. All of the pituitary extracts studied—guinea pig, mouse, rat, cat, and dog—crossreacted with the rabbit GH antiserum (Fig. 6). However, as is indicated by the more shallow slopes, the affinity of these extracts for the rabbit GH antibody is not as great as it is for rabbit GH itself.

Dilutions of other purified growth hormone preparations were also compared with the rabbit GH for ability to compete with the labeled rabbit GH for antibody to rabbit GH. In Fig. 7 it will be observed that, whereas rat and cat GH do crossreact with antibody to rabbit GH,

HGH, even at a concentration of 1000 mμg/ml does not inhibit the binding between labeled rabbit GH and its antibody.

Finally, in Fig. 8, dilutions of rabbit plasma are compared in the same way with rabbit GH. The values obtained for these plasma dilutions fall reasonably close to lines drawn parallel to that obtained for the purified rabbit GH. This has been taken as evidence that the material in rabbit plasma that inhibits the binding of labeled rabbit GH to its antibody is the rabbit GH in the plasma itself.

In spite of the evidence presented supporting the identity with GH of that material measured in rabbit plasma and rabbit pituitary extracts by the radioimmunoassay procedure, it was hoped that further evidence would be gained, if it were possible to show that physiological manipulation in the rabbit would produce plasma growth hormone changes similar to those observed in man and in other primates.

In man, the plasma GH level has been shown by Glick et al. [1965] and by Knopf, Conn, Fajans, Floyd, Guntsche, and Rull [1965] to respond to many factors. Among others, insulin-induced hypoglycemia, prolonged fasting, and the administration of certain amino acids will all result in high plasma GH levels. On the other hand, Glick et al. [1965] have shown that administration of glucose will depress the elevated plasma GH level of the hypoglycemic or fasting individual. The nembutalized rhesus monkey has been shown to respond with elevated plasma GH levels to hypoglycemia and to the administration of sheep hypothalamic extracts [Garcia and Geschwind, 1966] and Meyer and Knobil [1967] have shown that the conscious, restrained rhesus monkey will respond to a wide variety of stimuli with a release of GH.

As a laboratory animal, rabbits do offer at least one advantage in their readily available superficial vessels in the ear for injections and for the withdrawal of blood. All studies which we have carried out in the rabbit have been done in the conscious animal loosely restrained in a bleeding cage. All experiments were done on large males with the exception of a fasting experiment in which both males and females were used. For the acute studies the marginal vein in one ear was cannulated and was used as the injection site for all materials injected. The central artery of the other ear was also cannulated and was used for withdrawal of blood samples.

The effect of prolonged fasting was studied in 3 males and 3 females. The animals were bled prior to fasting from the 3rd to the 9th day of the fasting period, and on the 1st and 2nd days after refeeding was initiated. The GH levels found are presented in Fig. 9. Most of the plasma values measured during the fasting period are higher than the prefasting values. This is especially true for the females, in whom more than half the fasting values were greater than 25 mμg/ml. On refeeding, the GH values generally returned to the prefeeding values with the exception of 2 values in males which are still within the range of the fasting values for the males. These results in rabbits generally are in agreement with those observed in humans following fasting.

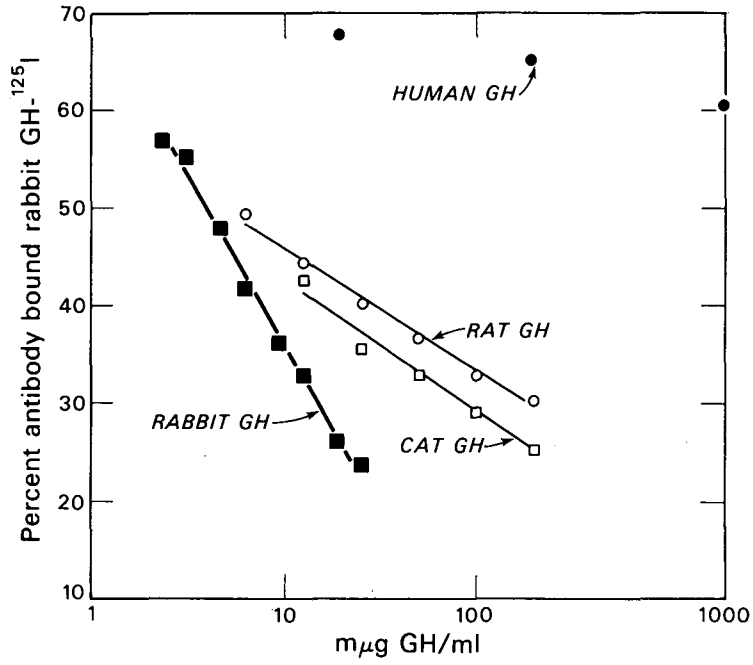

Fig. 7. Effect of varying concentrations of purified rat, cat, and human growth hormones in the radioimmunoassay for rabbit GH. Compare the slopes of the purified rat and cat hormones with those shown in Fig. 6 for their pituitary extracts.
DBL 678-1757

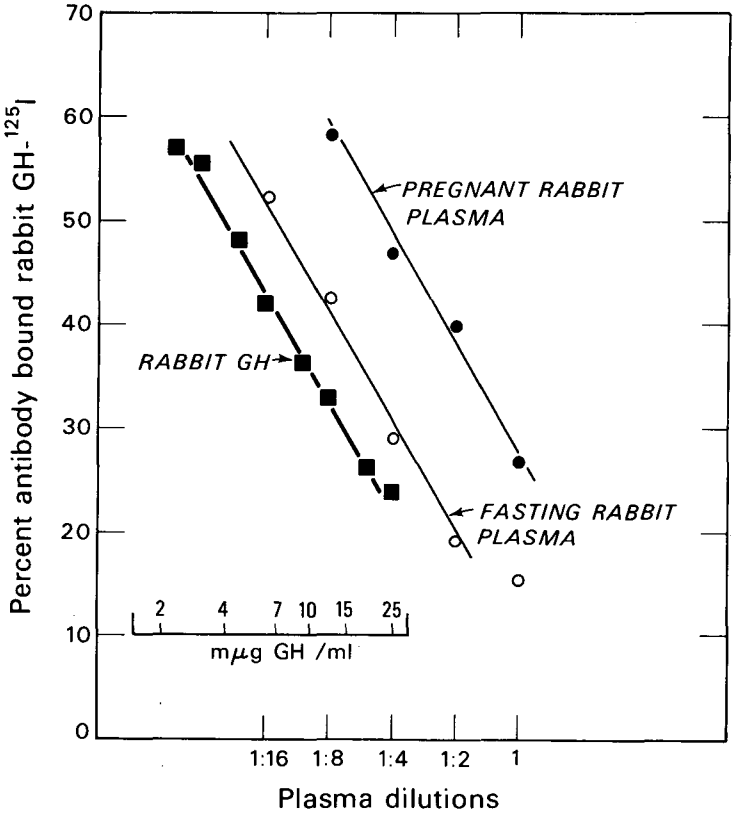

Fig. 8. Dilution-response curves given by fasting and pregnant rabbit plasma samples.
DBL 678-1756

Our studies in rabbits attempting to duplicate the results seen in humans and other primates to stimuli causing a more acute release of GH have not been as rewarding.

Experiments attempting the stimulating of GH release in response to insulin hypoglycemia in rabbits began with intravenous insulin doses of 0.5 U/kg and were progressively increased to 4 U/kg when no convincing GH release was observed. However, the blood glucose in rabbits did not fall to the low levels seen in other animals. A dose of 2 U/kg in rats will often depress blood glucose levels to 20 mg%. In Fig. 10 two studies in rabbits receiving 4 U insulin per kg are presented. Although there is a tendency for the plasma GH levels following the injection to be slightly higher than the preinsulin values, there is not the convincing release seen in the studies in primates. The lowest blood glucose level reached in one animal was 48 and in the other, 60 mg%. However, as a result of the rising blood sugar during the control period in the first animal, a decrease of over 100 mg% occurred in response to insulin in that animal. It is perhaps important to mention that all these studies were done in non-fasted animals. Also disappointing is the lack of depression of GH following the intravenous adminstration of glucose.

An infusion of arginine in the amount of 0.5 g/kg was given to two rabbits over a 30 min period (Fig. 11). Neither of the rabbits responded with increased GH levels during the 2 hr period studied following the infusion. In fact, in one rabbit all of the values after the infusion were lower than those observed before and during the infusion of the arginine.

The effect of intravenous administration of sheep hypothalamic extracts, similar to those that have produced consistent increases in GH levels in rhesus monkeys, was studied in two rabbits (Fig. 12). Here also, no significant rise in plasma GH concentration was observed over a 2 hr period following the injection.

Meyer and Knobil [1967] have observed a prompt release of GH in response to a large bleeding in the conscious monkey, and since our experiments did involve considerable blood sampling over a 4-5 hr period, we studied the effect of a massive bleeding in one rabbit. Sixty ml of blood was withdrawn over a 15 min period from a 4 kg rabbit, approximately 25% of the blood volume. This treatment also failed to produce a convincing rise in GH level (Fig. 13).

Finally, the disappearance from the plasma of intravenously administered rabbit GH was studied in 3 rabbits, and the results are presented in Fig. 14. Unanesthetized male rabbits weighing 3.8 to 4.5 kg were injected in the marginal vein in one ear with 34-45 μg of rabbit GH in 1 ml of normal rabbit plasma, and were bled from the central artery of the other ear. Over the first 20 min the GH concentration fell very rapidly with a half time of the order of 4 min. After approximately 30-40 min the GH values were not essentially different from the preinjection values. The extrapolated volume of distribution of the hormone at zero time was approximately 7.2% of the body weight.

In summary, the use of a radioimmunoassay for rabbit GH in rabbits has not as yet been

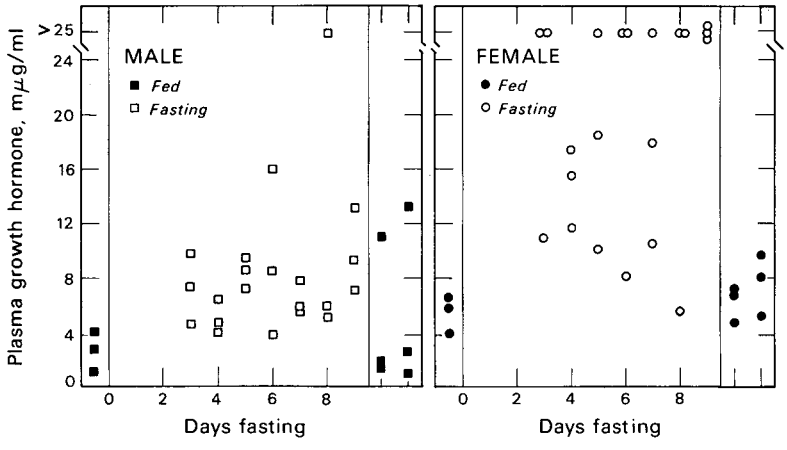

Fig. 9. Effect of a 9-day fast on plasma GH levels in male and female rabbits. Note the break in the ordinate scale.

DBL 678-1751

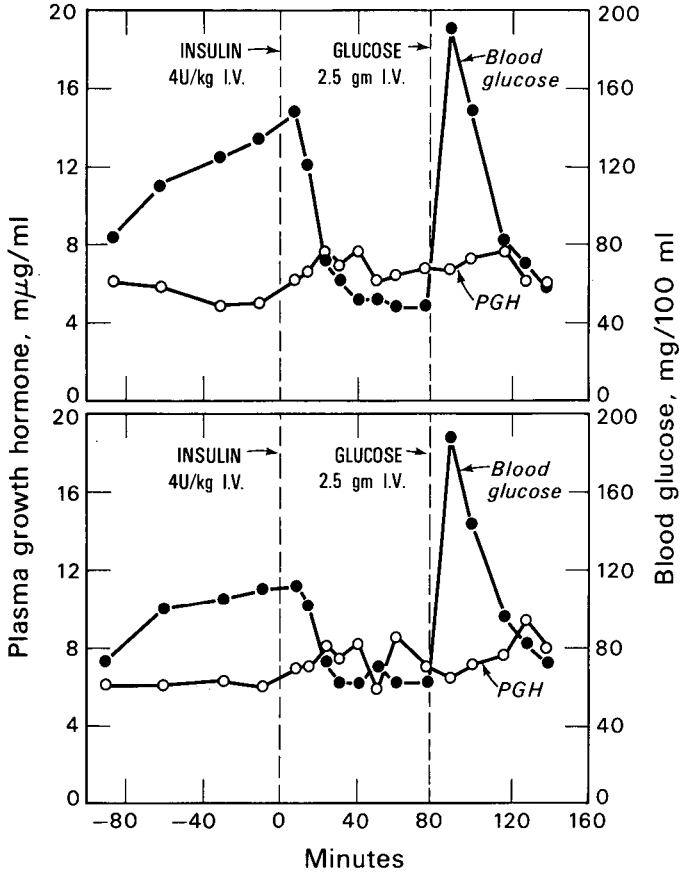

Fig. 10. The effect of intravenous insulin administration of plasma GH levels in the non-fasted rabbit. Note the rising blood glucose level during the pre-injection control period.

DBL 678-1750

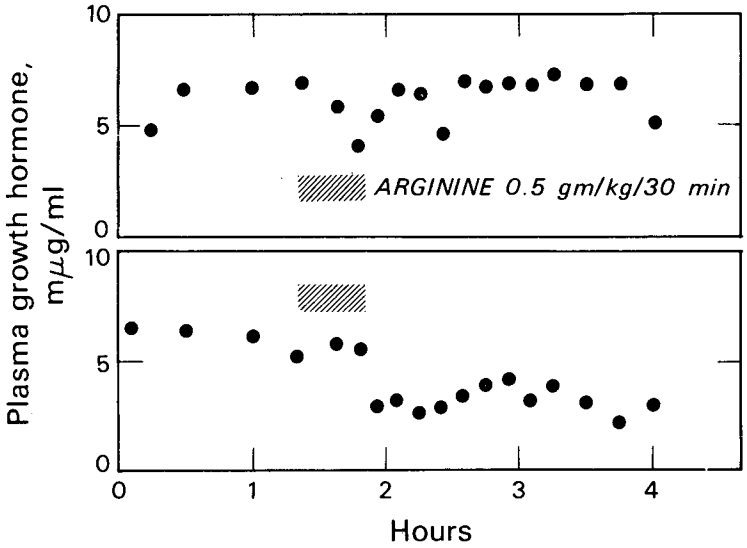

Fig. 11. The effect of an infusion of arginine on plasma GH levels in the rabbit.
DBL 678-1755

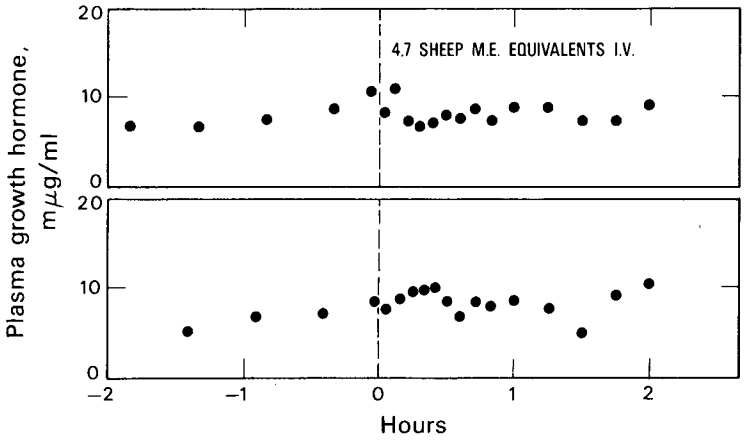

Fig. 12. The effect of an injection of sheep hypothalamic extract on plasma GH levels in the rabbit. Note the relative consistency of the values despite the multiple sample withdrawals.
DBL 678-1754

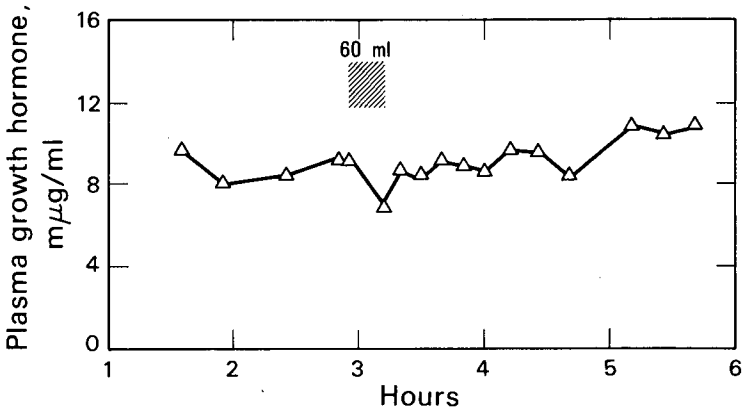

Fig. 13. The effect of bleeding 25% of the blood volume over a 15 minute period on the plasma GH level in the rabbit.
DBL 678-1745

particularly rewarding in the study of factors controlling the release of GH. In contrast to the responses seen in man and in the monkey, and in particular, those observed by Meyer and Knobil [1967] in the conscious monkey to a wide variety of stimuli, those in the rabbit appear virtually nonexistent, for the GH level appears very reluctant to change. Prolonged fasting does appear to result in higher plasma GH levels in rabbits, in agreement with results in humans. Whether the absence of responses in rabbits represents a species difference (in this vein, it must be pointed out that to our knowledge, with the exception of the experiments of Machlin et al. [1967] on infusion of hypothalamic extracts in the sheep, the rabbit is the only herbivorous animal yet studied in terms of GH release) or whether the radioimmunoassay itself or other features in the experimental design are at fault will remain the subject of future work.

STUDIES ON RATS AND MICE For the radioimmunoassay of rat GH we have used essentially the procedure described above for the radioimmunoassay of rabbit GH. Figure 15 shows a typical curve and also lists the amounts and dilutions of the various components used in the rat GH radioimmunoassay. The range of GH concentrations covered is similar to that for the rabbit GH assay, being linear from approximately 1 to 25 mμg/ml. A 1:50,000 dilution of the monkey antiserum to rat GH was required to achieve this range, and the slope of the curve did not improve with incubation periods greater than 4 days.

Studies similar to those done with the rabbit GH radioimmunoassay, comparing the ability of dilutions of pituitary extracts to compete with labeled rat GH for its antibody were carried out. In Fig. 16 are presented the results of studies on rat and mouse pituitary extracts. Both the rat and mouse pituitaries appear to react with antibody to rat GH with an affinity equal to that shown by the rat GH standard. Comparison of these dilution curves with the curve for the purified rat GH reveals a pituitary GH concentration of 29 μg/mg for the pregnant rat pituitary extract and 32 μg/mg for the male rat pituitary extract. The mouse pituitary extract, which was made from a pool of 5 pituitaries, had a GH concentration of 23 μg/mg. Also presented in this figure is the effect of dilutions of an extract of rat placenta. Although no line was drawn, it would appear that a line through these points would closely parallel that for rat GH, in contrast to extracts of human placenta which have a slope that is not as steep as that seen for HGH in a radioimmunoassay for HGH. The "GH" concentration in the rat placental extract, however, was quite high, with a value of 0.26 mμg/mg (260 mμg/g). This value is higher than any plasma GH concentration we have yet observed in the rat. Of further interest here is the point that if this does indeed represent a rat placental "GH," its production is not reflected in pregnant rat plasma in which Schalch and Reichlin [1966] have found normal levels of GH. This, too, would be in contrast to human placental "GH."

As an extension of these studies on rat and mouse pituitary extracts, we have determined the pituitary concentrations of GH in male and female Sprague-Dawley rats as a function of age. Previous studies in the rat have been reported by Solomon and Greep [1958] for female Sprague-Dawley and Wistar rats, and by Bowman [1961] for the male Long-Evans rat, over a period of time from 10 to approximately 600 days of age. These investigators were in agreement that the concentration of GH in the pituitary, as determined by bioassay, varied little

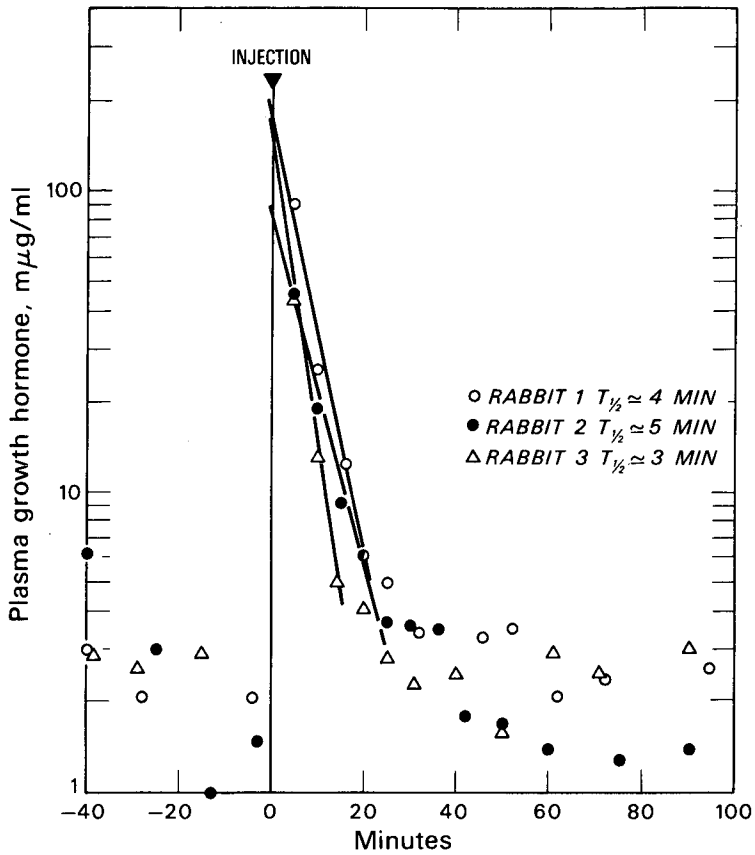

Fig. 14. The rate of change of plasma GH levels in the rabbit following the intravenous injection of 34 to 45 μg of rabbit GH.
DBL 678-1748

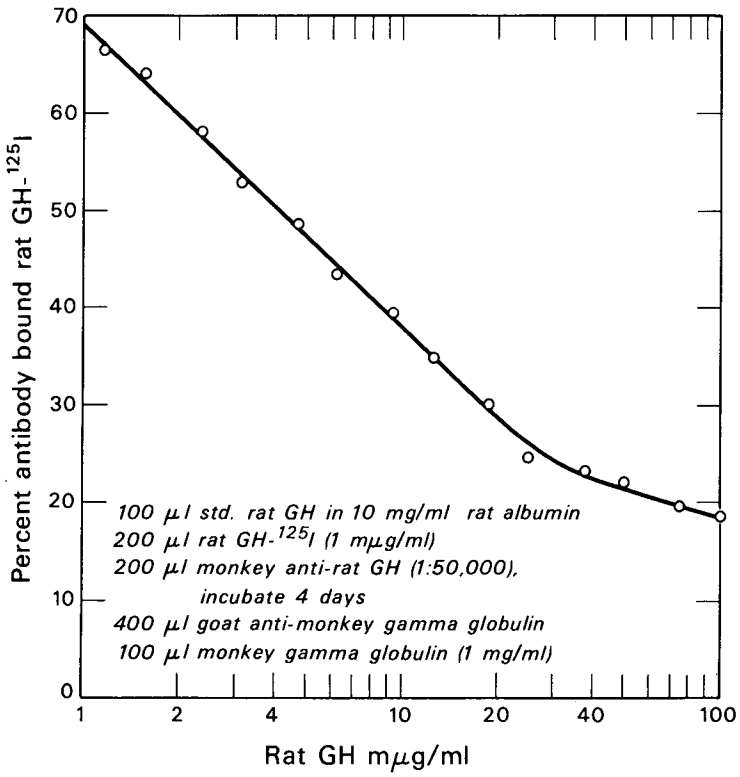

Fig. 15. The radioimmunoassay of rat GH: conditions, and a typical standard curve. The response is linear with the logarithm of GH concentration in the range of 1 to 25 mμg/ml.
DBL 678-1746

with age. Our results, shown in Table 1, indicate, however, that there is a steady increase in pituitary GH concentration in both the male and the female for at least the first 6 to 10 weeks of post-natal life. Our impression from spot checking of animals older than 10 weeks of age, is that the pituitary GH concentration plateaus in the female at about 30 to 35 μg/mg. It would appear from an analysis of the results of both Solomon and Greep and Bowman that increases were actually observed from 10 days to 6 to 9 weeks but that their significance was discounted.

Extracts of pituitaries of the guinea pig, rabbit, dog, and cat also crossreact with the antibody to rat GH as shown in Fig. 17. None of these, however, shows a strict parallel relationship with the curve for rat GH.

The purified GH preparations available to us were similarly compared in the rat GH radioimmunoassay (Fig. 18). Rabbit and cat GH crossreact with the antibody to rat GH. However, HGH at a concentration of 1000 mμg/ml does not compete with the labeled rat GH for antibody to rat GH.

Concentrations of GH in rat and mouse plasma, at halving dilutions, as read in a rat GH radioimmunoassay, are presented opposite their dilutions in Table 2. After correction for the dilution factor, the final GH concentrations appear relatively constant, indicating a reasonably parallel relationship with rat GH.

Most of the research on hypothalamic neurohumoral factors controlling the release of GH by the pituitary has been done in the rat, and profound decreases in rat pituitary GH have been reported following either the administration of such extracts or insulin or the imposition of cold stress or a fast. Therefore, we felt that the measurement of plasma GH levels in such animals should yield information pertinent to these previously described observations.

Our studies using the rat as an experimental animal, began with the use of large male (400-600 g) Sprague-Dawley rats. These studies were done for the most part on anesthetized animals. Initially ether, and in later experiments, methoxyflurane, was used as the anesthetic. A cannula was placed in the jugular vein for the withdrawal of serial (0.5 ml) blood samples, and injections of materials were made into the saphenous vein.

Plasma GH levels were followed in 3 anesthetized rats following the intravenous administration of insulin at a dose of 2 U/kg (Fig. 19). Although the blood glucose level fell to 40 mg% or below in all three animals, in only one animal was there evident an increase in GH concentration comparable to that observed in primates. The preinsulin GH concentration in this animal of approximately 3 mμg/ml increased to a concentration of 13 mμg/ml at 60 min following the insulin administration.* In several previous experiments, in which unanesthetized

*Rat plasma GH concentrations have been found to be distributed over a wide range, although repeated sampling in any one animal, as shown in Figs. 19 and 20, gives quite reproducible values. Although the former finding is in agreement with the findings of Schalch and Reichlin [1966], our estimate of mean GH levels in the plasma of male and female rats is very much lower than those reported by these investigators (cf. Tables 3 and 4).

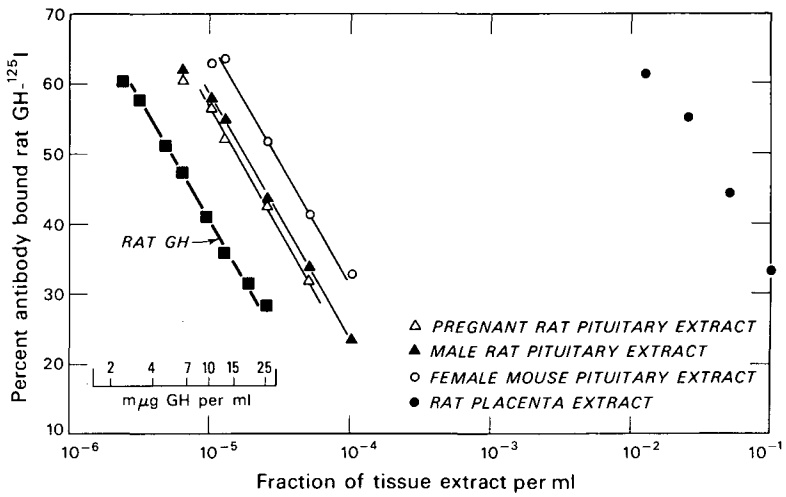

Fig. 16. The radioimmunoassay of rat GH, male rat, pregnant rat, and female mouse pituitary extracts, and rat placenta extract: dilution-response curves.
DBL 678-1752

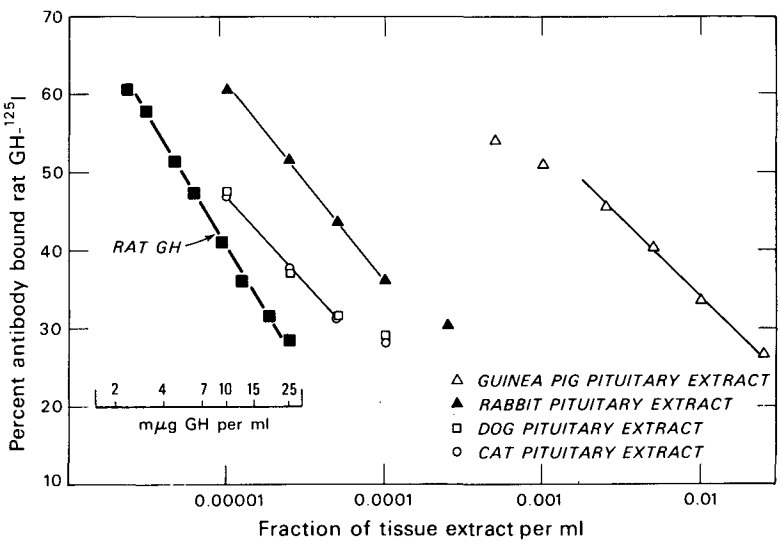

Fig. 17. Dilution-response curves for pituitary extracts of the guinea pig, cat, dog, and rabbit in the radioimmunoassay for rat GH. Compare the relative position of the guinea pig in these studies with that in the rabbit GH studies (Fig. 6).
DBL 678-1761

animals were injected intraperitoneally with the same amount of insulin and sampled by cardiac puncture at 60 min, the plasma GH concentrations were always less than those in saline-treated animals.

In similar animals the intravenous administration of a sheep hypothalamic extract equivalent to one hypothalamus failed to produce any change in the plasma GH concentration in 5 experiments. These rats were sampled over a 75 min period following the injection.

Subsequently, a rat hypothalamic extract, which was known to be capable of stimulating the release of LH from incubated rat pituitaries [Samli and Geschwind, 1967], was injected intracarotidly into 60-day-old male Sprague-Dawley rats. Twenty minutes later the animals were bled by heart puncture, and the pituitary was removed following decapitation. The

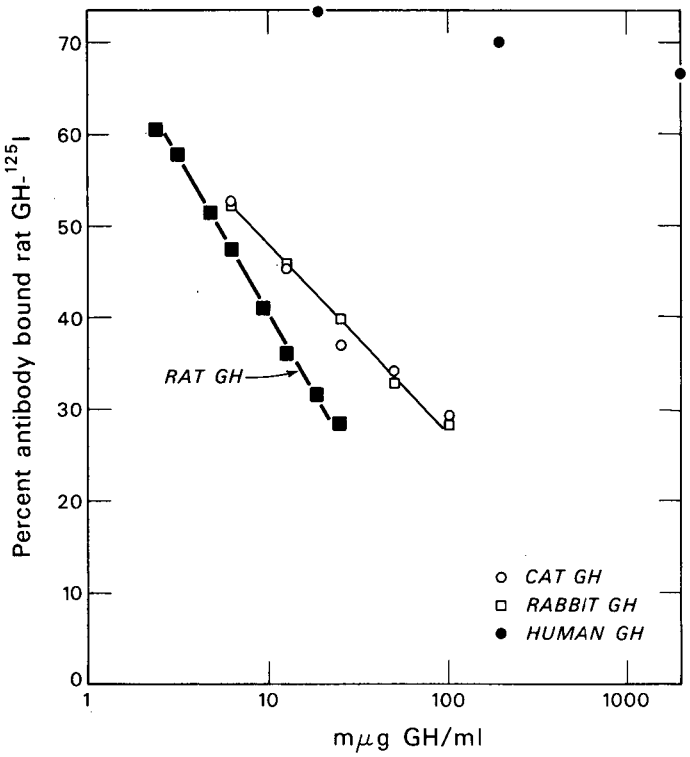

Fig. 18. Effect of varying concentrations of purified rabbit, cat and human growth hormones in the radioimmunoassay for rat GH. Compare the slope of rabbit GH with that shown in Fig. 17 for rabbit pituitary extract.
DBL 678-1760

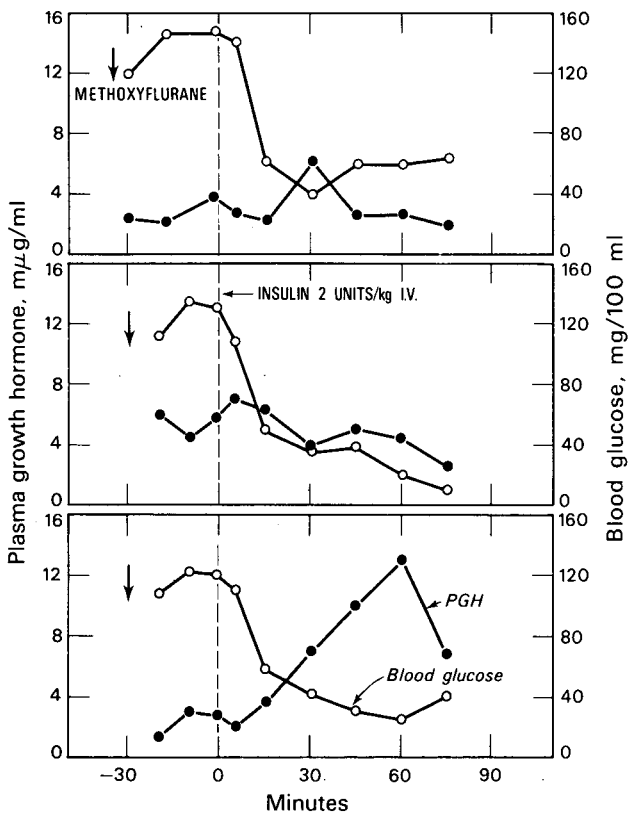

Fig. 19. The effect of intravenous insulin administration on plasma GH levels in the adult male Sprague-Dawley rat.
DBL 678-1744

Table 1. Pituitary GH concentrations in S-D rats as a function of age.*

	Age (days)	Weight (g)	Pituitary GH (μg/mg)†
Males	5	14	3.3
	10	24	7.0
	15	30	8.3
	20	45	13.1
	25	76	14.4
	45	222	30.4
	60	302	22.1
	75	369	43.1
Females	5	13	5.0
	10	24	4.7
	15	29	6.3
	20	42	11.4
	25	73	16.0
	45	152	19.2
	60	210	26.8
	75	258	33.7

*5 animals per group; all data in this table obtained in a single assay.

†5 pituitaries pooled.

Table 2. Plasma GH in dilutions of rat and mouse plasma.

	Dilution	GH conc. from curve (mμg/ml)	GH (mμg/ml, corrected for dilution)
Rat plasma	1:4	18.5	74.0
	1:8	7.2	57.6
	1:16	4.4	70.4
	1:32	2.0	64.0
Mouse plasma	1:2	9.0	18.0
	1:4	5.3	21.2
	1:8	2.8	22.4
	1:16	1.35	21.6

results, shown in Table 3, indicate that no significant change in either pituitary or plasma levels occurred.

In contrast to the experiments reported above, however, Müller's experiments have been consistently performed in the 30-day-old rat, and Pecile et al. [1965] and Krulich et al. [1965] have emphasized the greater responsiveness of the young rat to injections of hypothalamic extract. Similarly, Bernardis and Skelton [1967] have emphasized the greater effect of ventromedial nucleus lesions on growth in the weanling female rat. Consequently, some of the same experiments reported above were repeated exactly according to the conditions stipulated by Müller and Pecile and their co-workers in their various papers.

In Table 4 the results of two experiments in 30-day-old female Sprague-Dawley rats are reported. Neither intraperitoneal injection of 2 U insulin (Iletin^{R}), nor subjecting rats to a temperature of 4° C for 1 hr, affected the pituitary GH concentration, in contrast to the results reported by others using a bioassay. In keeping with our results we have found no increase in circulating GH levels; if anything, both insulin and cold have produced a decrease, similar to results reported above for the large rat, and to those reported earlier by Schalch [1966].

Finally, in Table 5 results are reported for an experiment in which hypothalamic extracts derived from 30-day-old rats were injected intracarotidly into 30-day-old female Sprague-Dawley rats under ether anesthesia; 15 min later the animals were bled by heart puncture and decapitated to allow removal of the pituitary. The age of the host animal has made no difference: no significant change is to be seen in either plasma or pituitary GH concentrations following injection of the extract.

The above results obtained with hypothalamic extracts and insulin were disappointing in view of the profound decreases in pituitary GH concentration observed by Müller et al. [1967a, b] in their experiments. In many of these, decreases in pituitary GH content in excess of 35% were reported, and in experiments in which hypothalamic extracts have been used, these decreases were seen after only 15 min.

Since the amount of GH disappearing from the pituitary is known in the experiments of Müller et al., it should be possible to calculate the expected levels of GH to be found in the circulation, if the hormone that has disappeared has been released into the circulation. For such a calculation both the half-life and distribution volume of rat GH must be known.

The disappearance of exogenously administered rat GH was studied in 4 rats, using the jugular vein for the blood-sampling site and the saphenous vein for the injection. Animals anesthetized with ether were injected with 2.0-3.8 μg of rat GH in 0.25 ml normal rat plasma. The results are presented in Fig. 20. An average half-time of approximately 7.5 min was obtained with an extrapolated volume of distribution of approximately 7.2% of the body weight. This half-life is in good agreement with that found by Schalch [1966] for exogenously administered rat GH.

Table 3. Plasma and pituitary GH in 60-day-old male S-D rats injected intracarotidly with rat hypothalamic extract.

	No.	Pituitary GH (μg/mg)	Plasma GH (mμg/ml)
Hypothalamic ext. (equiv. 3 rat hypo.)	4	20.5 ± 1.2*	17.6 ± 5.6
Saline	4	22.0 ± 9.5	9.4 ± 10.9†

*Mean ± standard deviation.

†p value 0.2 for plasma GH.

Table 4. Plasma and pituitary GH in 30-day-old female rats following insulin or cold.*

	Time (min)	Plasma GH (mμg/ml)	Pituitary GH (μg/mg)	P
Insulin	15	4.9 ± 2.9†	--	--
2 U/kg I. P.	30	1.9 ± 1.0	--	--
2 U/kg I. P.	45	2.0 ± 0.7	--	--
2 U/kg I. P.	60	2.1 ± 0.7	15.9 ± 2.5	< 0.5
Saline I. P.	60	11.7 ± 11.4	17.3 ± 1.1	
Cold 4°C	60	1.5 ± 0.6	17.4 ± 2.2	< 0.3
Uninjected	--	6.3 ± 5.1	20.2 ± 4.5	

*4 rats per group.

†Mean ± standard deviation.

Table 5. Plasma and pituitary GH in 30-day-old female rats 15 min after the intracarotid injection of rat hypothalamic extract* or saline.

Injection	Plasma GH (mμg/ml)	Pituitary GH (μg/mg)
Hypothalamic extract (8)†	2.9 ± 1.7‡	21.6 ± 5.1
Saline (6)	2.0 ± 0.3	20.9 ± 3.5

*2 SME equivalents.

†Number of animals.

‡Mean ± standard deviation.

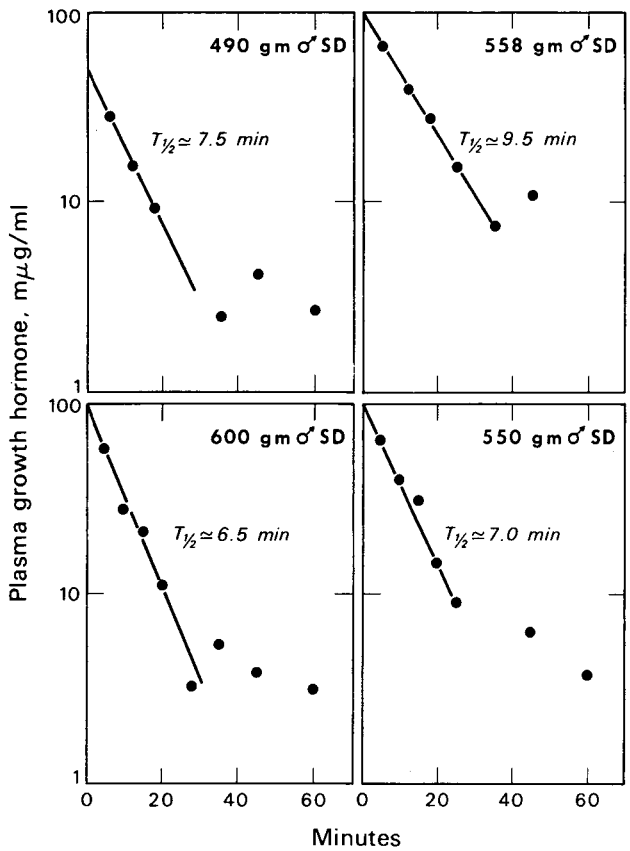

Fig. 20. The rate of change of plasma GH levels in the rat following the intravenous injection of 2.0 to 3.8 μg of rat GH.

DBL 678-1749

With the above values for the half-time and volume of distribution of rat GH (and assuming these values found in the 500 g male rat are valid for the 80 g female), and our own values for pituitary weights and GH concentrations we have made calculations on the expected plasma GH concentration in the 30-day-old rat used by Müller et al. 15 min after a 35% release of pituitary GH.* It will be noted that our values for pituitary GH concentrations are 1/3 to 1/4

*The 30-day-old female Sprague-Dawley rat weighs approximately 80 g, and therefore the volume available for dilution of GH is 80 × 0.072 = 5.8 ml. In the pituitary, which weighs approximately 3.5 mg, GH is present at a concentration of approximately 20 μg/mg. The total pituitary GH content is therefore 70 μg, and a decrease of 35% means a disappearance of about 24 μg of the hormone.

If the hormone is all released immediately in response to CRF administration, then at zero time the plasma concentration of the hormone has been increased by 4.1 μg/ml (24 + 5.8). Fifteen minutes later (two half-lives), 1/4 of this level, 1.0 μg/ml, should be present.

If instead the hormone is released evenly over the entire 15 min period, then the increase in secretion rate is 1.6 μg/min (24 + 15). The plasma concentration at any time in the steady state is related to the secretion rate by the relationship

$$\text{plasma concentration } (\mu g/ml) = \frac{\text{secretion rate } (\mu g/min) \times \text{half-life } (min)}{\text{distribution volume } (ml) \times 0.693};$$

substituting, we obtain

$$= \frac{(1.6)\,(7.5)}{(5.8)\,(0.693)} = 3.0\ \mu g/ml.$$

Both of these values, 1.0 and 3.0 μg/ml, are in terms of our rat GH standard. In terms of Müller's standard they would be 3 to 4 times higher. [Footnote continued on facing page.]

those reported by Müller and his co-workers; however, this difference can undoubtedly be accounted for by a difference in reference standard, since we have used as a standard a rat GH with a potency of 2.9 U/mg. If the GH is all released at zero time, then at 15 min the plasma concentration should be 1 μg/ml. (In terms of Müller's standard, it would be 3 to 4 μg/ml.) If instead it is evenly secreted over the 15 min period then the even higher plasma GH concentration of 3.0 μg/ml should be expected. Such levels are easily detectable in plasma even by the tibia test bioassay. (It is to be hoped that various investigators will carry out both bio- and immunoassays on the same samples of pituitary and plasma.)

The rat GH radioimmunoassay has been used in a few studies on mice. The effect of fasting was studied in female LAF_1 mice. Five animals were killed each day after having been fasted from 1 to 5 days. The animals were anesthetized with ether and bled by heart puncture. The plasma and pituitaries were pooled for each day of the fast. The total pituitary GH content and the plasma GH concentrations are presented in Table 6. Consistent with the results of Friedman and Reichlin [1965] in the rat, the total pituitary GH in mice appears to decrease with fasting. Correlated with this decrease is an increasing plasma GH concentration which rose from a prefasting value of 6 to a value of 44 mμg/ml after 5 days of fasting.

It was not possible to detect GH in the plasma of hypophysectomized mice, using the rat GH radioimmunoassay. Our attention then turned to a consideration of the genetic dwarf mouse. A group of dwarf mice and their normal litter mates were obtained from the Jackson Laboratory. The plasma and pituitary GH concentrations were assayed, using the rat radioimmunoassay. The results are presented in Table 7. Nine dwarf mice failed to shown any detectable GH in the plasma, whereas the eight normal female litter mates had plasma concentrations ranging from 4.3 to 35 mμg/ml. The five normal male litter mates had much lower plasma GH concentrations of from 1.6 to 2.2 mμg/ml. The pituitary GH concentration, although very low when compared with the normal litter mates (less than 1%), was nevertheless measurable in the dwarf mice. To our knowledge no quantitative bioassays for GH have ever been carried out on the dwarf mouse pituitary.

Finally, rat GH was injected intravenously (tail vein) into a group of 40 g male mice of the Swiss-Webster strain. Each mouse received 0.9 μg of rat GH dissolved in 0.1 ml of normal mouse plasma. Groups of 5 mice each were bled by heart puncture at 5, 10, 15, and 20 min after the injection. The plasma GH concentration was determined on each plasma sample, using the rat GH radioimmunoassay. These data yielded a plasma disappearance half-time of approximately 5.5 min and a volume of distribution of 8.2% for rat GH in mice.

These calculations are based on the assumption that the decrease in pituitary GH results from its release into the circulation. Another possibility is that it results from a decrease in synthesis. In the steady state, the removal rate, the secretion rate, and the synthetic rate are equal. If we solve the equation above for secretion rate, utilizing a normal plasma GH concentration of 15 mμg/ml, we obtain a value of 8.0 mμg/min. Thus, if synthesis were completely halted for 15 min, and release occurred normally, the pituitary GH concentration would decrease by 34 mμg/mg (8.0 × 15/3.5), a quantity that could not be accurately determined. Incidentally, if this rate of secretion is representative of the average rate during a day, the secretion rate of 11.5 μg/day in the 30-day-old rat would indicate that about 1/6 of the total pituitary GH is being turned over.

Table 6. Plasma and pituitary GH in fasting mice.*

Days fasting	Pituitary GH (μg, total)	Plasma GH (mμg/ml)
0	254	6
1	220	13
2	202	21
3	147	31
4	158	34
5	153	44

*Pooled pituitaries and plasma from 5 female mice.

Table 7. Plasma and pituitary GH concentrations in genetic dwarf mice (dw homozygotes) and their normal litter mates.

	Plasma GH (mμg/ml)	
Dwarf mice (9) (4 males, 5 females)	Undetectable	3 pituitaries 0.12 3 pituitaries 0.05 3 pituitaries 0.02
Normal female litter mates (8)	35.0 33.0 18.0 15.0 6.2 5.2 4.9 4.3	4 pituitaries 19.3 4 pituitaries 28.4
Normal male litter mates (5)	2.2 1.8 1.8 1.7 1.6	5 pituitaries 12.9

DISCUSSION

The experiments on control of GH release in the rabbit, rat, and mouse have, in a sense, been disappointing. We had expected that these animals would respond, as the primate does, to a set of trial stimuli: insulin and arginine administration, fasting, and stress. Having proven the point, we would then go on to the development of an acceptable in vivo assay for GRF, in which radioimmunoassay of circulating GH would be an integral part. We were therefore unprepared to find that with the exception of the stimulus of fasting, the aforementioned stimuli evoked either no response, or, as with Schalch's [1966] experience with stress in

rats, a response opposite to that found in primates. It is, parenthetically, most gratifying that the response to fasting is to be found in these non-primates, for it was from experiments in the rat that Russell developed the concept of GH as the hormone of the fasting state.

The failure to find the expected responses to these stimuli is all the more puzzling in the rat, in which animal a number of workers have reported profound decreases in pituitary GH within a short time after administration of insulin, or of submission of the animal to a cold stress. In these experiments, as in those in which an effect of crude or purified GRF's has been reported, GH was assayed by a bioassay—the tibia test. Thus, the problems to be resolved may, in fact, all be a facet of the problem of the adequacy of the radioimmunoassay in these animals.

Lack of specificity, offhand, does not appear to be a problem in the assay; that is, failure to obtain increases in GH levels in plasma in experiments in which bioassay has indicated a decrease in pituitary GH can hardly be explained in terms of non-specificity. Further, our own limited experience and the published findings of Hayashida and Contopoulos [1967] with other pituitary hormones derived from the rat and other animals would indicate instead great specificity for growth hormone for the antisera employed.

Other objections to the adequacy of the radioimmunoassay may, in part, be answered by the following considerations. After making allowances for the different standards employed and the terms in which the results are expressed, it would appear that both bioassay and radioimmunoassay give approximately the same value for the concentration of GH in the pituitary of the unmanipulated rat. It is only after manipulation of the animal (e.g., by insulin, cold, or hypothalamic extract) that bioassay gives much lower pituitary GH levels than does the immunoassay. Furthermore, in its favor, it can be said that the immunoassay is internally consistent; that is, failure to detect alterations in pituitary GH following manipulation of the animal is accompanied by a comparable failure to detect alterations in the plasma GH concentrations. As has been pointed out above, the decreases in pituitary GH found by bioassay must lead to enormous increases in circulating GH, if the hormone which disappears from the gland has been released into the circulation. It is difficult to believe that such increases would escape detection by the radioimmunoassay, which, for example, has detected the elevated plasma GH levels of the fasted rabbit and mouse, and of the fetal rabbit.

If one is willing to accept the adequacy and specificity of both bio- and immunoassays, then it would appear that the only explanation for the results observed may be the following: The biologically and immunologically active sites in pituitary GH are quite distinct, with little or no overlap. With certain appropriate stimuli, scission of the molecule takes place in the pituitary and the portion of the molecule with the biologically active site is released, leaving behind the fraction with the immunologically active site. One would then find no change in pituitary or plasma GH by immunoassay but a decrease in pituitary or plasma GH by bioassay. In order to explain the immunoassayable circulating GH, it is only necessary to assume that secretion under steady-state conditions is of the unfragmented molecule. As a corollary of the above, it would be presumed that the half-life and distribution volume of the exported

fragment would differ from those determined for the intact molecule.

The above speculation is divorced from present-day reality, being completely devoid of any supporting evidence. For the present, we are unable to explain the difference in results recorded by the two assay methods. In terms of the bioassay results, the rat at least is not greatly different from the primate, and the existence of a GRF has been reasonably well demonstrated. In terms of the radioimmunoassay results, it is only the stress of fasting that evokes similar responses in the various species, and the hypothalamic centers of the rabbit, rat, and mouse are not capable of detecting or responding to the other stimuli that provoke GH release in the primate.

Finally, it is the whole concept of a hypothalamic GRF which has suffered most from recent studies. Recent criticisms of the bioassay results by Rodger et al. [1967] have led to a reappraisal not of that assay procedure but of the statistical validity of the claims previously made. Our complete failure to demonstrate GRF effects either at the pituitary or plasma level of the rabbit and rat in in vivo experiments, and to show any change in rat pituitary or medium GH in unpublished 4 hr incubation studies (with Dr. M. H. Samli), along with Knobil's inability to detect changes in circulating GH in rhesus monkeys administered highly purified GRF all fit into an emerging pattern, at odds with reported 80% depletions in rat pituitary GH [Ishida et al., 1965]. That pattern is consistent with the notion that irrefutable evidence for a GRF has as yet not been presented. Perhaps what is needed is to determine the effect of hypothalamic extracts on weanling female rats bearing bilateral lesions of the ventromedial nucleus [Bernardis and Frohman, 1967], for these animals should be the most sensitive hosts in which to demonstrate the action of a GRF.

ACKNOWLEDGMENTS

The technical help of Mrs. Patricia Smith, Oskar Lang, Robert Dewey, and Eugene Mikuckis is gratefully acknowledged.

This work was supported in part by the U. S. Atomic Energy Commission (J. F. G.) and by NIH grant HO-00394 (I. I. G.).

REFERENCES

Bernardis, L. L., and Frohman, L. A. [1967]. Plasma and pituitary growth hormone levels in rats with hypothalamic lesions. Program of the 49th meeting of the Endocrine Society, 86.

Bernardis, L. L., and Skelton, F. R. [1967]. Growth and obesity in male rats after placement of ventromedial hypothalamic lesions at four different ages. J. Endocrinol. 38, 351.

Bowman, R. H. [1961]. Growth hormone activity of the anterior pituitary lobe of the male rat at various ages. Nature 192, 976.

Deuben, R. R., and Meites, J. [1964]. Stimulation of pituitary growth hormone release by a hypothalamic extract in vitro. Endocrinology 74, 408.

Friedman, R. C., and Reichlin, S. [1965]. Growth hormone content of the pituitary gland of starved rats. Endocrinology 76, 787.

Garcia, J. F., and Geschwind, I. I. [1966]. Increase in plasma growth hormone level in the monkey following administration of sheep hypothalamic extracts. Nature 211, 372.

Garcia, J. F., Linfoot, J. A., Manougian, E., Born, J. L., and Lawrence, J. H. [1967]. Plasma growth hormone studies in normal individuals and acromegalic patients. J. Clin. Endocrinol. Metab. 27, 1395.

Glick, S. M., Roth, J., Yalow, R. S., and Berson, S. A. [1965]. The regulation of growth hormone secretion. Recent Progr. Hormone Res. 21, 241.

Greenwood, F. C., Hunter, W. M., and Glover, J. S. [1963]. The preparation of ^{131}I-labelled human growth hormone of high specific radioactivity. Biochem. J. 89, 114.

Greenwood, F. C., and Landon, J. [1966]. Growth hormone secretion in response to stress in man. Nature 210, 540.

Hayashida, T., and Contopoulos, A. N. [1967]. Immunological studies with rat growth hormone. Program of the 49th meeting of The Endocrine Society, 72.

Hoffman, W. S. [1937]. A rapid photoelectric method for the determination of glucose in blood and urine. J. Biol. Chem. 120, 51.

Ishida, Y., Kuroshima, A., Bowers, C. Y., and Schally, A. V. [1965]. In vivo depletion of pituitary growth hormone by hypothalamic extracts. Endocrinology 77, 759.

Knobil, E. [1966]. The pituitary growth hormone: an adventure in physiology. The Physiologist 9, 25.

Knopf, R. F., Conn, J. W., Fajans, S. S., Floyd, J. C., Guntsche, E. M., and Rull, J. A. [1965]. Plasma growth hormone response to intravenous administration of amino acids. J. Clin. Endocrinol. Metab. 25, 1140.

Krulich, L., Dhariwal, A. P. S., and McCann, S. M. [1965]. Growth hormone-releasing activity of crude ovine hypothalamic extracts. Proc. Soc. Exptl. Biol. Med. 120, 180.

Machlin, L. J., Horino, M., Kipnis, D. M., Phillips, S. L., and Gordon, R. S. [1967]. Stimulation of growth hormone secretion by median eminence extracts in the sheep. Endocrinology 80, 205.

Meyer, V., and Knobil, E. [1967]. Growth hormone secretion in the unanesthetized rhesus monkey in response to noxious stimuli. Endocrinology 80, 163.

Müller, E. E., Saito, T., Arimura, A., and Schally, A. V. [1967a]. Hypoglycemia, stress and growth hormone release: blockage of growth hormone release by drugs acting on the central nervous system. Endocrinology 80, 109.

Müller, E. E., Sawano, S., Arimura, A., and Schally, A. V. [1967b]. Blockade of release of growth hormone by brain norepinephrine depletors. Endocrinology 80, 471.

Pecile, A., and Müller, E. E. [1966]. Control of growth hormone secretion. in: Neuroendocrinology [Martini, L., and Ganong, W. F., eds.], vol. 1, p. 537. Academic Press, Inc., New York.

Pecile, A., Müller, E. E., Falconi, G., and Martini, L. [1965]. Growth hormone-releasing activity of hypothalamic extracts at different ages. Endocrinology 77, 241.

Rodger, N. W., Beck, J. C., Burgos, R., and Guillemin, R. [1967]. Variability of response in the bioassay of ovine hypothalamic extracts for a somatotropin releasing factor. Program of the 49th meeting of the Endocrine Society, 88.

Samli, M. H., and Geschwind, I. I. [1967]. Some effects of the hypothalamic luteinizing

hormone releasing factor on the biosynthesis and release of luteinizing hormone. Endocrinology 81, in press.

Schalch, D. S. [1967]. Stress induced inhibition of growth hormone secretion in the rat. Program of the 48th meeting of the Endocrine Society, 57.

Schalch, D. S., and Reichlin, S. [1966]. Plasma growth hormone concentration in the rat determined by radioimmunoassay: influence of sex, pregnancy, lactation, anesthesia, hypophysectomy and extrasellar pituitary transplants. Endocrinology 79, 275.

Schally, A. V., Steelman, S. L., and Bowers, C. Y. [1965]. Effect of hypothalamic extracts on release of growth hormone *in vitro*. Proc. Soc. Exptl. Biol. Med. 119, 208.

Smith, G., Katz, S., Root, A., Dhariwal, A., Bongiovanni, A., Eberlein, W., and McCann, S. M. [1966]. Effect of crude ovine stalk median eminence extract on plasma growth hormone in rhesus monkeys. Program of the 48th meeting of the Endocrine Society, 35.

Solomon, J., and Greep, R. O. [1958]. Relationship between pituitary growth hormone content and age in rats. Proc. Soc. Exptl. Biol. Med. 99, 725.

The Measurement of the Effects of X Rays and Helium Ions on the Proliferative Capacity of Lymphoma Ascites Tumor Cells *in vivo*

Jose M. Feola, John H. Lawrence and Graeme P. Welch

INTRODUCTION

Although the greater biological effectiveness of heavy particles over electromagnetic radiation has been studied by J. H. Lawrence in normal tissues (1-3), as well as in neoplasms in animals (3-6), the need for a better understanding of the mechanisms of action of densely ionizing radiation, as well as the necessity of more precise measurement of the decrease of the oxygen effect with increasing linear energy transfer (LET), stimulated the initiation of a research program aimed at the clarification of these problems.

Studies of the biological effects of heavy ions on ascites tumor cells are particularly interesting because, unlike cultured cells, they are grown in vivo. In addition, parallel studies can sometimes be done by growing the same kind of cells in vivo as well as in vitro.

Quantitative studies of mammalian cellular radiobiology were limited to the precise techniques of culture in vitro until the methods first reported by Hewitt (7) and Hewitt and Wilson (8) allowed for measurement in vivo of cell viability by using cell dilution techniques.

Preliminary work done in this laboratory (9, 10) showed a greater relative biological effectiveness (RBE) for the 910 MeV helium ions at the Bragg peak than the same particles in the plateau region. Also, there was an indication that the oxygen effect was reduced to some extent, and the need for more quantitative studies was pointed out.

In the experiments reported here, improvements in the techniques used before have allowed us to make quantitative determinations of the oxygen enhancement ratio (OER) and the RBE of helium ions of different LET's. Our efforts in this direction are justified in view of the use of helium ions in therapy (11-13).

MATERIALS AND METHODS

THE TUMOR A murine lymphoma (near diploid) was used in the experiments reported here. This tumor line was obtained from Amos (14), and has been kept in ascites form by transplantation into A/Heston mice. This tumor "takes" in genetically closely related strains of mice such as A/Heston, LAF_1, A/JAX, and CAF_1. In these experiments we have used only LAF_1 female mice 12 to 16 weeks old and weighing 20 to 22 g. The tumor-forming

ability of the lymphoma cells (our designation L#2), as defined by the TD_{50} (the number of cells that produces 50% of tumors within 8 weeks of intraperitoneal injections) has not changed in 4 years. It is: $TD_{50} = 10 \pm 4$ cells (standard deviation indicated).

IRRADIATION CHAMBER Cells were irradiated in vitro, and Fig. 1 shows a cross section of a sample holder. Six were used and irradiated sequentially with the aid of a remotely controlled sample wheel. Each sample of ~71 mm^3 (~1.8×10^7 cells per chamber) was injected with a syringe through the 0.05 mm dialyzing paper cover into a 3.0-cm-diameter by 0.1-mm-deep depression in the lucite holder, and a 1/2-mil Mylar cover was placed over it. Neoprene "O" rings held the Mylar and dialyzing paper in place and sealed the cover to the holder.

For anoxic irradiations, nitrogen gas was passed through a bubbler and flow gauge to a manifold to which six 4-foot lengths of 1/2-mm glass capillary were attached. The flow rates from the capillaries were checked for independence, then the capillaries were individually connected to the sample holders with small plastic tubing. At a flow rate of 50 cm^3/min, the system flushed out in about one minute, and then the gas changed in each holder 2 to 3 times per minute. Twenty minutes was allowed for the oxygen in the samples to clear before the irradiations began.

For the hyperoxic irradiations, pure oxygen was used and the same procedure was followed as described for hypoxic irradiations.

We have kept the total flushing time for both hyperoxic and hypoxic irradiations at about 30 min, including the irradiation time. This was difficult in some cases when some technical problems arose after the flushing had been started.

IRRADIATIONS WITH X RAYS AND WITH HELIUM IONS ACCELERATED BY THE 184-INCH SYNCHROCYCLOTRON X-ray irradiations were done with a 250 kV Philips machine, operating at 230 kV and 15 mA. Filtration of 1 mm Al + 0.25 mm Cu was used, and the HVL in Cu was determined to be 1.4 mm. The TSD was 30 cm, and exposures were measured with a 250-R Victoreen ionization chamber. Calibration of this chamber was done by the National Bureau of Standards in August, 1966. The dose rate under these conditions is 210 ± 10 R/min.

The 184-inch synchrocyclotron was used for irradiations at the plateau region of the 910 MeV helium ions (LET = 17 MeV-cm^2/g), as well as at the Bragg peak region, which was obtained by placing 54 mm of copper absorber in front of the irradiation chamber.

Raju (15) has studied the energy distribution at the Bragg peak position by using a silicon detector 5 mm thick. Figure 2 shows the energy distribution as well as the LET distribution. The average energy is 85 MeV and the average LET is 100 MeV-cm^2/g.

Dose rates averaged 540 ± 100 rads/min.

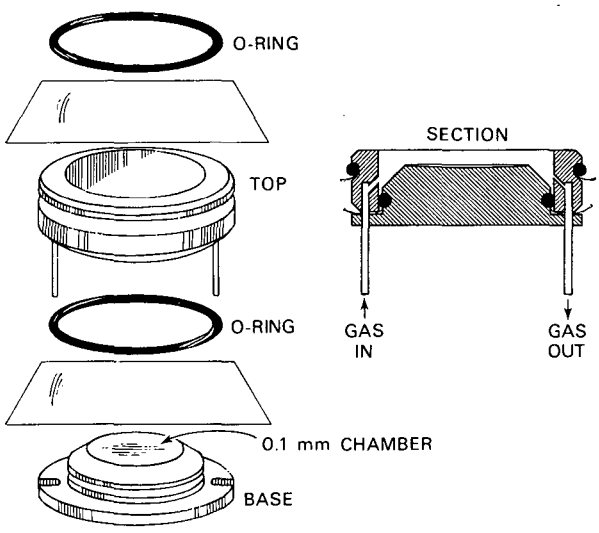

Fig. 1. Irradiation chamber. The lymphoma cells are irradiated under a 0.05 mm dialyzing paper cover. A 13 μ Mylar cover is placed on top. DBL 678-1772

IRRADIATIONS WITH THE 88-INCH SECTOR-FOCUSED CYCLOTRON Irradiations with helium ions of 118 MeV initial energy were done at the 88-inch sector-focused cyclotron. At the irradiation position, 60 ft from the cyclotron, the beam was brought to a focus with a quadrupole magnet. Then, in order to cover the sample uniformly, a 0.05 mm aluminum scattering foil was put into the beam 29 ft upstream from the target position. The maximum nonuniformity of this beam was approximately 5%, as determined by a diametrical scan with a 1 × 1 mm diode.

Full beam energy of 118 MeV was used for the low-LET irradiations at 80 MeV-cm^2/g. The low beam energy required for high-LET irradiations was obtained by absorption in lucite. Two remotely controlled wheels containing 1-1/2 in. diameter absorption discs were used first to obtain the Bragg curve, Fig. 3. Then the thickness that left a residual range of 0.09 g/cm^2 was placed in the beam, which yielded an LET of 220 MeV-cm^2/g at the sample. From the slope of the Bragg curve cutoff and the sample thickness, it is estimated that the LET ranged from 200 to 260 MeV-cm^2/g.

Doses were measured with a nitrogen-filled parallel-plate transmission ionization chamber with 6 μ aluminized Mylar electrodes. The electrodes were separated by 2 mm, and on the aluminum surface of one of them a 1 cm diameter circle was scratched to separate electrically the collecting electrode from its guard ring. The chamber's dimensions were measured with an optical comparator, and the dose corresponding to a microcoulomb of charge was calculated (16). A capacitor box and electrometer measured each irradiation's accumulated charge, from which the dose delivered was then determined.

The dose rate at the plateau region was 2800 ± 200 rads/min; at the peak it was 930 ± 250 rads/min.

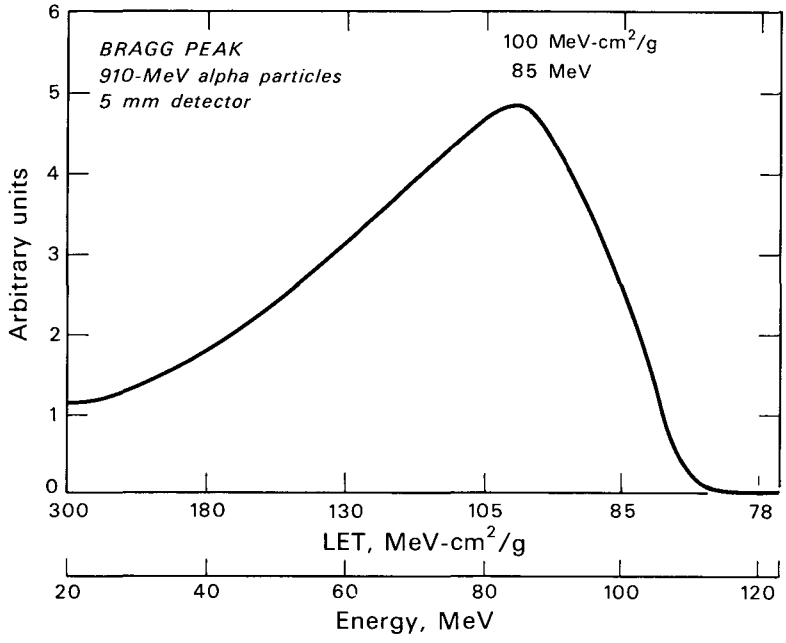

Fig. 2. Distribution of helium ion energy at the Bragg peak of the 910 MeV helium ion beam.
DBL 682-4597

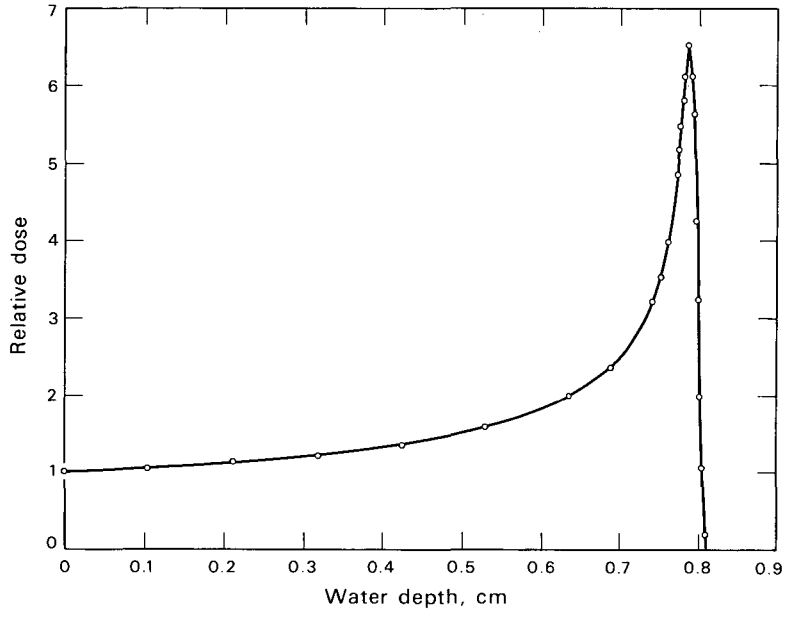

Fig. 3. Bragg curve of the 118 MeV helium ions accelerated by the 88-inch sector-focused cyclotron.
DBL 670-1838

THE ASSAY Seven days prior to the irradiations, LAF_1 mice were injected with 10^6 L#2 cells. Thirty minutes before irradiation time these animals were sacrificed, and the tumor cells contained in the ascitic fluid were then placed in the thin chambers by injection with a syringe and 27 gauge 3/4 in. hypodermic needle. The chambers were flushed for 20 min either with nitrogen or oxygen, and irradiations were performed while keeping the gas flow constant. The cells from each chamber were recovered and placed in test tubes which contained 2 ml of TC-199 medium. Counting was done with the hemocytometer, and serial dilutions were prepared for injection, using factors of 5 between dilutions. For each dose, as well as for controls, 5 groups of 10 animals each were intraperitoneally injected with 0.1 ml of fluid containing the different concentrations of cells.

Injected mice were kept in plastic cages housing 5 mice each, and the animals were examined for tumors twice a week for a period of 8 weeks.

SURVIVING FRACTION, MEAN LETHAL DOSE, AND RBE The percentage of animals taking the tumor at each level of cell inoculation allowed calculation of the TD_{50} (sometimes called "LD_{50}" because the tumor causes death in all cases). Because of the low precision of the accumulation method of Reed and Muench (17), and the serious doubts raised regarding its appropriateness (18, 19), Litchfield and Wilcoxon's method (20) was used to obtain the TD_{50}'s and their 95% confidence interval with occasional control of results by means of probit analysis (21, 22).

The ratios of the TD_{50} for the control group to those for the different doses of radiation gave the surviving fractions (S. F.), and plots of surviving fractions as a function of dose gave the survival curves. Straight lines fit most of the experimental curves well. When shoulders are present the extrapolation numbers range from 1.2 to 1.5.

The mean lethal dose (D_0, the dose in rads required to reduce to 0.37 the surviving fraction in the exponential region of survival curves) was used to estimate the RBE.

GAIN FACTOR The gain factor is defined as the ratio of the oxygen enhancement factor for X rays to that for helium ions. This factor gives an indication of how much one "gains" by using the different helium ions when treating anoxic cells. For equal injury to well-oxygenated tissues, the effect on anoxic cells is increased as if the dose to these cells only had been increased in the ratio given by the gain factor (23).

RESULTS

X-RAY IRRADIATIONS Figure 4 shows the survival curves obtained by irradiation with X rays. The mean lethal dose is indicated in the figure and all results have been summarized in Table 1.

The mean lethal dose under hypoxic conditions was 380 ± 50 rads, and under hyperoxic conditions it was 100 ± 10 rads. The ratio of these two values gave an oxygen enhancement ratio of 3.8 ± 0.9 as indicated in the 7th column of Table 1.

Table 1. Effects of helium ions and X rays on lymphoma cells irradiated *in vitro* and grown *in vivo*.

Accelerator	Radiation	LET ($MeV\text{-}cm^2/g$)	Number of animals*	D_0 (N_2)	D_0 (O_2)	$\frac{D_0(N_2)}{D_0(O_2)}$ †‡	RBE (N_2)‡	RBE (O_2)‡	Gain factor§
250 kV X rays	230 kV X rays	15-30	1500	380 ± 50	100 ± 10	3.8 ± 0.9	1	1	
184-inch synchro-cyclotron	910 MeV He ions, plateau	17	500	330 ± 50	130 ± 30	2.5 ± 1.0	1.2 ± 0.3	0.8 ± 0.3	1.5
184-inch synchro-cyclotron	85 MeV He ions, peak§	100**	1000	210 ± 30	100 ± 20	2.1 ± 0.7	1.8 ± 0.5	1.0 ± 0.3	1.8
88-inch cyclotron	118 MeV He ions, plateau	80	1000	330 ± 70	115 ± 25	2.9 ± 1.2	1.2 ± 0.4	0.9 ± 0.3	1.3
88-inch cyclotron	36 MeV He ions, near peak	220	1000	200 ± 20	110 ± 20	1.8 ± 0.5	1.9 ± 0.4	0.9 ± 0.3	2.1

*Each experiment involves about 250 mice.

†Oxygen enhancement ratio.

‡Standard errors are indicated.

§The ratio of the oxygen enhancement factor for X rays to that for helium ions.

**Averages of energy and LET distributions are indicated.

Points on both curves at the same dose level indicate values obtained in independent experiments. In the case of X rays, all laboratory procedures, irradiations, and injections were performed in the same building. When the irradiations were performed with the 184-inch synchrocyclotron or with the 88-inch sector-focused cyclotron, the timing of the experiments was more difficult, and greater variability was expected and actually observed.

IRRADIATIONS PERFORMED WITH HELIUM IONS

184-Inch Synchrocyclotron Figure 5 shows the survival curves obtained by irradiation of the lymphoma cells at the plateau region of the 910 MeV helium ions under hyperoxic and hypoxic conditions.

For the hypoxic irradiation: $D_0 = 330 \pm 50$ rads.

For the hyperoxic irradiation: $D_0 = 130 \pm 30$ rads.

The ratio of these two quantities gave an OER = 2.5 ± 1.0.

RBE's were estimated by the ratios of the mean lethal dose for X rays to that of the helium ions both under hypoxic and hyperoxic conditions. The values for 910 MeV helium ions were obtained the following way:

$$\text{RBE } (N_2) = \frac{380 \pm 50}{330 \pm 50} = 1.2 \pm 0.3 \quad \text{(8th column in Table 1)},$$

$$\text{RBE } (O_2) = \frac{100 \pm 10}{130 \pm 30} = 0.8 \pm 0.3 \quad \text{(9th column in Table 1)}.$$

Finally, the gain factor was obtained as the ratio of the oxygen enhancement ratio for X rays to that for the helium ions. In the case we are exemplifying:

$$\text{G. F.} = 3.8/2.5 = 1.5 \quad \text{(last column in Table 1)}.$$

Survival curves for the Bragg peak of these particles are shown in Fig. 6, and the estimated values of D_0, OER, RBE, and GF are given in Table 1. The energy and the LET are the averages found by Raju (15) as shown in Fig. 2.

88-Inch Sector-Focused Cyclotron Figure 7 shows survival curves obtained by irradiation of the lymphoma cells at the plateau region, at an energy of 118 MeV, and Fig. 8 shows the survival curves obtained by irradiation at the Bragg peak. The shape of the Bragg curve for these particles can be seen in Fig. 3. Results have been summarized in Table 1.

DISCUSSION

The end point of these studies was the tumor-forming ability of the lymphoma cells. No matter by which mechanisms the tumor-forming ability was impaired, it showed up in the slope of the survival curves. When the irradiations were performed under hyperoxic conditions, the same dose of different kinds of radiation impaired the tumor-forming ability to the same proportion, within the limits of the experimental errors.

The presence of oxygen seems to make the impairment of the tumor-forming ability a function only of the dose given. On the other side, survival curves obtained under hypoxic conditions showed a clear dependency on the LET of the helium ions used, in spite of the short span of the LET's explored in these experiments. The RBE's and gain factors calcu-

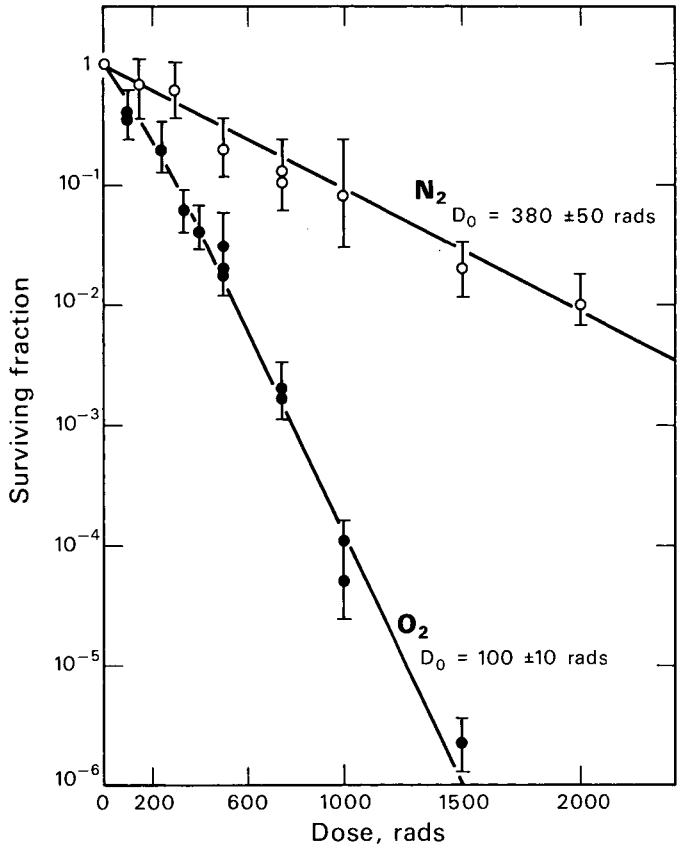

Fig. 4. Lymphoma cells irradiated with 230 kV X rays under hypoxic and hyperoxic conditions. Points at the same dose level show degree of reproducibility obtained.
$D_0(N_2)$ = 380 ± 50 rads; n = 1.0,
$D_0(O_2)$ = 100 ± 10 rads; n = 1.8.
In all figures, open circles indicate hypoxic conditions and solid circles show hyperoxic conditions.
XBL 672-777

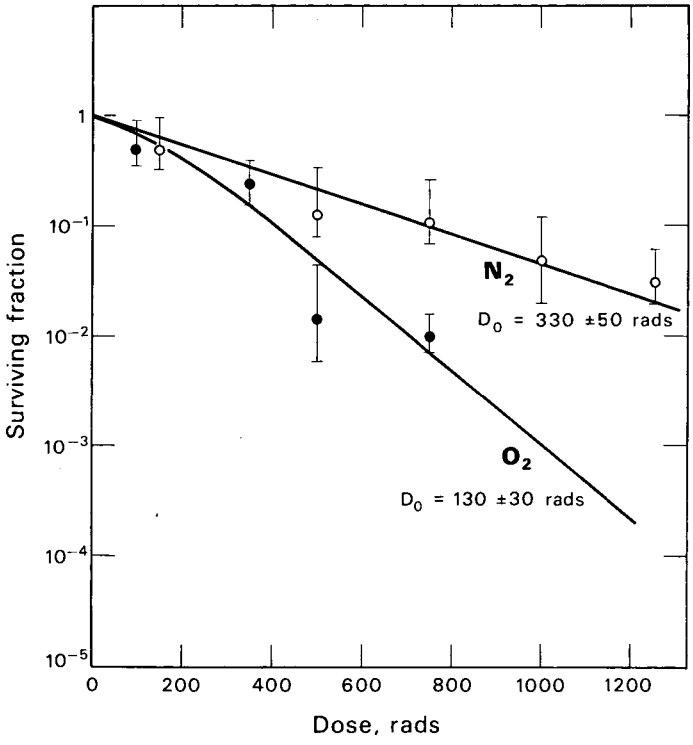

Fig. 5. Survival of lymphoma cells irradiated with the 910 MeV ^{4}He ions accelerated by the 184-inch synchrocyclotron. $n(N_2)$ = 1.0; $n(O_2)$ = 1.7.
DBL 670-1830

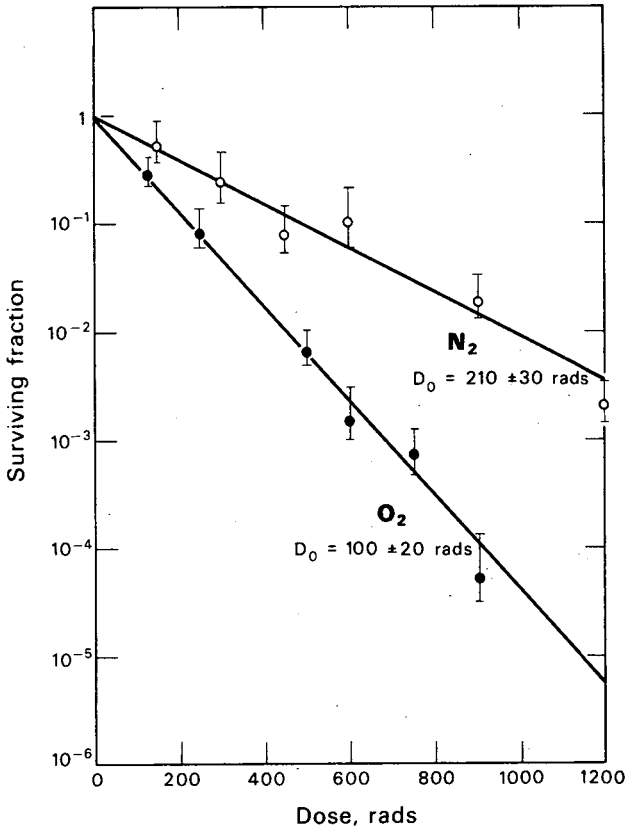

Fig. 6. Effects of ^{4}He ions accelerated by the 184-inch synchrocyclotron on the lymphoma cells when irradiated at the Bragg peak region (average energy 85 MeV). $n(N_2) = n(O_2) = 1.0$.
DBL 670-1831

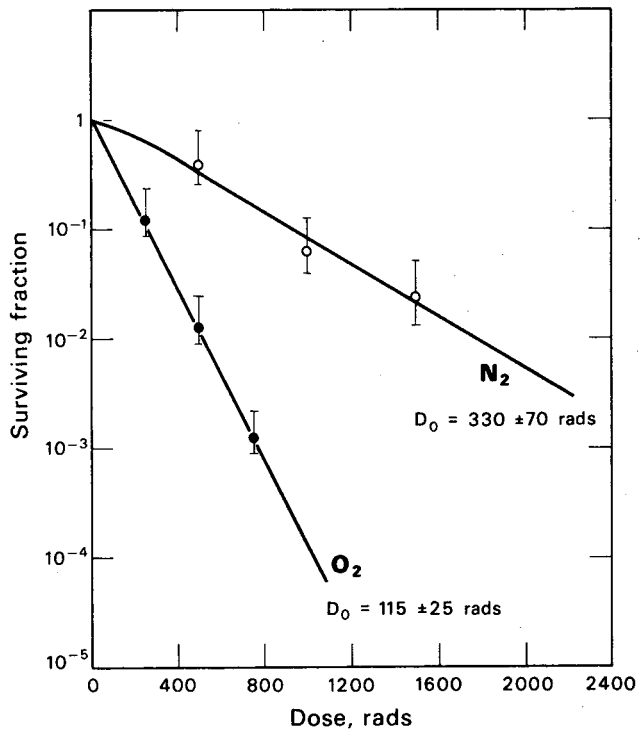

Fig. 7. Survival of lymphoma cells irradiated with 118 MeV ^{4}He ions accelerated by the 88-inch sector-focused cyclotron. $n(N_2) = 1.2$; $n(O_2) = 1.1$.
DBL 670-1829

lated for the helium ions quantitatively showed the greater effectiveness of the Bragg peak over the plateau and over X rays, as well as the partial overcoming of the oxygen effect.

The assay we have used "certainly measures the net result of a number of radiation-initiated processes, all of which can lead ultimately to the failure of a cell to carry out unlimited proliferation" (24).

Qualitative differences between the action of alpha and X rays on lymphoma cells in vitro have been pointed out by Alexander (25). He also thought it was unlikely that DNA synthesis was involved in the events leading to cell death, since DNA continued to be made at the normal rate for many hours by the irradiated cultures.

Bacq and Alexander (26) have indicated that "the fact that oxygen enhances the biological damage of radiations with low LET could arise from the fact that an isolated ionization initiates an autoxidation chain, thereby breaking these barriers which are made up in part of phospholipids in the same way as do several ionizations close together" (p. 97). This would explain why the mean lethal dose under hyperoxic conditions is the same regardless of the type of radiation used. In all cases enough damage is produced, although by different mechanisms, which results in similar impairment of the proliferative capacity. The fact that densely ionizing radiation has a higher RBE than ^{60}Co gamma rays has already been shown by Loughman et al. for these lymphoma cells using polyploidy induction as an end point (27). This increasing RBE with increasing LET showed up when the irradiations took place under hypoxia. In the absence of oxygen, helium ions are more effective, not only in causing chromosome damage, but also in producing cell membrane malfunctioning, organelles damage, releasing of proteolytic enzymes, etc., all of which would impair the ability of the cell to proliferate, and then would be measured in an assay for loss of proliferative capacity (24).

Small shoulders are present in some of the survival curves. The extrapolation number ranges from 1.2 to 1.5 in those cases, in agreement with nearly shoulderless survival curves obtained by Bush and Bruce (32) and Silini and Maruyama (30) with lymphoma cells.

Comparison of the mean lethal doses obtained by us by irradiating in vitro with values reported in the literature for in vitro and in vivo irradiations gives good agreement for hypoxic conditions. Berry and Andrews (28) reported a value of D_0 = 365 rads for the P-388 lymphocytic leukemia; Belli and Andrews (29) obtained a D_0 = 415 R for the P-388 lymphocytic leukemia irradiated in vivo as an ascites 7-day-old tumor; and Silini and Maruyama (30) gave a D_0 = 437 R for the LSA ascites lymphoma irradiated in the C57BL dead mice.

Mendelsohn (31) has pointed out the little spread observed for different tumors and techniques, and has given an average value of 358 R for anoxic cells.

Regarding the hyperoxic irradiations, Mendelsohn (32) gave an average value of D_0 = 131 R, which compares well with the value obtained by us with X rays (D_0 = 100 ± 10 rads). In comparing results for "well-oxygenated" cells, one has to be careful, however. For example,

the value of D_0 = 160 rads reported by Berry and Andrews (28) was obtained by injection of hydrogen peroxide prior to irradiation, and this value, as well as the one reported by Silini and Maruyama (30) of D_0 = 170 R for in situ irradiations, seems to indicate that the cells were not well oxygenated. This seems to be clear by comparison with the value reported by Belli and Andrews (29) for the 1-day-old tumor, namely, $D_0 = 110 \pm 11$ rads, which agrees well with ours. When the irradiation is performed under vigorous bubbling of oxygen (95% O_2, 5% CO_2), as in the experiments done by Bush and Bruce (32) irradiating lymphoma cells in suspension and assaying by the spleen colony method, the conditions are closer to those in our chambers, and the mean lethal dose reported by them ($D_0 = 114 \pm 4$ rads) for ^{60}CO gamma-ray irradiations compares well with our values for X-ray irradiations.

Considering the complexity of the factors involved, we think all these results are in essential agreement, and they point out the need of measuring the oxygen pressure in vivo as well as in vitro. The careful work of Deschner and Gray (33) has shown the difficulties of this task, as well as its potential in radiation research, especially for measurements in the ascitic fluid.

We have done some preliminary experiments to correlate pO_2 measurements with mean lethal dose. We have done these measurements in vivo by introducing a Beckman microelectrode housed in an 18-gauge needle into the peritoneal cavity instead of taking samples of the ascitic fluid (30). Calibration at four points at 37°C gave a straight line in most cases. A survival curve for a 7-day-old tumor is shown in Fig. 9. The $D_0 = 260 \pm 40$ rads indicated that some oxygen was present, since the mean lethal dose for anoxic cells is higher. However, the value of 21.0 ± 7.0 mm Hg obtained by measuring 10 animals with the same age tumors seems slightly high, and we are in the process of repeating these experiments in tumors from 3 to 8 days old.

The oxygen enhancement ratio is known to decrease with increasing LET (34-37), and consequently the gain factor increases. The range of gain factors obtained by us (1.5 to 2.1) is of the same order as values reported by other workers who used fast neutrons in their experiments (35-38).

The method used by us was not sensitive enough to show differences due to dose rate, and the same was true regarding survival under hyperoxia. Differences may exist, as has been shown with more precise techniques (39, 40). The RBE values reported here are in the range expected on the basis of previous work done in this laboratory with mammalian cells in vitro (39) and with techniques similar to ours (9, 41).

ACKNOWLEDGMENTS

We wish to thank Miss Alice Beckmann and Miss Henriette C. Cozza for their technical assistance in this project.

We are grateful to Dr. John T. Lyman and Messrs. Jerry Howard and David D. Love for their advice and help with the irradiations at the 184-inch synchrocyclotron.

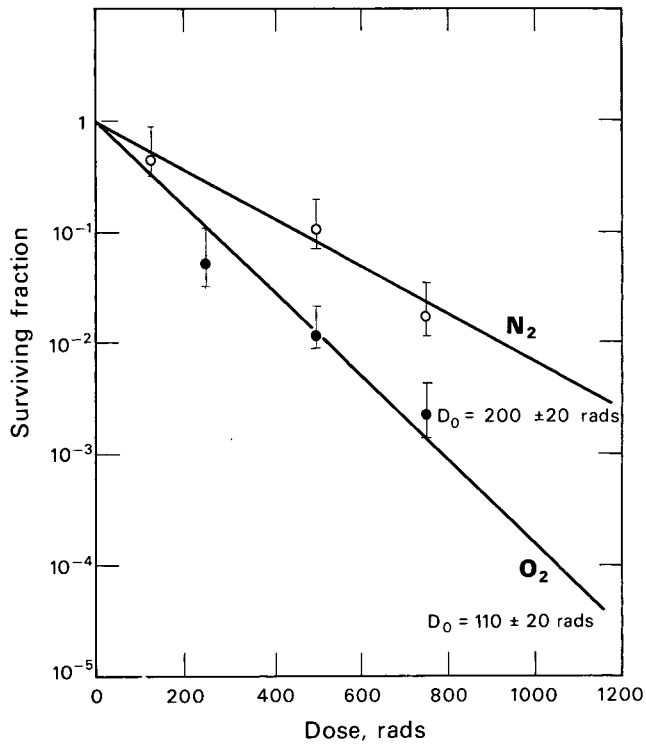

Fig. 8. Survival of lymphoma cells irradiated at the Bragg peak region of the ^{4}He ions accelerated by the 88-inch sector-focused cyclotron. $n(N_2) = n(O_2) = 1.0$.
DBL 670-1832

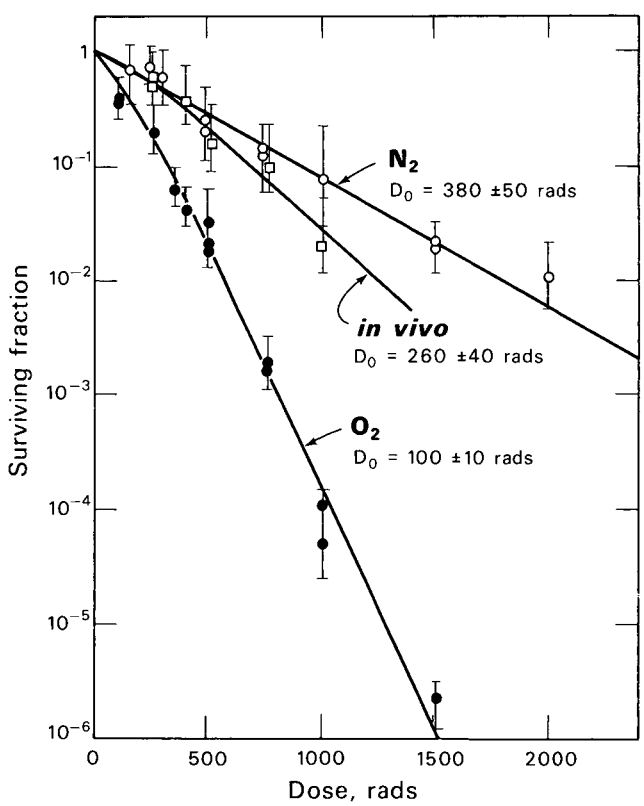

Fig. 9. Survival of lymphoma cells irradiated in vivo (7-day-old tumor) as compared with the irradiations performed in vitro.
n (in vivo) = 1.2.
DBL 678-1769

REFERENCES

1. Lawrence, J. H., and Lawrence, E. O.; The biological action of neutron rays. Proc. Natl. Acad. Sci. 22: 124-233, 1936.
2. Lawrence, J. H., and Tennant, R.; The comparative effects of neutrons and X-rays on the whole body. J. Exptl. Med. 66: 667-688, 1937.
3. Lawrence, J. H.; Aebersold, P. C., and Lawrence, E. O.; The comparative effects of X-rays and neutrons on normal and tumor tissue. Proc. Natl. Acad. Sci. 22: 543-557, 1936.
4. Lawrence, J. H.; Horn, R., and Strong, L. C.; Radiation studies on mammary carcinoma of mice. Yale J. Biol. Med. 10: 145-154, 1938.
5. Axelrod, D.; Aebersold, P. C., and Lawrence, J. H.; Comparative effects of neutrons and x rays on 3 tumors irradiated "in vitro." Proc. Soc. Exptl. Biol. Med. 48: 251-256, (1941).
6. Aebersold, P. C., and Lawrence, J. H.; Physiological effects of neutron rays. Ann. Rev. Physiol. 4: 25-48, 1942.
7. Hewitt, H. B.; Studies of the dissemination and quantitative transplantation of a lymphocytic leukemia of CBA mice. Brit. J. Cancer 12: 378-401, 1958.
8. Hewitt, H. B., and Wilson, C. W.; A survival curve for mammalian leukaemia cells irradiated in vivo (Implications for the treatment of mouse leukaemia by whole-body irradiation). Brit. J. Cancer 13: 69-75, 1959.
9. Sillesen, K.; Lawrence, J. H., and Lyman, J. T.; Heavy-particle ionization (He, Li, B, Ne) and the proliferative capacity of neoplastic cells "in vivo." Acta Isotopica 3: 107-126, 1963.
10. Schmidlin, Y.; Lawrence, J. H.; Sillesen, K.; Welch, G., and Lyman, J.; Effect of heavy particles on the proliferative capacity of ascites tumor cells (lymphoma) grown in vivo; in Semiannual Report, Donner Laboratory, Lawrence Radiation Laboratory Report UCRL-11833, 1964, pp. 80-94.
11. Lawrence, J. H., and Tobias, C. A.; Heavy particles in medicine; in Progress in Atomic Medicine, New York, Grune & Stratton, Inc., 1965, Chap. 6.
12. Tobias, C. A., and Todd, P. W.; Heavy charged particles in cancer therapy. Natl. Cancer Inst. Monograph No. 24, 1965.
13. Lawrence, J. H., and Tobias, C. A.; Heavy particles in therapy; in Modern Trends in Radiotherapy, edited by T. J. Deeley and C. A. P. Wood, Butterworths, 1967, Chap. 15.
14. Amos, D. B.; Serological differences between comparable diploid and tetraploid lines of three mouse ascites tumors. Ann. N. Y. Acad. Sci. 63: 706-710, 1956.
15. Raju, M. R.; Heavy particle studies with silicon detectors. Lawrence Radiation Laboratory Report UCRL-16534, 1965.
16. Birge, A. C.; Anger, H. O., and Tobias, C. A.; Heavy charged beams; in Radiation Dosimetry, edited by G. J. Hine and G. L. Brownell, New York, Academic Press, Inc., 1956, p. 623.
17. Reed, L. J., and Muench, H.; A simple method of estimating fifty per cent endpoints. Am. J. Hyg. 27: 493-497, 1938.
18. Finney, D. J.; Statistical Method in Biological Assay, 2nd ed., New York, Hafner Publishing Co., 1964.

19. Meynell, G. G.; Inherently low precision of infectivity titrations using a quantal response. Biometrics 13: 149-163, 1957.
20. Litchfield, J. T., and Wilcoxon, F.; A simplified method of evaluating dose-effect experiments. J. Pharmacol. Exptl. Therap. 96: 99-113, 1949.
21. Finney, D. J.: Probit Analysis, 2nd ed., Cambridge, 1962.
22. Dixon, W. J., Ed.: Biomedical Computer Programs, University of California at Los Angeles, BMD 03S, 1964, p. 357.
23. Fowler, J. F., and Morgan, R. L.; Pre-therapeutic experiments with the fast neutron beam from the Medical Research Council Cyclotron, VIII, General Review. Brit. J. Radiol. 36: 115-121, 1963.
24. Whitmore, G. F., and Till, J. E.; Quantitation of cellular radiobiological responses. Ann. Rev. Nucl. Sci. 14: 347-374, 1964.
25. Alexander, P., Qualitative differences between the action of α and X rays on lymphoma cells in vitro. Brit. J. Radiol. 35: 361, 1962.
26. Bacq, Z. M., and Alexander, P.: Fundamentals of Radiobiology, New York, Pergamon Press, Inc., 1961.
27. Loughman, W. D.; Feola, J. M.; Raju, M. R., and Winchell, H. S.; RBE of π^- beams in the Bragg peak region using polyploidy induction in mammalian cells irradiated in vivo, to be published in Radiation Research.
28. Berry, R. J., and Andrews, J. R.; Quantitative studies of radiation effects on cell reproductive capacity in a mammalian transplantable tumor system in vivo. Ann. N. Y. Acad. Sci. 95: 1001-1008, 1961.
29. Belli, J. A., and Andrews, J. R.; Relationship between tumor growth and radiosensitivity. J. Natl. Cancer Inst. 31: 689-703, 1963.
30. Silini, G., and Maruyama, Y.; Studies of the LSA ascites lymphoma of C57BL mice. I. Transplantation characteristics and radiosensitivity of cells during serial passages. J. Natl. Cancer Inst. 35: 841-849, 1965.
31. Mendelsohn, M. L.; Radiation effects in tumors; in Radiation Research, edited by G. Silini, Amsterdam, North-Holland Publishing Co., 1967, pp. 659-675.
32. Bush, R. S., and Bruce, W. R.; The radiation sensitivity of transplanted lymphoma cells as determined by the spleen colony method. Radiation Res. 21: 612-621, 1964.
33. Deschner, E. E., and Gray, L. H.; Influence of oxygen tension on X-ray-induced chromosomal damage in Ehrlich ascites tumor cells irradiated in vitro and in vivo. Radiation Res. 11: 115-146, 1959.
34. Alper, T.; Effects on subcellular units and free-living cells; in Mechanisms in Radiobiology, edited by M. Errera and A. Forssberg, New York, Academic Press, Inc., 1961, Chap. 5, p. 382.
35. Bewley, D. K., and Hornsey, S.; Radiobiological experiments with fast neutrons, with reference to the possible value of neutron therapy; in Biological Effects of Neutron and Proton Irradiations, Vienna, IAEA, Vol. II, 1964, pp. 173-183.
36. Fowler, J. F.; Neutrons in radiotherapy: slow neutrons, fast neutrons and other heavy particles; in Biological Effects of Neutron and Proton Irradiations, Vienna, IAEA, Vol. II, 1964, pp. 185-214.
37. Fowler, J. F.; Radiation biology as applied to radiotherapy; in Current Topics in Radia-

tion Research, Vol. II, edited by M. Ebert and A. Howard, Amsterdam, North-Holland Publishing Co., 1966, p. 332.

38. Hornsey, S., and Silini, G.; Comparisons of the effects of x-rays and cyclotron neutrons on mouse ascites tumours, mouse testis and chick embryos. Brit. J. Radiol. 36: 92-97, 1963.

39. Todd, P. W.; Reversible and irreversible effects of densely ionizing radiations upon the reproductive capacity of cultured human cells. Med. College of Virginia Quarterly 1: 2-14, 1966.

40. Barendsen, G. W.; Mechanism of action of different ionizing radiations on the proliferative capacity of mammalian cells; in Theoretical and Experimental Biophysics, edited by A. Cole, New York, M. Dekker, Inc., 1967, pp. 167-231.

41. Berry, R. J.; "Small clones" in irradiated tumour cells in vivo. Brit. J. Radiol. 40: 285-291, 1967.

Use of a Modified Insulin Tolerance Test to Measure Growth Hormone Reserve in Pituitary Diseases

John A. Linfoot, Joseph F. Garcia, Norton J. Snyder, Edward Manougian, Richard A. Carlson, Robert A. Fink, James L. Born and John H. Lawrence

INTRODUCTION

The adaptation of the radioimmunoassay technique originally described for insulin by Berson and Yalow (1), to pituitary protein and peptide hormones (2, 3), has provided an invaluable means of studying pituitary physiology. The sensitivity of the radioimmunoassay has made it possible to measure human growth hormone (HGH) levels in acromegaly and gigantism as well as levels in normal individuals. However, fasting levels of HGH are often inadequate to distinguish hypopituitary states. The observation by Roth et al. (4) that hypoglycemia was a potent stimulus for HGH secretion suggested its application as a test of HGH reserve. This has been pursued by a number of investigators, including Franz and Rabkin (5) in adults, Kaplan and Grumbach (6) in children with disorders of growth and development, and Cornblath et al. (7) in infants.

Since the degree of insulin sensitivity varies in different endocrine and metabolic states, and because prolonged hypoglycemia is not without risk in patients with panhypopituitarism, the routine use of the standard insulin tolerance test (8) has certain disadvantages. The observation by Knopf et al. (9) that plasma HGH increased following intravenous administration of amino acids led to the introduction of arginine infusion (10) as a means of assessing HGH release in pituitary disease. While the safety of the arginine test is well established and it has been considered as the test of choice in the diagnosis of HGH deficiency (11), a number of patients have been demonstrated to respond to a hypoglycemic stimulus after failing to respond to arginine stimulus. Furthermore, it has been our experience as well as others' (12) that both tests are required for an accurate diagnosis of hyposomatotrophinism. Thus, it would be desirable to modify the insulin tolerance test in such a fashion that the problems of prolonged hypoglycemia are avoided. In this paper we describe a modified insulin tolerance test in which a standard amount of insulin is employed, regardless of the endocrine status. The duration of hypoglycemia is shortened and terminated in a routine fashion without significantly blunting the HGH response. The results of the modified tests, performed in patients with acromegaly, chromophobe adenomas, Chiari-Frommel syndrome, Cushing's disease, and a number of patients with hypopituitarism following surgical hypophysectomy and heavy particle pituitary irradiation from the 184-inch synchrocyclotron, are presented.

MATERIALS AND METHODS

The details of the method used for the radioimmunoassay of GH have been presented previously (13). Human growth hormone (kindly supplied by Professor C. H. Li, University of California, Berkeley) was used to immunize rabbits, and also labeled with iodine-125, using the Chloramine-T method of Greenwood et al. (2). The antibody-bound HGH-iodine-125 was precipitated using a goat anti-rabbit gamma globulin serum. The percentage of the labeled HGH which was bound to antibody was plotted against the logarithm of the concentration of standard HGH (a gift from Professor A. E. Wilhelmi, Emory University, Atlanta, Georgia. Lot No. HS503A had a specific activity of 1.7 I.U./mg, standardized in terms of the bovine growth hormone international standard). The concentrations of HGH were read directly off such a curve and are therefore expressed in millimicrograms per millimeter of the standard HGH.

Intravenous insulin tolerance tests (ITT) were performed using 0.1 unit/kg of glucagon-free insulin (kindly supplied by Dr. John A. Galloway, Eli Lilly & Company). Patients were fasted overnight and maintained at bedrest during the entire procedure. Since many of the patients had varying degrees of hypopituitarism, the standard ITT was modified so that hypoglycemia was interrupted 30 min after the injection of insulin by allowing the patients to eat a normal hospital breakfast. Blood samples were obtained fasting and at 10, 20, 30, 45, 60, and 90 min following insulin injection. Blood glucose determinations were performed on an Autoanalyzer, using a modification of the method of Hoffmann (14). Maximal hypoglycemia was achieved in all patients within 20-30 min; however, peak HGH levels lagged slightly and usually did not occur until 30-60 min.

RESULTS

Typical HGH response patterns in two normal subjects are shown in Fig. 1. Hypoglycemia was interrupted at 30 min by permitting the subjects to eat breakfast. In both subjects approximately a 100-fold increase in HGH was observed. The effects of heavy particle pituitary irradiation on HGH reserve are shown in Fig. 2. Serial studies were performed in a patient (Lin) with mammary carcinoma. Initially, the fasting values were elevated but further increase occurred during insulin hypoglycemia. Gradual obliteration of HGH response was observed following treatment.

Figure 3 presents the results of modified-ITT studies in a variety of conditions associated with anatomic or functional pathology of the pituitary gland. The fasting and maximum HGH levels in a group of normal individuals is included for comparison. A group of patients with active acromegaly and with elevated fasting HGH levels was uniformly resistant to insulin hypoglycemia and failed to show HGH increase.

Five patients with non-functioning pituitary adenomas and no other clinical evidence of hypopituitarism had nearly absent HGH responses following the modified ITT. Similar responses were observed in patients with post-surgical panhypopituitarism. Blunted HGH responses were also seen in 2 patients with Chiari-Frommel syndrome. The patients with Chiari-Frommel were all exquisitely insulin sensitive; one of the patients showed a slightly

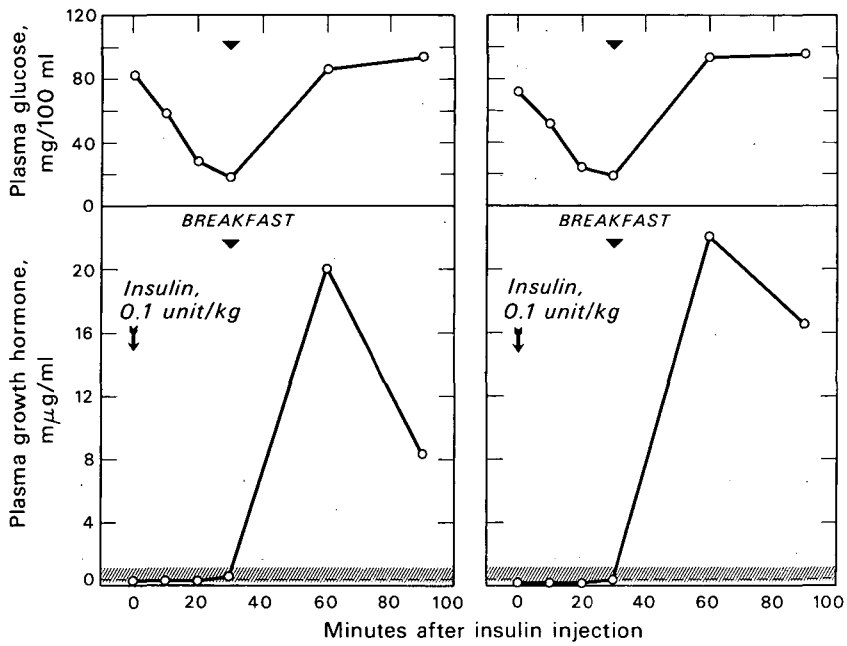

Fig. 1. Plasma HGH responses in 2 normal males during modified insulin tolerance tests.
MUB-9736

greater HGH rise but was clinically indistinguishable from the other case. In a group of patients with Cushing's disease due to bilateral adrenal hyperplasia, HGH response to hypoglycemia was suppressed compared to normals. These patients were all quite sensitive to insulin in spite of high levels of circulating adrenal cortisol.

Modified ITT's were performed in a number of patients receiving heavy particle pituitary irradiation for breast cancer and diabetic retinopathy. Figure 4 illustrates HGH responses to insulin-induced hypoglycemia in these disorders. The normals are again included for comparison. The patients with mammary carcinoma were studied before heavy particle pituitary irradiation. The fasting growth hormone levels were elevated in several of these cases for unknown reasons. All of these patients showed a definite HGH response to hypoglycemia, although the response was less than that of the normal subjects. After heavy particle pituitary irradiation, which was delivered in amounts anticipated to produce more than 50% histologic destruction of the pituitary gland, HGH secretion was markedly depressed. A similar depression was observed in a small group of non-obese, adult-type diabetic patients 2-3 years after pituitary suppressive therapy for diabetic retinopathy but with minimal or absent clinical or laboratory signs of hypopituitarism.

DISCUSSION

It is generally accepted that fasting HGH studies are inadequate for distinguishing hypopituitary states. The HGH rise following insulin hypoglycemia has been used for this purpose. While the stimulus for HGH response has been shown to follow extracellular hypoglycemia, the studies with 2-deoxyglucose suggest intracellular glucose deficiency is the ultimate stimulus (15).

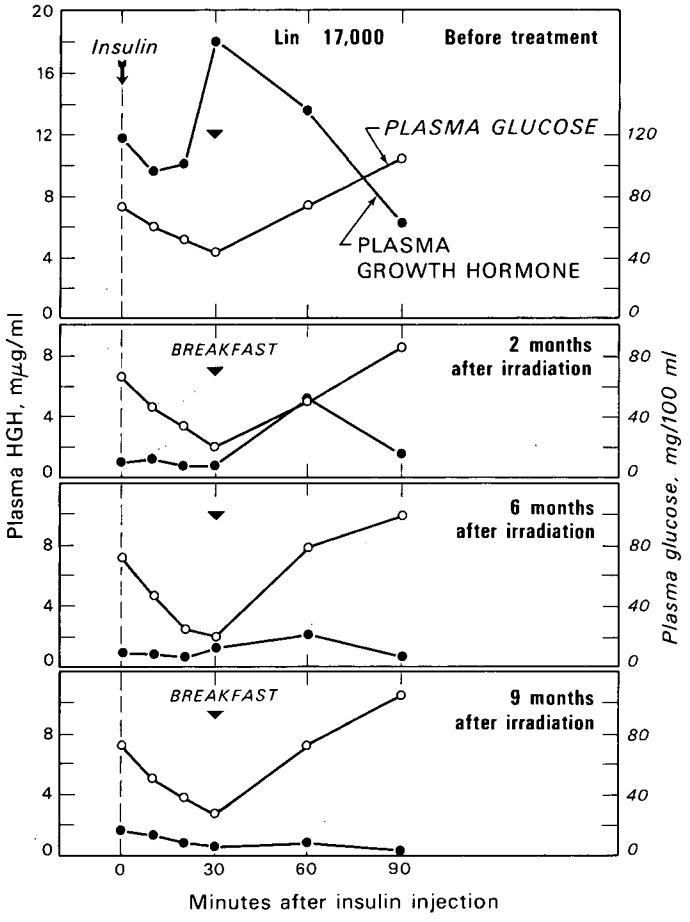

Fig. 2. Serial changes in HGH reserve following heavy particle pituitary irradiation in a patient with mammary carcinoma. MUB-10643

Insulin resistance is characteristic of acromegaly. The minimal changes in HGH observed in acromegalics during modified insulin tolerance tests may reflect incomplete hypoglycemic stimulus and perhaps larger doses of insulin might have induced greater HGH response. However, such studies carried out by Beck et al. (16) using standard ITT were similar to ours. We have concluded that many of the pituitary adenomas secreted HGH largely autonomously. The impaired HGH reserve in patients with chromophobe adenomas is not too surprising; however, the lack of other evidences of altered pituitary trophic function demonstrates the sensitivity of the test in detecting pituitary pathology. When radioimmunoassays for ACTH, TSH, LH, and FSH become more generally available, subtle changes in these hormones may also be detectable.

The cause of blunted HGH release in Chiari-Frommel syndrome is uncertain. The presence of a small pituitary adenoma of insufficient size to produce anatomical change by X ray or, equally likely, some alteration in the hypothalamic pituitary axis, are two possible explanations. Blunted HGH secretion following adrenal steroid administration and in Cushing's syndrome has been reported by Franz and Rabkin (5) and Hartog et al. (17). We have con-

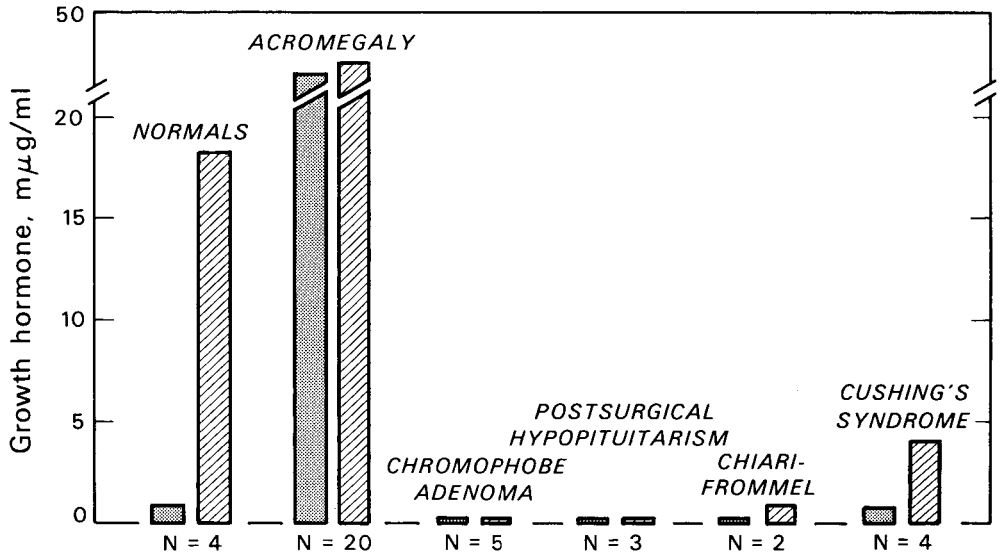

Fig. 3. Comparison of the fasting and maximal HGH levels during modified insulin tolerance tests in patients with a variety of pituitary pathologies. The fasting values are indicated by the shaded bars and the maximal responses by the hatched bars. MUB-10967

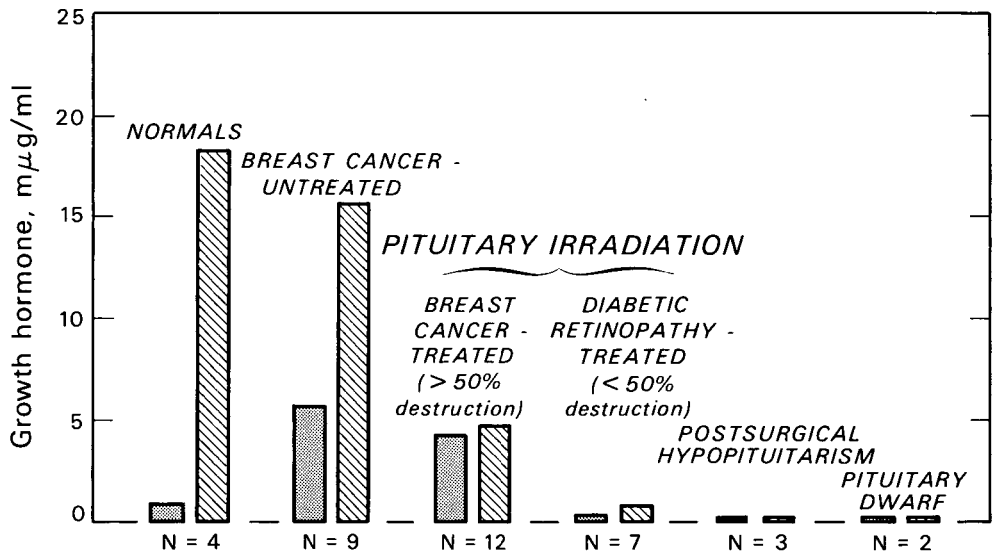

Fig. 4. Fasting and maximal HGH responses in patients with mammary carcinoma and diabetic retinopathy who had received suppressive heavy particle pituitary irradiation. Patients with postsurgical hypopituitarism and idiopathic pituitary dwarfism are presented for comparison. MUB-10968

firmed these observations. The normal insulin sensitivity in patients with Cushing's disease suggests that the insulin-induced hypoglycemia is more dependent on HGH availability than on the secretion of adrenal cortical steroids.

The primary limitation of insulin provocative studies lies in the discomfort and danger of resultant protracted hypoglycemia. This is particularly hazardous in hypopituitary states, in which it has been suggested the ITT be abandoned and replaced by the arginine infusion test (11). Because of the occasional disparity of the results of arginine and insulin data in states with depressed HGH (growth retardation, delayed pubescence, and Chiari-Frommel syndrome), we feel both mechanisms of HGH stimulation are vital to the definition of hyposomatotrophinism. From our experience with 250 procedures, modified insulin tolerance tests were free from untoward effects, though many patients were hypopituitary. The abbreviated period of hypoglycemia minimizes physician supervision of the tests. With the minimized side effects, patients are seldom reluctant to have repeat tests performed.

CONCLUSION

We have suggested a modification of the standard insulin tolerance test by termination of hypoglycemia by a normal hospital meal at 30 min. The application of this test to studies of HGH reserve is reviewed in a variety of pathologic pituitary states. Serial studies utilizing this test illustrate the decline in HGH response after heavy particle pituitary irradiation. Extensive experience with this modified insulin tolerance test in hypopituitary states has been uncomplicated by any significant side effects and provided a highly sensitive test of pituitary function.

REFERENCES

1. Berson, S. A., and Yalow, R. S.; J. Clin. Invest, 39: 1157, 1960.
2. Hunter, W. M., and Greenwood, F. C.; Biochem. J. 85: 39, 1962.
3. Glick, S. M.; Roth, J.; Yalow, R. S., and Berson, S. A.; Nature 119: 784, 1963.
4. Roth, J.; Glick, S. M.; Yalow, R. S., and Berson, S. A.; Science 140: 987, 1963.
5. Franz, A. G., and Rabkin, M. T.; New Engl. J. Med. 271: 1375, 1964.
6. Kaplan, S. L.; Abrams, C. A. L.; Bell, J. J.; Conte, F. A., and Grumbach, M. M.; J. Pediat. 67: 956, 1966.
7. Cornblath, M.; Parker, M. L.; Reisner, S. H.; Forbes, A. E., and Daughaday, W. H.; J. Clin. Endocrinol. Metab. 25: 209, 1965.
8. Fraser, R. W.; Albright, F., and Smith, P. A.; J. Clin. Endocrinol. Metab. 1: 297, 1941.
9. Knopf, R. F.; Conn, J. N.; Fajans, S. S.; Floyd, J. C.; Guntsche, E. M., and Rull, J. A.; J. Clin Endocrinol. Metab. 25: 1140, 1965.
10. Merimee, T. J.; Lillicrap, D. A., and Rabinowitz, D.; Lancet 2: 668, 1965.
11. Parker, M. L.; Hammond, J. M., and Daughaday, W. H.; J. Clin. Endocrinol. Metab. 27: 1129, 1967.
12. Raiti, S.; Davis, W. T., and Blizzard, R. M.; Lancet 2: 1182, 1967.
13. Garcia, J. F.; Linfoot, J. A.; Manougian, E.; Born, J. L., and Lawrence, J. H.; J. Clin. Endocrinol. Metabl. 27: 1395, 1967.

14. Hoffman, W. S.; J. Biol. Chem. 120: 51, 1937.
15. Roth, J.; Glick, S. M.; Yalow, R. S., and Berson, S. A.; Metabolism 12: 577, 1963.
16. Beck, P.; Schalch, D. S.; Parker, M. L.; Kipnis, D. M., and Daughaday, W. H.; J. Lab. Clin. Med. 66: 366, 1965.
17. Hartog, M.; Gafaar, M. A., and Fraser, R.; Lancet 2: 376, 1964.

Delayed Radionecrosis of the Central Nervous System

Larry W. McDonald, John H. Lawrence, James L. Born and John T. Lyman

Until recent years the adult central nervous system was commonly thought to be radioresistant. That this radioresistance is relative and not nearly as great as previously believed is now generally recognized. In contrast to investigations of 25 years ago, when the main concern of the investigator in this area was whether or not the central nervous system was affected by ionizing radiation, present-day studies are concerned with mechanisms producing immediate and late radiation effects. Along with this the detailed morphological studies of both early and late radiation lesions in the CNS continue with greater precision in both man and (especially) in the experimental animal. In the experimental studies of the late effects, attention is generally focused on the role of blood vessels and glial cells in producing tissue necrosis. The possible role of DNA and RNA turnover in glial cells has also been discussed in some of the recent reports. The importance of volume of tissue irradiated has been well established as a factor in the development of delayed radionecrosis in the experimental animal: the smaller the volume, the greater the dose required to produce delayed radionecrosis. In addition, animal experimental studies have shown that the larger the radiation dose, the earlier a delayed radiation lesion will appear.

LITERATURE PRIOR TO 1955

The earliest report of delayed radionecrosis of the central nervous system of man was that of Fischer and Holfelder (1) in 1930. In one of their two cases, epilepsy developed 7 years after radiation had been given for an epithelioma of the scalp. Biopsy of the brain showed evidence of old hemorrhage, necrosis, and hyaline and amyloid-like changes of blood vessels. In the period between 1930 and 1955 twelve other reports (2-13) of 1 to 4 cases each of delayed radionecrosis of brain appeared in the world literature. Two of these reports with a total of 3 cases, in which surgical removal of an area of radionecrosis of brain was successful, were those of Lowenberg-Scharenberg and Bassett (13) and Pennybacker and Russell (6). During this same period six reports, which included histological description of myelitis attributable to radiation, appeared (12, 14-18). In general the histological picture of the radiation lesions has been similar to that described by Fischer and Holfelder (1).

When one turns to experimental animal studies, one finds some mention of delayed effects as early as 1902 when Rudis-Jicinsky (19) described small hemorrhages in the central nervous systems of guinea pigs 50 days post-irradiation. The next year Danysz (20) described similar changes in adult mice 10 to 44 days after radiation. Up to 1955 there were occasional other papers by various authors describing late changes of the brain of various animal species following radiation. Two of these papers presented work of greater significance in clearly

defining the delayed radiation lesions than most of the others. The first of these papers was that of Scholz (21). He described an "early" delayed reaction occurring 4 to 5 weeks following radiation and a "late" delayed reaction occurring several months later in dogs. The "early" delayed reaction consisted of infiltration of lymphocytes in perivascular areas. The "late" delayed reaction consisted of diffuse and focal perivascular hemorrhage with some evidence of tissue necrosis. The second paper presenting experimental work of particular significance here was that of Russell et al. (22). In this work, radiation conditions and dosimetry were emphasized and various post-irradiation survival times were studied. The hyaline changes of blood vessels and hemorrhages about small blood vessels were found. No changes were observed with doses below 2440 R, some rabbits having been kept over 2 years.

With the exception of a few animal experimental papers such as the paper by Russell et al. (22), most of the earlier work on late effects is of limited value for comparison with present-day experiments because of the poor or limited dosimetry in the early work. Some dose determinations were attempted by several authors prior to 1955 in cases of radionecrosis of human brain. The results of these studies were summarized by Lindgren (23) as shown in Table 1. The tolerance doses have generally been of the same order of magnitude as those found in more recent studies.

LITERATURE SINCE 1955

In the past 10 years there have been a number of reports of delayed radiation lesions in human brain. Only those papers which in our judgment had good dosimetry data or those in which the morphologic data is superior will be mentioned. Both from the standpoint of number of cases studied and the effort made to determine dose-effect relationships, the paper by Lindgren (23) adds much information as to the radiation tolerance of the human brain. From the 13 cases from the literature and the 4 additional cases described by Lindgren (23), a radiation dose of 3.2 kR given over a 10 day fractionation period may produce radionecrosis of brain in some cases. Using a modified Strandquist diagram and the same slope found for human skin, the single dose which might lead to a great risk of radionecrosis is 1888 R.

Two cases of delayed radionecrosis of brain were reported by Zulch (24). The histological features of these cases were similar to those already described. The radiation data are not given in detail, but the doses were well up in the range where delayed necrosis might occur (Table 2). In one of these cases the patient survived surgical removal of the area of necrosis. There is another recent report of a case in which an area of radionecrosis was successfully removed surgically 19 years following use of radon seeds to treat a fibrosarcoma of the right temple at the age of 41 years. In this report by Chandler et al. (25) the radiation dose to the involved brain was between 2000 and 7000 R. Some of the cysts extended well below areas of brain receiving less than 1800 R.

The case reported by Toga et al. (26) is also of interest because of the long time interval (78 months) between irradiation and the appearance of clinical signs of an expanding lesion of the frontal lobes. The original tumor was a meningioma which was excised and followed by radiation with the large dose of 10 kR through 4 ports. The quality factors and fractionation

Table 1. Literature cases of radionecrosis of brain with histologic verification and dosage data (reported prior to 1955).*

Author/year	Primary diagnosis	Age	kV	HVL (mm)	Field size (cm^2)	Total tumor dose (kR/days)	Interval, treatment to death (months)
Scholz & Hsu 1938 (3)	Schizophrenia	26	180	0.67 Cu	80-150	4.3 kR/2	17
	Schizophrenia	32	180	0.67 Cu	80-150	4.3 kR/2	19
Wachowski & Chenault 1945 (5)	Glioblastoma multiforme	44	190-220	1.56 Cu	10×10	7.8 kR/105	7.5
	Astrocytoma	30	190-220	0.75 Cu	10×10	8.7 kR/84	15
	Colloid carcinoma	52	190-220	0.75 Cu	10×10	8.8 kR/87	18
Pennybacker & Russell 1948 (6)	Ulcus rodens capillitii	58	230	1.3 Cu	7 cm	2.3 single air; at 2 cm depth: 1.9 single	Living after extirpation of necrosis†
Zeman 1949 (8)	Brain-stem tumor astrocytoma	37	180	1.0 Cu	Pendulum irradiation	6.0 kR/30	45
Boden 1950 (7)	Acoustic neurinoma, middle ear	38	250	1.65 Cu	19-31	6.0 kR/17	19
		43	250	1.65 Cu	19-31	5.9 kR/17	15
Foltz, Holyoke, & Heyl 1953 (9)	Basal cell epithelioma of the scalp	45	120	1.0 Al	25	2.9 single skin; at 2 cm depth: 1.3 single	
Arnold, Bailey, & Harvey 1954 (10)	Brain-stem glioma	--	400	--	--	4.5 kR/30	12
	Brain-stem glioma	--	400	--	--	4.5 kR/30	12
	Ependymoma of the 4th ventricle	--	23×10^3 X ray†	--	--	7.5 kR/18	14
Malamud et al. 1954 (12)	Sarcoma in parieto-occipital region	37	1000	2.6 Pb	100	3.6 kR/25 (at 2 cm depth)	44
Dugger et al. 1954 (11)	Carcinoma of the scalp	54	150	0.5 Cu	5 cm	4.3 kR/10 (at 2 cm depth)	27
Lowenberg-Scharenberg & Bassett 1950 (13)	Basal cell carcinoma of lt. temporal region	42	150	0.25 Cu	5.7×4.1 cm^2	< 6.0 kR/10+ < 3.6/30 (2 yr later)	71‡
	Carcinoma right parietal region	53	110-130 (?)	N. S.§	N. S.	3.5 kR/1	40‡

*From Lindgren (23) except last two cases, which were added from original literature.

†Equivalent to 4.5 kR of 400 kV X rays.

‡Area of necrosis removed surgically and patients survived.

§N. S. = not specified.

Table 2. Cases of late radionecrosis of brain (reported since 1955).

Author/year	Primary diagnosis	Age	kV	HVL (mm)	Field size (cm^2)	Total tumor dose (kR/days)	Interval, treatment to death or operation (months)
Zulch 1956 (24)	Meningioma	50	N. S.*	N. S.	N. S.	9.0 kR/30 (2 treatments)	60
	Glioma	24	N. S.	N. S.	N. S.	6.0 kR/? 4.2 kR/? (3 yr later)	63
Lindgren 1958 (23)	Astroblastoma	41	170	1.0 Cu	35-100	7.25 kR/38	15
	Glioblastoma	56	170	1.0 Cu	35-100	7.25 kR/27	8
	Medulloblastoma	37	170	1.0 Cu	35-100	5.1 kR/26	43
	Medulloblastoma	32	170	1.0 Cu	35-100	6.6 kR/31	27
Toga, Berard, & Sommer 1961 (26)	Meningioma	48	N. S.	N. S.	4 ports, size not specified	10.0 kR/?	78
Crompton & Layton 1961 (27)	Chromophobe adenoma	55	250	2.1 Cu	6 × 4	4.5 kR/28	17
	Pituitary adenoma	51	200	1.5 Cu	--	6.25 kR/42	24
Boellaard & Jacoby 1962 (28)	Basal cell carcinoma of skin, left para-sagittal (case No. 1)	50	N. S.	N. S.	N. S.	2.0 kR/?	30
	Basal cell carcinoma of skin, right temple (case No. 2)	48	N. S.	N. S.	N. S.	23.3 kR (2.0-8.0 kR given per treatment over 6 yr)	200 (from 1st irradi-ation)
	Parasagittal glioma (case No. 3)	48	N. S.	N. S.	N. S.	11.1 kR in 2 divided doses 1 yr apart	120
	Medulloblastoma (case No. 4)	5	N. S.	N. S.	N. S.	4.9 kR/?	60
	Right temporal lobe glioblastoma multi-forme (case No. 5)	37	N. S.	N. S.	N. S.	5.0 kR/? 3.2 kR/? 1 yr later	19
	Left central tumor, probably glioma (case No. 6)	35	N. S.	N. S.	N. S.	4.9 kR/?	34
Bignami, Giuffie, & Riccio 1963 (29)	Pituitary tumor	29	^{60}Co γ ray	--	N. S.	10.0 kR/?	14

Lampert & Davis 1964 (46)	Carcinoma tonsil Astroblastoma	64 19	200 1000	1.5 Cu --	6 × 8 10 × 10	5.7 kR/32 8.3 kR/35	3-1/2† 144
Almquist, Dahlgren, Notter, & Sunborn 1964 (30)	Cushing's disease	29	200	0.7 Cu	4 cm circle, full rotation	5.0 kR/29 necrosis in areas receiving 1.8-3.0 kR/29	1-1/2†
Chandler, Tucker, & Herzberger 1964 (25)	Sarcoma	40	‡	‡	‡	N. S. ; necrosis extending to areas receiving less than 1.8 kR	228§

*N. S. = not specified.

†Lesions in this case were limited primarily to perivascular round cell accumulation, focal demyelination, and focal gliosis. Hemorrhage was prominent in the case of Almquist et al.

‡Radiation from radon seeds.

§Patient surviving; area of radionecrosis removed surgically.

schedule were not specified. Surgical exploration revealed no residual tumor, but an expanding area of radionecrosis was found. The histological description of this lesion is reported in detail and similar to the lesions previously described. Lymphocytes in perivascular spaces were fairly prominent. Hyaline amyloid-like material was abundant; hyalinization of vessel walls and intimal accumulation of lipid-filled histiocytes were prominent features. As in many other earlier reports, white matter was more involved than cortex. Although they did not observe eosinophiles as did Crompton and Layton (27), an immunological mechanism appealed to Toga et al. (26).

Two cases of delayed radionecrosis of human brain were reported by Crompton and Layton (27) in 1961. Both occurred in patients with acromegaly following pituitary irradiation. Their first case was a 55-year-old woman who developed clinical signs of brain damage 12 months after irradiation of the pituitary. The tumor dose was 4 to 4.8 kR with brain tissue receiving similar doses over a 4 week fractionation period. The detailed histological description of the lesion generally agrees with those of earlier reports. Hemorrhage was limited to the area near radionecrosis. Their second case was a 51-year-old male who received between 3.3 and 6.25 kR to brain tissue over a 6 week period. There was a gradual loss of vision and 20 months after radiation he was confused and lethargic. He died 2 years following irradiation. Microscopically there was evidence of old hemorrhage as in most earlier reported cases. The usual amyloid-like material was again noted along with reactive astrocytes about areas of necrosis. As in other cases white matter was more involved than grey. In this second case an unusual feature was the presence of large numbers of eosinophiles in some of the areas of necrosis. On this basis and on the basis of the presence of round cells about vessels, the authors suggested that an allergic mechanism may have been involved.

Six cases of delayed radionecrosis of human brain following treatment for basal cell carcinoma (two cases) or brain tumor (four cases) have been collected and reported by Boellaard and Jacoby (28). All of these cases had complete excision of the area of necrosis or a biopsy of the area; the histological descriptions are good. However, the descriptions of dosimetry are very sketchy and more specific details, such as voltages and specific fractionation details, are lacking. Four of their six cases showed histological changes like the "early" delayed lesion of Scholz (21), although vessel wall sclerosis was fairly marked in their case No. 4. Only in two of their cases (their Nos. 4 and 5) did they observe the amyloid-like material which is commonly described in the delayed lesion. All of these except for one (their case No. 4) did well post-operatively and it appeared that excision of the area of radiation damage was curative. One case died with a meningioma which was apparently radiation induced and appeared clinically 6 years following radiation for a glioma (their case No. 3).

A case of a 28-year-old woman who received ^{60}Co gamma ray therapy to the pituitary for a "complex multiglandular dysendocrine syndrome" was described by Bignami (29). 5000 R was given to the area of the pituitary through each of 2 lateral ports in a single treatment. Eight months after irradiation the patient became extremely cachectic and died 6 months later. The autopsy revealed typical lesions of delayed radionecrosis extensively involving the hypothalamus. There were perivascular round cell infiltrates which made the lesion appear to

represent the "early" delayed necrosis as described by Scholz (21).

Almquist et al. (30) reported clinical signs of radionecrosis developing in a patient with Cushing's disease 3 weeks following pituitary irradiation. The radiation factors are shown in Table 2. The lesions were definitely of the early type as described in the studies in dogs done by Scholz (21). Brain necrosis with hemorrhage was observed in areas of the frontal lobe receiving 1.8 to 3.0 kR in 29 days. Perivascular lymphocytic infiltration was also prominent. Typical late changes of vessel hyalinization and accumulation of proteinaceous lakes of amyloid-like material were not seen. Interestingly, this patient was hypertensive and this may account for the severe rapidly developing radiation lesion appearing after such low radiation exposure over a prolonged fractionation period. In experimental studies using rats and in a clinical case Asscher and Anson (31) have shown arterial hypertension to lower the threshold for radionecrosis of the spinal cord. In one patient hypertension, 180/120 mm Hg, was definitely implicated in increasing the radiosensitivity of the spinal cord. In this patient, a man 42 years old with ankylosing spondylitis, 1.0 kR given over 1 month in 4 divided doses produced paraplegia 15 months later. The patient died of a urinary tract infection. The sections of spinal cord from the autopsy showed "multiple vascular necrotic foci as well as necrosis of neural tissue."

On concluding this survey of reported cases of delayed radiation changes in the human brain, the omission of two groups of papers should be explained. First, papers in which implanted radioactive materials were used in the brain have been omitted because precise dosimetry is usually difficult to ascertain. The paper by Bailey et al.(32) will be mentioned, however, because of its fine histological description of the late lesions in which all of the typical histological features of the delayed radiation lesions are described. These lesions were found in the frontal lobes about ^{60}Co implants. The second group of papers omitted are those in which whole body radiation was received either as a result of atomic bomb explosions, reactor accidents, fallout exposure, systemically administered radioisotopes, or whole body therapeutic irradiation. In these cases the radiation received was below that which will produce direct effects on the brain during the period of survival. Most effects on the brain which have been observed in such cases are probably more related to the total effects of the radiation on the organism than to a direct effect on the brain.

Cases of late necrosis of the spinal cord reported since 1955 are tabulated in Table 3. The cases tabulated are restricted to those in which there has been histological study of the cord lesions, generally at autopsy. The 10 cases reported by Dynes and Smedal (33) may not have all been delayed necrosis of the spinal cord since they were not confirmed by histological examination except in 2 cases. For this reason only the 2 cases (their case I and case VII) are in Table 3. From the 7 of the 10 cases which developed hemiplegia or paraplegia without evidence of recurrence of their neoplasm, between 2500 and 5000 rads fractionated over 18 days appears to be required to produce necrosis in 11 months [case I of Dynes and Smedal, (33)]. In the paper by Pallis et al. (34) 5 cases of radiation myelopathy are described clinically, but in only 1 case (case 2) was the lesion examined histologically. The complete description of the lesion was "a vascular lesion which had all the appearance of an infarct."

Table 3. Cases of late radiation necrosis of spinal cord (reported since 1955).

Author/year	Primary diagnosis	Age	kV	HVL (mm)	Length of cord irradiated	Estimated cord dose (kR/days)	Interval, treatment to death or symptoms (months)
Itabashi, Bebin, & DeJong 1957 (47)	Lymphoepithelioma of tongue	72	250	3 Cu	> 10 cm	6.1 kR/27	15
	Laryngeal carcinoma	22	250	2-3 Cu	< 10 cm	4.7 kR/38	4-1/2; stationary at 39
Dynes & Smedal 1960 (33)	Giant follicular lymphoma (case I)	42	2000	N.S.*	> 10 cm	2.5-5.0 kR/18	11
	Carcinoma of lung (case VII)	45	2000	N.S.	> 10 cm	6.0 kR/49	33
Alajouanine, Lhermitte, Cambien, & Gantier 1961 (48)	Epithelioma, nasal cavity	39	^{60}Co γ ray	N.S.	> 10 cm	< 20.7 kR/40	12
Pallis, Louis, & Morgan 1961 (34)	Pharyngeal carcinoma (case 2)	47	8 MeV	N.S.	< 10 cm	4.6-6.8 kR/32	7
Asscher & Anson 1962 (31)	Ankylosing spondylitis†	42	N.S.	N.S.	> 10 cm	1.0 kR/1	15
Verjaal 1964 (35)	Carcinoma of lung	67	^{60}Co γ ray	N.S.	8 cm	4.5 kR/30 2.4 kR/1 (10 months following 1st irradiation)	6

*N.S. = not specified.

†This patient also had hypertensive cardiovascular disease.

A report of one case of radiation myelopathy with a detailed histological description of the lesion was made by Verjaal (35). The initial radiation dose to the cord was less than 4500 R. Because it was thought the patient had metastatic tumor involvement of the spinal cord, a second radiation dose of 2400 R was given 10 months later. The cord was examined at autopsy 1 month later. Sclerosis of vessels was a marked finding. In addition to necrosis of the radiated segments of the spinal cord there was moderate glial reaction and ascending and descending degeneration, but no residual tumor in the spinal cord.

Another 5 cases of clinical radiation myelopathy were reported by Schinz (36). Histological examinations were not done in any of these cases and for this reason they are not included in Table 3. The lowest dose which produced myelopathy was 4400 rads. Very little dosimetry data is given.

EXPERIMENTAL STUDIES SINCE 1955

Of the many experimental papers which have appeared since 1955 only those which appear to represent a general approach to the subject will be mentioned. First will be mentioned work we have done which explores the possibility of an immune mechanism in delayed radionecrosis of rabbit brain (37). In this study animals were sensitized with Freund's adjuvant and spinal cord tissue to produce a minimal low-level experimental encephalitis. With the dosage schedules used, no effect on the delayed radiation lesion in the rabbit could be found. Another approach is the ultrastructural study of the capillaries when the late effects are just beginning to appear, in order to determine if alterations in these structures precede the development of the more advanced radiation lesions. We have been doing such studies and have reported some of the results (38). Capillary basement membrane thickening, vacuolation and swelling of endothelial cells, and increased density of fibers in perivascular astrocytic foot processes appear to precede or occur concomitantly with delayed radiation necrosis. Cervos-Navarro (39) has reported somewhat similar delayed changes.

The experimental studies of Asscher and Anson (31) mentioned above have shown that hypertension increases the radiosensitivity of the rat spinal cord.

The most complete and extensive study of radionecrosis in the rodent is that of Berg and Lindgren (40). In this study they have explored the effect of dose fractionation and shown that a single dose of 1.7 krads may produce distinct necrosis. They present the detailed histology of the radiation lesions and point out that amyloid-like deposits are less frequently observed in the experimental lesion than in the human cases. In the log plot of dose against days of fractionation they find a slope of 0.34 rather than the 0.22 found by Strandquist (41) for human skin and skin tumors. They observed early changes in blood vessel endothelium which they interpreted as being related to the delayed necrosis.

In another study using the rabbit, Berg and Lindgren (42) have shown the effect of volume of brain tissue irradiated on the frequency with which radionecrosis was produced. Animals were killed at 1 year if they survived to that time. From their experimental results, 18,000 R and a field width of 2 mm produces about the same number of discrete lesions and severe lesions per unit volume as 5000 R with a 6 mm field width or 3000 R with an 8 mm field width. When the data were put on a scatter diagram with a log scale (field width vs. radiation dose), a straight line was approximated.

In studying delayed radionecrosis in the rat spinal cord, Zeman (43) has found that there is increased uptake of tritiated thymidine by glial cell nuclei in the few days immediately preceding the development of delayed radionecrosis, indicating an increased DNA synthesis. A similar but less marked increase in tritiated cytosine uptake was found. The total number of glial cells is increased during the few days preceding necrosis. These changes occur in white matter primarily. He suggests two possible interpretations: 1) cells are stimulated to divide following radiation and die after mitotic division, some surviving long enough to increase the total number of cells, but after almost 5 months cells begin to die at a rapidly increasing rate and necrosis soon ensues, or 2) acute cell loss following radiation stimulates mitotic activity

and thus accounts for the increased labeling and increased numbers of cells. He favors the first interpretation and relates this to radiogenic damage at sites for RNA synthesis. It has been shown by others, however, that tritiated thymidine labeling of glial cells is increased about sites of tissue damage. Thus it may be that the increased number and increased labeling reflect reaction of glial cells to areas of tissue damage. Thus the findings would also be consistent with the primary damage being in capillaries and/or their associated astrocytes.

REPORT OF CASES

During the course of post-mortem examination of brains from patients dying of metastatic breast cancer who had also received pituitary irradiation using the heavy particle beam, 8 examples of delayed radionecrosis were found. These occurred among a group of patients with advanced breast cancer who no longer responded to conventional forms of therapy and for whom suppression of pituitary function or hypophysectomy seemed advisable. In all there were over 150 such patients treated during the period 1954-1966. In the early period 1954-1958 relatively large doses to the sellar area were used in order to bring about cessation of pituitary function as rapidly as possible, and the risk of brain damage seemed to be justified. Since then, however, non-damaging doses have been used, bringing about more slowly suppression or cessation of pituitary function.

The 8 cases are recorded in Table 4 with the pertinent irradiation treatment data. They are all high-dose cases and are of particular interest to the purposes of this study since the average duration of life after pituitary irradiation was 3 years. Five of these patients had an excellent prolonged remission of their disease and survived for 2, 2.5, 3.5, 4, and 6 years respectively after treatment. Clinically there were signs of temporal lobe involvement in only 4 of the 8 cases but these signs were generally not severe and controllable with Dilantin. All of these patients had varying degrees of functional disturbance of cranial nerves, some of which improved (chiefly 3rd, 4th, and 6th nerves). All of the patients eventually died of metastatic disease except for one who died of fat embolism following a traumatic fracture of the hip. It was apparent to the clinician and the patients that any untoward or damaging effects of the radiation were outweighed by the extension of comfortable life.

Figure 1 shows one of the most extensive gross lesions encountered in this series* along with a representative isodose diagram for this technique of radiation, the details of which have been described elsewhere (44 and 45). The isodose diagram shows less than 5% of the pituitary dose at points 1 cm anterior or posterior to the sella. There is very little scatter of particle radiation so that there is almost no radiation outside of the beam path.

Blocks of the temporal lobes were taken from the formalin fixed brains through the anterior portion of the amygdala and sections stained with hematoxylin and eosin. Myelin sheaths

*Two of the authors who followed this patient for the entire course of 6 years, during the last 2 of which she had temporal lobe aura easily controllable by Dilantin, were greatly surprised at post-mortem to see the degree of brain damage in view of the mild clinical picture. This patient had a fairly long remission as the result of pituitary irradiation, but at post-mortem examination there was extensive and widespread metastatic carcinoma including skeletal metastases.

Table 4. Cases of radionecrosis.

Case No.	Age	Duration of treatment (days)	Particle	Dose lateral to center of pituitary (krads)		Strandquist corr. dose to 12 days treatment		Survival post-irradiation (days)	Necrosis	PAS-positive bodies	Astroglial reaction	Demyelination*
				2.1 cm	1.5 cm	2.1 cm	1.5 cm					
20	47	12	α++	2.62	5.25	2.6	5.2	495	+	0	+	2
65	48	21	p+	2.89	5.73	2.55	5.06	431	+	1	0	3
28	65	11	α++	3.30	6.54	3.3	6.5	527	+	1	+	2
68	51	21	p+	3.60	7.37	3.2	6.56	2107	+	1(1)	0(+)	3
37	48	22	α++	3.65	7.15	3.0	6.0	1722	+	0	+	3
40	60	13	α++	3.76	7.52	3.7	7.5	1371	+	3	+	3
54	60	12	α++	>5.0	>10.0	>5.0	>10.0	758	+	0	+	3
58	74	12	α++	>5.0	>10.0	>5.0	>10.0	1261	+	-	Inadequate fix.	

*Demyelination was graded from 0 to 3.

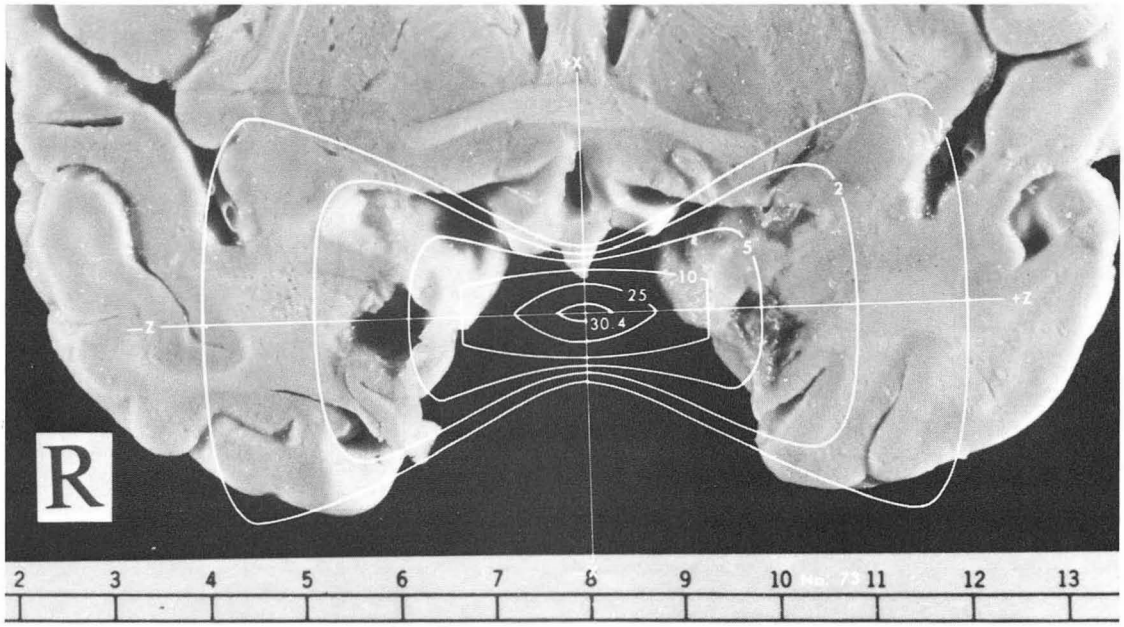

Fig. 1. Photograph of gross specimen showing cystic area of necrosis involving the cortex of the uncus and adjacent underlying tissue. There has probably been some shifting of the area of necrosis laterally because of loss of support medially. The isodose lines are in krads. Case No. 40.

JHL-3398

and polysaccharide were stained with Luxol fast blue and periodic acid-Schiff stain, mucopolysaccharide with Alcian blue, and glial fibers by the Holzer method.

In addition, many sections were stained for Nissl substance with cresyl violet, for free fat with Sudan black, for nerve cell processes with an adaptation of a Cajal rapid silver method, for calcium with alizarin red S, and for ferric iron with Perls stain. Sections were also taken outside of the radiation field, namely from the hippocampus in the coronal plane including the pineal body.

In the 8 cases the dose to the center of the pituitary was more than 22.8 krads, and the dose to the surface of the temporal cortex more than 5.0 krads. There appears to be no selective damage to white matter, but this may be because the radiation dose is always much greater in the cortical grey matter. The damage is present in the areas of maximum dose involving the inferior portion of the uncal cortex, the adjoining temporal cortex, amygdala, and the white matter immediately adjacent to the inferior and medial border of the amygdala. The extent of the lesion is least in cases No. 65, 28, and 37. In case No. 40 there is a distinct cystic space filled with a grossly tan translucent gelatinous material (Fig. 1). This is a characteristic feature of 4 cases showing the greatest damage (cases 20, 40, 54, and 58).

Microscopically, when present the central cystic space of the area of damage contains a few scattered round cells in a loose palely basophilic network of fibers. At several points along the edge of the cystic space there are lakes of eosinophilic material with a glassy homogenous appearance and a few vacuoles. This material is periodic acid-Schiff positive, Alcian blue negative, and stains negatively for collagen in the Van Giesen stain. Most parts of the wall of the cystic space consist of loosely arranged, poorly staining, intermeshing fibers in which small round cells, presumably lymphocytes, are focally abundant (Fig. 2). Next, peripheral to this, is a layer in which there are ghost outlines of blood vessels, often with thickened walls. In this area the fibers are more compact and are sometimes continuous with the zone of astrogliosis which is located next peripherally. Here the walls of blood vessels, particularly small arterioles, show poorly staining areas between nuclei of the muscular coat. Small mononuclear cells are often found in the vascular sheath (Fig. 3), and bodies staining positively with the periodic acid-Schiff stain are abundant. Astrocytes with numerous large processes extending peripherally are seen in this zone. Many of these astrocytes have large vesicular nuclei. The gliosis extends farthest peripherally in the white matter, where it appears to be spatially related to degenerated axis cylinders. Gitter cells are often present about blood vessels. Silver stains show fragmentation of axis cylinders in these areas. As an aid in outlining the general appearance of the damaged tissue, three zones may be recognized proceeding from the center peripherally as follows:

1) Central area containing an occasional round cell in a very loose palely basophilic network of fibers. Fibers stain deeply in Holzer stain. Focal lakes of eosinophilic material are sometimes present along the edges of the central cavity. This material is Alcian blue negative and periodic acid-Schiff positive.

2) Zone 2 consists of poorly staining fibers in which round cells may be focally collected. In addition, there are occasionally groups of typical gitter cells here. More compactly arranged fibers, in which ghost outlines of blood vessels can be seen, make up the more peripheral part of this zone. The blood vessels are prominent in the Holzer stain. A few astrocytes are recognizable here. This zone is 100 to 300 μ thick.

3) In zone 3, astrogliosis is intense centrally. Round-cell infiltration about arterioles is often present. Bodies which are both periodic acid-Schiff and Alcian blue positive are present near some small veins. Zone 3 is 0.5 to 4 mm thick.

Both case 37 and case 65 have poor differentiation between zones 1 and 2, the area of damage being very small (Fig. 4). In case No. 40 there are plasma cells in the layer of pia-arachnoid which folds into some areas of the cystic cavity.

The pia-arachnoid covering the uncus usually remains, although showing increased dense fibrous connective tissue, and it is sometimes infiltrated by round cells. This is regardless of the nature and degree of pathological change that may be present in the underlying parenchymal tissue. The pia-arachnoid was located in an area of greater radiation exposure than the underlying cortex and white matter that have undergone necrosis. Small arteries in the pia-arachnoid also often appear unaltered. A small part of the molecular layer of the cortex often remains with the pia. Bodies which are both periodic acid-Schiff and Alcian blue positive

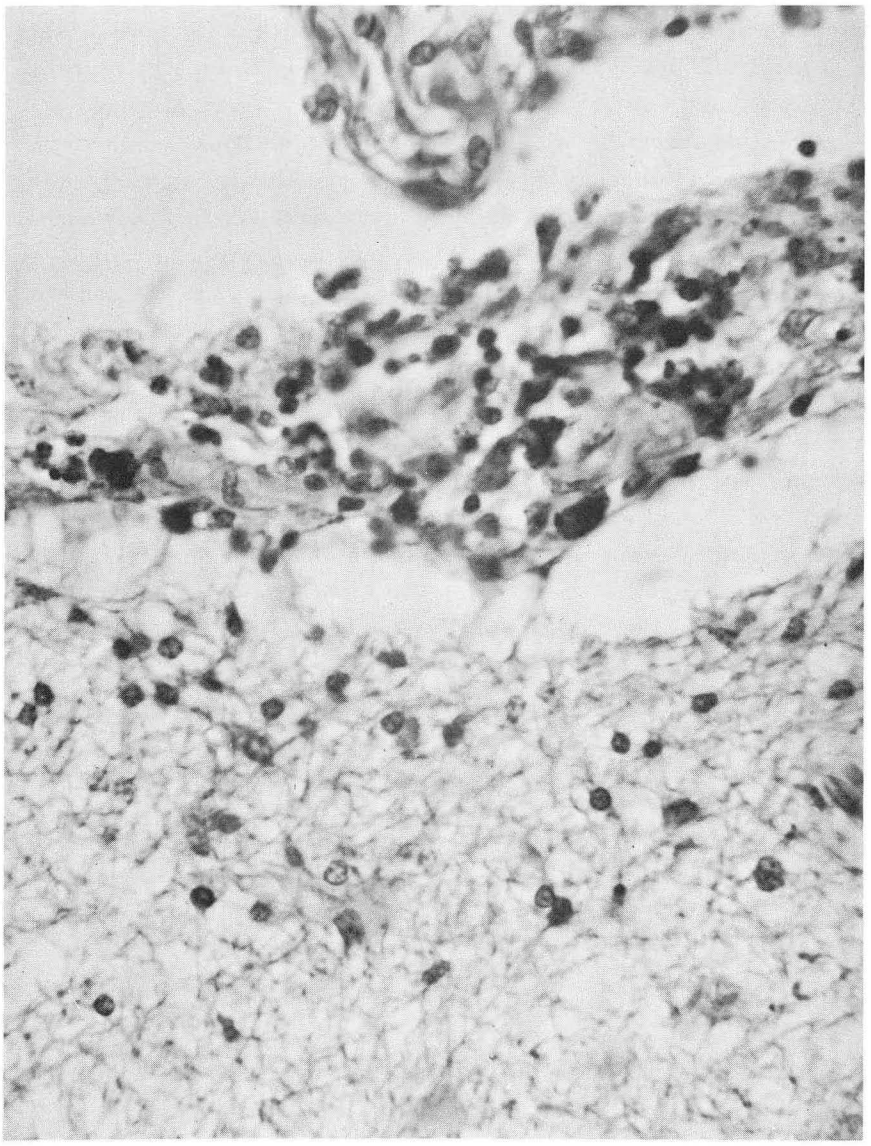

Fig. 2. Photomicrograph of wall of cystic area of necrosis. The contents of the cystic area of necrosis have mostly been lost from the section at the top of the photograph, although a few round cells in the loose palely basophilic network of fibers can be seen (zone 1). The eosinophilic material is not present in this field. The intermeshing fibers with round cells forming the wall of the cyst are seen across the central part of the photograph. At the bottom of the photograph the more compactly arranged fibers are seen (zone 2). × 240. Hematoxylin and Eosin stain. Case No. 40.

JHL-5020

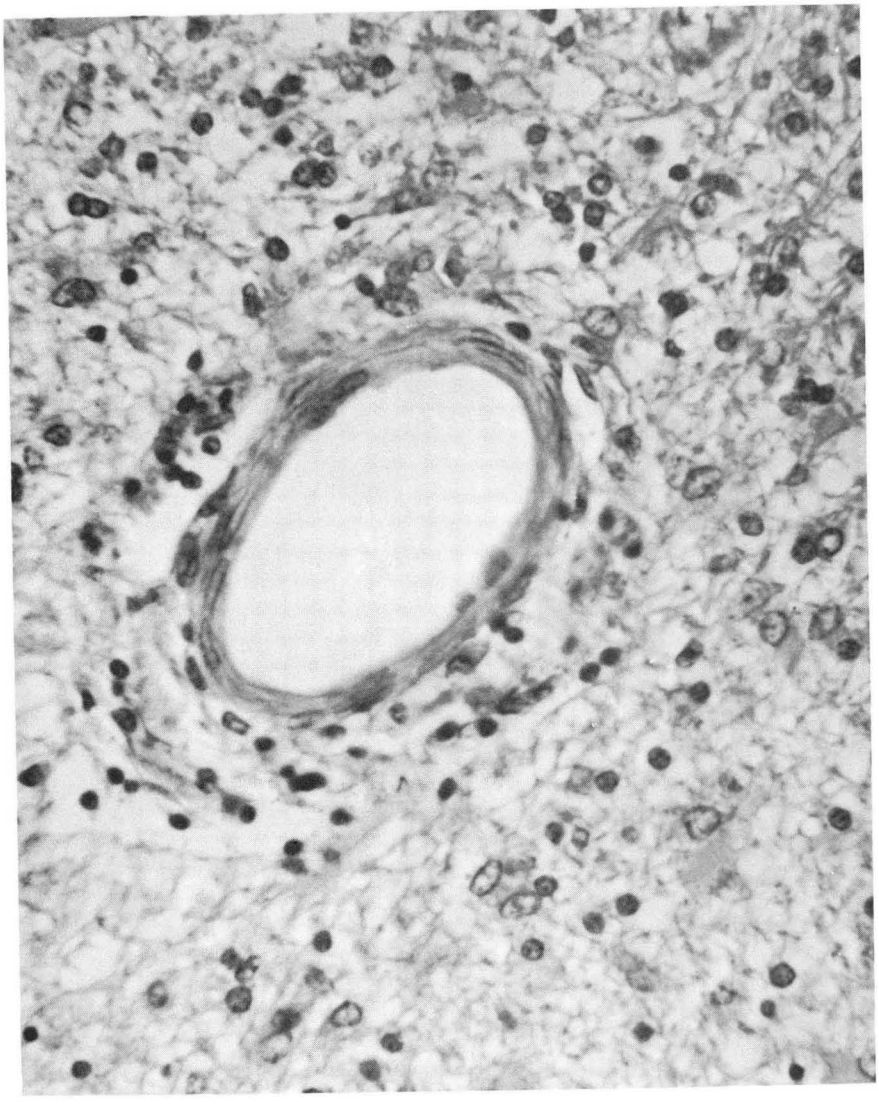

Fig. 3. Small arteriole from tissue near necrosis (zone 2). Infiltration of adjacent areas by small round cells is moderate. × 400. Hematoxylin and Eosin stain. Case No. 40.

JHL-5021

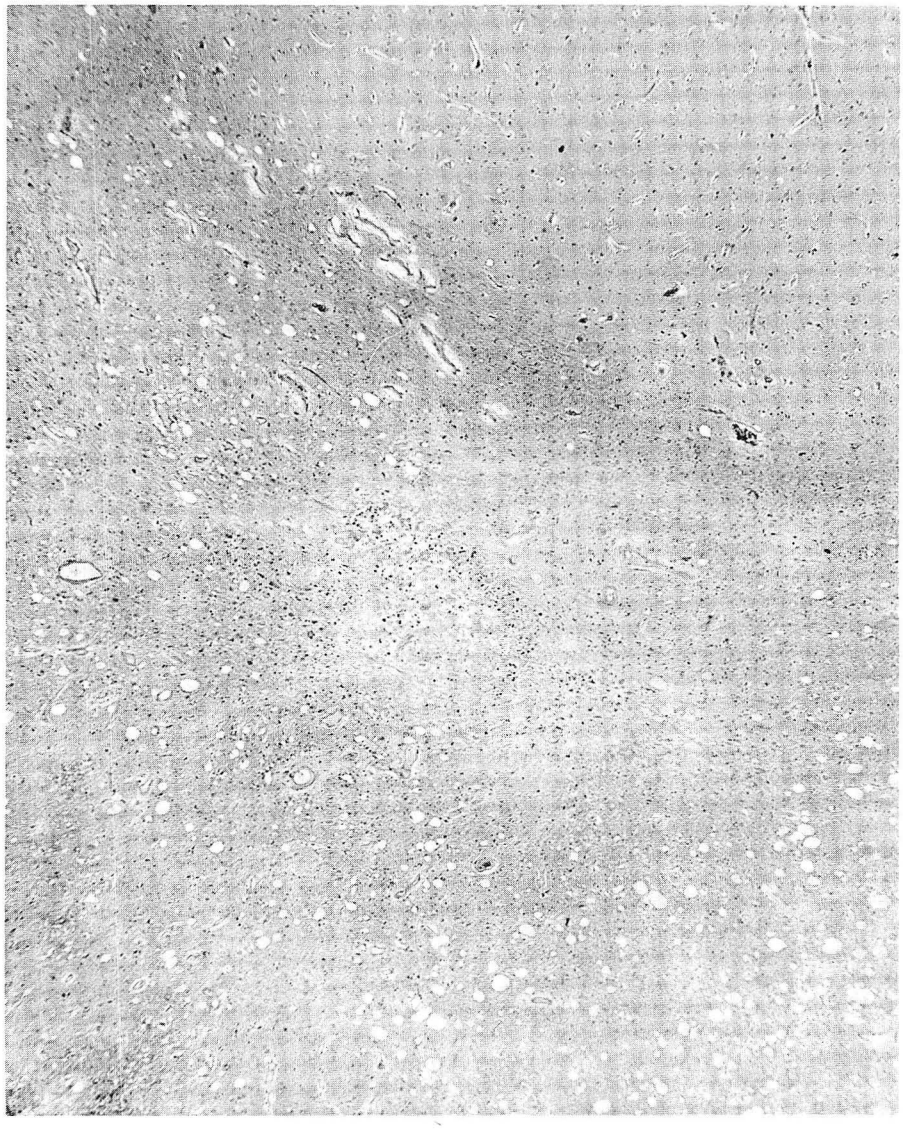

Fig. 4. Photomicrograph of band of white matter medial to the amygdala of case No. 65. This was a proton-irradiated case. An area of necrosis is seen in the center of the field. At the left margin of the field the necrosis extends to involve deeper layers of the cortex. × 36. Hematoxylin and Eosin.

XBB 683-1012

are abundant in this remaining superficial layer of the cortex. Nerve cells generally remain unaltered even when adjacent to an area of necrosis.

Vessel sclerosis or hyalinization is present to a severe extent in 6 of the 8 instances of tissue radionecrosis. Eosinophiles are not present in any of the cases.

DISCUSSION

From the cases reported here it would appear that between 2.6 and 5.2 krads may produce radionecrosis in 495 days. When the 8 cases are plotted on a log scale (Fig. 5) in a manner similar to that used by Strandquist (46) and the threshold dose for necrosis projected to a 1 day treatment, a dose of 1.9 krads is found. This is in general agreement with the cases cited in the literature where doses of 1.8 krads given in a single exposure (6) produced delayed radionecrosis in one instance, and similar or higher dose over unspecified periods of treatment produced delayed radionecrosis in two other instances (25 and 28).

The general histology of the delayed radiation lesion produced by the particle beam is similar to that described previously by others for X ray. The lesion, however, is more limited in extent and does not selectively involve white matter. This is probably because of the dose distribution being such that the grey matter of the uncus received twice the radiation dose as that received by the white matter. Such marked difference in the dose received by adjacent tissues is not possible with X ray.

Vessel sclerosis in the lesion area was a marked finding in most of these heavy particle irradiated cases. All of the lesions were of the late delayed radionecrosis type as described by Scholz (3) in the dog, although in case 40 there was significant perivascular round cell infiltration (Fig. 3). Eosinophiles were not observed in any of the cases.

CONCLUSIONS AND SUMMARY

1) From a review of the literature there appears to be great individual variation in the susceptibility to the development of late radionecrosis in the central nervous system. With large fields it appears that a few percent of the population will develop late radionecrosis with single doses as low as 1500 rads to the brain or spinal cord.

2) From both human studies and animal experimental data, the following factors increase the likelihood of a given radiation dose producing late radionecrosis:

a) youth
b) large volume of tissue irradiated
c) short fractionation interval and, probably,
d) disease involving blood vessels.

3) In the eight cases of radionecrosis reported here, the lowest fractionated dose producing radionecrosis was 26 krads in 12 days. The general histology of the delayed radiation lesion following particle irradiation is similar to the lesions reported in the literature following X ray.

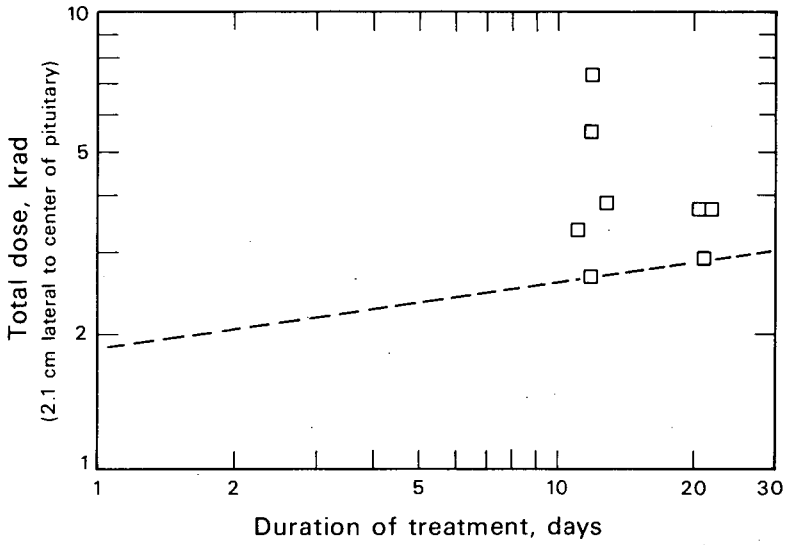

Fig. 5. Radiation dose in krads plotted against duration of treatment in days on a log scale for the 8 cases of delayed radionecrosis.

DBL 682-4599

4) General features of the delayed radiation lesions of the central nervous system are:

a) necrosis of a coagulation type which may go on to liquifaction in some cases
b) hyalinization and thickening of walls of blood vessels
c) accumulation of an amyloid-like material, especially about blood vessels
d) astrogliosis which may be marked in some instances
e) selectivity of lesions for white matter
f) focal hemorrhage occasionally.

REFERENCES

1. Fischer, A. W., and Holfelder, H.; Lakales Amyloid im Gehirn; Eine Spatfalge von Roentgenbestrahlungen. Dtsch. Z. Chir. 227: 475-483, 1930.
2. Markiewicz, T.; Uber Spatschadigungen des menschlichen Gehirns durch Roentgenbestrahlen. Z. ges. Neurol. Psychiat. 1952: 548-568, 1935.
3. Scholz, W., and Hsu, Y. K.; Late damage from Roentgen irradiation of human brain. Arch. Neurol. Psychiat., Chicago, 40: 928-936, 1938.
4. O'Connel, J. E. A., and Brunschweig, A.; Observations on Roentgen treatment of intracranial gliomata with especial reference to the effects of irradiation upon the surrounding brain. Brain 60: 230-258, 1937.
5. Wachowski, T., and Chenault, H.; Degenerative effects of large doses of Roentgen rays on the human brain. Radiology 45: 227-246, 1945.
6. Pennybacker, J., and Russell, D. S.; Necrosis of brain due to radiation therapy: clinical and pathological observations. J. Neurol., Neurosurg., Psychiat. n. s. 11: 183-198, 1948.
7. Boden, G.; Radiation myelitis of the brain stem. J. Fac. Radiol., London, 2: 79-94, 1950.
8. Zeman, W.; Zur Frage der Roentgenstrahlenwirkung am Tumorkranken Gehirn. Arch. f. Psychiat. 182: 713-730, 1949.

9. Foltz, E. L.; Holyoke, J. B., and Heyl, A. L.; Brain necrosis following X-ray therapy. J. Neurosurg. 10: 423-429, 1953.
10. Arnold, A.; Bailey, P., and Harvey, R. A.; Intolerance of primate brainstem and hypothalamus to conventional and high energy radiations. Neurology 4: 575-585, 1954.
11. Dugger, G. S.; Stratford, J. G., and Bouchard, J.; Necrosis of brain following Roentgen irradiation. Am. J. Roentgenol. 72: 953-960, 1954.
12. Malamud, N.; Boldrey, E. B.; Welch, W. K., and Fadell, E. J.; Necrosis of brain and spinal cord following X-ray therapy. J. Neurosurg. 11: 353-362, 1954.
13. Lowenberg-Scharenberg, K., and Bassett, R. C.; Amyloid degeneration of the human brain following X-ray therapy. J. Neuropathol. Exptl. Neurol. 9: 93-102, 1950.
14. Boden, G.; Radiation myelitis of the cervical spinal cord. Brit. J. Radiol. 21: 464-469, 1948.
15. Stevenson, L. D., and Eckhardt, R. E.; Myelomalacia of the cervical portion of the spinal cord, probably the result of Roentgen therapy. Arch. Pathol. 39: 109-112, 1945.
16. Ahlborn, H. E.; The results of radiotherapy of hypopharyngeal cancer at the radiumhemmet, Stockholm, 1930-1939. Acta Radiol., Stockholm, 22: 155-171, 1941.
17. Smothers, D. W.; Clarkson, J. R., and Stron, J. A.; The Roentgen treatment of cancer of the esophagus. Amer. J. Roentgenol. 49: 606, 1943.
18. Jacobson, F.; Cancer of the hypopharynx. Acta Radiol., Stockholm, 35: 1-21, 1951.
19. Rudis-Jicinsky, J.; Experimental investigations with Roentgen rays upon living tissue. New York Med. J. 76: 850, 1902.
20. Danysz, J.; De l'action du radium sur les differents tissues. Compt. Rend. Acad. de Sci., Paris, 137: 1296-1298, 1903.
21. Scholz, W.; Uber die Empfindlichkeit des Gehirns fur Roentgen und Radiumstrahlen. Klin. Wschn. 14: 189-193, 1935.
22. Russell, D. S.; Wilson, C. W., and Tansley, K.; Experimental radionecrosis of the brain in rabbits. J. Neurosurg. Psychiat. 12: 187-195, 1949.
23. Lindgren, M.; On tolerance of brain tissue and sensitivity of brain tumors to irradiation. Acta Radiol., Suppl. No. 170, 1958, pp. 1-73.
24. Zulch, K.; Biologie und Pathologie der Hirngeschwulste; in Handbuch der Neurochirurgie, Bd. 3, edited by H. Olivecrona and W. Tonnis, Berlin, Springer-Verlag, 1956, pp. 1-702, 492.
25. Chandler, A.; Tucker, F. C., and Herzberger, E. E.; Late radiation necrosis of the brain. Wisconsin Med. J. 63: 297-300, 1964.
26. Toga, M.; Berard, M., and Sommer, D.; Observation anatomo-clinique d'un das de radio-necrose cerebrale. Arch. Anat. Pathol. 11: 175-180, 1963.
27. Crompton, M. R., and Layton, D. D.; Delayed radionecrosis of the brain following therapeutic X-radiation of the pituitary. Brain, Part I, 84: 85-101, 1961.
28. Boellaard, J. W., and Jacoby, W.; Roentgenspatschaden des Gehirns. Acta Neurochir. 10: 533-564, 1962.
29. Bignami, A.; Giuffre, R., and Riccio, A.; Radionecrosi tardiva del chiasma dei nervi ottici e dell' ipotalamo consequente a cobalto-terapia dell'ipofsi e simulante un processo espansivo. Rivista di Neurologia 33: 709-730, 1963.

30. Almquist, S.; Dahlgren, S.; Notter, G., and Sunborn, L.; Brain necrosis after irradiation of the hypophysis in Cushing's disease. Acta Radiol. 2: 179-188, 1964.

31. Asscher, A. W., and Anson, S. G.; Arterial hypertension and irradiation damage to the nervous system. Lancet 2: 1343-1346, 1962.

32. Bailey, O. T.; Woodard, J. S., and Putnam, T. J.; Tissue reactions of the human frontal white matter to gamma radiation; in Response of the Nervous System to Ionizing Radiation, edited by T. J. Haley and R. S. Snider, Boston, Little, Brown and Company, 1964, pp. 3-18.

33. Dynes, J. B., and Smedal, M. I.; Radiation myelitis. Am. J. Roentgenol. 83: 78-87, 1960.

34. Pallis, C. A.; Louis, S., and Morgan, R. L.; Radiation myelopathy. Brain 84: 460-479, 1961.

35. Verjaal, A.; Roentgen myelopathie. Ned. Tijdschr. Geneesk. 108: 1123-1127, 1964.

36. Schinz, H. R.; Strahlenschaden des Ruckenmarkes. Deut. Med. Wochschr. 89: 796-797, 1964.

37. McDonald, L. W., and Welch, G. P.; Role of immunity in brain radionecrosis. J. Neuropathol. Exptl. Neurol. 25: 169, 1966 (abstract).

38. McDonald, L. W., and Hayes, T. L.; The role of capillaries in the pathogenesis of delayed radionecrosis of brain. Am. J. Pathol. 50: 745-763, 1967.

39. Cervos-Navarro, V.; Elektronenmikroskopische Befunde an den Capillaren des Kaninchengehirns nach der Einwirkung ionisierender Strahlen. Arch. fur Psychiatrie and Zeitschrift f. d. ges Neurologie 205: 204-222, 1964.

40. Berg, N. O., and Lindgren, M.; Time-dose relationship and morphology of delayed radiation lesions of the brain in rabbits. Acta Radiol. Suppl. 167, 1958.

41. Strandquist, M.; Studien uber die kumulative Wirkung der Roentgenstrahlen bei Fraktionierung. Erfahr. aus dem Radiumhemmet an 280 Haut-und Lippenkarzinomen. Acta Radiol., Suppl. 55, 1944.

42. Berg, N. O., and Lindgren, M.; Relation between field size and tolerance of rabbit's brain to Roentgen irradiation (200 kV) via a slit-shaped field. Acta Radiol. 1: 147-168, 1963.

43. Zeman, W.; Disturbances of nucleic acid metabolism preceding delayed radionecrosis of nervous tissue. Proc. Natl. Acad. Sci. U.S. 50: 626-630, 1963.

44. Lawrence, J. H., and Tobias, C. A.; Radioactive isotopes and nuclear radiations in treatment of cancer. Cancer Res. 16: 185-193, 1956.

45. Tobias, C. A., et al.; Pituitary irradiation with high-energy proton beams—a preliminary report. Cancer Res. 18: 121-134, 1958.

46. Lampert, P. W., and Davis, R. L.; Delayed effects of radiation on the human central nervous system. Neurology 14: 912-917, 1964.

47. Itabashi, H. H.; Bebin, J., and DeJong, R. N.; Post-irradiation cervical myelopathy. Neurology (Minneapolis) 7: 844-852, 1957.

48. Alajouanine, T.; Lhermitte, F.; Cambien, V., and Gantier, J. C.; Late post-radiation therapy lesions of the CNS (concerning anatomo-clinical observations of cervical myelopathy). Rev. Neurol. 105: 9-21, July 1961.

Heavy Particle Radiosurgery in Cushing's Disease

John A. Linfoot, Edward Manougian, Cornelius A. Tobias, James L. Born, Norton J. Snyder, Richard A. Carlson and John H. Lawrence

INTRODUCTION

Satisfactory heavy particle radiosurgery in breast cancer, diabetic retinopathy, acromegaly, and other pituitary tumors prompted extension of heavy particles to Cushing's syndrome. Five factors prompted our direct approach to the pituitary: 1) abundant pathophysiological evidence indicating that the majority of cases of bilateral adrenal hyperplasia result from a primary disturbance in the hypothalamus or anterior pituitary resulting in an excess or inappropriate secretion of ACTH, the secretion of ACTH by extra-pituitary neoplasms being an exception to this, of course (1); 2) the recognition of pituitary tumors in 15-25% of these patients either before or subsequent to bilateral adrenalectomy (2); 3) in reviewing the results of cases of Cushing's syndrome, it became apparent that complete remissions were infrequent and often temporary in patients receiving conventional forms of radiation (3); 4) it did appear, however, that there was a somewhat higher incidence of permanent and satisfactory remission with larger doses of radiation (4, 5); 5) and finally, heavy particles could be safely delivered teletherapeutically (6).

All of the patients received between 6,000 and 12,000 rads of heavy particle pituitary irradiation delivered by the 184-inch synchrocyclotron at the Lawrence Radiation Laboratory in Berkeley. This technique has been described in detail elsewhere (7). Several points should be emphasized, however. First, the radiation is delivered in such a fashion that the entire pituitary gland is covered with a rapid fall-off of the radiation superiorly and laterally preserving the parasellar structures. Furthermore, the isodose curve is such that the hypothalamus receives less than 20% of the radiation administered; thus the pituitary is almost exclusively the structure affected by heavy particles. Finally, the amount of heavy particles or dose has been selected arbitrarily on the basis of prior experience and the duration of therapy (6 treatments in 11 days) determined by previous treatment protocols.

RESULTS AND DISCUSSION

Since 1959 we have treated 15 cases of Cushing's disease with heavy particle pituitary irradiation. Four of these patients had Nelson's syndrome (8) and are considered separately in our analysis, since intensive irradiation such as provided by heavy particles would be obviously desirable in the management of these clinically apparent adenomas, which are rather distinctive in their biological properties as well as their tendency to invasiveness and malignant degeneration. There appear to be two clinically distinct groups with hyperpigmentation, however. Two patients developed obvious enlargement of the sella turcica several years

after bilateral adrenalectomy and thus may be considered classical examples of Nelson's syndrome. Plasma ACTH determined by bioassay was elevated in both of these cases while on replacement therapy. The two other cases had a similar hyperpigmentation but had normal sellas and only slight or normal ACTH levels by bioassay. The response to radiation in these two groups had differed as illustrated in the following case histories.

The first patient with a pituitary tumor was a 32-year-old secretary who originally had been treated with a subtotal, and later total, adrenalectomy in 1955 and 1957, respectively. Hyperpigmentation and ballooning of the sella was present at the time of initial therapy. There was a gradual loss of pigmentation beginning 6 to 8 months following treatment, but an interval of 2-1/2 years elapsed before a striking degree of pigmentary loss was observed. Further pigmentary loss has continued to occur. A similar course was observed in the other patient with sellar enlargement. The two patients without sellar enlargement have failed to pigment further, but to date have not demonstrated the pigmentary loss observed in the two preceding cases, although they received comparable doses of heavy particles. This suggests but does not prove that the mechanism responsible for pigmentation may be different.

The first patient treated with heavy particle therapy as a primary form in the management of bilateral adrenal hyperplasia subsequently had a unilateral adrenalectomy for diagnostic purposes; she has remained in complete clinical remission for 8-1/2 years. There were two especially impressive features in this case. First of all, there was prompt restoration of her menses within one month after treatment although she had been previously amenorrheic for some 18 months. Secondly, the exaggerated response to metyrapone, which was present prior to treatment, disappeared quite promptly after treatment, even before the basal excretion of urinary 17-hydroxycorticosteroids had fallen.

Ten additional patients have now received heavy particle pituitary irradiation ranging from 6,000 to 12,000 rads. The pretreatment hormonal data on these patients is summarized in Table 1. Two patients, J. V. and J. A., have had previous adrenal surgery; but hypercorticism recurred due to hypertrophy of an adrenal remnant in J. V. and presumably to accessory adrenal tissue in J. A. Another patient, M. D., had shown no response to a unilateral adrenalectomy. The remaining 9 patients had heavy particle therapy as a primary form of treatment. You will note in the third column that all of the patients had a slightly (indicated by the tilted arrow) or a moderately increased value of urinary 17-hydroxycorticosteroid. Urinary 17-ketosteroids were normal in some, slightly increased in several, and low or decreased in the two patients who had had previous adrenalectomies. All of the patients except the latter two patients, J. V. and J. A., had an exaggerated response to the oral administration of metyrapone. These two patients also failed to show a significant increase in adrenal secretion in response to ACTH, while the remainder of the cases all had marked responses to intravenous ACTH administration. While the suppression with a low dose or the 2 mg dose of dexamethasone was variable in this group of patients, all patients except J. V. and J. A., who appeared to have fixed secretion rates, or at least circulating levels of corticoids, showed a 50% or greater suppression of urinary adrenal steroids following 3 or more days of "high-dose" (8 mg per day) dexamethasone administration. All of the patients had altered circadian

Table 1.

Patient	Sex	Age	17 OHCS	17 KS	Metyrapone	ACTH	Dexamethasone	Circadian rhythm
R. K.	F	37	↑	N	↑	↑	↓	A
R. S.	F	45	↑	N	↑	↑	↓	A
R. C.	M	17	↑	N	↑	↑	↓	A
D. M.	F	35	↑	N	↑	↑	↓	A
J. V.*	F	56	↗	↓	→	→	→	A
J. A.*	M	24	↑	↓	↘	→	↓	A
J. D.	F	38	↗	↗	↑	↑	↓	A
P. O.	F	34	↑	↗	↑	↑	↓	A
P. D.	F	19	↑	↗	↗	↑	↓	A
R. D.*	M	46	↑	↓	↑	↑	↓	A
M. D.	M	42	↑	↗	↑	↑	↓	A

*Previous adrenalectomy.

↑ = increased ↗ = slight increase → = no change

↓ = decreased ↘ = slight decrease

N = normal A = abnormal R = reversed

rhythm with only slight or no significant difference between their 8 a.m. and 4-6 p.m. plasma steroid values. Amenorrhea was present in all but one of the premenopausal women, and an abnormal glucose tolerance test was present in all but two patients.

All of the patients were treated conservatively with the idea in mind that an optimal result would be to control altered ACTH secretion without inhibiting completely other anterior lobe functions, realizing that the hypercorticism could be controlled by bilateral adrenalectomy at a later date. With the exception of the first patient treated and the two recent cases, all of the patients would be described as having mild to moderate signs and symptoms of hypercorticism. The results of treatment are summarized in Table 2 and illustrated in the following case summaries.

A typical response in steroid secretion was seen in patient R. C., a 17-year-old boy with Cushing's syndrome of some 3 to 4 year's duration. The basal level of the adrenocorticosteroid excretion was elevated, and there was an exaggerated response to metyrapone, as well as ACTH. There was definite suppression of urinary steroids following administration of the 8 mg dose of dexamethasone. This patient's plasma steroids also lacked the normal circadian rhythm. You will note that there was a change in the metyrapone response within 3 months after treatment, although the basal level of adrenal steroids remains elevated. The basal level gradually fell, as did the response to metyrapone, and the patient is currently in chemical and clinical remission 36 months after treatment. One interesting phenomenon that has been observed in this patient is a reversal in circadian rhythm, with a significantly higher

Table 2.

Patient	Sex	Age	Treat-ment	Months post Rx	17 OHCS	17 KS	Metyra-pone	ACTH	Dexa-metha-sone	Circadian rhythm
R. K.	F	37	5-5-57	90	N	N	↓	↓	--	A
R. S. (a)	F	45	4-12-63	55	N/↑	N	↓/↑	↓/↑	--	R
R. C.	M	17	1-24-64	46	N	N	↓	↓	↓	R
D. M. (b)	F	35	1-24-64	46	N/↑	N	↓/↑	↓/↑	--	R
J. V.*	F	56	7-2-65	28	N	N	→	→	↓	N
J. A.*	M	24	1-21-66	22	N	N	→	→	--	A
J. D.	F	38	1-17-66	21	→	→	↓	--	--	N
P. O.	F	34	5-20-66	18	N	N	↓	--	--	N
P. D.	F	19	10-19-66	13	↓	↓	→	--	--	N
R. D.* (c)	M	46	2-17-67	9	--	--	--	--	--	--
M. D. (d)	M	42	4-28-67	7	N/↑	↓/↑	↓/↑	↓/↑	--	A

(a) Relapse 24 months.
(b) Relapse 12 months.
(c) Relapse 8 months.
(d) Relapse 6 months.
*Previous adrenalectomy.
↑ = increased → = no change ↓ = decreased
N = normal A = abnormal R = reversed

value of plasma 17-hydroxycorticosteroids in the afternoon compared with the morning. A similar rise in afternoon and evening plasma steroids was observed in 3 other patients who also had a fall in steroid excretion and similar changes in their other tests.

Additional data on the change in circadian rhythm is illustrated by patient J. V., a 56-year-old female with recurrent hypercorticism due to the hypertrophy of the small adrenal remnant. This patient showed little or no difference in her morning or afternoon plasma levels or urinary excretion of steroids. The patient had a prompt fall in adrenal steroid excretion at 3 months following treatment; and, although her plasma steroid level has fallen tremendously, there is now a higher value in the afternoon and in the evening. The altered daytime and nighttime excretion of steroids is less evident in the urine but may have been partially obscured by not carrying out more frequent fraction collection during the 24-hour period. Her altered circadian rhythm seems to be persisting, yet she remains in excellent clinical remission 2-1/2 years following treatment.

All of the patients have shown an initial fall in steroid excretion within 1 to 6 months following heavy particle therapy. In addition, the steroid response to metyrapone has decreased. Four patients, all of whom received 10,000 rads, have relapsed following treatment after showing an initial response. The time of relapse varied from 6 to 24 months. Typical data

in these cases can be illustrated by patient D. M., a 32-year-old Caucasian female who developed meningitis at the age of 11 months and was subsequently left neurologically handicapped. Three years before treatment she developed amenorrhea, hirsutism, and hypertension and was found to have classical tests compatible with Cushing's syndrome. In addition, she had periods of alternating consciousness, hyperkinetic movements, and hyperhidrosis with marked fluctuations in blood pressures suggestive of a hypothalamic syndrome. This patient received 10,000 rads of heavy particle therapy, resumed menses, and showed a dramatic improvement in her tests during the first 3 months following treatment, but subsequently relapsed with resumption of amenorrhea and a return of the exaggerated metyrapone response. Because of this patient's condition, she is in a convalescent hospital, and further therapy has not been carried out at this time.

All of the other patients have shown a fall in total urinary steroid excretion, both in the 17-hydroxycorticosteroids as well as in the 17-ketosteroids. Furthermore, those that had abnormal metyrapone responses prior to treatment showed a loss of this exaggerated response. Persistence of this change appears to indicate continued remission. ACTH tests have not been repeated in all cases, although in those that have been repeated, there is a less marked response which would suggest some decrease in the total adrenal mass or sensitivity to ACTH. Dexamethasone tests have not been repeated in a sufficient number of patients to draw any conclusions. The circadian rhythm by and large has remained abnormal in 2 of the patients, probably has returned to normal in 2, and shows a reversal in 4.

CONCLUSION

In conclusion, we have summarized our experience with radiosurgery in the treatment of 15 patients with Cushing's disease. Four of the patients with ACTH secreting pituitary adenomas have shown a highly satisfactory response to treatment. Eleven additional patients were treated primarily for hypercorticism. All of the patients have shown a fall in urinary steroid output and a less exaggerated response to the administration of metyrapone. The 4 patients who relapsed at 6 to 24 months showed a return of this rather characteristic abnormality. These results we interpret as encouraging but preliminary. The results have by and large been obtainable without major change in other trophic hormone function, and insofar as we know, have been completely free of side effects with the exception of the first patient treated who developed a third nerve palsy 7 years after treatment.

REFERENCES

1. Liddle, G. W.; Island, D., and Meador, C. K.; Recent Prog. Hormone Res. 18: 125, 1962.
2. Salassa, R. M.; Kearns, T. P.; Kernohan, J. W.; Sprague, R. G., and MacCarthy, C. S.; J. Clin. Endocrinol. Metab. 19: 1523, 1959.
3. Soffer, L. J.; Iannaccone, A., and Gabrilove, L.; Am. J. Med. 30: 129, 1961.
4. Dohan, F. C.; Raventos, A.; Boucot, N., and Rose, E.; J. Clin. Endocrinol. Metab. 17: 8, 1957.
5. Molinatti, G. M.; Camanni, F.; Massara, F., and Messina, M.; J. Clin. Endocrinol. Metab. 27: 861, 1967.

6. Lawrence, J. H.; Tobias, C. A.; Born, J. L.; Linfoot, J. A., and D'Angio, G. J.; J. Am. Med. Assoc. 196: 166, 1966.
7. Tobias, C. A.; Anger, H. O., and Lawrence, J. H.; Am. J. Roentgenol., Radium Therapy Nucl. Med. 67: 1, 1952.
8. Nelson, D. H.; Meakin, J. W.; Dealy, J. B., Jr.; Matson, D. D., and Thorn, G. W.; New Engl. J. Med. 259: 161, 1958.

Staff Publications

Anger, H. O.; Radioisotope cameras; in Instrumentation in Nuclear Medicine, Vol. 1, edited by G. J. Hine, New York and London, Academic Press, Inc., 1967, pp. 485-552.

Anger, H. O.; Powell, M. R.; Van Dyke, D. C.; Schaer, L. R.; Fawwaz, R. A., and Yano, Y.; Recent applications of the scintillation camera; in Radioaktive Isotope in Klinik und Forschung, Vol. 7, edited by K. Fellinger and R. Hofer, Munich and Berlin, Urban & Schwarzenberg, 1967, pp. 70-93.

Anger, H. O.; The scintillation camera for radioisotope localization; in Radioisotope in der Lokalizationsdiagnostik, edited by G. Hoffman and K. E. Scheer, Stuttgart, F. K. Schattauer-Verlag, 1967, pp. 1-21.

Ashikawa, J. K.; Sondhaus, C. A.; Tobias, C. A.; Kayfetz, L. L.; Stephens, S. O., and Donovan, M.; Acute effects of high-energy protons and alpha particles in mice; in Workshop Conference on Space Biology, University of California, Berkeley, 1965, Proceedings, edited by P. E. Schambra, G. E. Stapleton, and N. F. Barr. Radiation Res. Suppl. 7: 312-324, 1967.

Baker, R. M., and Haynes, R. H.; UV-induced enhancement of recombination among lambda bacteriophages in UV-sensitive host bacteria. Molec. Gen. Genetics 100: 166-177, 1967.

Barr, J. L., and Hayes, T. L.; Virus particles associated with immune responses to Ehrlich ascites tumor cells. Mikroskopie 21: 293-297, 1967.

Brustad, T.; On the mechanisms of radiation inactivation of enzymes in dilute solutions; in International Congress of Radiation Research, 3rd, Cortina d'Ampezzo, 1966, Radiation Research, edited by G. Silini, Amsterdam, North-Holland Publishing Co., New York, John Wiley & Sons, Inc., 1967, pp. 384-396.

Budinger, T. F., and Howerton, R. J.; Characterization of the time variations of reproductive processes in living cells. Nature 214: 397-399, 1967.

Curtis, S. B.; Energy-loss distributions and fractional cell lethality; in Special Sessions on Radiation Transport and Biological Effects, Pittsburgh, Pa., Nov. 1, 1966, Proceedings, edited by D. K. Trubey, Oak Ridge National Laboratory, Tennessee, report ANS-SD-4, 1967, pp. 97-115.

Curtis, S. B.; The physical characteristics of solar flares; in Workshop Conference on Space Biology, University of California, Berkeley, 1965, Proceedings, edited by P. E. Schambra, G. E. Stapleton, and N. F. Barr. Radiation Res. Suppl. 7: 38-42, 1967.

Curtis, S. B.; Two hazard-evaluation criteria--dose equivalent and fractional cell lethality; in International Symposium on the Biological Interpretation of Dose from Accelerator-Produced Radiation, 1st, Lawrence Radiation Laboratory, Berkeley, 1967, Proceedings, edited by R. W. Wallace. CONF-670305, 1967, pp. 230-240.

de Serres, F. J.; Webber, B. B., and Lyman, J. T.; Mutation-induction and nuclear inactivation in Neurospora crassa using radiations with different rates of energy loss; in Workshop Conference on Space Biology, University of California, Berkeley, 1965, Proceedings, edited by P. E. Schambra, G. E. Stapleton, and N. F. Barr. Radiation Res. Suppl. 7: 160-171, 1967.

Dewey, D. L.; DNA breaks in coliphage T_7 after irradiation with argon nuclei, Intern. J. Radiation Biol. 12: 497-503, 1967.

Dobson, E. L.; Kelly, L. S., and Finney, C. R.; Kinetics of the phagocytosis of repeated injections of colloidal carbon: a blockade, latent period or stimulation? A question of timing and dose; in International Symposium on Atherosclerosis and the Reticuloendothelial System, Como, Italy, 1966, The reticuloendothelial system and atherosclerosis, edited by N. R. LiLuzio and R. Paoletti, New York, Plenum Press, 1967, pp. 63-73.

Durbin, P. W.; Jeung, N.; Williams, M. H., and Arnold, S.; Construction of a growth curve for mammary tumors of the rat, Cancer Res. 27: 1341-1347, 1967.

Fawwaz, R. A.; Winchell, H. S.; Pollycove, M., and Sargent, T.; Hepatic iron deposition in humans. I. First-pass hepatic deposition of intestinally absorbed iron in patients with low plasma latent iron-binding capacity. Blood 30: 417-424, 1967.

Feola, J. M.; Loughman, W. D., and Richman, S. P.; Pion radiobiology; in International Symposium on the Biological Interpretation of Dose from Accelerator-Produced Radiation, 1st, Lawrence Radiation Laboratory, Berkeley, 1967, Proceedings, edited by R. W. Wallace. CONF-670305, 1967, pp. 368-381.

Fred, S. S., and Smith, W. W.; Radiation sensitivity and proliferative recovery of hemopoietic stem cells in weanling and compared to adult mice. Radiation Res. 32: 314-326, 1967.

Freifelder, D.; Lack of a relation between deoxyribonucleic acid methylation and thymineless death in Escherichia coli. J. Bacteriol. 93: 1732-1733, 1967.

Garcia, J. F.; Linfoot, J. A.; Manougian, E.; Born, J. L., and Lawrence, J. H.; Plasma growth hormone studies in normal individuals and acromegalic patients. J. Clin. Endocrinol. Metab. 27: 1395-1402, 1967.

Gilmore, R. A.; Super-suppressors in Saccharomyces cerevisiae. Genetics 56: 641-658, 1967.

Glaeser, R. M., and Scott, T. B.; Surface structure of nucleated animal cells: carbon replicas; in Electron Microscopy Society of America Twenty-Fifth Anniversary Meeting, Chicago, 1967, Proceedings, edited by C. J. Arceneaux, Baton Rouge, Claitor's Book Store, 1967, pp. 120-121.

Grendon, A.; Public reactions to nuclear facilities. Am. J. Public Health 57: 1263-1268, 1967.

Gunter, T. E.; Electron paramagnetic resonance studies of the radiolysis of H_2O in the solid state. J. Chem. Phys. 46: 3818-3829, 1967.

Hanawalt, P. C., and Haynes, R. H.; Reparatur schadhafter Desoxyribonucleinsäure. Umschau Wiss. Tech. 67: 553-559, 1967.

Hayes, T. L.; Pease, R. F. W., and Camp, A. S.; Stereoscopic scanning electron microscopy of living Tribolium confusum. J. Insect Physiol. 13: 1143-1145, 1967.

Hildreth, P.; Developmental effects of X rays on embryos of Drosophila melanogaster. Proc. Natl. Acad. Sci. U. S. 58: 1924-1929, 1967.

Howard, A. N.; Gresham, G. A.; Hales, C. N.; Lindgren, F. T., and Katzberg, A. A.; Atherosclerosis in baboons: pathological and biochemical studies; in International Symposium on the Baboon and Its Use as an Experimental Animal, 2nd, San Antonio, 1966, Proceedings, Vol. 2, Austin, University of Texas Press, 1967, pp. 333-350.

Humphreys, W. J.; Hayes, T. L.; and Pease, R. F. W.; Transmission and scanning electron microscopy of cryptobiotic cytoplasm; in Electron Microscopy Society of America Twenty-Fifth Anniversary Meeting, Chicago, 1967, Proceedings, edited by C. J. Arceneaux, Baton Rouge, Claitor's Book Store, 1967, pp. 50-51.

Johnston, J. R., and Mortimer, R.; Influence of temperature on recombination in yeast. Heredity 22: 297-303, 1967.

Jones, H. B.; Radiation exposure limits and their biological basis; in International Symposium on the Biological Interpretation of Dose from Accelerator-Produced Radiation, 1st, Lawrence Radiation Laboratory, Berkeley, 1967, Proceedings, edited by R. W. Wallace. CONF-670305, 1967, pp. 289-296.

King, J. L.; Frequency of homozygotes. (Letter to the Editors) J. Heredity 58: 63, 1967.

Lawrence, J. H.; Radiobiological studies with heavy particles as related to therapy; in Workshop Conference on Space Biology, University of California, Berkeley, 1965, Proceedings, edited by P. E. Schambra, G. E. Stapleton, and N. F. Barr. Radiation Res. Suppl. 7: 360-368, 1967.

Linfoot, J. A.; Kimura, S. J., and Caygill, W.; Vascular complications of diabetes mellitus; in Heavy Particle Irradiation of the Pituitary, St. Louis, Mosby & Co., 1967, Chap. 17, pp. 219-226.

Lindgren, F. T.; Freeman, N. K., and Ewing, A. M.; Ultracentrifugal analysis of serum lipoproteins; in Progress in Biochemical Pharmacology, Vol. 2, edited by D. Kritchevsky, R. Paoletti, and D. Steinberg, Basel/New York, S. Karger, 1967, pp. 475-499.

Lochaya-Vimokesant, S.; Winchell, H. S.; Fish, M. B., and Pollycove, M.; Decreased de novo DNA-thymine synthesis and increased thymidine-^{3}H incorporation into DNA by human bone marrow cultured with aminopterin. Proc. Soc. Exptl. Biol. Med. 126: 621-624, 1967.

Lossow, W. J.; Lindgren, F. T., and Jensen, L. C.; Lead uptake of rat serum protein by $S_f > 400$ lymph chylomicrons in vitro. Biochim. Biophys. Acta 144: 670-677, 1967.

Loughman, W. D.; Sargent, T. W., and Israelstam, D. M.; Leukocytes of humans exposed to lysergic acid diethylamide: lack of chromosomal damage. Science 158: 508-510, 1967.

Lyman, J. T.; Radiation environment parameters and the biophysicist; in International Symposium on the Biological Interpretation of Dose from Accelerator-Produced Radiation, 1st, Lawrence Radiation Laboratory, Berkeley, 1967, Proceedings, edited by R. W. Wallace. CONF-670305, 1967, pp. 277-297.

Lyman, J. T., and Haynes, R. H.; Recovery of yeast after exposure to densely ionizing radiation; in Workshop Conference on Space Biology, University of California, Berkeley, 1965, Proceedings, edited by P. E. Schambra, G. E. Stapleton, and N. F. Barr. Radiation Res. Suppl. 7: 222-230, 1967.

Maccabee, H. D., and Raju, M. R.; Ionization fluctuations in cells and thin dosimeters; in International Symposium on the Biological Interpretation of Dose from Accelerator-Produced Radiation, 1st, Lawrence Radiation Laboratory, Berkeley, 1967, Proceedings, edited by R. W. Wallace. CONF-670305, 1967, pp. 221-229.

McDonald, L. W.; The effect of high-energy particle irradiation on the vestibular mechanism in rabbits; in Workshop Conference on Space Biology, University of California, Berkeley, 1965, Proceedings, edited by P. E. Schambra, G. E. Stapleton, and N. F. Barr. Radiation Res. Suppl. 7: 451-458, 1967.

McDonald, L. W.; Pease, R. F. W., and Hayes, T. L.; The use of the scanning electron microscope for the examination of sectioned tissue; in Electron Microscopy Society of America Twenty-Fifth Anniversary Meeting, Chicago, 1967, Proceedings, edited by C. J. Arceneaux, Baton Rouge, Claitor's Book Store, 1967, pp. 254-255.

Nakai, S., and Mortimer, R.; Induction of different classes of genetic effects in yeast using heavy ions; in Workshop Conference on Space Biology, University of California, Berkeley, 1965, Proceedings, edited by P. E. Schambra, E. Stapleton, and N. F. Barr. Radiation Res. Suppl. 7: 172-181, 1967.

Nichols, A. V.; Human serum lipoproteins and their interrelationships; in Advances in Biological and Medical Physics, Vol. 11, edited by J. H. Lawrence, J. W. Gofman, and T. L. Hayes, New York and London, Academic Press, Inc., 1967, pp. 109-158.

Nohr, M. L.; Inefficacy of erythropoietic response of BALB/c mice to hypoxia. Am. J. Physiol. 213: 1285-1289, 1967.

Oda, N. and Lyman, J. T.; Secondary-electron distribution for heavy ions; in Workshop Conference on Space Biology, University of California, Berkeley, 1965, Proceedings, edited by P. E. Schambra, G. E. Stapleton, and N. F. Barr. Radiation Res. Suppl. 7: 20-32, 1967.

Parker, H.; Data from various occupational groups; in International Symposium on the Biological Interpretation of Dose from Accelerator-Produced Radiation, 1st, Lawrence Radiation Laboratory, Berkeley, 1967, Proceedings, edited by R. W. Wallace. CONF-670305, 1967, pp. 88-93.

Paulus, J. M., and Mel, H. C.; Viability studies on megakaryocytes in mechanically and enzymatically suspended rat bone marrow. Exptl. Cell Res. 48: 27-38, 1967.

Pease, R. F. W., and Hayes, T. L.; Scanning electron microscopy using cathodoluminescence; in Electron Microscopy Society of America Twenty-Fifth Anniversary Meeting, Chicago, 1967, Proceedings, edited by C. J. Arceneaux, Baton Rouge, Claitor's Book Store, 1967, pp. 122-123.

Raju, M. R.; Heavy-particle studies with silicon detectors; in Workshop Conference on Space Biology, University of California, Berkeley, 1965, Proceedings, edited by P. E. Schambra, G. E. Stapleton, and N. F. Barr. Radiation Res. Suppl. 7: 43-52, 1967.

Raju, M. R.; Richman, C., and Curtis, S. B.; A review of the physical characteristics of pion beams; in International Symposium on the Biological Interpretation of Dose from Accelerator-Produced Radiation, 1st, Lawrence Radiation Laboratory, Berkeley, 1967, Proceedings, edited by R. W. Wallace. CONF-670305, 1967, pp. 349-357.

Resnick, M. A.; Tippetts, R. D., and Mortimer, R. K.; Separation of spores from diploid cells of yeast by stable-flow free-boundary electrophoresis. Science 158: 803-804, 1967.

Richman, S. P.; Richman, C.; Raju, M. R., and Schwartz, B.; Studies of Vicia faba root meristems irradiated with a π^- beam; in Workshop Conference on Space Biology, University of California, Berkeley, 1965, Proceedings, edited by P. E. Schambra, G. E. Stapleton, and N. F. Barr. Radiation Res. Suppl. 7: 182-189, 1967.

Sargent, T. W.; Israelstam, D. M.; Shulgin, A. T.; Landaw, S., and Finley, N. N.; A note concerning the fate of the 4-methoxyl group in 3, 4-dimethoxyphenethylamine (DMPEA). Biochem. Biophys. Res. Commun. 29: 126-130, 1967.

Schoenbrun, R. L., and Adey, W. R.; Space-flight-related stresses on the central nervous system; in Workshop Conference on Space Biology, University of California, Berkeley, 1965, Proceedings, edited by P. E. Schambra, G. E. Stapleton, and N. F. Barr. Radiation Res. Suppl. 7: 423-438, 1967.

Schooley, J. C.; Hayes, J. M.; Cantor, L. N., and Havens, V. W.; Studies on the behavior of erythropoietin-sensitive cells in the mouse during recovery from 200 roentgens of whole-body irradiation. Radiation Res. 32: 875-883, 1967.

Taketa, S. T.; Castle, B. L.; Howard, W. H.; Conley, C. C.; Haymaker, W., and Sondhaus, C. A.; Effects of acute exposure to high-energy protons on primates; in Workshop Conference on Space Biology, University of California, Berkeley, 1965, Proceedings, edited by P. E. Schambra, G. E. Stapleton, and N. F. Barr. Radiation Res. Suppl. 7: 336-359, 1967.

Tippetts, R. D.; Mel, H. C., and Nichols, A. V.; Stable-flow free-boundary (STAFLO) electrophoresis: three-dimensional fluid flow properties and applications to lipoprotein studies; in Chemical Engineering Symposium, 33rd, University of Cincinnati, 1966,

Chemical engineering in medicine and biology, edited by D. Hershey, New York, Plenum Press, 1967, pp. 505-540.

Tobias, C. A., and Schambra, P. E.; Summary of Workshop; in Workshop Conference on Space Biology, University of California, Berkeley, 1965, Proceedings, edited by P. E. Schambra, G. E. Stapleton, and N. F. Barr. Radiation Res. Suppl. 7: 459-463, 1967.

Todd, P. W.; Heavy-ion irradiation of cultured human cells; in Workshop Conference on Space Biology, University of California, Berkeley, 1965, Proceedings, edited by P. E. Schambra, G. E. Stapleton, and N. F. Barr. Radiation Res. Suppl. 7: 196-207, 1967.

Van Dyke, D. C.; Shkurkin, C. J.; Price, D. C.; Yano, Y., an Anger, H. O.; Differences in distribution of erythropoietic and reticuloendothelial marrow in hematologic disease. Blood 30: 364-374, 1967.

Van Dyke, D. C.; Similarity in distribution of skeletal blood flow and erythropoietic marrow. Clin. Orthop. 52: 37-51, May-June 1967.

White, M.; Grendon, A., and Jones, H. B.; Effects of urethane dose and time patterns on tumor formation; in Fifth Berkeley Symposium on Mathematical Statistics and Probability, Proceedings, Vol. 4, Biology and Problems of Health, edited by L. M. LeCam and J. Neyman, 1967, Berkeley, University of California Press, 1967, pp. 721-743.

Windsor, A. A.; Rich, T. H.; Doyle, R. E., and Lindgren, F. T.; Automatic acceleration and speed control for an analytic ultracentrifuge. Rev. Sci. Instr. 38: 949-952, 1967.

Yamanaka, W.; Winchell, H. S., and Ostwald, R.; Erythrokinetics in dietary hypercholesteremia of guinea pigs. Am. J. Physiol. 213: 1278-1284, 1967.

Author Index

Adamson, G. L. 95
Anger, H. O. 58
Born, J. L. 166, 173, 193
Cantor, L. N. 15
Carlson, R. A. 166, 193
Coggiola, E. L. 95
Curtis, S. B. 108
Duffy, F. 58
Feola, J. M. 151
Fink, R. A. 166
Forte, G. M. 74
Freeman, N. K. 89
Garcia, J. F. 123, 166
Geschwind, I. I. 123
Glaeser, R. M. 50, 64, 74
Havens, V. W. 15
Hayes, J. M. 15
Hayes, T. L. 50
Higashino, S. 58
Jensen, L. C. 85, 89, 102
Landaw, S. A. 1
Lawrence, J. H. 151, 166, 173, 193
Lew, V. C. 89
Lindgren, F. T. 85, 95, 102
Linfoot, J. A. 166, 193
Lossow, W. J. 102
Loughman, W. D. 48
Lyman, J. T. 173
Manning, J. S. 50
Manougian, E. 166, 193
McDonald, L. W. 173
McKey, T. J. 38
Mortimer, R. K. 26, 43
Murchio, J. C. 102
Nakai, S. 26
Nichols, A. V. 74, 95
Nohr, M. L. 23
Raju, M. R. 108
Resnick, M. A. 43
Rich, T. H. 85
Schooley, J. C. 15
Snyder, N. J. 166, 193
Strisower, E. H. 95
Tennant, B. 23
Tobias, C. A. 193
Van Dyke, D. C. 23, 58
Welch, G. P. 151
Wilson, J. 58

Personnel

Senior Staff

John H. Lawrence, Director
Hal O. Anger
Max W. Biggs
James L. Born
Ernest L. Dobson
Norman K. Freeman
Joseph F. Garcia
Thomas L. Hayes
Robert H. Haynes
Hardin B. Jones
Thomas H. Jukes
Frank T. Lindgren
Howard C. Mel
Robert K. Mortimer
Alexander V. Nichols
Howard G. Parker
Donald J. Rosenthal
John C. Schooley
William E. Siri
Cornelius A. Tobias
Donald C. Van Dyke
Harry Saul Winchell

Medical Investigator Staff

Max W. Biggs
James L. Born
Thomas F. Budinger
Richard A. Carlson
Claude Y. Chong
William G. Donald, Jr.
Stephen A. Landaw
John H. Lawrence
John A. Linfoot
Edward Manougian
Larry W. McDonald
Howard G. Parker
James Price
Donald J. Rosenthal
Norton J. Snyder
Henry H. Stauffer
Donald C. Van Dyke
Harry Saul Winchell

Research Staff

Henry Aceto
Lawrence Adams
Nabil Amer
Gerald Connell
Stanley B. Curtis
Patricia Durbin-Heavey
Rashid A. Fawwaz
Jose M. Feola
Cornelius T. Gaffey
Robert M. Glaeser
Thomas E. Gunter
Jerry Howard
Lin C. Jensen
W. Barrie G. Jones
Lola S. Kelly
Jack L. King
Walter J. Lossow
William D. Loughman
David D. Love
John T. Lyman
James McRae
Myron Pollycove
Douglas W. Pounds
Mudundi R. Raju
Thornton W. Sargent
Richard L. Schoenbrun
Carol J. Shkurkin
John V. Slater
Edward H. Strisower
Chiyoko Tokunaga
Graeme P. Welch
Margaret R. White
Yukio Yano

Postdoctoral Fellows

Brenda Buckhold
H. John Burki
Michael G. Chen
John C. Cummings
Gertrude M. Forte
David M. Israelstam
John T. Leith
Howard D. Maccabee
Tran Manh Ngo
John P. Sandblom
Martin D. Shetlar
Burton H. Slanger
Patric Tauro

Technical Staff

Gerald L. Adamson
Paul M. Aebersold
Hilda M. Alexander
Cathryne C. Allan
Alice Beckmann
Adrienne Berkowitz
Patricia J. Blanche
Catharine D. Boerke
Carol S. Bohlen
John F. Bohn
Jonathan Bokelman
Deortra Brooks
Gerald L. Brooks
Dorothy A. Carpenter
Emanuela N. Catena
Elaine L. Coggiola
Karen R. Colyear
Mary J. Cornell
Henriette C. Cozza
Susan J. Daniels
Theodora M. Davis
Rosalee Demostene
Michael P. Donovan
Robert E. Doyle
Doris L. Dunn
Gregory C. Eggling
Ora B. Ellington
Nancy C. Finley
Carolee R. Finney
Myrtle L. Foster
Roscoe Frazier
Charlie M. Fuller
Patricia A. Garbutt
Queen E. Gipson
Lois R. Gumz
Dawn C. Hammond
Virginia C. Havens
Judith M. Hayes
Beverly D. Heinze
Jerilyn Hirshberg
Walter K. K. Ho
Deanna Honbo
Willie M. Jackson
Karen Jarrett
Nylan M. Jeung
Kay M. Johnson
Natalia Kusubov
Phoebe J. Lindsay
Cynthia Lippincott
Jennie M. London
Jean R. Luce
Josephine A. Lundberg
Justine J. Lynch
Larry E. Marbley
Patricia C. Mason
Tommie C. Mathews
Johnie A. Maxion
Lafayette McIntosh, Jr.
Tommy J. McKey
Velma B. McNeal
Victor J. Montoya
William D. Nance
Mary L. Nohr
Virginia I. Obie
Anne K. Poley
Rosanne B. Raley
Camille M. Reed
Ralph L. Reynolds
Willie H. Sanders
Thea B. Scott
Barbara A. Shipley
Patricia P. Smith
Virginia M. Spamer
Robert W. Springsteen
Gary R. Stevens
Sandra K. Stoddard
Velta Suna
Frances B. Taylor
Charles Thompson, Jr.
Cole Ulrichs
Elnora Walker
Susan M. Walker
Marilyn A. Williams
Robert D. Wills
Elaine H. Yokoyama
Philip E. Yost

Graduate Students

Ann S. Amer
Raymond Baker
Steven A. Beckwitt
Martin L. Brown
Jeremy N. Bruenn
Elizabeth J. Clark
Robert A. Everson
Robert Foreman
David E. Garfin
Michael M. Graham
Martin Haas
Mark N. Herman
William J. Horsley
Latife Ismail
Gary E. Jones
Michael W. Kaplan
Gustave H. Langner, Jr.
Lawrence R. Lawlor
David H. Lin
Max S. Lin
Roderick D. Macgregor, Jr.
Udipi Madhvanath
Abdel M. Mamoon
JaRue Manning
Bambino I. Martins
Peter C. Nosler

Graduate Students (cont.)

Paul H. Olague
George F. Oster
James B. Pawley
Esther B. Perry
David A. Pistenma
Robert G. Plantz
Donald L. Puppione
Theodore Regimbal
Michael A. Resnick
Ubaldo S. Rodarteyramon
Guy Roy
Werner T. Schlapfer
Bernard Schwartz
Paul T. Shafer
Sylvia Spengler
Tom S. Tenforde
Junarden Williams
Myonggeun Yoon
David A. Zelman

Engineering and Technical Support Staff

Robert C. Aker
Elbert L. Benjamine
Delbert H. Coleman
Robert D. Creedy
Dewey D. Dean
Dorothy E. Denney
John A. Despotakis
Edward F. Dowling
James H. Edwards
John P. Flambard
John R. Gurule
Edward A. Heilstad
David A. Hoopes
Victor P. Jensen
Edward J. Lampo
Van L. Miller
Ellis H. Myers
Karen A. Peterson
Marjory H. Simpson
John M. Sweeney
Pamela C. Symmes
Frank T. Upham
Alfred A. Windsor

Administrative and Office Staff

Igor R. Blake
Baird Whaley
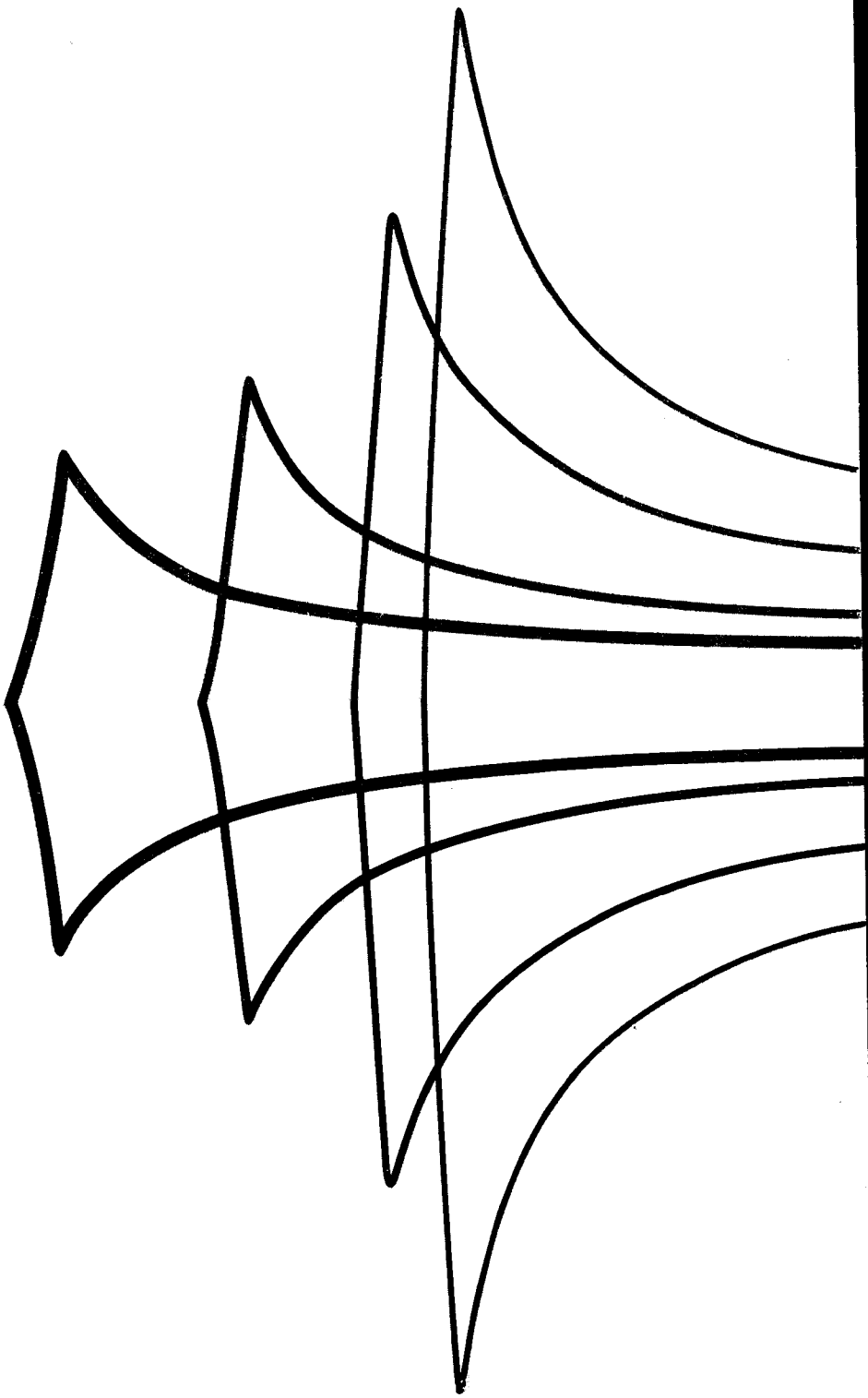
Betty M. Allen
Sandra L. Bazyouros
Mary M. Bryan
Janice C. DeMoor
Marian F. Edelen
Fern V. Forsberg
Mary C. Harmon
Dorothy B. Hedquist
Donna E. Kennedy
June M. Lattin
Judith S. Manning
Pamela A. Mott
Barbara J. O'Rourke
Shirley C. Peterson
Beverly A. Rovner
Ruth T. Showalter
Dorothy S. Sprague
Grace H. Walpole